Ras regulation of mitochondrial fission promotes tumor growth

Aldo Nascimento
Silver Spring, MD

A.B. Harvard University 2011

A Dissertation presented to the Graduate Faculty of the University of Virginia in Candidacy for the Degree of Doctor of Philosophy

Department of Microbiology, Immunology and Cancer Biology

University of Virginia
July, 2018

Abstract

Pancreatic cancer ranks 4th in the United States for cancer associated deaths. Despite recent advances in our understanding of cancer biology, pancreatic cancer patients have the poorest prognosis of all cancer types. The median survival rate for pancreatic cancer is 6 months and the 5-year survival rate of roughly 8%. Due to these high mortality statistics, there is an urgent need to better understand pancreatic cancer biology in order to discover novel pathways and targets that may be exploited for therapeutic benefit. Under this premise, this dissertation set out to understand the contribution of mitochondrial dynamics to pancreatic cancer growth.

One of the primary mutations in pancreatic cancer occurs in KRas, a master signaling protein which is responsible for controlling a variety of cellular processes. The best characterized pathway downstream of KRas is the MAPK pathway which promotes cell growth and proliferation. KRas mutations render the GTPase constitutively active which results in perpetual signaling through its downstream effector pathways including the MAPK pathway. Recently, studies have shown that in diseases and abnormal metabolic states such as Alzheimer's disease and hyperglycemia, respectively, MAPK activation can cause changes in mitochondrial dynamics. Due to the ability of KRas to activate the MAPK pathway in pancreatic cancer, we examined whether the MAPK pathway causes changes to mitochondrial morphology in cancer and if tumor growth ensues as a result of these changes.

Thus, in chapter 2 we demonstrate that HRas signals through the MAPK pathway to phosphorylate dynamin related protein 1 (Drp1) which in turn causes mitochondrial fission in HEK cells and pancreatic cancer cell lines. Furthermore, this Ras-mediated Drp1 induced mitochondrial fission is necessary for tumor growth in a xenograft model. In chapter 3, we show that HRas can partially inhibit mitochondrial fusion as well, which acts to shift the mitochondrial morphology of mutant Ras cells further toward the fragmented state. In chapter 4, we utilize *in vitro* and *in vivo* models of pancreatic cancer to study the contribution of Drp1 to tumor growth in

a more physiologically relevant system. We find that KRas-Drp1 signaling causes increased cell accumulation as well as glycolytic metabolism in MEF cells, partially through upregulation of the glycolytic enzyme hexokinase 2 (HK2). *In vivo*, we show that loss of Drp1 in a pancreatic cancer mouse model results in a 45-day survival advantage. Drp1 null tumor cells derived from these mice have undergone global metabolic reprogramming to maintain glycolytic flux and HK2 expression. Furthermore, these cells have compromised mitochondrial function and an increase in catabolism of lipids, which suggests that after Drp1 loss, these cells may attempt to compensate for lost mitochondrial function. Taken together, the data presented in this thesis support a model whereby KRas signals to promote Drp1 activation which in turn results in metabolic rewiring of tumor cells that support their tumorigenic properties.

Table of Contents

List of Figures

Chapter 1: Introduction

Pancreatic cancer is currently the fourth leading cause of cancer associated death in the United States. Pancreatic cancer patients have a median survival rate of approximately 6 months and the lowest 5-yr survival rate of any cancer at 8% (Hezel et al., 2006). By 2030, the number of deaths due to pancreatic cancer is projected to surpass liver and colorectal cancer to become the second leading cause of cancer deaths among Americans (Rahib et al., 2014). The rapid rise in pancreatic cancer mortality highlights the need for pioneering research to understand the factors that contribute to disease initiation and progression.

The primary aim of this thesis is to elucidate the relationship between oncogenic signaling pathways downstream of the Rat Sarcoma (Ras) protein, namely the Mitogen-Activated Protein Kinase (MAPK) pathway, and mitochondria to reveal how they promote pancreatic cancer progression. This chapter will provide a review of pancreatic cancer development and pathology followed by current treatments of the disease. Next will be a discussion of the genetic and biological classification of pancreatic cancer including a review of general Ras biology, primary Ras effector pathways as well as a review of key mutations that occur in pancreatic ductal adenocarcinoma (PDAC). Afterward, a review of general mitochondrial biology and the regulation of mitochondrial dynamics will lead into the relationship between Ras and mitochondria in cancer. Finally, the chapter will provide an outline of the central questions to be addressed by the research compiled in this thesis.

1.1 Pancreatic cancer development and pathology

1.1.1 Pancreatic Intraepithelial Neoplasia

A majority of pancreatic cancer lesions initiate at the head of the pancreas and spread to neighboring tissue including the spleen and peritoneal cavity with common metastasis to the liver

(Figure 1.1) (Hezel et al., 2006). Pancreatic cancer precursor lesions have been categorized into three subtypes: pancreatic intraepithelial neoplasm (PanIN), mucinous cystic neoplasm (MCN) and intraductal papillary mucinous neoplasm (IPMN) (Scarlett et al., 2011). PanIN in the most common type of precursor lesion found among patients and is graded from stages I to III. The PanIN stages are widely believed to represent a progression in dysplastic characteristics and neoplastic potential (Scarlett et al., 2011). PanIN-1 is divided into two categories, PanIN-1A and PanIN-1B (Hruban et al., 2001). PanIN-1A lesions are identified by their flat but tall columnar appearance while maintaining typical basal localization of the nucleus along with abundant mucinous epithelium. PanIN-1B are identified by minimal nuclear atypia and the formation of short papillary structures (Figure 1.2). PanIN-2 maintain the papillary structures but they exhibit more moderate nuclear atypia including nuclear crowding and enlargement. In progression from PanIN-2, PanIN-3 lesions are characterized by the formation of cribriform structures along with the papillary structures. At this stage there is loss of nuclear polarity and a significant increase in the nuclear:cytoplasmic ratio. PanIN-3 is classified as an *in situ* tumor due to its intact basement membrane and thus containment of the lesion (Hruban et al., 2001; Hruban and Fukushima, 2007). At the PanIN-3 stage, the carcinomas can progress to complete PDAC as evidenced by invasion into the basement membrane (Figure 1.2).

1.1.2 Pancreatic Ductal Adenocarcinoma

The main type of pancreatic cancer is known as pancreatic ductal adenocarcinoma (PDAC), as it comprises over 85% of pancreatic cancer cases. PDAC is characterized by the similarity of cancer cells to pancreatic duct cells based on their morphology (Li et al., 2004). PDAC tumors are firm, white-yellow masses with extensive desmoplastic stroma surrounding the cancer (Hruban et al., 2001). Patients with pancreatic cancer often present with a vague abdominal pain (Modolell et al., 1999). Symptoms can also include jaundice, asthenia and anorexia. Weight loss

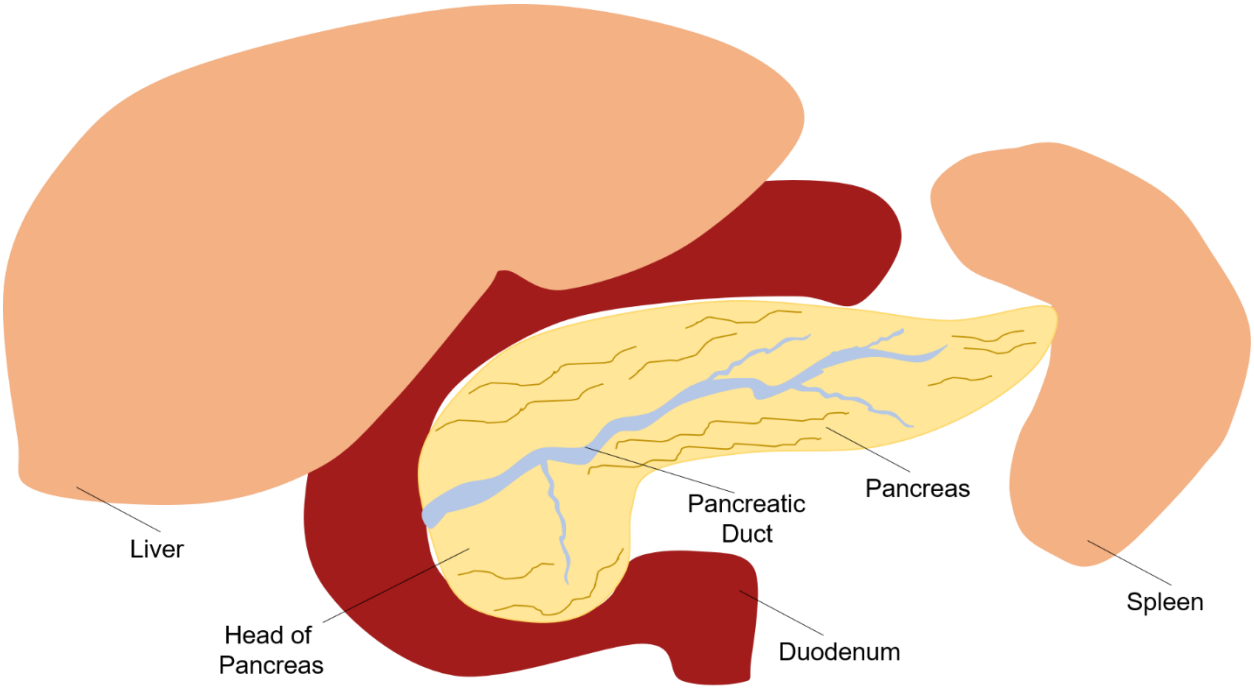
Liver
Pancreatic
Duct
Pancreas
Spleen
Head of
Pancreas
Duodenum

Figure 1.1. Diagram of Pancreas and surrounding tissues.

The pancreas is surrounded by the liver, duodenum and spleen. The head of the pancreas is where the majority of pancreatic tumors form.

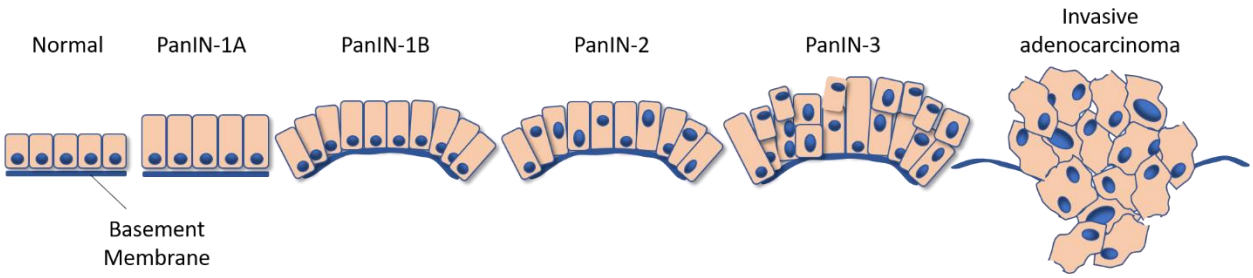
Normal
PanIN-1A
PanIN-1B
PanIN-2
PanIN-3
Invasive adenocarcinoma
Basement Membrane

Figure 1.2. Schematic representation of PanIN progression.

This diagram displays the morphology of ductal epithelial cells during the progression from normal tissue to invasive adenocarcinoma.

is common in pancreatic cancer patients as a secondary effect of complications arising from compromised pancreatic function. Patients also commonly present with diabetes (Ryan et al., 2014). As PDAC remains one of the most lethal cancers, current treatment strategies will be discussed in further detail.

1.2 Current Treatments for Pancreatic Cancer

1.2.1 Surgical Resection

Treatment options for pancreatic cancer patients remain limited. Thus far, the only potentially curative therapy for pancreatic cancer is surgical resection (Ryan et al., 2014). However, there are two key factors that determine patient compatibility for resection. First is the proximity of the tumor to the surrounding vasculature and whether or not there is evidence of distant metastasis (Vauthey and Dixon, 2009). Based on these factors, there are three types of tumor classifications: resectable, unresectable/locally advanced pancreatic cancer (LAPC) and metastatic. Due to the advanced stage of pancreatic cancer at which most patients are diagnosed, only 15-20% of patients are suitable for resection. Tumors from resectable candidates in the head and neck of the pancreas are removed via a procedure known as a pancreaticoduodenectomy (Whipple procedure). Recently, variations of the Whipple procedure have been developed in an effort to improve patient outcomes, however they have proven to be unsuccessful at providing any significant survival benefit (Martin et al., 2009). Tumors in the body and the tail of the pancreas are removed in a procedure known as distal pancreatectomy, which often requires a splenectomy (Ryan et al., 2014). As surgical resection is not an option for a majority of cancer patients, other types of therapies are more prevalent for treatment of PDAC patients.

1.2.2 Adjuvant Therapies

Surgery alone has proven to be ineffective in terms of improving survival outcomes. Indeed, during surgery, a majority of resectable candidates are found to be positive for lesions at

resection margins (Konstantinidis et al., 2013). Thus, the potential of locoregional failure after surgery has prompted the incorporation of adjuvant therapies for patient treatment. The different types of therapy include chemotherapy, radiation therapy (radiotherapy) and chemoradiotherapy. Chemotherapy involves the administration of anti-cancer drugs to fight disease while radiotherapy involves the exposure of patients to high doses of ionizing radiation. Chemoradiotherapy is the combination of chemotherapy and radiotherapy. Several studies have demonstrated the value of adjuvant chemotherapy with the pyrimidine analogues gemcitabine or fluorouracil, however, there is a disagreement in the field regarding the benefit of adjuvant radiotherapy and chemoradiotherapy. For example, one study by Neoptolemos et al. (Neoptolemos et al., 2004) found that patients with resected pancreatic tumors who receive fluorouracil alone had a 5-yr survival rate of 21% compared to 8% in the observational group. However, patients who received chemoradiotherapy (20 Gy over a two-week period plus fluorouracil) had a 5-yr survival rate of 10% versus 20% in the group that did not receive chemoradiotherapy. This study contrasts with previous clinical trials (GISTG, 1987; Klinkenbijl et al., 1999) that found that chemoradiotherapy provides a survival benefit. Currently, there is an ongoing clinical trial to address the effectiveness of chemoradiotherapy for survival outcomes of patients with resected tumors (NCT01013649). An alternative treatment for resectable candidates was to administer chemoradiotherapy before tumors are resected, a strategy classified as neoadjuvant therapy, however this approach did not produce any appreciable effect in patient outcomes (Ryan et al., 2014).

1.2.3 Combinatorial Therapeutics

Recently, efforts have shifted to the use of multiagent chemotherapy regimens, the foremost known as FOLFIRINOX (Ychou et al., 2003). FOLFIRINOX is composed of four drugs: Folinic acid (FOL), a vitamin B derivative that alleviates the adverse affects of fluorouracil, fluorouracil (F), irinotecan (IRIN), a topoisomerase inhibitor and Oxaliplatin (OX) which is a platinum-based DNA synthesis inhibitor. FOLFIRINOX has shown promising results in patients

presenting with metastatic disease. Compared to gemcitabine alone, the current standard of therapy for metastatic patients, FOLFIRINOX increased patient survival from 6.8 months to 11.1 months and progression-free survival from 3.3 months to 6.8 months (Conroy et al., 2011). Similar to the FOLFIRINOX study, Von Hoff et al. demonstrated that a combinatorial therapy of gemcitabine plus albumin bound paclitaxel particles (nab-paclitaxel) yielded an increase to 8.5 month median survival compared to 6.7 months with gemcitabine alone for patients with metastatic disease. (Von Hoff et al., 2013). Based on the success of combinatorial regimens for patients with metastatic cancer, clinicians have initiated combinatorial therapies for LAPC and for resectable patients in neoadjuvant and adjuvant regimens. A study by Faris et al. showed that neoadjuvant FOLFIRINOX led to a median progression-free survival of 11.7 months in LAPC patients. Furthermore, the group showed that 20% of LAPC patients converted to resectability following treatment with FOLFIRINOX (Faris et al., 2013). However, there were recurrences in three of the five patients who had tumors resected, highlighting the need for continuing research into effective combinatorial therapeutics for both resectable and unresectable patients.

Recently, there has been interest in identifying prognostic biomarkers that can predict disease progression. SMAD4 has gained prominence as a putative biomarker in pancreatic cancer, as patients with reduced SMAD4 expression correlated with more metastatic disease whereas patients with intact SMAD4 had fewer metastases and more locally contained disease (Iacobuzio-Donahue et al., 2009). Indeed, there is an extensive effort being put forth in terms of identifying and categorizing the specific genetic and molecular markers underlying pancreatic cancer in an effort to stratify patients into regimens according to local vs. metastatic disease. Based on the significance of understanding the genetic and molecular determinants of pancreatic cancer, this chapter will now summarize some of the key mutations and biological aspects of pancreatic cancer.

1.3 Biological and Genetic classification of Pancreatic Cancer

1.3.1 Ras

The molecular and genetic defects in pancreatic cancer have been stratified based on their association with the progressive stages of PDAC. These genetic lesions include activation of some of the well-established oncogenes, namely KRas, as well as inactivation of some canonical tumor suppressor genes. Furthermore, there is a growing catalogue of putative biomarkers whose expression correlates with histological pancreatic cancer stage. This section will summarize the function and regulation of the primary pancreatic cancer mutations and the biomarkers correlated with these mutations at respective pancreatic cancer stages. This section will also review current therapeutic strategies designed to target the mutated proteins and pathways.

1.3.1.1 Ras Structure and function

The *RAS* genes were originally identified from studies of viruses that could cause cancer in rats resulting in the name rat sarcoma (Ras)(Harvey, 1964). The *RAS* genes have since been implicated as master regulators of cell cycle progression, proliferation, survival, differentiation and metabolism (Bryant et al., 2014; Cox and Der, 2010; Hezel et al., 2006). The three oncogenes of the Ras family are *HRAS, KRAS* and *NRAS* which encode 21 kDa GTPases that share 82-90% sequence identity (Cox and Der, 2010). As a result of splice variation at exon 4, *KRAS* encodes the proteins KRas4A and KRas4B, which have different c-terminal sequences. KRas4B is mainly expressed in untransformed cells, however KRas4A has recently been found to be more widely expressed than KRas4B in cancer cells (Cox and Der, 2010; Tsai et al., 2015). All Ras proteins are composed of an N-terminal G domain, a hypervariable (HV) region and a CAAX moiety at the C-terminus. The G domain contains 6 conserved motifs necessary for binding GDP/GTP as well as the core effector domain (E), which mediates effector binding specificity (Karnoub and Weinberg, 2008). Also within the G domain are the Switch 1 and Switch 2 regions that regulate

stabilization of GDP/GTP binding (Fernandez-Medarde and Santos, 2011). The HV region accounts for the main differences between the Ras isoforms and contains domains necessary for post-translational modifications that target Ras to the plasma membrane (Karnoub and Weinberg, 2008). Finally, the CAAX moiety accounts for the final four amino acids of Ras proteins and is comprised of a cysteine (C) two aliphatic amino acids (AA) and a terminal amino acid (X), which is also involved in targeting Ras to the plasma membrane (Wright and Philips, 2006).

1.3.1.2 Regulation

The Ras proteins are prenylated at the cysteine residue of the CAAX moiety (Cox and Der, 2010). The addition of farnesyl or geranylgeranyl isoprenoid groups is determined by the terminal X amino acid and is carried out by farnesyltransferases (FTase) or geranylgeranyltransferases (GGTase), respectively (Cox and Der, 2010). Once the cysteine residue has been prenylated, Ras is trafficked to the endoplasmic reticulum (ER) where the Ras and a-factor converting enzyme-1 (Rce1) cleaves the AAX residues of the CAAX motif. Once the AAX residues have been removed, carboxyl methylation of the cysteine isoprenoid group is catalyzed by the isoprenylcysteine carboxyl methyltransferase (Icmt), a modification believed to significantly increase hydrophobicity, which facilitates plasma membrane association (Karnoub and Weinberg, 2008; Wright and Philips, 2006). After the cysteine residue of the CAAX has been fully modified, a second modification in the HV region is required to target Ras to the plasma membrane. Protein acyltransferases (PATs) at the ER mediate the addition of palmitate fatty acids to cysteine residues immediately upstream of the CAAX moiety in HRas and NRas (Cox and Der, 2010; Karnoub and Weinberg, 2008). Palmitoylation of HRas and NRas allows them to be transported through the classical secretory pathway by way of the Golgi to eventually arrive at the plasma membrane (Karnoub and Weinberg, 2008). KRas4B doesn't undergo palmitoylation and instead has a series of lysine residues immediately upstream of its CAAX moiety termed the

polybasic region (PBR), which allow it to bypass secretory pathway trafficking to arrive at the plasma membrane (Cox and Der, 2010).

At the plasma membrane, Src homology 2 domain containing protein (Shc) binds activated growth factor receptors and recruits growth factor bound protein 2 (Grb2) (Steelman, 2011). Grb2 recruits the normally cytosolic son of sevenless1 (Sos1) protein to the plasma membrane where it can activate newly recruited Ras (Quilliam, 1994). As Ras is in its "off" state when it is bound to GDP, Sos1 functions as a guanine nucleotide exchange factor (GEF) that disrupts GDP nucleotide binding by displacing Switch 1 and distorting Switch 2, providing a mechanistic basis for GEF-enhanced GDP release. As the concentration of GTP is ten times higher than GDP in the cytosol, GTP is expected to bind to the empty pocket that switches Ras into the "on" state (Boriack-Sjodin, 1998). Ras inactivation is mediated by cytosolic GTPase activating proteins (GAPs) that induce a 300-fold acceleration of hydrolysis of GTP bound to Ras, which converts GTP back to GDP. This conversion returns Ras to the "off" state (Trahey, 1987) (Figure 1.3A)

1.3.1.3 Role of KRas in Pancreatic Cancer

In pancreatic cancer, KRas is the Ras family member that is almost exclusively mutated (Cox et al., 2014; Zeitouni et al., 2016). KRas is primarily mutated at one of three residues, which causes it to be insensitive to GAP activity and thus renders it constitutively active: G12, G13 and Q61. It is interesting to note that all three of these residues surround the guanine nucleotide binding site, which is essential for Ras activity. (Barbacid, 1987) (Figure 1.3B). G12 and G13 are found in the p-loop of the Ras G domain and are involved in binding phosphate groups (Schubbert et al., 2007). When the G12 site is mutated (mainly from GGT to GAT (Asp, D) or GTT (Val, V)), the positively charged catalytic "arginine finger" of a RasGAP is no longer able to insert into the p-loop of Ras. This prevents the RasGAP from neutralizing the negatively charged β- and γ-phosphate groups of GTP when it is bound to Ras. Thus the bond between the β- and γ-phosphate groups cannot be cleaved and Ras remains in the GTP bound, active state

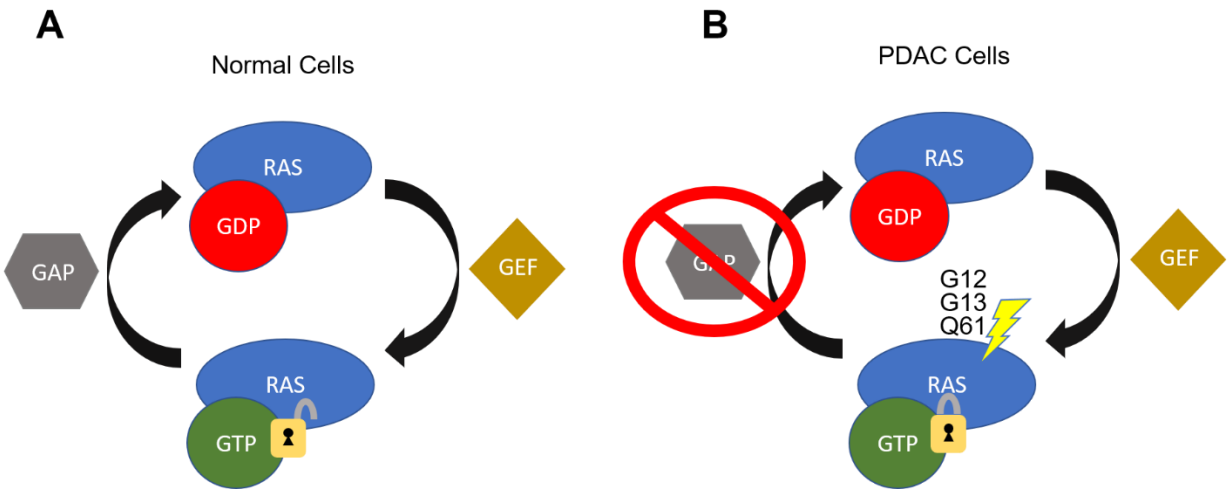
A
Normal Cells
RAS
GDP
GAP
GEF
RAS
GTP
B
PDAC Cells
RAS
GDP
GEF
G12
G13
Q61
RAS
GTP

Figure 1.3. Schematic of the Ras activity state in normal cells vs cancer cells.

(A) In normal cells, wild-type KRas switches from an inactive state (GDP-bound) to an active state (GTP-bound). This process is mediated by a guanine nucleotide exchange factor (GEF). Ras GTPase activity is activated by a GTPase activating protein (GAP) which causes Ras to hydrolyze GTP into GDP, converting Ras back to its inactive state. (B) In pancreatic cancer cells, KRas is mutated at one of three residues, G12, G13 or Q61. All of these mutations cause Ras to become insensitive to GAP activity so it can no longer hydrolyze GTP. The result of this insensitivity to GAP activity causes Ras to become permanently GTP-bound, locked in its active state.

(Scheffzek et al., 1997). Ras Q61 is located in the switch II region and when mutated, it is no longer able to activate the water molecule that is required to assist in the cleavage of the γ-phosphate group of GTP. Again, this causes Ras to remain GTP-bound and in its active conformation (Rajalingam et al., 2007). These activating KRas mutations are some of the earliest genetic lesions to occur during pancreatic cancer initiation and they persist throughout pancreatic cancer progression (Moskaluk et al., 1997). For example, KRas mutations are found in 30-40% of early PanIN lesions and in well over 90% of advanced stage lesions leading up to and including PDAC (Klimstra and Longnecker, 1994). Moreover, several studies have shown the necessity of mutant KRas expression for the progression and maintenance of pancreatic tumors (Fleming et al., 2005). For example, a study by Collins et al. showed that in a mouse model of pancreatic cancer, induction of $KRas^{G12D}$ expression following tissue damage led to precursor lesions and progression to pancreatic cancer. Inactivation of the $KRas^{G12D}$ in early lesions as well as in established tumors caused regression in tumor size, tumor grade, tissue damage and induced remodeling of pancreatic architecture to a more normal state (Collins et al., 2012).

1.3.1.4 Therapeutic Strategies targeting Ras

Due to the significance of KRas for tumor growth, extensive efforts have been made over the past several years to exploit the therapeutic potential of the protein. However, an effective pharmacological inhibitor has remained elusive (Cox and Der, 2010). Initial attempts to develop anti-Ras strategies focused on inhibiting FTase, an enzyme responsible for the post-translational prenylation of Ras which allows it to localize to the plasma membrane and signal to downstream effectors (Bryant et al., 2014). The FTase inhibitors (FTIs) initially demonstrated promising preclinical results, efficiently blocking HRas association with the plasma membrane and inducing cell growth arrest in tumor cells. However, clinical trials showed no appreciable effect on patient outcomes with KRas and NRas mutations. This was due to the unanticipated finding that the other Ras isoforms could be alternatively prenylated by GGTase-I, thus allowing Ras to bypass FTI

activity and continue to localize to the plasma membrane (Appels et al., 2005; Whyte et al., 1997). These early setbacks originally led to the classification of Ras as an “undruggable” target. However, the paradigm is shifting away from this view through renewed efforts to exploit other methods of Ras regulation. Recent studies have focused on (1) developing small-molecule ligands to inhibit the interaction between Ras and its GEFs, effectively preventing GTP binding (Maurer et al., 2012); (2) targeting the prenyl-binding pocket of the Ras membrane transporter phosphodiesterase delta (PDEδ) (Zimmermann et al., 2013); (3) using a multivalent small-molecule to directly target multiple Ras “effector-protein” binding sites at once (Welsch et al., 2017). Despite the advances in Ras targeting, a recent study by Muzumdar et al. utilized clustered regularly interspaced short palindromic repeat (CRISPR)/Cas9 genome editing to completely inhibit KRas expression in pancreatic cancer cell lines, effectively modeling the consequences of the most potent KRas inhibition (Muzumdar et al., 2017). They showed that complete loss of KRas is sufficient to drive reduced cell viability and colony formation in pancreatic cancer cells. However, there were a subset of cells that were no longer dependent on KRas function. In these KRas null tumor cells, there was increased mitogen-activated protein kinase (MAPK) signaling that is dependent on phosphoinositide 3-kinase (PI3K). This compensatory signaling cascade was shown to be critical for the survival of these cells as they developed an increased sensitivity to PI3K inhibitors. Interestingly, this group also showed that KRas null cells exhibited a genetic profile that is consistent with increased metastatic potential, suggesting that the presence of mutant KRas may actually suppress metastasis-related genes in pancreatic tumors. Collectively, these studies show that. while blocking KRas function in pancreatic tumors may ultimately prove to be an achievable goal, PDAC cells can still develop resistance to KRas inhibition. Thus, it will be critical to consider combinatorial therapeutic strategies to target any compensatory pathways. As Ras is known to be a master regulator of proliferative signaling, the three best characterized pathways downstream of activated Ras that are associated with oncogenic transformation will be summarized in the following sections.

1.3.1.5 Ras signaling Pathways

1.3.1.5.1 MAPK Pathway

The MAPK pathway is involved in mediating signals that drive the growth and proliferation of cells. Simply, once Ras is at the plasma membrane and is bound to GTP, it can recruit the Ras-binding kinase rapidly accelerated fibrosarcoma (Raf), which becomes activated to phosphorylate dual-specificity kinases mitogen activated protein kinase kinase (Mek)1 and Mek2, which in turn phosphorylate extracellular signal related kinase (Erk)1 and Erk2 (Figure 1.4). Erk functions to alter the levels and activities of transcription factors that regulate genes that promote cell growth and proliferation (Kolch, 2000).

The MAPK pathway is primarily regulated at the Raf activation step. There are three Raf kinase members, C-Raf, B-Raf and A-Raf that share similar structure and regulation. Of the three members, C-Raf is the cellular homolog expressed in a variety of tissues (Kolch, 1991). C-Raf is a multi-domain protein that consists of an N-terminal auto-inhibitory Ras-GTP binding domain (RBD), a hinge region and a C-terminus that contains the kinase domain (Kolch, 2000). When Ras is bound to GDP, Raf is in the inactive confirmation where the N-terminal auto-inhibitory domain is folded over the kinase domain, physically blocking its catalytic site (Cutler, 1998). 14-3-3 proteins form dimers and bind to phosphorylated serine residues on Raf and function as molecular restraints keeping Raf folded over itself (Kolch, 2000). The Raf RBD has such a high affinity for GTP-bound Ras that it will release the kinase domain in order to bind active Ras. Meanwhile phosphatases remove the phosphorylations at the serine residues, detaching the 14-3-3 proteins and further exposing the Raf kinase domain. At this point c-Raf can form homodimers or heterodimers with the other Raf family members and autophosphorylate serine and threonine

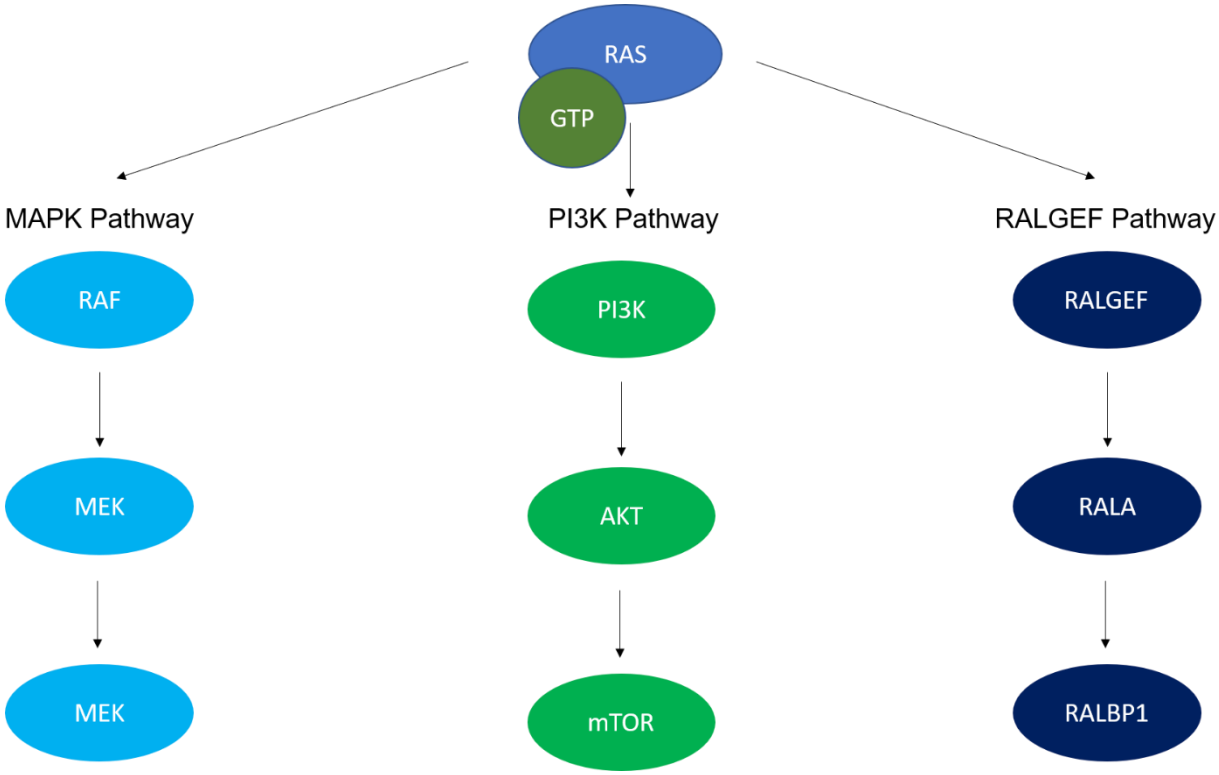
RAS
GTP
MAPK Pathway
PI3K Pathway
RALGEF Pathway
RAF
MEK
MEK
PI3K
AKT
mTOR
RALGEF
RALA
RALBP1

Figure 1.4. Diagram of the primary Ras effector pathways.

The best characterized pathways downstream of Ras that have been implicated in cancer are the MAPK pathway, the PI3K pathway and the RALGEF pathway. In the MAPK pathway, Ras activates RAF, which in turn phosphorylates MEK, and MEK phosphorylates Erk. In the PI3K pathway, Ras activates PI3K and PI3K recruits AKT to the plasma membrane where it can be activated. Once activated, AKT can activate mTOR. For the RALGEF pathway, Ras activates RALGEF which goes on to activate RALA by promoting it's binding to GTP. Once RALA is bound to GTP it can activate RALBP1.

residues in the activation loop of the Raf kinase domain (Matallanas et al., 2011). Phosphorylation of Ser339 and Tyr342 near the N-terminal of the kinase domain also promotes activation of Raf. Once phosphorylated, the activation loop uncovers the catalytic site, which allows ATP to bind and primes Raf to phosphorylate MEK (Chong and Guan, 2003). After MEK is phosphorylated, it is able to phosphorylate Extracellular signal related kinase 1,2 (Erk1/2) on T202, and Y204 and Erk2 on T185 and Y187 (Chang et al., 2003). Signaling through the MAPK pathway is ultimately terminated by Erk feedback phosphorylation of inhibitory residues on Raf and phosphatase removal of activating residues (Shin et al., 2009).

Among the MAPK pathway components, Raf is the main effector found mutated in cancers such as melanoma, colorectal, ovarian and rarely in PDAC. However, due to upstream activation of KRas, PDAC cell lines are susceptible to genetic and pharmacological inhibition of the MAPK pathway. Gysin et al. showed that pharmacological MEK inhibition caused G0-G1 cell cycle arrest instead of outright cell death (Gysin et al., 2005). Similarly, a recent study by Hayes et al. demonstrated that prolonged pharmacological inhibition at the level of Erk results in cellular senescence in pancreatic tumor cells mediated by myelocytomatosis gene (MYC) degradation (Hayes et al., 2016). Thus, the MAPK pathway has been implicated as driving tumor growth in many cancer types with mutated Ras.

1.3.1.5.1 PI3K/Akt Pathway

The PI3K pathway has been found to be involved in promoting cell proliferation while simultaneously providing resistance to apoptosis signals (Castellano and Downward, 2011). PI3K is divided into three different classes, I-III, based on the nature of the binding partners and regulation. Class I PI3Ks are the most widely studied of the three families due to their association with cancer (Yuan and Cantley, 2008). Class I PI3K is a heterodimeric molecule composed of a regulatory subunit, p85, and a catalytic subunit, p110 (Carpenter, 1990), which can be activated in a manner of ways including through Ras (Castellano and Downward, 2011).

Similar to activation of the MAPK pathway, signaling through the PI3K pathway begins with the activation of a receptor tyrosine kinase (RTK), which dimerize and autophosphorylate its tyrosine residues (Castellano and Downward, 2011). Src Homology 2 (SH2) domain containing proteins recognize the phosphorylated tyrosine residues and bind Son of sevenless homolog 1 (SOS1), which activates Ras. In this scenario, GTP-bound Ras can directly interact with the p110 subunit and activate PI3K independently of p85 (Castellano and Downward, 2011). However, other studies demonstrated that the interaction between p85 and the RTK-associated growth factor receptor-bound protein 2 (Grb2)/Grb2-associated-binding protein (GAB) complex is necessary for HRas mediated activation of p110 (Chan, 2002). Ras association with p110 is thought to induce a conformational change at the p110 substrate-binding site to stabilize p110 association with the plasma membrane (Pacold, 2000; Vanhaesebroeck, 1997). After PI3K is activated, it phosphorylates phosphatidylinositol 4,5-bisphosphate (PIP_2) and converts it into phosphatidylinositol 3,4,5-triphosphate (PIP_3). PIP_3 is able to recruit Protein Kinase B (PKB/Akt) and phosphoinositide-dependent kinase-1 (PDK1) through their pleckstrin homology domains (Franke, 1997) at which point PDK1 can partially activate Akt through phosphorylation at threonine 308. Akt becomes fully activated after it is phosphorylated at serine 473 by the transducer of regulated CREB protein 2 (TORC2) complex (Steelman, 2011). Fully activated Akt has a range of downstream effectors that enable it to regulate proliferation and apoptosis but one of the key effectors is the mammalian target of Rapamycin (mTOR). mTOR is activated by the GTPase Ras homologue enriched in brain (Rheb) (Steelman, 2011). Akt phosphorylation of the GAP TSC2 deactivates the TSC1/TSC2 complex, which is responsible for deactivating Rheb, and as a result activates mTOR (Castellano and Downward, 2011) (Figure 1.4). mTOR has a variety of downstream effectors involved in protein synthesis and cell growth (Steelman, 2011).

While mutations in the PI3K pathway components have been associated with several kinds of cancer, they are relatively rare in PDAC (Samuels and Velculescu, 2004). However,

numerous studies have shown that pancreatic tumors rely on perturbations in downstream PI3K signaling for initiation, maintenance as well as for compensatory resistance mechanisms to KRas inhibition. Lim and Counter demonstrated that PI3K signaling is important for tumor initiation. However, once tumors were established, the tumors no longer depended on KRas and instead required PI3K pathway activity for maintenance (Lim and Counter, 2005). The DePinho group demonstrated that the tumor suppressor phosphatase and tensin homolog (PTEN) is frequently deleted in primary PDAC tumor specimens and this phenomena is corroborated in genetic mouse models (Ying et al., 2011). PTEN is a negative regulator of the PI3K pathway, responsible for converting PIP_3 to PIP_2 which prevents activation of Akt. Decreased PTEN expression has also been shown to be regulated at the epigenetic level via promoter hypermethylation (Asano et al., 2004). Conversely, Akt2, a PI3K effector, has been shown to be upregulated in roughly 20% of PDAC cases, which would result in increased signaling and downstream proliferative effects (Schlieman et al., 2003). Accordingly, studies have shown that inhibiting mTOR, which lies downstream of Akt2, inhibits growth of PDAC cell lines (Asano et al., 2005). Recently, studies have shown that resistance to direct pharmacological Erk inhibition or complete genetic KRas ablation was mediated by increased basal PI3K-AKT signaling (Hayes et al., 2016; Muzumdar et al., 2017). These more recent studies provide insight into the previous findings that demonstrate the effectiveness of combined MEK and PI3K inhibition on PDAC tumors *in vitro* as well as *in vivo* (Alagesan et al., 2015).

1.3.1.5.3 RalGEF-Ral Pathway

The least characterized of the three major pathways downstream of activated Ras is the RalGEF pathway (Cox and Der, 2010). Briefly, GTP-bound Ras is able to activate RalGEF family proteins, which in turn activate RalA and RalB. RalA and RalB have a wide range of immediate downstream effectors including Sec5 and RalBP1, which mediate, cell proliferation, survival, exocytosis as well as actin reorganization (Neel et al., 2011). The activated Ral proteins bind their

downstream effectors and promote their recruitment to the sites where effectors such as RalBP1, a GAP protein, can carry out their various cellular functions. The first RalGEF identified was Ral guanine nucleotide dissociation stimulator (RalGDS) through a mouse cDNA library screen for genes with strong homology to RasGEFs (Albright, 1993). The additional human RalGEFs called RalGEF-like 1-3 (Rgl, Rgl2, Rgl3) were identified through two-hybrid screens for various Ras family GTPases (Neel et al., 2011).

The Ral GTPases are recruited to the plasma membrane in a manner very similar to Ras (Neel et al., 2011). Ral GTPases contain a CAAX motif prenylated by GGTs and go through AAX cleavage and carboxyl-methylation by Rce1 and Icmt, respectively. However, Ral GTPases contain a PBR region upstream of the CAAX that allow them to bypass the Golgi on their way to the plasma membrane (Kinsella, 1991). At the membrane, the four human RalGEFs can interact with Ras to become activated. While RalGDS binds to Ras, it does not appear to act on Ras and only promotes guanine nucleotide exchange for RalA and RalB. The RalGEF pathway is deactivated by RalGAPs, which are structurally and functionally similar to the TSC1/TSC2 GAP complexes that act on Rheb (Neel et al., 2011).

In PDAC, studies have shown that RalA is activated in human pancreatic tissue samples as well as in a variety of PDAC cell lines and that it is critical for anchorage-independent and tumorigenic growth. Further, these studies demonstrate that RalA is required for PDAC tumor maintenance and that another RalGEF pathway effector, RalB is required for PDAC metastatic potential (Lim et al., 2005; Lim et al., 2006). More recently, Neel et al. found that in PDAC, mutant KRas signaling to RalB but not RalA is necessary for the formation of actin-rich membrane protrusions known as invadopodia, which are thought to facilitate metastasis (Neel et al., 2012). More upstream in the RalGEF pathway, RalGEFs themselves have also been found to be upregulated in human PDAC samples and promote the tumorigenic capabilities of PDAC tumor cell lines (Vigil et al., 2010).

Taken together, these sections demonstrate the extensive roles of KRas and its downstream effector pathways in driving as well as maintaining pancreatic tumors. Along with KRas, the other Ras isoforms have been shown to play a role in promoting pancreatic cancer as well. Even though HRas and NRas are rarely mutated in pancreatic cancer, a study by Lim et al. showed that in pancreatic cancer cell lines, there was a dependence on wild-type HRas and NRas for tumorigenicity (Lim et al., 2008). The authors first observed that oncogenic KRas-mediated activation of AKT resulted in the activation of endothelial nitric oxide synthase (eNOS). Activation of eNOS led to the S-nitrosylation and subsequent activation of endogenous wild-type HRas and NRas. The activation of HRas and NRas by eNOS was necessary for the tumorigenic properties of pancreatic cancer cell lines *in vivo* and *in vitro* as knockdown of wild-type HRas or NRas led to reduced xenograft growth and colony formation. Expression of wild-type HRas or NRas in the pancreatic cancer cell lines rescued the loss of tumor growth and colony formation (Lim et al., 2008). Thus, the other isoforms of wild type Ras provide alternative pathways for pancreatic cancer cells to maintain their proliferative signaling. Due to the numerous routes available to Ras to signal through compensatory pathways, research into the interplay between critical nodes of downstream Ras signaling will guide future treatments in the hopes of improving patient survival outcomes. As mentioned earlier in the chapter, combinatorial therapeutics shed light on promising avenues for further advances in cancer treatment.

1.3.2 CDK2NA: $p16^{INK4A}$ and $p19^{ARF}$ tumor suppressors

Cyclin-dependent kinase inhibitor 2A (CDK2NA) is a found at the *9q21* locus and encodes two tumor suppressors, $p16^{INK4A}$ (p16) and $p19^{ARF}$ (p19). p16 regulates cell cycle progression by binding cyclin dependent kinase 4 and 6 (CDK4/6) thus preventing their phosphorylation of retinoblastoma protein (Rb) (Rayess et al., 2012). p19 prevents aberrant cell cycle progression by mediating the degradation of mouse double minute 2 homolog (MDM2), an E3 ubiquitin ligase responsible for the degradation of p53 (Zhang et al., 1998).

In PDAC, the significance of p16 tumor suppressor capability has been demonstrated by the identification of germline as well as sporadic mutations in pancreatic cancer patients (Rozenblum et al., 1997; Yarbrough et al., 1999). As early pancreatic lesions progress from early staged PanIN-1, they accumulate an increasing array of genetic mutations. In moderately advanced lesions that demonstrate features of dysplasia, there is loss of function of p16 in 80-95% of sporadic PDAC cases. This loss of function can be caused by deletion, mutation or promoter hypermethylation (Hustinx et al., 2005; Rozenblum et al., 1997). Furthermore, loss of p16 function has been shown to cooperate with KRas as well as p53 mutations in driving disease progression (Bardeesy et al., 2006). Initially, studies in mouse and human fibroblasts showed that Ras activation caused accumulation of p16 and p19 which in turn led to premature senescence as would be expected (Drayton et al., 2003; Serrano et al., 1997). Consequently, Collado et al. demonstrated that in mouse models where mutant KRas is expressed endogenously in lung and pancreatic ducts, premalignant lesions expressed p16 along with other markers of senescence. However, when they analyzed frank tumors of each tumor type, they found that the invasive tumors had fully lost expression of p16 (Collado et al., 2005). While these earlier studies seem to suggest a direct relationship between KRas and induction of p16 and p19, subsequent work by several groups demonstrate that expression of endogenous levels of activating KRas mutations provided a proliferative benefit in very early passage mouse and human fibroblasts without inducing senescence (Benanti and Galloway, 2004; Tuveson, 2004). Thus, these studies led to the conclusion that once KRas is activated in early Pan-IN lesions, intermediary events may occur, such as increases in the protein level of activated KRas, growth factor signaling or reactive oxygen species (ROS) production that could induce a selective pressure for loss of p16 and p19 and thus provide a route for the lesion to progress to PDAC (Hezel et al., 2006).

1.3.3 p53 Tumor suppressor

p53, encoded by *TP53*, is a 53 kD sequence-specific DNA binding protein that regulates transcription (Kastenhuber and Lowe, 2017). p53 is composed of two N-terminal transactivation domains that are upstream of a conserved proline-rich domain, a central DNA-binding domain and a C-terminal domain that consists of an oligomerization domain and nuclear localization sequences (Laptenko and Prives, 2006). In response to cellular stressors such as DNA damage or oncogenic signaling, p53 can become activated by phosphorylation, which prevents MDM2-dependent proteolysis of p53, or by p19-mediated inhibition of MDM2, respectively (Pomerantz et al., 1998; Shieh et al., 1997). The primary consequences of p53 activation include cell cycle arrest, senescence or apoptosis (Kastenhuber and Lowe, 2017). The role of p53 as a cell cycle regulator was first elucidated by studies in the early 1990s that demonstrated that p53 is necessary for the G1 checkpoint induced by DNA damage (Kastan et al., 1991). Subsequent studies showed that p53 regulation of G1 checkpoint entry is dependent, in part, on p53 transcriptional activation of the p21 cyclin-dependent kinase inhibitor gene (El-Deiry et al., 1993). The G1 checkpoint initiated after DNA damage is thought to allow the cell time to implement DNA repair mechanisms to ensure the fidelity of DNA for the proceeding stages of the cell cycle. In terms of aberrant growth signaling, overactivation of an oncogene can induce p53-mediated cellular senescence through a mechanism preventing the phosphorylation of Rb (Serrano et al., 1997). The regulation of apoptosis depends on p53 induction of pro-apoptotic cellular responses. Studies by Miyashita et al. demonstrated that p53 is able to simultaneously decrease the expression of the apoptosis-suppressing gene *bcl-2*, while increasing the expression of *bax*, a gene responsible stimulating apoptosis. (Miyashita, 1994; Toshiyuki and Reed, 1995).

The ultimate consequences of p53 activation in mediating senescence, cell cycle arrest or apoptosis are two-fold. In one instance p53 is able to retard the earliest stages of cancer initiation because of its ability to stop the accumulation of oncogenic mutations by stopping the

cell cycle after DNA damage or killing off cells with irreparable DNA (Livingstone et al., 1992). The other scenario in which p53 is able to deter cancerous outgrowth is by impeding the proliferation of cells with activated oncogenes/loss of tumor suppressors, thus negating the biological effects of these oncogenic mutations (Serrano et al., 1997). These tumor suppressing functions of p53 have led to the colloquial classification of the protein as the “guardian of the genome”, an appropriate title underscored by the fact that *TP53* is the most commonly mutated gene in all human cancers (Kastenhuber and Lowe, 2017).

In PDAC specifically, late stage PanIN lesions harbor missense mutations in the p53 DNA-binding domain in roughly 50% of patients (Maitra et al., 2003; Rozenblum et al., 1997). The occurrence of p53 mutations in higher grade PanINs may point to a selective pressure within the tumor to eliminate p53 function. These selective pressures may arise as a result of increased genetic damage due to the buildup of reactive oxygen species (ROS) or telomere erosion, mechanisms that would allow the cell to proliferate with accumulating chromosomal instability (Hezel et al., 2006). The high rates of aneuploidy associated with PDAC tumors may accelerate disease progression as well as provide mechanisms for therapeutic resistance, thus highlighting the importance of p53 in maintaining genetic fidelity (Harada et al., 2008).

Recently, another role for p53 in PDAC disease progression has been identified at the level of metastasis. Weissmueller et al. found that gain-of-function mutant p53 can drive a pro-metastatic phenotype in a murine model of PDAC through cell-autonomous stabilization of platelet-derived growth factor receptor b (PDGFRb). PDGFRb expression was further shown to correlate with poor prognosis not only in PDAC, but in colon and ovarian cancers as well (Weissmueller et al., 2014). From a clinical perspective, mutant p53 was found to stimulate chemoresistance to gemcitabine in pancreatic cancer cell lines through expression of *Cdk1* and *CCNB1* genes. This activity could be reversed through the addition of p53-reactivating drugs used in combination with gemcitabine (Fiorini et al., 2015). Finally, p53 has been shown to have some

prognostic potential in determining the survival of patients who qualify for resection. In this study, Xiang et al. used a tumor tissue microarray screen, PDAC cell lines and a mouse model to demonstrate that overexpression of mutant p53 upregulated cavin-1, an RNA binding protein responsible for regulating transcription, and patients with high mutant p53 and cavin-1 expression had the shortest survival after resection (Xiang et al., 2016).

The sections above highlight the depth of research regarding the numerous genetic lesions and their consequences for pancreatic cancer initiation and progression. As these findings have progressed through the years, the direction of pancreatic research is evolving to question the contribution of broader cellular biology aspects to disease progression. One of the most promising fields of research in this regard concerns the primary energy producer of the cell, the mitochondria. The following sections will review some of the basic biology of mitochondria, including the regulation of their dynamic nature as well as the role mitochondria play in concert with Ras to affect pancreatic cancer growth.

1.4 Mitochondria and Mitochondrial Dynamics

1.4.1 Mitochondrial Fission

Mitochondria are double-membrane-bound organelles in eukaryotic cells that are highly dynamic and primarily responsible for meeting the energy requirements of the cell by regulating ATP production through oxidative phosphorylation (Corrado et al., 2012; Grandemange et al., 2009; Westermann, 2012). Mitochondria also play an essential role in mediating the programmed cell death cascade known as apoptosis (Corrado et al., 2012). An important requirement for proper mitochondrial function is tightly regulated mitochondrial morphology (Chan, 2012). Changes to mitochondrial morphology allow the mitochondria to meet different cellular demands and is defined as the shape, number and size of mitochondria and is mediated by continuous cycles of fusion and fission (Kageyama et al., 2011). Mitochondrial fission is necessary for appropriate segregation of mitochondria during cell division as well as for fragmenting damaged

mitochondria for clearance. Fusion on the other hand is necessary for content mixing and mitochondrial DNA complementation to maintain mitochondrial function. The balance between fusion and fission events is collectively termed mitochondrial dynamics and is regulated by distinct sets of large dynamin-related GTPases (Westermann, 2012). Simply, fusion of mitochondrial membranes is regulated by Mitofusin 1 and 2 (Mfn1, Mfn2) and Optic Atrophy 1 (Opa1) whereas fission is regulated primarily by dynamin-related protein 1 (Drp1) (Chan, 2012). Shifts in the balance of fission and fusion events result in rapid changes in mitochondrial morphology and function, underlining the importance of the balance between these two processes (Cerveny et al., 2007). Due to the varied energetic demands as well as physiological conditions of different cell types, there is an extensive variation of mitochondrial morphology (Westermann, 2012). Thus, mitochondrial morphologies in different cell types run the gamut of conformations, ranging from extensive interconnected networks to small, punctuate like structures (Benard and Rossignol, 2008; Kuznetsov et al., 2009). Defects in the mitochondrial machinery that cause deregulation of mitochondrial dynamics result in various neurodegenerative diseases as well as cancer (Boland et al., 2013; Corrado et al., 2012; Grandemange et al., 2009; Martin, 2012). Due to the emerging importance of mitochondrial fission and fusion for cellular homeostasis as well as disease progression, the basics of mitochondrial dynamics are reviewed below.

A key component of overall cellular function is the balance between mitochondrial fusion and fission, which allows mitochondria to change their morphology to accommodate various physiological demands (Archer, 2013; Benard, 2007; Soubannier and McBride, 2009). For example, mitochondrial fission is important for mitochondrial autophagy (mitophagy) whereby damaged mitochondria need to be separated from healthy mitochondria through fission and degraded via autophagosomes (Gomes and Scorrano, 2013). In neurons, fission facilitates the transport of mitochondria to cellular extremities such as the synapse, which require high ATP

consumption (Ishihara et al., 2009). Furthermore, mitochondrial fission is necessary for proper mitochondrial inheritance during mitosis (Taguchi et al., 2007).

As a counter to fusion, mitochondrial fission is largely mediated by the large GTPase dynamin related protein 1 (Drp1). Briefly, mitochondrial fission is initiated when Drp1 is recruited to the outer mitochondrial membrane (OMM) where it can oligomerize into concentric spirals around the mitochondria. Drp1 hydrolyzes GTP in order to constrict its oligomeric spiral structures, thus constricting the underlying mitochondria. At this point, dynamin-2 (Dyn2) is able to form oligomeric structures around the mitochondria. Dyn2 also hydrolyzes GTP in order to constrict and eventually sever the mitochondria, resulting in mitochondrial fission (Lee et al., 2016).

1.4.1.1 Drp1 structure and function

Drp1 is a member of the dynamin-like protein family (Labrousse, 1999; Smirnova, 2001; Smirnova, 1998). Drp1 is composed of a GTPase domain at its N-terminus, followed by a middle domain (MID) and a variable domain (VD) and GTPase effector domain (GED) at the C-terminus (Figure 1.5) (Strack and Cribbs, 2012). The MID forms part of the stalk along with the GED while VD functions as an auto-inhibitory domain that regulates Drp1 oligomerization and activity. The MID specifically contains a short α-helical stretch containing the Arg-376 residue, which is responsible for the interaction between Drp1 and mitochondrial fission factor (Mff) (Strack and Cribbs, 2012). Drp1 exists in four isoforms; the longest of the isoforms is primarily expressed in neurons while the shortest is expressed ubiquitously in mammalian cells (Macdonald et al., 2015). Drp1 primarily functions to drive membrane fission of mitochondria as well as peroxisomes (Demarquoy and Le Borgne, 2015). Drp1 is mainly a cytosolic protein with approximately only 3% of the total protein found to be localized to the outer mitochondrial membrane (Smirnova, 2001). Although the mechanism of Drp1 recruitment to the mitochondria remains largely unknown, there are four OMM bound adaptor proteins that associate with Drp1: Fis1, Mitochondrial fission factor (Mff), Mitochondrial dynamics protein of 49 kDa (MiD49) and MiD51 (Chan, 2012). Fis1 has been

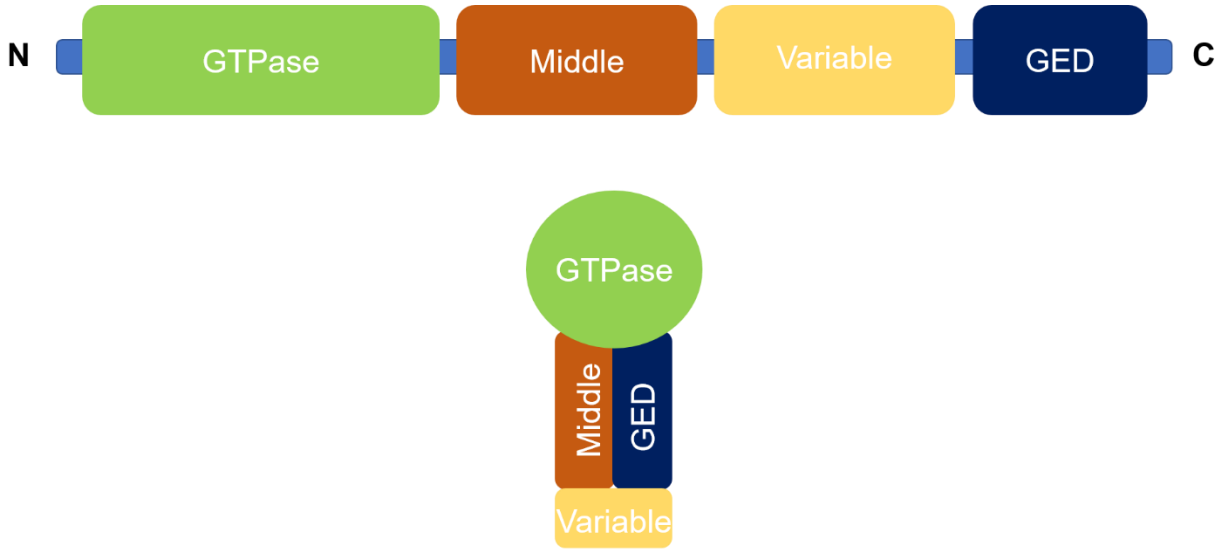
N
GTPase
Middle
Variable
GED
C
GTPase
Middle
GED
Variable

Figure 1.5. Representation of Drp1 structure.

Drp1 is composed of a GTPase domain at its N-terminus, followed by a middle domain (MID) and a variable domain (VD) and GTPase effector domain (GED) at the C-terminus. The MID forms part of the stalk along with the GED while VD functions as an auto-inhibitory domain that regulates Drp1 oligomerization and activity. The MID specifically contains a short α-helical stretch containing the Arg-376 residue ,which is responsible for the interaction between Drp1 and mitochondrial fission factor (Mff).

shown to recruit Drp1 to the mitochondria in yeast but such a role has not been identified for the mammalian ortholog hFis1 (Lee et al., 2004). Currently there is a debate about the necessity of Fis1 for fission, as some studies have demonstrated that it is required whereas others have demonstrated that it is dispensable (Chan, 2012; Grandemange et al., 2009; Otera et al., 2010). A recent study has proposed that hFis1 promotes fission through sequestration of MiD51 (Zhao et al., 2011). Mff is currently accepted as the primary mammalian receptor for Drp1 on the OMM, evidenced by the loss of Drp1 at the mitochondria in the absence of Mff (Otera et al., 2010). The MiD proteins have been found to bind Drp1 but their role in promoting fission remains controversial, as MiD51 has been demonstrated to inhibit Drp1 GTPase activity and thus fission (Chan, 2012; Zhao et al., 2011).

Before Drp1 is recruited to the mitochondria, ER tubules wrap around the mitochondria in order to constrict the OMM and form pre-fission sites prior to the arrival of Drp1 (Figure 1.6). ER-associated mitochondrial division (ERMD) is thought to reduce the 1 μm mitochondrial tubule diameter down to a size where the 100 nm Drp1 oligomers can spiral around the mitochondria (Friedman et al., 2011; Ingerman et al., 2005; Kageyama et al., 2011). Meanwhile, cytoplasmic Drp1 forms dimers and tetramers and is subsequently recruited to ER-OMM contact sites and associates with Mff at the OMM (Figure 1.6). (Macdonald et al., 2014; Otera et al., 2010). Recent studies suggest that ER mediated calcium transfer into the mitochondria assists in Drp1 recruitment (Ortiz-Sandoval et al., 2014). Once at the OMM, Drp1 oligomerizes to form ring-like structures around the mitochondria (Figure 1.6) (Soubannier and McBride, 2009) but only a subset of these structures yields a productive fission event (Chan, 2012; Friedman and Nunnari, 2014). The Drp1 oligomers subsequently hydrolyze GTP, which results in constriction and splitting apart of the Drp1 ring structures. The consequence of this Drp1 GTP hydrolysis and constriction is a transient super-constriction state of the mitochondria. (Figure 1.6) (Benard and Karbowski, 2009; Lee et al., 2016). The super-constricted mitochondria allow for Dyn2 assembly downstream

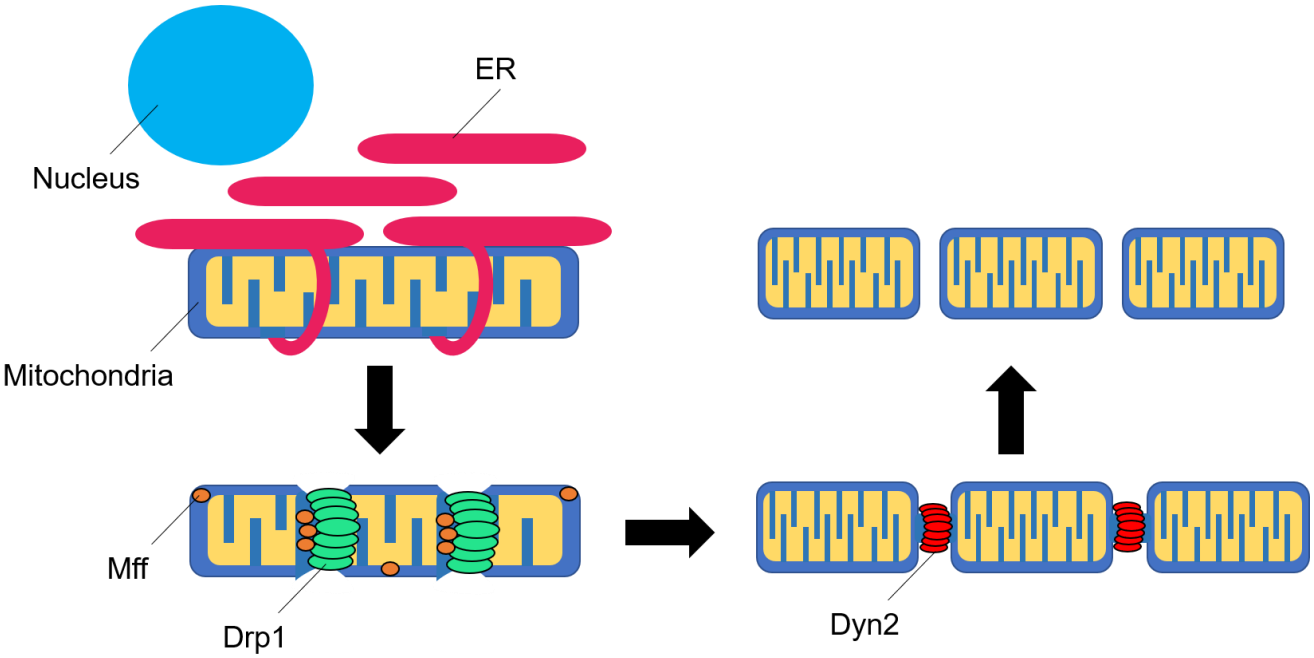
ER
Nucleus
Mitochondria
Mff
Drp1
Dyn2

Figure 1.6. Schematic Representation of Mitochondrial Fission.

Mitochondrial fission is initiated when endoplasmic reticulum (ER) tubules wrap around the mitochondria at sites of pending mitochondrial fission. The ER will constrict the mitochondria to a diameter that will allow Drp1 to form oligomers around the mitochondria. Drp1 is recruited to the mitochondria and binds to mitochondrial fission factor (Mff). At this point, Drp1 will hydrolyze GTP in order to constrict the mitochondria down to an even smaller diameter. At this point, Dynamin2 (Dyn2) is able to oligomerize around the mitochondria and complete the scission of the mitochondria, resulting in mitochondrial fragmentation.

of Drp1 (Figure 1.6). Dyn2 has recently been shown to mediate the final mitochondrial constriction that induces membrane fission and ultimately leads to mitochondrial division (Figure 1.6) (Lee et al., 2016).

In laboratory and clinical settings, Drp1 has been proven to be essential for proper organismal development. In a whole-animal mouse model of Drp1 loss, Wakabayashi et al. demonstrated that improper placental development *in utero* led to embryonic lethality by embryonic day E11.5. Furthermore, the group showed that brain-specific Drp1 loss resulted in faulty neuronal development, demonstrating the physiological importance of Drp1 at the whole-animal level as well as its contribution to tissue-specific development (Wakabayashi et al., 2009). In the clinical setting, a germ-line, dominant negative Drp1 mutation was identified in an infant who suddenly died 37 days after birth. The patient presented with numerous neurologic and metabolic defects and poor overall health, recapitulating some of the characteristics of tissue-specific Drp1 loss in mice (Waterham et al., 2007).

1.4.1.2 Post-translational modifications of Drp1

Inherent in the role of Drp1 as a regulator of mitochondrial fission are the number of post-translational modifications that mediate its activity (Cerveny et al., 2007; Chang and Blackstone, 2010; Grandemange et al., 2009). Drp1 can undergo phosphorylation, ubiquitination, as well as SUMOylation. Each modification has been shown to have differing impacts on Drp1 function. Drp1 has been identified to be phosphorylated at Ser637 by cyclic-AMP dependent protein kinase (PKA), which inhibits its GTPase activity and thus fission activity. The phosphatase calcineurin is able to dephosphorylate Drp1 at S637 to reactivate Drp1 and induce mitochondrial fission (Chang and Blackstone, 2007). Phosphorylation of Drp1 at Ser616 by Cdk1/Cyclin B has been demonstrated to drive fission but has no impact on Drp1 GTPase activity, thus the mechanism of this phosphorylation in promoting fission has yet to be determined (Taguchi et al., 2007). More recently, we have demonstrated that MAPK activated Erk2 can directly phosphorylate Drp1 on

S616 to promote mitochondrial fission (Chapter 2) (Kashatus et al., 2015). Ubiquitination of Drp1 is mediated by membrane associated RING CH V (MARCHV), an E3 ubiquitin ligase, which is anchored to the OMM and capable of binding Drp1. Overexpression of inactive MARCHV mutants leads to abnormal accumulation of Drp1 on the OMM associated with distinct differences in mitochondrial morphology, suggesting that MARCHV plays a role in regulating trafficking and/or assembly of Drp1 fission complexes (Karbowski et al., 2007). Finally, the small ubiquitin like modifier1 SUMO1 and its conjugating enzyme Ubc9 are binding partners of Drp1. SUMOylation appears to stabilize Drp1 at the mitochondria and thus drives fission, as loss of SUMO1 results in mitochondrial elongation (Harder et al., 2004).

1.4.2 Mitochondrial Fusion

Mitochondrial fusion occurs in two stages; the first in outer membrane fusion followed by inner membrane fusion. The physiological role of mitochondrial fusion at the cellular level remains incompletely understood. Recent theories postulate that one function of mitochondrial fusion is to maintain mitochondrial health through content mixing of adjoining mitochondria to complement damaged mitochondrial DNA or electron transport chain subunits with functional ones, as well as to dilute any detrimental molecules generated by normal respiration (Schrepfer and Scorrano, 2016). Another theory for the functional relevance of mitochondrial fusion in the cell is to evade autophagic degradation as the fused mitochondria are physically too large to be engulfed by the autophagosome. The spared, elongated mitochondria are thus able to undergo more efficient oxidative metabolism due to the extended mitochondrial network (Gomes et al., 2011). Furthermore, studies have shown that more elongated mitochondria also allow for more efficient transport of metabolic substrates throughout the mitochondrial network (Rambold, 2011).

Similar to mitochondrial fission, proper regulation of mitochondrial fusion has important implications for organismal health and development. Mfn1 as well as Mfn2 knockout mice exhibit embryonic lethality through differing mechanisms; Mfn2 null embryos suffer from dysfunctional

placenta development while the cause of embryonic lethality in Mfn1 null mice remains under investigation. Mutations in Mfn2 have been characterized in patients with Charcot-Marie-Tooth Disease Type 2A (CMT2A), an axonal sensimotor neuropathy that affects the lower extremities (Züchner et al., 2004). Additionally, Mfn2 deficiency has been found to be associated with pulmonary arterial hypertension in humans (Ryan et al., 2013). Inner membrane components also play a role in development and human disease. Homozygous mutation of Opa1 in mice is embryonic lethal by embryonic day 13.5, however the cause remains poorly understood (Davies et al., 2007). Dominant optic atrophy, a condition characterized by bilateral degeneration of the optic nerves which results in visual loss, is most commonly caused by mutations in the OPA1 gene (Archer, 2013).

1.4.2.1 Outer Membrane Fusion

The mitochondrial double membrane consists of the outer mitochondrial membrane (OMM) and the inner mitochondrial membrane (IMM) separated by the intermembrane space (IMS). The fusion of the OMM is mediated by Mfn1 and Mfn2 (Archer, 2013). Between Mfn1 and 2, Mfn1 has higher GTPase activity and seems to play a greater role in mediating fusion of the adjacent OMMs whereas Mfn2 seems to be more important for regulating ER-mitochondria contact sites as well as calcium imported from the ER, two processes that are important for division (Chan, 2012; Scorrano, 2013). The Mfns are anchored to the OMM by a bipartite transmembrane domain in a manner whereby both the N-terminal GTPase and the coiled-coil C-terminal domains face the cytosol (Santel, 2001). Hydrolysis of GTP through activation of Mfn GTPase activity results in conformational changes that allow Mfn1 and Mfn2 to form homo- and hetero-oligomeric complexes on OMM surfaces of adjacent mitochondria (Figure 1.7) (Chen et al., 2003b). In order for fusion to occur, the adjacent mitochondria are first brought into close proximity via cytoskeletal elements (Meeusen and Nunnari, 2005). Once they are close enough, the coiled-coil C-terminal domains of the Mfn1 and Mfn2 complexes undergo “tethering”, bringing

the membranes in even closer proximity resulting in “docking”. The molecular mechanism of the final fusion event remains unknown but it is speculated to take place in a manner similar to that of SNARE mediated membrane fusion (Koshiba et al., 2004).

1.4.2.2 Inner Membrane Fusion

In regards to the inner membrane, the fusion is primarily regulated by Opa1 (Cerveny et al., 2007; Meeusen et al., 2006; Meeusen and Nunnari, 2005). However there have been studies that demonstrate the requirement of Mfn1 in Opa1-mediated membrane fusion (Cipolat et al., 2004). In humans, eight different Opa1 isoforms have been identified due to splice variations of Opa1 mRNA (Delettre, 2000). Opa1 variants are imported into the mitochondrial matrix where constitutive cleavage of its bipartite-type mitochondrial targeting sequence (MTS) by the mitochondrial processing peptidase (MPP) converts them to the long isoform (l-Opa1) (Griparic et al., 2007; Ishihara, 2006). The inner-membrane ATPase associated with diverse cellular activities (i-AAA) protease Yme1L as well as the matrix-AAA (m-AAA) protease are involved in generating and maintaining l-Opa1, respectively (Ishihara, 2006; Song et al., 2007). After cleavage, l-Opa1 isoforms anchor to the IMM facing the IMS through an N-terminal transmembrane region where it can be further cleaved into a short isoform (s-Opa1), which is soluble and remains in the IMS (Cerveny et al., 2007; Ishihara, 2006; Olichon, 2002). l-Opa1 and s-Opa1 are maintained at approximately equal amounts in mitochondria and combinations of each isoform are required for IMM fusion (Figure 1.7) (Cerveny et al., 2007; Ehses et al., 2009; Song et al., 2007). The molecular mechanism of IMM fusion has yet to be identified but it is thought that direct interactions between long and short Opa1 assemblies bring adjacent IMMs in close enough proximity for tethering and that actual fusion may take place via a SNARE-like membrane fusion event (Meeusen et al., 2006). Furthermore, numerous studies have demonstrated that the electrochemical potential ($\Delta\psi_m$) across the IMM is required for Opa1 processing and fusion, as disruption or dissipation of the $\Delta\psi_m$ results in the conversion of all l-Opa1 isoforms to s-Opa1

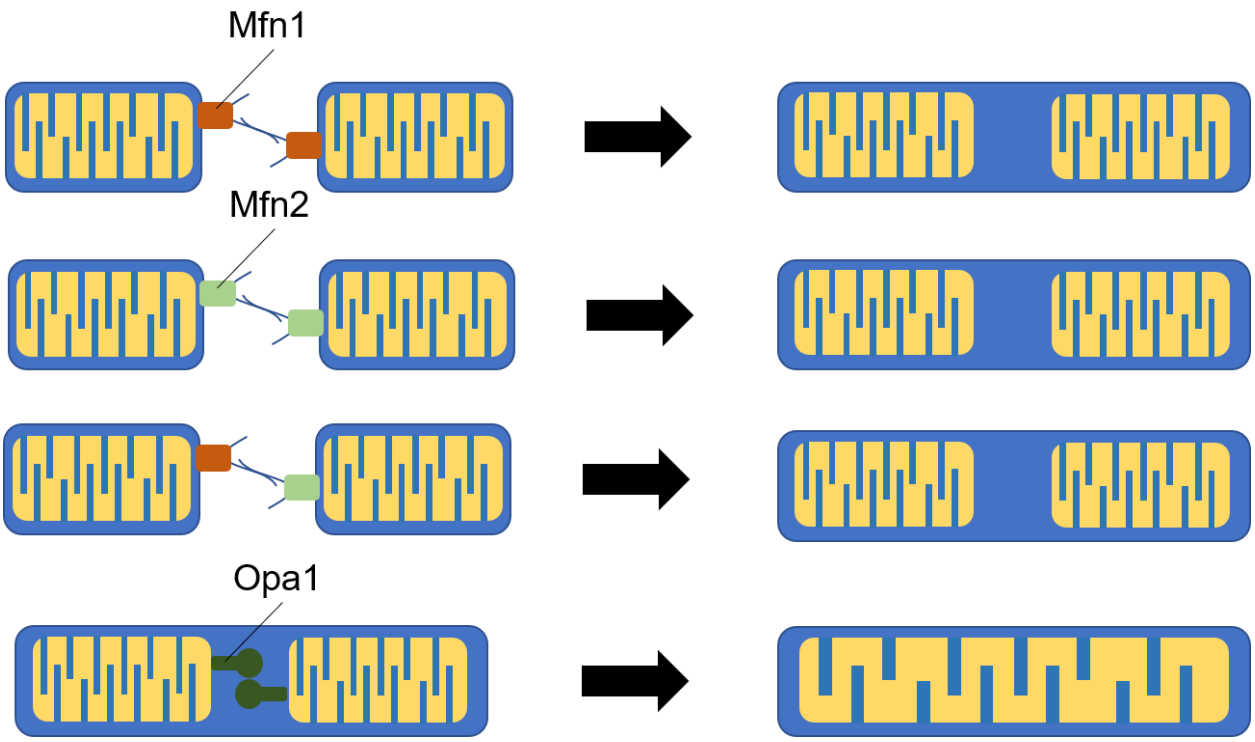
Mfn1
Mfn2
Opa1

Figure 1.7. Schematic Representation of Mitochondrial Fusion.

Mitochondrial fusion occurs in two steps: outer membrane fusion and inner membrane fusion. Outer membrane fusion is mediated by the large GTPases Mfn1 and Mfn2. Mfn1 and Mfn2 can form homo and heterodimers to bring mitochondrial outer membranes in close enough proximity that they eventually undergo fusion. Once the outer membrane is fused, the inner membrane can undergo fusion. Inner membrane fusion is mediated by the large GTPase OPA1. OPA1 forms homodimeric complexes and mediates inner membrane fusion in a manner similar to Mfn1/2.

isoforms by the metallopeptidase OMA1, which ultimately leads to inhibition of fusion (Duvezin-Caubet et al., 2006; Ishihara, 2006; Meeusen et al., 2004).

The sections above emphasize the importance of mitochondrial dynamics in proper development and organismal health. As cancer is believed to be a disease in which developmental growth pathways have gone awry, the contribution of mitochondrial dynamics to these processes has emerged as a promising new avenue in terms of understanding tumor biology. The following section aims to review the connections between Ras signaling and the regulation of mitochondrial dynamics in cancer.

1.5 Ras and Mitochondria in Cancer

While the role of Ras signaling pathways in promoting cancer is well established, Ras-mediated regulation of mitochondrial dynamics is emerging as an important contributor to tumorigenesis. However, studies have shown that the effect of mitochondrial dynamics on tumor growth may depend on tissue/cell type as well the type of stress acting on the cell. In general, the arguments in favor of fission and fragmented mitochondria for driving tumorigenesis are that fragmentation impairs efficient oxidative phosphorylation by disrupting cristae formation and respiratory complexes and thus may drive the cell to respire through glycolysis in what is known as the “Warburg Effect” (Boland et al., 2013; Warburg, 1956). Furthermore, under hypoxic conditions, HIF-1alpha can drive mitochondrial fragmentation and perinuclear clustering of the mitochondria, which may function to facilitate tumor-promoting ROS signaling (Al-Mehdi et al., 2012). Studies have shown that mitochondrial fusion may also contribute to tumorigenesis. Under conditions of nutrient deprivation, mitochondrial fusion and mitophagy coordinate to join functional mitochondrial while depleting cells of depolarized mitochondria, effectively maximizing oxidative phosphorylation efficiency, which serves to promote cell growth (Guo et al., 2011). Additionally, mitochondrial elongation induced by GSK-3β phosphorylation of Drp1 protects cells from undergoing apoptosis (Chou. C.H.; Lin, 2012).

Ras has been shown to initiate and drive many cellular reprogramming events that position tumor cells to thrive, including increased growth and proliferation as well as rewiring metabolism (Nagdas and Kashatus, 2017). Numerous studies have demonstrated that mitochondria change shape in order to accommodate different cellular demands and energetic states (Obre and Rossignol, 2015; Rossignol et al., 2004). Due to the overlap between processes regulated by Ras and mitochondria, several links have been found implicating Ras upstream of changes in mitochondria morphology, with functional consequences for the cell. This section will provide a brief review of the most recent studies that describe ways in which Ras signaling pathways shift the balance of mitochondrial fusion and fission in different tumor settings.

1.5.1 MAPK signaling to mitochondria

An association between the MAPK pathway and mitochondrial fission was reported by Yu et al. demonstrating that Erk1 can phosphorylate Drp1 *in vitro* to promote mitochondrial fission and that inhibition of the MAPK pathway can decrease mitochondrial fragmentation (Yu, 2011). A later study by Gan et al. verified these initial findings in cybrid neurons containing platelet mitochondria from Alzheimer's disease patients (Gan et al., 2014). The connection between MAPK-mediated mitochondrial fragmentation and tumor growth was recently characterized by work that will be described in further detail in the following chapter. Briefly, it was found that Erk2 can phosphorylate Drp1 at S616 to promote mitochondrial fission *in vitro* as well as in human embryonic kidney cells (HEK) expressing mutant $HRas^{G12V}$ and in PDAC cell lines. Interestingly, mutation of Drp1 at the fission-promoting S616 residue to an alanine compromised growth in a xenograft model, suggesting that Drp1 and by extension mitochondrial fission are required for tumor growth (Kashatus et al., 2015). These findings were further corroborated in an accompanying study that used melanoma cell lines harboring $B\text{-}Raf^{V600E}$ (Serasinghe et al., 2015). Serasinghe et al. also demonstrated that MAPK signaling can increase Drp1 mRNA levels

suggesting that the MAPK pathway can not only directly regulate mitochondria at the morphological level, but also indirectly by mediating transcription of the mitochondrial machinery.

Ras signaling has been further implicated in driving mitochondrial fragmentation by inversely inhibiting mitochondrial fusion, suggesting that mitochondrial fusion may impede tumor growth. In work that will be further described in chapter 3 of this dissertation, it was demonstrated through high-throughput mitochondrial imaging that the presence of mutant $HRas^{G12V}$ in immortalized HEK cells moderately inhibited mitochondrial fusion (Nascimento et al., 2016). Studies by Pyakurel et al. substantiated this finding as they showed that Erk can inhibit Mfn1 fusion activity via phosphorylation at T562 in mouse embryonic fibroblasts (MEFs) (Pyakurel et al., 2015b). An inverse relationship has also been reported between Ras and mitochondrial fusion machinery. Chen et al. showed that the mitochondrial fusion machinery can directly inhibit Ras activity. Mfn2, in B cell lymphoma cell lines and in rat vascular smooth muscle cells, has shown the ability to bind Ras resulting in antiproliferative effects (Chen et al., 2014; Chen et al., 2004).

Recently, work by Prieto et al. provided some further insight into the functional consequences of mitochondrial fragmentation in developing cells that can be co-opted for tumor growth through MAPK signaling. In their study, Prieto et al. recapitulated previous work demonstrating that Erk can activate Drp1 to promote mitochondrial fission (Kashatus et al., 2015). They went on to convey that mitochondrial fragmentation downstream of MAPK activation is a necessary early step in the transition of somatic cells to induced pluripotent stem (iPS) cells and that knockdown of Drp1 inhibits this process (Prieto et al., 2016). These findings have interesting implications in cancer, as a shift in normal cells to pluripotency has been well documented (Visvader and Lindeman, 2012).

1.5.2 PI3K signaling to mitochondria

Studies involving the PI3K/Akt/mTOR pathway suggest that Akt signaling promotes mitochondrial fission in tumors. For example, in melanoma cells that harbor increased PI3K-Akt signaling, Brown et al. demonstrated that expression of PTEN, an inhibitor of PI3K-Akt signaling, promotes canonical Wnt/β-catenin-mediated mitochondrial fusion, thus altering the bioenergetic potential of these cells. These findings suggest PI3K signaling contributes to the fragmented mitochondrial phenotype of melanoma cells (Brown et al., 2017). Moreover, a study by Caino et al. found that prostate cancer cell lines with mutations that render PI3K constitutively active displayed a fragmented mitochondrial morphology and pharmacological inhibition of PI3K results in mitochondrial elongation (Caino et al., 2015).

Intriguingly, the mitochondrial fusion machinery has also been shown to inhibit the PI3K/Akt/mTOR pathway, effectively inactivating proliferative signaling. For example, in breast cancer cells, loss of Mfn2 results in increased cell viability, colony formation, transwell invasion as well as increased xenograft growth (Xu et al., 2017). Consistent with the previously mentioned study, Guo et al. demonstrated that in rat vascular smooth cells, Mfn2 inhibited Akt activation. They further showed that it is not the fusion activity of Mfn2 that promotes apoptosis in smooth muscle cells, but instead Mfn2's inhibitory effects on Akt activation (Guo et al., 2007)

1.5.3 RalGEF signaling to mitochondria

The least well-characterized of the three pathways downstream of Ras that have been implicated in cancer, the RalGEF pathway has also shown the capacity to regulate mitochondrial morphology. The primary study that connects RalGEF signaling to mitochondria establishes a link during mitosis, when equal distribution of mitochondria to daughter cells is necessary for proper cell division. Kashatus et al. showed that Aurora A phosphorylates RalA causing it to localize to the mitochondria and recruit RalBP1. RalBP1 is thought to act as a scaffold for Drp1 and one of

its kinases, Cdk1, allowing Cdk1 to phosphorylate Drp1 at S616 and drive mitochondrial fission during mitosis (Kashatus et al., 2011). Consistent with a role for the RalGEF pathway in mediating mitochondrial dynamics in cancer, Ral activity has been shown to be upregulated in a variety of cancers including pancreatic, bladder and colon cancer. Furthermore, these studies demonstrate the necessity of RalA for tumorigenic potential in various cancer cell lines. (Lim et al., 2006; Martin et al., 2011; Smith et al., 2007).

1.5.4 Proliferation

At a fundamental level, the physiological functions of dynamic mitochondria promote progression through the various stages of the cell cycle and perturbations in the balance of mitochondrial fusion and fission have tumor-promoting consequences (Kashatus, 2017). In preparation for entry into the cell cycle, cells at the G1/S stage require an increased energy supply for nucleotide biosynthesis. They meet this energetic demand by upregulating mitochondrial fusion, resulting in increased ATP production (Mitra et al., 2009). The mitochondrial fusion at this stage also promotes content mixing between mitochondria, which minimizes the inheritance of damaged mitochondrial components by complementing them with healthy ones (Paola et al., 2017). Further, mitochondrial elongation at this stage promotes the build-up of cyclin E and allows for entry into S phase (Mitra et al., 2009). Mitochondria undergo increasing fragmentation as they progress through the cell cycle, culminating in a hyper fragmented state at mitosis to permit the proper allocation of mitochondria between dividing cells (Nagdas and Kashatus, 2017).

At mitosis, mitochondrial fission is coordinated downstream of Ras activation by RalA-mediated relocalization of RalBP1 to the OMM. Here, RalBP1 acts as a scaffold between Drp1 and one of its kinases cyclin B/Cdk1. Cdk1 phosphorylates Drp1 at S616 to drive mitochondrial fission, allowing mitochondria to be equally distributed between daughter cells to progress through mitosis (Kashatus et al., 2011). Drp1 is subsequently degraded by APC/C-Cdh1 ubiquitin ligase, which permits mitochondrial elongation after mitosis, amid the reset of the cell cycle at G1 (Horn

et al., 2011). Disruptions in the balance between fission and fusion have detrimental effects on cell cycle progression. Mitra et al. found that prolonged inhibition of Drp1, which results in fused mitochondria, results in dysfunctional chromosomal alignment (Mitra et al., 2009). Additionally, Qian et al. observed that inhibition of Drp1 in breast cancer cells results in hyperfused mitochondria and that the cell proliferation defects in Drp1 knockdown cells are caused by cell cycle delay at the G2/M transition (Qian et al., 2012). The hyperfused mitochondria in Drp1 knockdown cells resulted in overamplification of centrosomes and chromosomal instability which led to aneuploidy and replication stress. Conversely, Chen et al. demonstrated that perpetual mitochondria fragmentation in MEFs by double knockout of Mfn1 and Mfn2 or Opa1 knockout resulted in defects in mitochondrial membrane potential and respiration. These studies reinforce the concept that mitochondrial fusion promotes organelle health and energy production while mitochondrial fission is necessary for proper chromosomal segregation during mitosis. It is tempting to speculate that the fragmented mitochondrial phenotype, which is promoted by oncogenic Ras and found in many Ras-driven cancers, serves to prevent the levels of aneuploidy and chromosomal instability from reaching a point of critical failure for the cell, allowing the cancerous cell to continue to divide and select for mutations that provide a proliferative advantage.

1.5.5 Metabolism

One of the hallmarks of cancer is dysregulated metabolism. Mitochondria represent a significant hub for various metabolic processes, including ATP production through oxidative phosphorylation with inputs from glycolysis, amino acid metabolism as well as lipid metabolism (Vyas et al., 2016). A key metabolic characteristic of cancer cells is an increased reliance on glycolysis even in the presence of oxygen, a phenomenon known as the “Warburg Effect” (Warburg, 1956). Several studies over the last few decades have revealed that cancer cells rely on glycolysis to provide intermediates for the biosynthetic processes that lead to macromolecule synthesis, a requirement for rapidly growing cells (Kashatus, 2017). When the Warburg effect was

first described, it was postulated that oxidative metabolism was decreased due to dysfunctional mitochondria in tumor cells and this lead to the upregulation of glycolysis. In recent years, it has been well established that many tumors possess functional mitochondria and that oxidative mitochondrial respiration is critical for some tumor types (Vyas et al., 2016). This section will briefly review the main aspects of glycolysis as well as oxidative metabolism that coordinate with Ras-mediated regulation of mitochondria.

1.5.5.1 Glycolysis

Glycolytic metabolism has been well characterized in numerous cancer types with growing links to oncogenic Ras signaling (Kashatus, 2017; Vyas et al., 2016). For glycolysis to commence, glucose must first be transported into the cell via numerous glucose transporters (GLUT) and then it must be phosphorylated by hexokinases (HK) so that it can remain in the cell to be further processed through the glycolytic pathway (Figure 1.8) (Pedersen, 2007). A study by Ying et al. demonstrated the importance of KRas in maintaining glucose uptake and retention in PDAC via upregulation of GLUT1 as well as HK1 and HK2, but they also discovered that KRas drives glycolytic intermediates away from the TCA cycle and instead diverts them into the nonoxidative arm of the pentose phosphate pathway as well as into the hexosamine biosynthesis pathway (Ying et al., 2012). Several studies have demonstrated the importance of fragmented mitochondria for cancer cells, which suggests KRas-mediated mitochondrial fission may be contributing to the upregulation of glycolytic intermediates and enzymes downstream of KRas. The mechanisms by which this is happening remain to be elucidated, however, less efficient oxidative phosphorylation associated with fragmented mitochondria may play a role. One mechanism cancer cells may use to reduce oxidative metabolism involves downregulating oxidative phosphorylation proteins. Schell et al. showed that in numerous colon cancer cell lines with KRas mutations, there was downregulation as well as deletion of the mitochondrial pyruvate carrier gene *MPC1* and this is correlated with poor prognosis in patients. MPC1 is localized to the

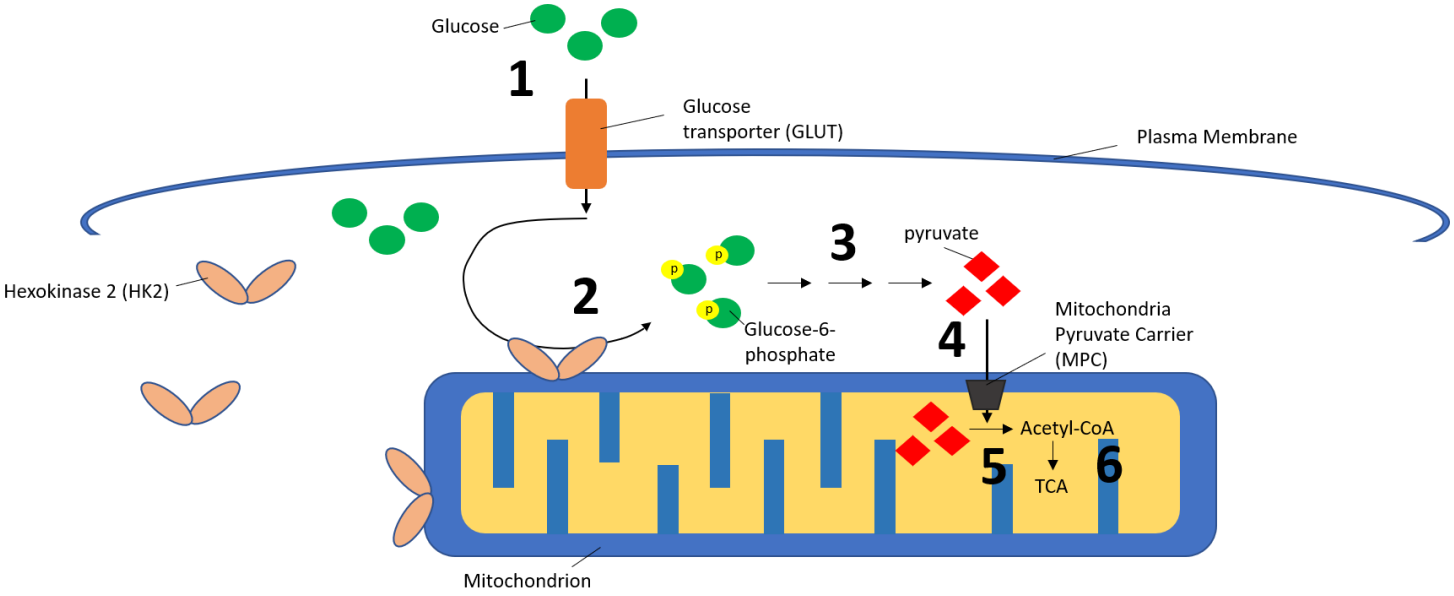
Glucose
1
Glucose
transporter (GLUT)
Plasma Membrane
Hexokinase 2 (HK2)
2
3
pyruvate
Glucose-6-
phosphate
4
Mitochondria
Pyruvate Carrier
(MPC)
Acetyl-CoA
5
TCA
6
Mitochondrion

Figure 1.8. Initiation of Glycolysis and transportation of pyruvate into mitochondria.

(1) Glucose enters the cell through glucose transporters (GLUT). (2) In order to remain inside the cell, glucose must be phosphorylated into glucose-6-phosphate. (3) Once glucose is phosphorylated, it can be further processed through glycolysis to generate pyruvate. (4) Pyruvate is then transferred into the mitochondrial matrix by the mitochondrial pyruvate carrier (MPC). (5) In the mitochondrial matrix, pyruvate is oxidized to form Acetyl-CoA. (6) Acetyl-CoA can be further processed through the TCA cycle to eventually generate ATP.

inner mitochondrial membrane and its primary function is to transport pyruvate into the mitochondrial matrix where it is oxidized to generate Acetyl-CoA (Figure 1.8). Acetyl-CoA is further processed through the TCA cycle to generate ATP during oxidative metabolism (Figure 1.8) (Bender and Martinou, 2016). Re-expression of MPC1 and MPC2 in MPC-low cancer cells causes a reduction in growth of 3D cultures as well as xenografts (Schell et al., 2014). The downregulation of MPC1 in KRas-driven cancers which exhibit fragmented mitochondria, suggests that mitochondrial fission prompts cancer cells to actively block pyruvate utilization through the TCA cycle in favor of biosynthetic processes that promote glycolysis (Bender and Martinou, 2016).

Another way in which tumors divert glycolytic intermediates from feeding into the TCA cycle is via preferential upregulation of pyruvate kinase (PKM). Cells contain two isoforms of PKM, PKM1 and PKM2, which converts phosphoenolpyruvate (PEP) into pyruvate (Bender and Martinou, 2016). In non-transformed cells with oxidative metabolism, cells preferentially utilize PKM1 which has higher activity than PKM2, thus converting more PEP into pyruvate which can then be transported to the mitochondria. However, cancer cells specifically upregulate PKM2, which has lower activity than PKM1, and thus reduces the amount of pyruvate produced after glycolysis. The reduced pyruvate conversion causes an accumulation of the upstream glycolytic intermediates allowing them to be shunted off in to anabolic pathways that support rapid proliferation (Christofk et al., 2008).

1.5.5.2 Oxidative Phosphorylation

The Warburg effect originally postulated that tumor cells upregulate anaerobic glycolytic metabolism to compensate for dysfunctional mitochondria that have a reduced capacity for oxidative phosphorylation (Warburg, 1956). A study by Hu et al. found that $KRas^{G12V}$ can promote this shift to glycolytic metabolism from oxidative phosphorylation. Their work suggests that in HEK 293 cells transduced with a tetracycline inducible $KRas^{G12V}$, KRas associates with the

mitochondria and causes suppression of complex I of the electron transport chain as well as disruption of mitochondrial membrane potential by interfering with the cyclosporin-sensitive permeability transition pore. These insults to mitochondrial components result in dysfunctional mitochondria with a decreased capacity for oxidative phosphorylation (Hu et al., 2011). However, there is a growing body of evidence that suggests that mitochondria in cancer cells with increased glycolysis are still functional and are responsible for a significant proportion of a cancer cell's energy supply (Paola et al., 2017). Furthermore, there is a growing appreciation for the heterogeneity of tumor cells in terms of their dependence on glycolysis or oxidative phosphorylation. Indeed, there are tumor cells in which there is increased glycolysis with a corresponding decrease in oxidative phosphorylation capacity, tumor cells that simply have increased glycolysis with negligible defects in oxidative metabolism as well as tumor cells that rely primarily on oxidative metabolism instead of glycolysis (Moreno-Sánchez et al., 2007). In terms of promoting oxidative phosphorylation, studies suggest that oncogenic Ras can induce oxidative metabolism in early transformed cells. Funes et al. found that mesenchymal stem cells transformed with mutant HRas exhibit increased oxidative phosphorylation without an increase in glycolysis for ATP production (Funes et al., 2007). Other groups have demonstrated similar increases in oxidative metabolism after initial transformation in MEFs with mutant HRas, however, over time the MEFs began to display increased glycolysis with a corresponding increase in tumor forming potential *in vitro* (de Groof et al., 2009). These studies suggest that during transformation, cells with mutant Ras require increased oxidative metabolism, perhaps to increase the production of ROS that are necessary as signaling molecules for tumor initiating processes (Weinberg et al., 2010).

1.6 Significance and Overview

The primary aim of this dissertation is to understand the role of Drp1 in regulating mitochondrial dynamics to promote cancer progression in the context of oncogenic Ras. Up to

one third of all cancers harbor mutations in the Ras gene and subsequent studies have demonstrated the necessity of Ras in transforming cells through an extensive network of signaling pathways (Cox and Der, 2010). The physiological consequences that arise as a result of these constitutively activated signaling pathways involve some of the hallmarks of cancer defined by Hanahan and Weinberg, including increased proliferation, reprogrammed metabolism and resistance to death pathways (Hanahan and Weinberg, 2011). Interestingly, several studies have demonstrated that dysregulation of mitochondrial dynamics can also lead to the physiological changes seen under Ras activation, which lead us to question whether there is a link between Ras signaling and mitochondrial dynamics in cancer. Previously, twp groups demonstrated that activated Ras could indeed lead to activation of Drp1 and subsequent mitochondrial fragmentation in disease models such as hyperglycemia and Alzheimer's disease (Gan et al., 2014; Yu et al., 2006). However, the importance of the MAPK-Drp1 signaling pathway for cancer progression had yet to be elucidated. In chapter 2, we demonstrate that oncogenic Ras can signal through Erk2 to phosphorylate Drp1 at S616, its activating residue, to promote mitochondrial fission. This fission activity is required for Ras-driven tumor growth in xenograft models and we show that the signaling pathway as well as corresponding mitochondrial morphology is intact in a panel of pancreatic cancer cell lines. These studies suggest that Ras-mediated Drp1 activation of mitochondrial fission promotes cancer progression.

Similar to fission, the fusion machinery can also be regulated in several ways that have physiological consequences for the cell (Li et al., 2014; Zhao et al., 2013a). Furthermore, shifts in mitochondrial morphology are often brought about by coordinated reciprocal regulation of the fission and fusion machinery (Chen et al., 2003a; Zhao et al., 2011; Zhao et al., 2013a). Interestingly, Ras has previously been reported to carry out coordinated reciprocal regulation of other cellular processes (Dajee et al., 2002). Thus, in chapter 3, we sought to determine if Ras

could coordinately downregulate mitochondrial fusion while upregulating fission to more fully understand the scope of Ras mediated regulation of mitochondrial morphology.

Finally, we set out to determine the role of Drp1 in promoting KRas driven pancreatic cancer *in vivo*. In chapter 2, we explored the contribution of Drp1 to tumor growth in xenograft models using HEK cells transduced with HRas as well as with pancreatic cancer cell lines with KRas mutations. However, it had not been previously reported if Drp1 can promote pancreatic cancer in a mouse model. Therefore, in chapter 4, we investigated the physiological changes that occur after Drp1 loss in an *in vitro* system and used these data to inform us on the physiological changes that take place after loss of Drp1 *in vivo*. The data presented in this chapter suggest that Drp1 can promote metabolic rewiring to support tumor growth and that loss of Drp1 causes mitochondrial dysfunction. In order to ameliorate the defects associated with decreased mitochondrial function, tumor cells from this model may increase breakdown of fatty acids to possibly maintain cellular energy.

The findings presented in this dissertation provide a new understanding of how mutant Ras regulates mitochondrial dynamics to promote tumor growth. However, there remain important gaps in our knowledge. In chapter 5, these gaps will be explored along with future experiments to elucidate the contribution of mitochondrial dynamics to changes in other physiological processes that can promote tumor growth. The discussion will also include an analysis of the potential of Drp1 as a therapeutic target in pancreatic cancer.

Chapter 2: Erk2 phosphorylation of Drp1 promotes mitochondrial fission and MAPK-driven tumor growth

**This chapter is adapted from Kashatus, Nascimento et al., Molecular Cell 2015*

2.1 Introduction

Mutations in *RAS* render the encoded small GTPase constitutively GTP-bound and active (Bos, 1989; Downward, 2003; Shields et al., 2000). In this state Ras stimulates downstream effectors that increase proliferation, block differentiation, reprogram metabolism and suppress apoptosis to drive oncogenesis (Shields et al., 2000). Despite this, direct pharmacological inhibition of Ras has been unsuccessful (Downward, 2003), so much attention has been focused on targeting critical Ras effector pathways, including the Raf, PI3K, and RalGEF pathways (Shields et al., 2000). Pharmacological inhibitors targeting the MAPK (Sebolt-Leopold and Herrera, 2004) and PI3K (Luo et al., 2003) pathways have been developed and shown to have anti-tumor activity, and there are numerous clinical trials testing such inhibitors for the treatment of a broad spectrum of cancers (Liu et al., 2009; Montagut and Settleman, 2009).

Several of the biological processes affected by Ras signaling, including apoptosis, proliferation, metabolic reprogramming and autophagy, are tightly linked to mitochondrial function and each of these processes can be affected by alterations in the balance of mitochondrial fusion and fission, suggesting that changes in mitochondrial morphology may underlie many of the phenotypes that drive tumorigenic growth (Liesa and Shirihai, 2013; Mitra, 2013; Youle and Karbowski, 2005). In support of this, mitochondrial fragmentation has been observed in tumor cells (Arismendi-Morillo, 2009; Inoue-Yamauchi and Oda, 2012; Rehman et al., 2012) and inhibition of mitochondrial fission decreases proliferation and increases apoptosis in models of lung cancer (Rehman et al., 2012) and colon cancer (Inoue-Yamauchi and Oda, 2012). Furthermore, the protein Survivin promotes increased glycolysis and tumorigenesis through

increased mitochondrial fission (Hagenbuchner et al., 2013), mitochondrial fission is increased in invasive breast cancers and associated with increased metastatic potential (Zhao et al., 2013a) and the mitochondrial fusion mediator Mfn2 is downregulated in gastric cancer (Zhang et al., 2013b), and its knockdown promotes proliferation in B-cell lymphoma cells (Chen et al., 2014; Zhang et al., 2013b). These studies support a link between mitochondrial fragmentation and tumor growth, but the mechanisms through which tumor cells promote this phenotype are not known and the physiological advantages gained from fragmentation have not been explored in detail.

Our previous work showed that the RalGEF-Ral pathway, an effector pathway downstream of oncogenic Ras, promotes mitochondrial fission during mitosis through mitochondrial recruitment and phosphorylation of the fission-mediating GTPase Drp1, suggesting a potential link between Ras and mitochondrial fission (Kashatus et al., 2011). As such, we hypothesized that altering the balance of mitochondrial fusion and fission might be a mechanism through which Ras promotes a number of the phenotypes associated with tumor progression and represent an attractive therapeutic target.

In support of this hypothesis, we find that expression of oncogenic Ras promotes a fragmented mitochondrial phenotype and that inhibition of this phenotype, through knockdown of Drp1, blocks tumor growth. Ras promotes this phenotype through activation of the MAPK pathway, as it is phenocopied through expression of activated cRaf and Mek1 and inhibited by treatment with the Mek inhibitor PD325901. Activation of the MAPK pathway promotes this phenotype, at least in part, through the direct phosphorylation of Serine 616 on Drp1 by Erk2 and levels of this phosphorylation are elevated in tissues and cells derived from pancreatic cancer patients. The importance of this phosphorylation is underscored by the fact that expression of wildtype, but not S616A, Drp1 reverses the mitochondrial elongation and loss of tumor growth observed upon knockdown of Drp1. These data suggest that induction of mitochondrial fission

through phosphorylation of Drp1 is a critical event in tumor growth driven by Ras or MAPK and that inhibitors targeting this process might have therapeutic potential for the treatment of tumors associated with the activation of these pathways.

2.2 Results

2.2.1 Expression of HRas^{G12V} promotes Drp1-dependent mitochondrial fragmentation

To determine whether activation of Ras affects mitochondrial dynamics, we expressed HRas^{G12V} in human embryonic kidney cells immortalized with SV-40 large and small T antigens and hTert (HEK-TtH) (Hahn et al., 1999) and analyzed the mitochondrial morphology by staining with MitoTracker Red (Figure 2.1A, 2.1B). Expression of HRas^{G12V} promoted a shift in mitochondrial morphology, with greater than 80% of cells exhibiting a fragmented morphology compared to less than 25% of control cells (Figure 2.1A, 2.1C).

Mitochondrial morphology is determined by a balance of the processes of fusion and fission, which are mediated by large GTPases of the dynamin family (Westermann, 2010). To determine the importance of mitochondrial fission for the shift towards a fragmented mitochondrial phenotype, we used shRNA to knock down expression of the fission-mediating GTPase Drp1 (Figure 2.1B). Expression of the Drp1 shRNA reversed the fragmented phenotype and caused the cells to exhibit an interconnected phenotype (Figure 2.1A, 2.1C). This change was not associated with major changes in mitochondrial function, as the basal oxygen consumption rate was unchanged following knockdown of Drp1 (Figure 2.S1A). Likewise, there was no decrease in membrane potential, as measured by TMRE loading (Figure 2.S1B). The only difference observed following knockdown of Drp1 was an increase in mitochondrial mass (Figure 2.S1C) along with an increase in spare respiratory capacity (Figure 2.S1A).

Figure 2.1

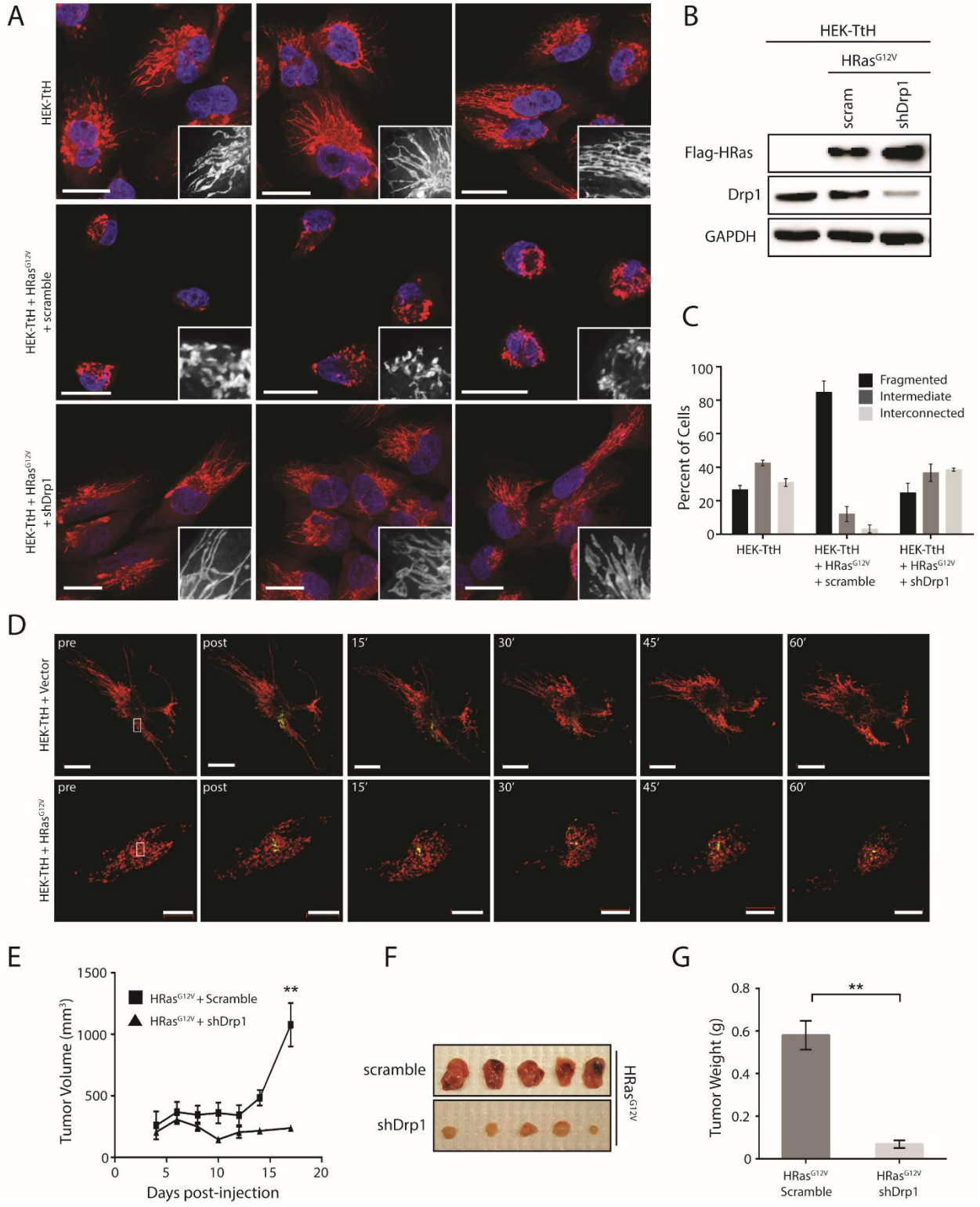
A
HEK-TtH
HEK-TtH + HRasG12V + scramble
HEK-TtH + HRasG12V + shDrp1
B
HEK-TtH
HRasG12V
scram
shDrp1
Flag-HRas
Drp1
GAPDH
C
Percent of Cells
Fragmented
Intermediate
Interconnected
HEK-TtH
HEK-TtH + HRasG12V + scramble
HEK-TtH + HRasG12V + shDrp1
D
HEK-TtH + Vector
HEK-TtH + HRasG12V
pre
post
15′
30′
45′
60′
E
Tumor Volume (mm3)
HRasG12V + Scramble
HRasG12V + shDrp1
Days post-injection
F
scramble
shDrp1
HRasG12V
G
Tumor Weight (g)
HRasG12V Scramble
HRasG12V shDrp1

Figure 2.1. Ras-induced mitochondrial fission is required for tumor growth. (Figure 2.1E-G contributed by Kashatus, JA).

(A) Mitochondrial morphologies of HEK-TtH cells or HEK-TtH cells stably expressing $HRas^{G12V}$ plus scramble or Drp1 shRNA. Red: MitoTracker Red; Blue: DAPI. Scale Bar = 20μm. (B) Immunoblot of Flag-$HRas^{G12V}$ and Drp1 in cells visualized in (A). GAPDH = Loading control. (C) Quantitation of mitochondrial morphologies observed in cells described in (A). n>50 cells, blindly scored by 3 people, 3 independent experiments; Error bar: S.E.M of mean percentages from 1 representative experiment. (D) HEK-TtH cells expressing vector or $HRas^{G12V}$ were transfected with mito-dsRed and mito-PA-GFP. mito-PA-GFP was activated by a 405-nm laser pulse in a 4μm region of interest (white box) then green fluorescence was tracked over a 1 hour time course. (E-G) HEK-TtH cell expressing $HRas^{G12V}$ and an shRNA targeting either scramble control or Drp1 were injected into mice and tumor volume (E) was measured over time. Tumors were removed at day 17 to be photographed (F) and weighed (G). n=5 tumors per cell line; error bars: S.E.M. of mean tumor volume (E) or tumor weight (G). ** Two-tailed student t-test, p=0.00749 (E) or p=0.00242 (G).

Figure 2.S1

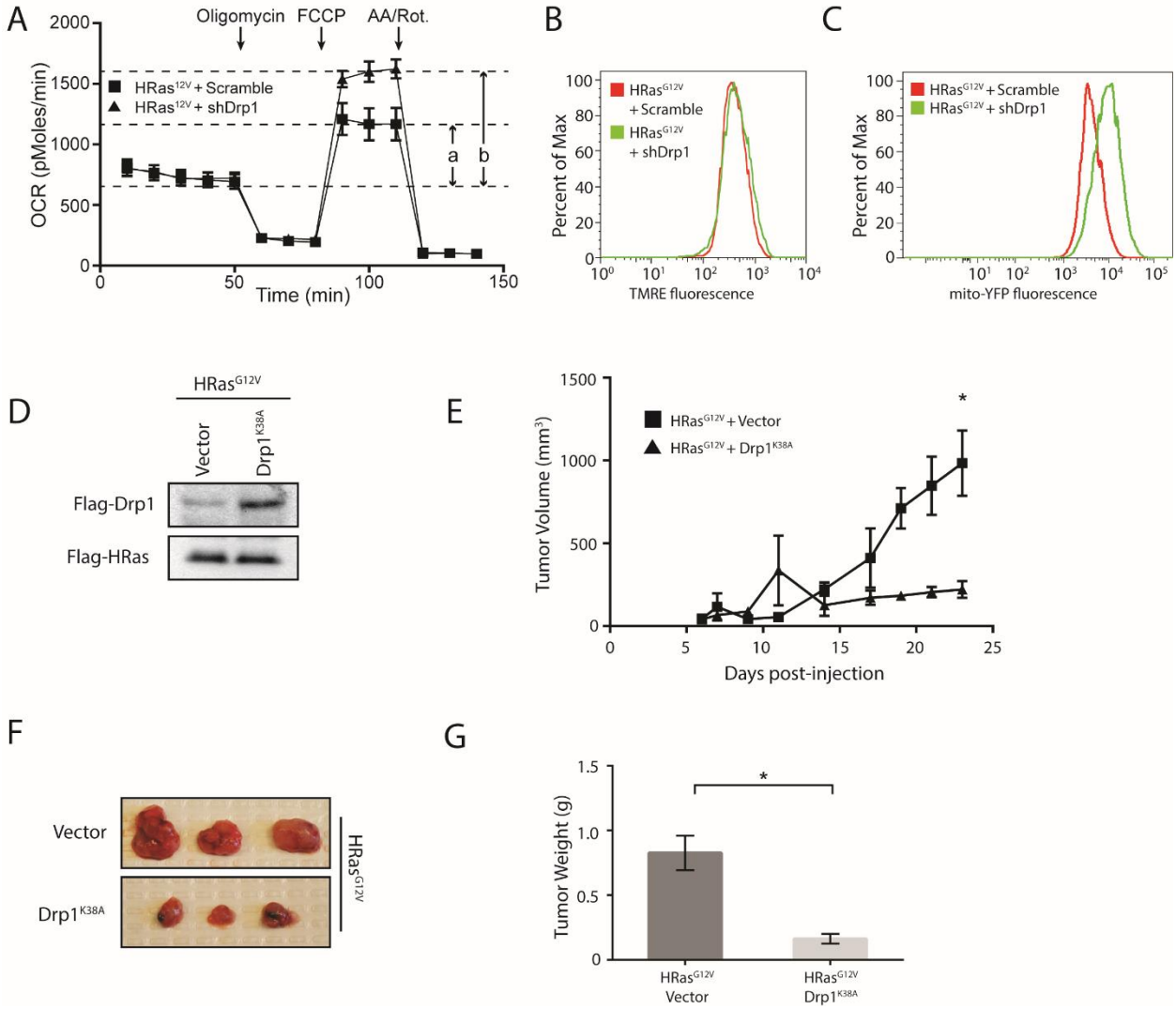
A
Oligomycin
FCCP
AA/Rot.
OCR (pMoles/min)
HRas12V + Scramble
HRas12V + shDrp1
a
b
Time (min)
B
HRasG12V + Scramble
HRasG12V + shDrp1
Percent of Max
TMRE fluorescence
C
HRasG12V + Scramble
HRasG12V + shDrp1
Percent of Max
mito-YFP fluorescence
D
HRasG12V
Vector
Drp1K38A
Flag-Drp1
Flag-HRas
E
HRasG12V + Vector
HRasG12V + Drp1K38A
Tumor Volume (mm3)
Days post-injection
F
Vector
Drp1K38A
HRasG12V
G
Tumor Weight (g)
HRasG12V Vector
HRasG12V Drp1K38A

Figure 2.S1. Inhibition of Drp1 in Ras-expressing HEK-TtH Cells. (Related to Figure 2.1). (Figure 2.S1A contributed by Byrne, FL, Figure 2.S1B-G contributed by Kashatus, JA).

(A) Oxygen consumption rate was measured using an XF24 extracellular flux analyzer in HEK-TtH cell expressing HRasG12V and an shRNA targeting either scramble control or Drp1. Oligomycin, FCCP, Rotenone and Antimycin A were added at the indicated timepoints (arrows). Spare respiratory capacity is measured as the difference between basal oxygen consumption rate and the FCCP uncoupled oxygen consumption rate (a,b). B. TMRE was added to HEK-TtH cell expressing HRasG12V and an shRNA targeting either scramble control or Drp1 and fluorescence was measured by flow cytometry. C. The levels of fluorescence in HEK-TtH cells expressing mito-YFP, HRasG12V, and an shRNA targeting either scramble control or Drp1 were analyzed by flow cytometry. D. HEK-TtH cells stably expressing HRasG12V and either empty vector or Drp1K38A were analyzed by immunoblot for expression of Flag-Drp1 and Flag-HRas. E. The cells were injected into SCID/Beige mice and tumor volume was measured over time. F-G. Tumors were removed at day 24 to be photographed and weighed. n=3 tumors per cell line; error bars: S.E.M. of mean tumor volume (E) or tumor weight (G). * Two-tailed t-test, p=0.0352 (E) or p=0.0280 (G).

To further analyze the effects of Ras expression on mitochondrial dynamics, we employed a mitochondria-targeted photoactivatable Green Fluorescent Protein (mt-PA-GFP) (Karbowski et al., 2004). Activation of mt-PA-GFP in vector control cells led to a rapid diffusion of the fluorescent signal throughout the entire mitochondrial network (Figure 2.1D). In the $HRas^{G12V}$-expressing cells, on the other hand, the GFP signal did not readily diffuse despite some observable fusion events. These data indicate that Ras-induced mitochondrial fragmentation requires Drp1, but that a concomitant decrease in fusion activity cannot be ruled out. Furthermore, the data are consistent with the previously observed association between oncogenic transformation and mitochondrial fragmentation, and suggest a potential mechanistic link between Ras activity and altered mitochondrial morphology.

2.2.2 Ras-driven tumor growth requires Drp1

HEK-TtH cells expressing $HRas^{G12V}$ are able to form tumors in immunocompromised mice (Hamad et al., 2002), making them a useful model to study Ras-mediated tumorigenesis. To test whether mitochondrial fragmentation is important for tumor growth, we injected the HEK-TtH cells expressing $HRas^{G12V}$ and either scramble or Drp1 shRNA subcutaneously (Figure 2.1E) and found that expression of Drp1 shRNA caused a significant reduction in tumor volume ($p=0.00749$) and tumor weight ($p=0.00242$) (Figure 2.1E-2.1G). These results were recapitulated by expression of the dominant-negative $Drp1^{K38A}$ (Pitts et al., 2004) (Figure 2.S1D-G), suggesting that the loss in tumor growth is not an off-target effect of the Drp1 shRNA. These data are consistent with a previous report that over-expression of the fusion GTPase Mfn2 or intratumoral injection of the Drp1 inhibitor Mdivi-1 can inhibit the tumorigenic growth of a lung adenocarcinoma cell line (Rehman et al., 2012) and suggest that Drp1 is a potential therapeutic target in tumors expressing oncogenic Ras.

2.2.3 Erk2 is a Drp1 kinase

We next sought to explore the mechanism through which Ras expression changes mitochondrial morphology. The observed fragmented phenotype is dependent on Drp1, consistent with an induction of fission activity. Mitochondrial fission is regulated through recruitment of Drp1 to mitochondrial membranes, its assembly into a ring structure and the constriction of that ring (Westermann, 2010). These processes are regulated by specific protein-protein interactions between Drp1 and mitochondrial membrane proteins, as well as post-translational modifications, including phosphorylation of S616, which promotes Drp1 activity (Taguchi et al., 2007), and S637 which inhibits its activity (Chang and Blackstone, 2007). We previously showed that the GTPase RalA and its effector RalBP1 drive mitochondrial fission during mitosis by promoting Cdk1-mediated phosphorylation of S616 and recruitment to the mitochondrial outer membrane (Kashatus et al., 2011). While this pathway is one potential mechanism through which activation of Ras promotes mitochondrial fragmentation, the persistence of the fragmentation throughout all phases of the cell cycle observed in $HRas^{G12V}$-expressing cells (Figure 2.1A) led us to speculate that Ras signals to the mitochondrial fission machinery through additional routes. Interestingly, our analyses of the sequences surrounding S616 revealed that it represents a perfect consensus sequence for phosphorylation by Erk2 (Carlson et al., 2011) and that this site is conserved throughout vertebrate evolution (Figure 2.2A). Furthermore, Erk activity has previously been shown to promote mitochondrial fission, and *in vitro* kinase assays using recombinant Erk1 have suggested that Erk1 may directly phosphorylate Drp1 (Gan et al., 2014; Yu, 2011). As the MAPK pathway is a key effector pathway downstream of activated Ras (Shields et al., 2000), phosphorylation of Drp1 by Erk2 would provide an additional potential mechanism for the Ras-induced mitochondrial fragmentation we observe. To test whether Erk2 phosphorylates Drp1, we incubated recombinant, constitutively active $Erk2^{R67S}$ (Levin-Salomon et al., 2008) and γ^{32}P-ATP with recombinant GST or GST fused to the C-terminal

219 amino acids of Drp1 ($Drp1^{518-736}$) in either the wildtype or S616A configuration. Erk2 phosphorylated wildtype Drp1, but not the S616A mutant or GST alone (Figure 2.2B). We repeated the experiment using non-radioactive ATP and an S616 phospho-specific antibody, finding that only the combination of activate Erk2 and wildtype Drp1 resulted in a detectable signal (Figure 2.2C). These experiments confirm that Erk2 is a kinase for S616 on Drp1 and provide a potential mechanism through which Ras promotes mitochondrial fission.

2.2.4 Drp1 S616 is phosphorylated following activation of the MAPK pathway.

To determine whether Erk2 phosphorylation of Drp1 occurs in a more physiological setting, we used gain- and loss-of-function approaches. First, we incubated HEK-TtH cells overnight in the absence of serum and the presence of the Mek inhibitor PD325901 to inhibit Erk signaling (Sebolt-Leopold and Herrera, 2004). Following the incubation, we replaced the media with fresh media containing 10% fetal bovine serum and evaluated the phosphorylation of both Erk and Drp1 over an 8-hour timecourse. Addition of serum led to an increase in phospho-Erk1/2 (T202/Y204), indicating activation of the MAPK pathway, closely followed by an increase in S616-phosphorylated Drp1 (Figure 2.2D). Conversely, when we treated cells grown in serum with increasing concentrations of PD325901, we observed a dose-dependent decrease in Drp1 phosphorylation that closely tracked the inhibition of Erk phosphorylation (Figure 2.2E). Identical effects were observed when we treated HEK-TtH cells stably expressing $HRas^{G12V}$, suggesting that the serum-induced effects are through Ras and its downstream signaling pathways (Figure 2.2F). To more specifically test the ability of the MAPK pathway to promote Drp1 phosphorylation, we transiently transfected serum-starved HEK-TtH cells with a constitutively active mutant of c-Raf (Raf-22W) (Stanton, 1989). Raf-22W expression led to increased Erk phosphorylation as well as increased phosphorylation of Drp1 (Figure 2.2G). To rule out the possibility that this is peculiar to our HEK-TtH system, we repeated this experiment in HeLa cells and confirmed that expression of Raf-22W led to an increase in both Erk and Drp1 phosphorylation (Figure 2H).

Figure 2.2

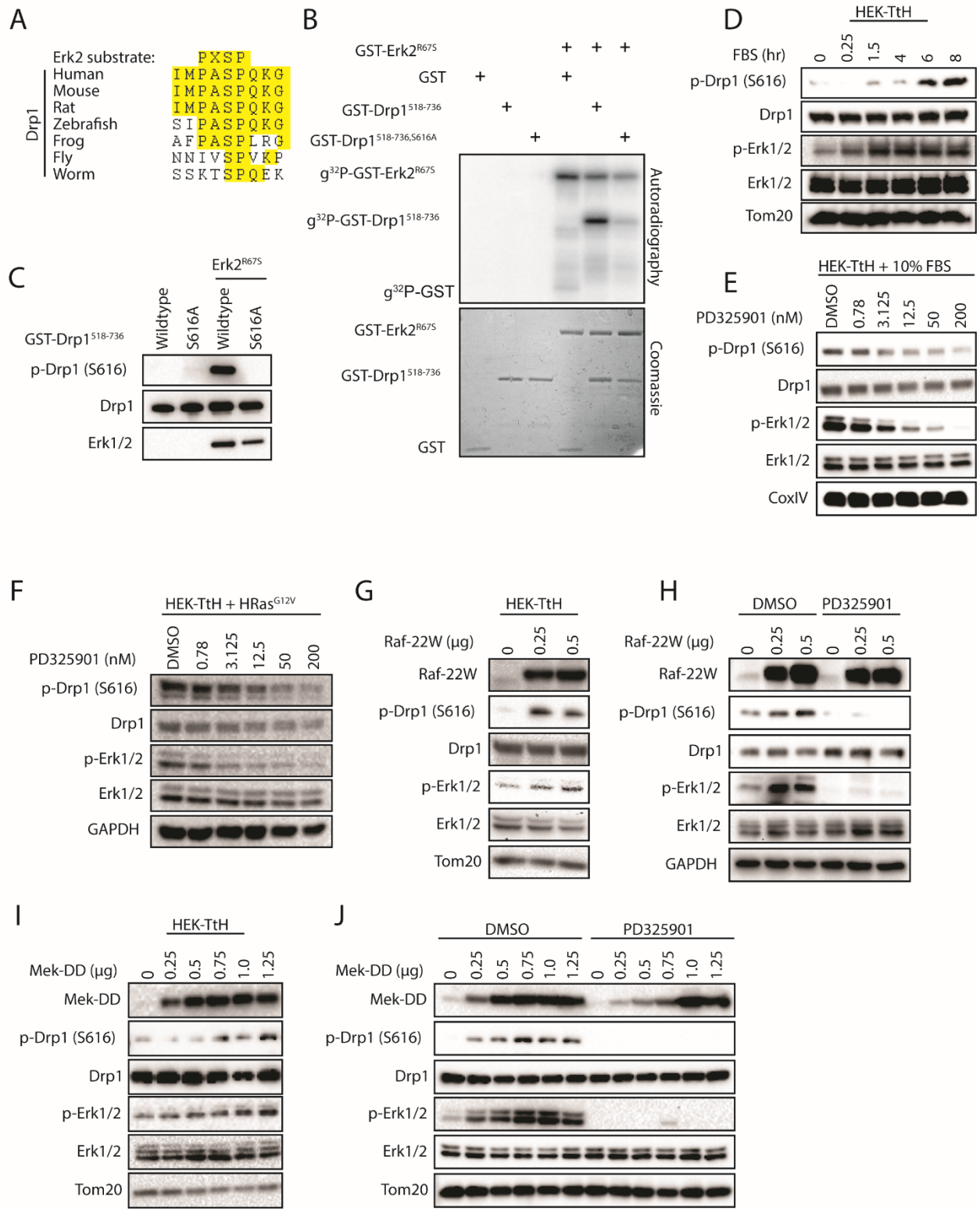
A
Erk2 substrate: PXSP
Drp1
Human IMPASPQKG
Mouse IMPASPQKG
Rat IMPASPQKG
Zebrafish SIPASPQKG
Frog AFPASPLRG
Fly NNIVSPVKP
Worm SSKTSPQEK
B
GST-Erk2R67S
GST
GST-Drp1518-736
GST-Drp1518-736,S616A
g32P-GST-Erk2R67S
g32P-GST-Drp1518-736
g32P-GST
GST-Erk2R67S
GST-Drp1518-736
GST
Autoradiography
Coomassie
C
Erk2R67S
Wildtype
S616A
Wildtype
S616A
GST-Drp1518-736
p-Drp1 (S616)
Drp1
Erk1/2
D
HEK-TtH
FBS (hr) 0 0.25 1.5 4 6 8
p-Drp1 (S616)
Drp1
p-Erk1/2
Erk1/2
Tom20
E
HEK-TtH + 10% FBS
PD325901 (nM) DMSO 0.78 3.125 12.5 50 200
p-Drp1 (S616)
Drp1
p-Erk1/2
Erk1/2
CoxIV
F
HEK-TtH + HRasG12V
PD325901 (nM) DMSO 0.78 3.125 12.5 50 200
p-Drp1 (S616)
Drp1
p-Erk1/2
Erk1/2
GAPDH
G
HEK-TtH
Raf-22W (µg) 0 0.25 0.5
Raf-22W
p-Drp1 (S616)
Drp1
p-Erk1/2
Erk1/2
Tom20
H
DMSO
PD325901
Raf-22W (µg) 0 0.25 0.5 0 0.25 0.5
Raf-22W
p-Drp1 (S616)
Drp1
p-Erk1/2
Erk1/2
GAPDH
I
HEK-TtH
Mek-DD (µg) 0 0.25 0.5 0.75 1.0 1.25
Mek-DD
p-Drp1 (S616)
Drp1
p-Erk1/2
Erk1/2
Tom20
J
DMSO
PD325901
Mek-DD (µg) 0 0.25 0.5 0.75 1.0 1.25 0 0.25 0.5 0.75 1.0 1.25
Mek-DD
p-Drp1 (S616)
Drp1
p-Erk1/2
Erk1/2
Tom20

Figure 2.2. Erk2 phosphorylates Drp1 Serine 616. (Figure 2.2A-D contributed by Kashatus, DF).

(A) Alignment of the consensus Erk2 target sequence with amino acids 612-620 of human Drp1 (isoform 1) and the corresponding sequence from the indicated species. (B-C) Recombinant, active GST-Erk2^{R67S} was incubated with either GST alone, GST-Drp1$^{518-736}$ or GST-Drp1$^{518-736, S616A}$ in the presence of γ^{32}P-ATP (B) or ATP (C) and resolved by SDS-PAGE. Drp1 phosphorylation was detected by autoradiography (B) or immunoblot (A). (D-J) Phosphorylation of Drp1 (P616) and Erk1/2 (Y202/T204) were monitored by immunoblot in the following cells: (D) HEK-TtH cells grown in serum-free DMEM supplemented with 10μM Mek inhibitor PD325901 for 16 hrs, then supplemented with 10% FBS over an 8-hour time course; (E) HEK-TtH cells supplemented with 10% FBS and treated with 0.78-200nM of PD325901 for 8 hrs. (F) HEK-TtH cells stably expressing HRas^{G12V} treated with 0.78-200nM of PD325901 for 8 hrs; (G) HEK-TtH cells transfected with increasing amounts of Raf-22W; (H) HeLa cells transfected with increasing amounts of Raf-22W in the presence of DMSO or PD325901; (I) HEK-TtH cells transfected with increasing amounts of MEK-DD; (J) HeLa cells transfected with increasing amounts of active MEK-DD in the presence of DMSO or PD325901; Tom20, CoxIV, GAPDH: Loading Controls.

Further, when we transfected cells simultaneously treated with PD325901, we observed a near complete loss of both Erk and Drp1 phosphorylation, indicating that Raf-induced Drp1 phosphorylation is dependent on Mek activity (Figure 2.2H, lanes 4-6). Notably, neither inhibition of Mek activity in the presence of serum or $HRas^{G12V}$, nor expression of Raf-22W, led to changes in the levels of the fusion proteins Mfn1, Mfn2 and Opa1 (Figure 2.S2A,B,C).

The Mek dependence of S616 phosphorylation led us to test whether expression of an activated mutant of Mek also promotes Drp1 phosphorylation. As with Raf-22W, transient expression of an activated Mek1 mutant (Mek-DD) (Brunet, 1994) led to an increase in Drp1 phosphorylation in both HEK-TtH (Figure 2.2I) and HeLa cells (Figure 2.2J) and this increase was abolished by treatment with PD325901 (Figure 2.2J, lanes 7-12).

These data indicate that activation of the MAPK pathway through several routes leads to a Mek-dependent increase in Drp1 phosphorylation and, with the *in vitro* data, are consistent with the hypothesis that Ras activation of the MAPK pathway promotes phosphorylation of Drp1 S616 by Erk2.

2.2.5 Activation of MAPK signaling induces mitochondrial fragmentation

As phosphorylation of Drp1 S616 promotes mitochondrial fission, we evaluated whether activation of the MAPK pathway is necessary to induce the fragmented mitochondrial phenotype induced by oncogenic $HRas^{G12V}$. As such, we treated HEK-TtH cells expressing $HRas^{G12V}$ with DMSO or PD325901 and visualized the mitochondrial morphology. Treatment with the inhibitor led to a complete reversal of the Ras-induced mitochondrial phenotype, with >80% of the drug-treated cells exhibiting an interconnected phenotype, compared with <5% of the vehicle-treated cells (Figure 2.3A,B).

These results indicate that the MAPK pathway is *necessary* for Ras-induced mitochondrial fragmentation. To test whether the pathway is *sufficient* for fragmentation, we utilized the

constitutively activated mutants of Raf and Mek. Transient expression Raf-22W or Mek-DD completely phenocopied the mitochondrial fragmentation observed following expression of activated Ras and this fragmentation was completely reversed by treatment with PD325901 (Figure 2.3C-3F). These data suggest that Ras-mediated activation of the MAPK pathway is both necessary and sufficient to promote a fragmented mitochondrial phenotype. Thus, while the RalGEF pathway promotes mitochondrial fission during mitosis (Kashatus et al., 2011), the MAPK plays a dominant role in promoting the fragmented phenotype in the context of constitutive Ras activity.

2.2.6 Drp1 is phosphorylated in pancreatic cancer cell lines

As exogenous expression of oncogenic Ras, or activation of MAPK signaling, promotes phosphorylation of Drp1 and mitochondrial fragmentation, we examined whether the *endogenous* activation of these pathways observed in pancreatic cancer promotes the same phenotype. Thus, we analyzed the levels of phosphorylated Drp1 and the mitochondrial morphology in a series of patient-derived, KRas-mutant pancreatic cancer cell lines: Capan-1, Capan-2, CFPAC-1, PANC-1, L3.6PL, MPanc96 and VMP 608t (Bruns et al., 1999; Deer et al., 2010; Moore et al., 2001; Stokes et al., 2011) and one cell line with wildtype Ras: BxPC-3 (Diep et al., 2011). Each of the cell lines had detectable levels of S616-phosphorylated Drp1 by immunoblot (Figure 2.4A). Treatment of MPanc-96 cells with PD325901 led to a dose-dependent decrease in Drp1 S616 phosphorylation that temporally followed a decrease in Erk phosphorylation, suggesting that the MAPK pathway contributes to the phosphorylation (Figure 2.4B,C). Like HEK-TtH cells, treatment with the inhibitor had no observable effect on the levels of fusion proteins (Figure 2.S3A). Additionally, the mitochondrial morphology of each of the cell lines exhibited a highly fragmented phenotype (Figure 2.4D and 2.S3B), similar to what we observed in HEK-TtH cells expressing $HRas^{G12V}$.

Figure 2.S2

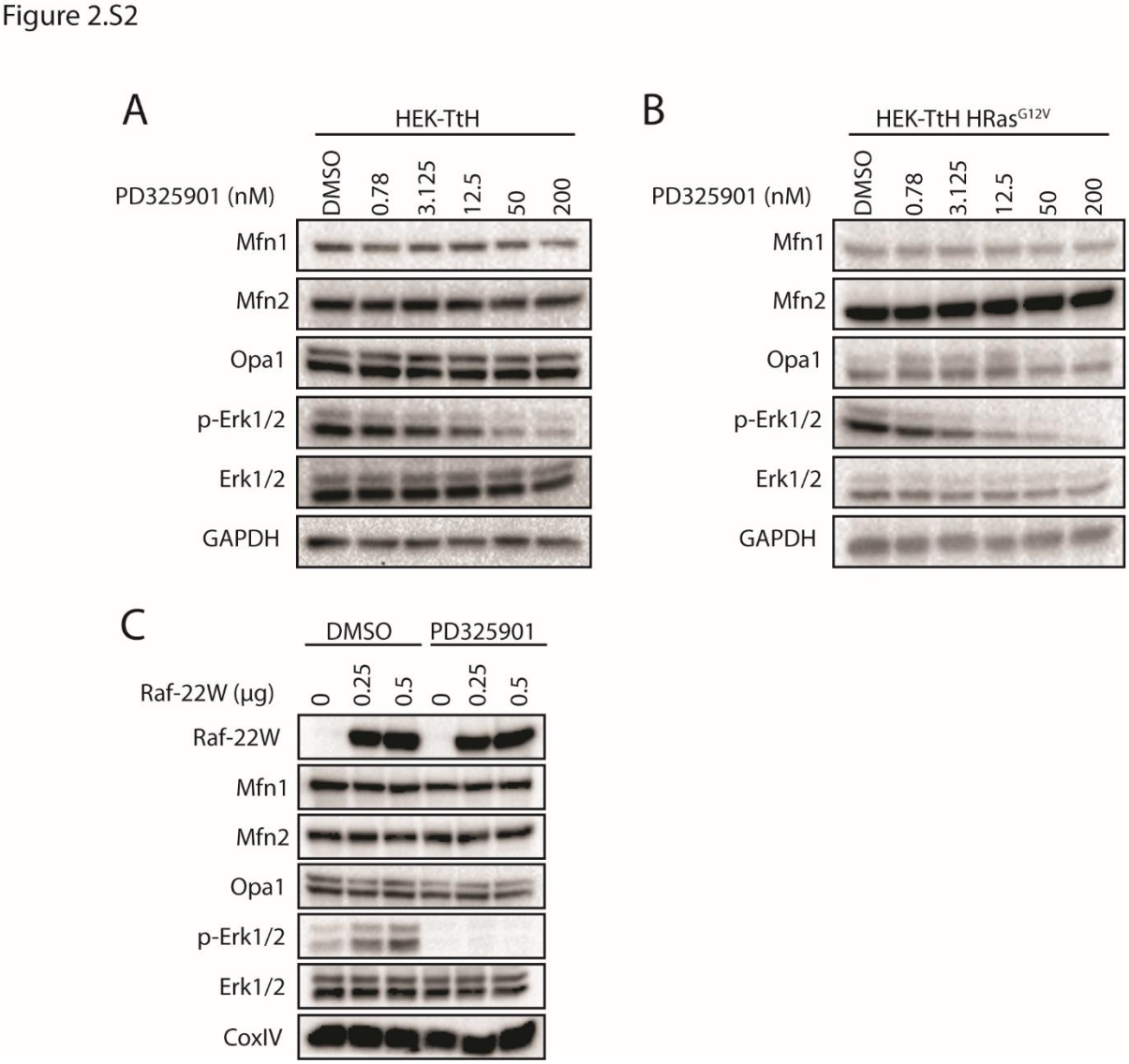
A
HEK-TtH
PD325901 (nM)
DMSO
0.78
3.125
12.5
50
200
Mfn1
Mfn2
Opa1
p-Erk1/2
Erk1/2
GAPDH
B
HEK-TtH HRas^{G12V}
PD325901 (nM)
DMSO
0.78
3.125
12.5
50
200
Mfn1
Mfn2
Opa1
p-Erk1/2
Erk1/2
GAPDH
C
DMSO
PD325901
Raf-22W (µg)
0
0.25
0.5
0
0.25
0.5
Raf-22W
Mfn1
Mfn2
Opa1
p-Erk1/2
Erk1/2
CoxIV

Figure 2.S2. Inhibition of Mek/Erk signaling does not affect levels of fusion proteins. (Related to Figure 2.2)

(A) HEK-TtH cells, supplemented with 10% FBS, were treated with 0.78-200nM of the MEK inhibitor PD325901 and the levels of Mfn1 and Mfn2, the processing of Opa1 and the phosphorylation of Erk1/2 (Y202/T204) were analyzed by immunoblot. GAPDH: Loading Control. B. HEK-TtH cells stably expressing HRasG12V were treated with 0.78-200nM of the MEK inhibitor PD325901 and the levels of Mfn1 and Mfn2, the processing of Opa1 and the phosphorylation of Erk1/2 (Y202/T204) were analyzed by immunoblot. GAPDH: Loading Control. C. HeLa cells were transfected with increasing amounts of active Raf-22W in the presence of DMSO or MEK inhibitor PD325901 and the levels of Mfn1 and Mfn2, the processing of Opa1 and the phosphorylation of Erk1/2 (Y202/T204) were analyzed by immunoblot. GAPDH: Loading Control.

Figure 2.3

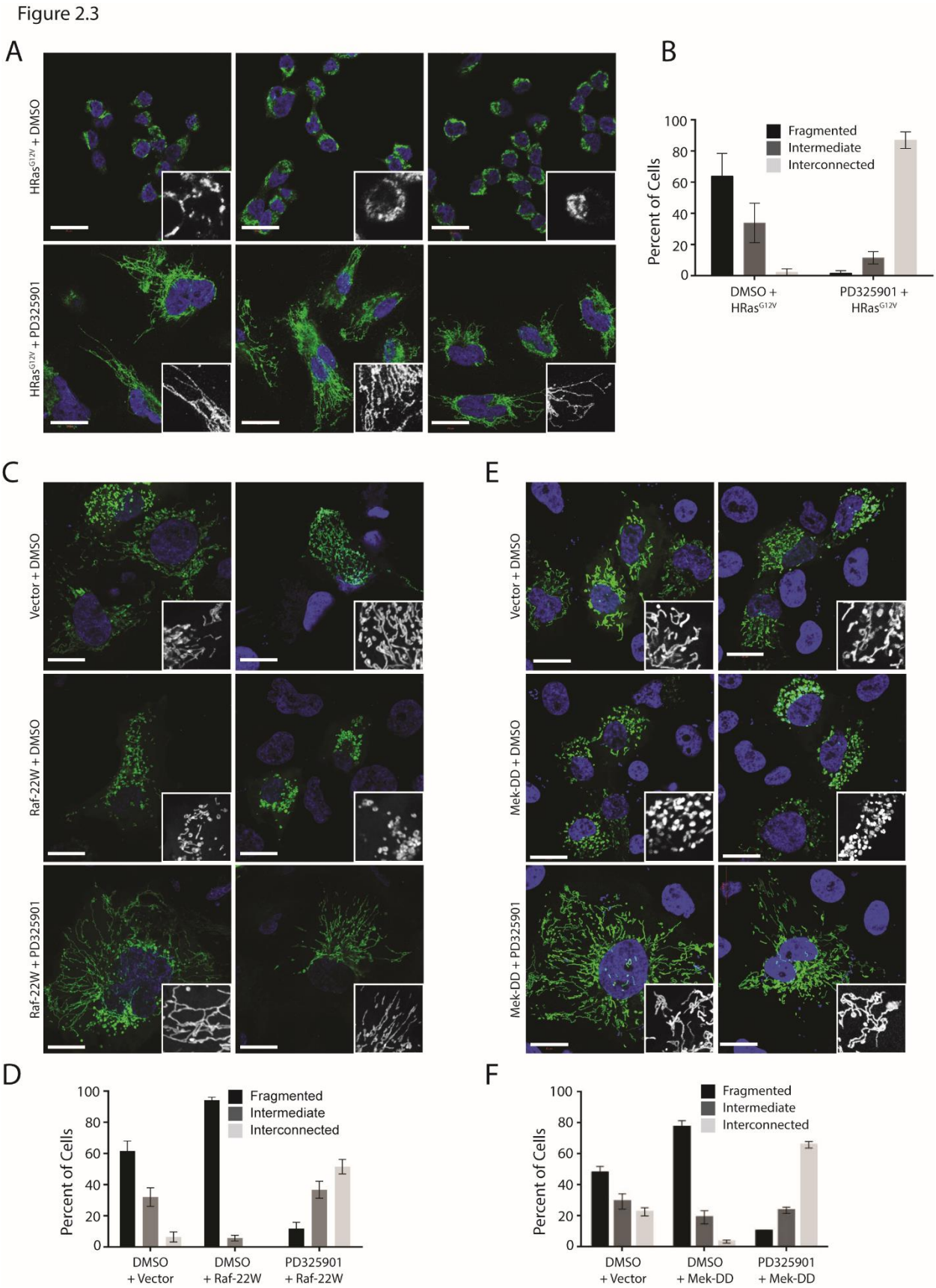
A
HRas^{G12V} + DMSO
HRas^{G12V} + PD325901
B
Percent of Cells
100
80
60
40
20
0
Fragmented
Intermediate
Interconnected
DMSO + HRas^{G12V}
PD325901 + HRas^{G12V}
C
Vector + DMSO
Raf-22W + DMSO
Raf-22W + PD325901
D
Percent of Cells
100
80
60
40
20
0
Fragmented
Intermediate
Interconnected
DMSO + Vector
DMSO + Raf-22W
PD325901 + Raf-22W
E
Vector + DMSO
Mek-DD + DMSO
Mek-DD + PD325901
F
Percent of Cells
100
80
60
40
20
0
Fragmented
Intermediate
Interconnected
DMSO + Vector
DMSO + Mek-DD
PD325901 + Mek-DD

Figure 2.3. Activation of Ras or MAPK signaling leads to Mek-dependent mitochondrial fragmentation.

(A) Mitochondrial morphologies of HEK-TtH cells stably expressing mito-YFP and $HRas^{G12V}$ and treated with either DMSO or 200nM PD325901 for 24 hours. Green: mito-YFP; Blue: DAPI. Scale Bar = 20μm. (B) Quantitation of mitochondrial morphologies observed in cells described in (A). n>50 cells, blindly scored by 5 people, 3 independent experiments; Error bar: S.E.M of mean percentages from 1 representative experiment. (C-F) Mitochondrial morphologies of HEK-TtH cells transfected with mito-YFP plus either vector, Raf-22W or Mek-DD and treated with either DMSO or 200nM PD325901 for 24 hours as indicated. Green: mito-YFP; Blue: DAPI. Scale Bar = 20μm; Quantitation of mitochondrial morphologies: n>50 cells, blindly scored by 5 people, 3 independent experiments; Error bar: S.E.M of mean percentages from 1 representative experiment.

To determine if Mek-dependent phosphorylation of Drp1 is important for the observed fragmented mitochondrial phenotype, MPanc96 cells were treated with PD325901 for 24 hrs and the mitochondrial morphology analyzed. Consistent with the data from HEK-TtH cells, inhibition of Mek led to a reversal of the fragmented phenotype, with 50% of the PD325901-treated cells exhibiting an interconnected phenotype, compared to less than 5% of controls (Figure 2.4E).

2.2.7 Stable knockdown of Drp1 inhibits pancreatic tumor growth

To determine the importance of mitochondrial fission for tumor growth, we stably knocked down Drp1 in BxPC3 cells, which have wildtype Ras but high levels of MAPK activity and rely on MAPK signaling for their tumorigenic growth (Diep et al., 2011; Holcomb et al., 2008). Knockdown of Drp1 had a significant effect on BxPC3 tumor growth, with a significant delay observed in cells expressing the Drp1 shRNA compared with the scramble controls (Figure 2.4F,G). Furthermore, the size of the tumors that arose from the Drp1 knockdown was variable, and immunoblots of the tumor lysates indicated that the larger tumors expressed higher levels of Drp1 (Figure2.4H). These data suggest that there is selective pressure against knockdown of Drp1 and that cells with higher basal levels have a distinct growth advantage *in vivo*, lending support to the idea that Erk-induced Drp1 activity is important for tumor growth.

We performed the same analysis with two additional pancreatic cancer cell lines, L3.6PL and MPanc96, but observed no effect on tumor growth following knockdown of Drp1 (Figure 2.S3C, S3D). However, like the BxPC3 cells, analysis of the tumors revealed re-expression of Drp1 in the tumors that arose (Figure 2.S3E, 2.S3F), suggesting selective pressure against Drp1 knockdown and indicating that alternative methods of inhibition will be required to test the requirement of Drp1 more broadly.

Figure 2.4

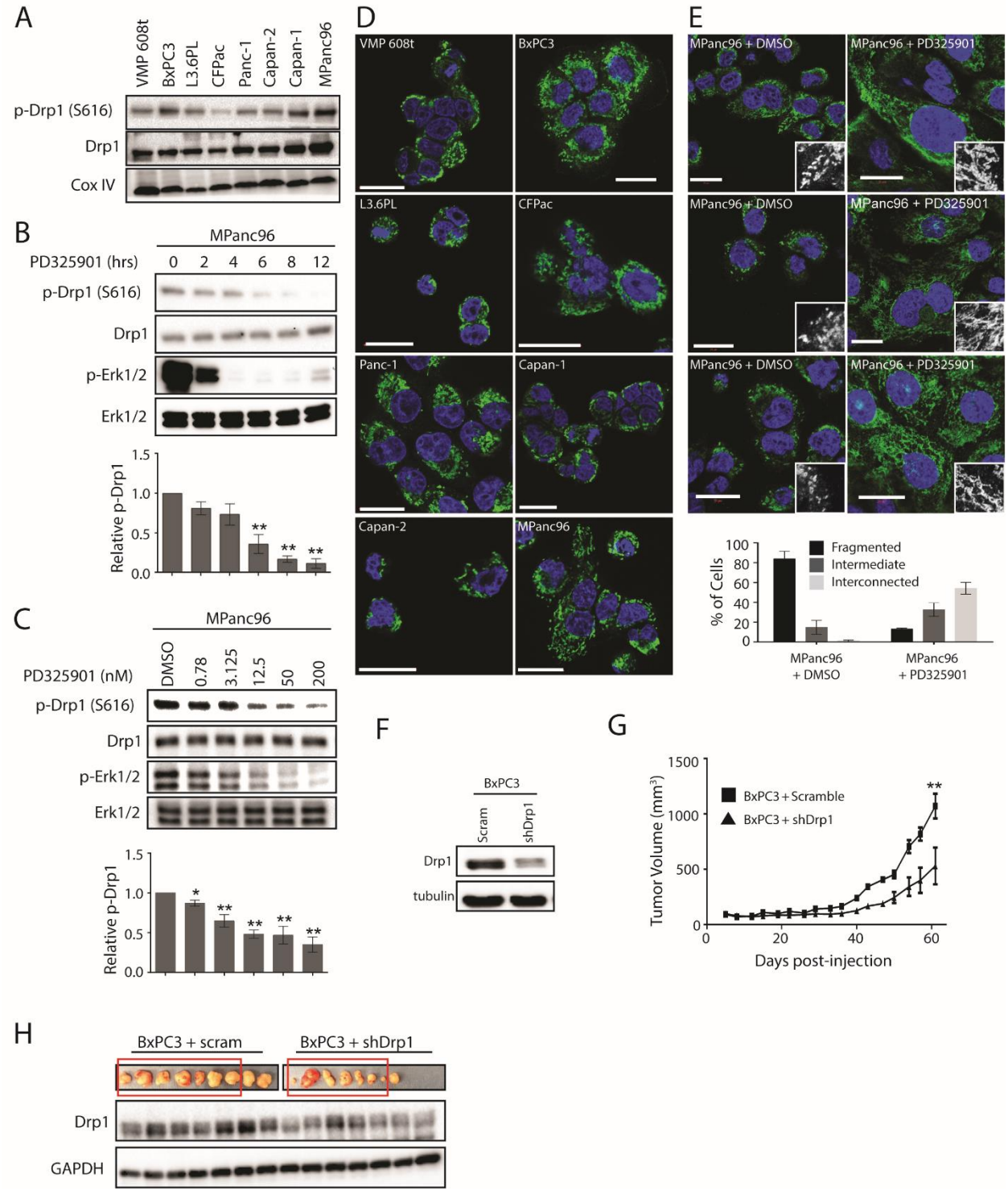
A
VMP 608t
BxPC3
L3.6PL
CFPac
Panc-1
Capan-2
Capan-1
MPanc96
p-Drp1 (S616)
Drp1
Cox IV
B
MPanc96
PD325901 (hrs)
0 2 4 6 8 12
p-Drp1 (S616)
Drp1
p-Erk1/2
Erk1/2
Relative p-Drp1
C
MPanc96
PD325901 (nM)
DMSO 0.78 3.125 12.5 50 200
p-Drp1 (S616)
Drp1
p-Erk1/2
Erk1/2
Relative p-Drp1
D
VMP 608t
BxPC3
L3.6PL
CFPac
Panc-1
Capan-1
Capan-2
MPanc96
E
MPanc96 + DMSO
MPanc96 + PD325901
% of Cells
Fragmented
Intermediate
Interconnected
F
BxPC3
Scram
shDrp1
Drp1
tubulin
G
BxPC3 + Scramble
BxPC3 + shDrp1
Tumor Volume (mm³)
Days post-injection
H
BxPC3 + scram
BxPC3 + shDrp1
Drp1
GAPDH

Figure 2.4. Patient-derived pancreatic cancer cell lines are characterized by Mek-dependent Drp1 phosphorylation and mitochondrial fragmentation. (Figure 2.4F-G contributed by Myers, LJ).

(A) Immunoblot analysis of phospho-Drp1 (P616) and Drp1 in a panel of 8 patient-derived pancreatic cell lines. CoxIV: Loading Control. (B-C) Immunoblot analysis of MPanc96 cells treated with 200nM PD325901 over a timecourse of 12 hours (C) or treated with 0.78-200nM for 8 hours (D). Graph: p-Drp1 levels normalized to total Drp1 levels; n=3, Error bars: S.E.M. Two-tailed student t-test comparing treatment to control, **p<0.01; *p<0.05. (D) Mitochondrial morphology of 8 patient-derived pancreatic cancer cell lines. Green: anti-Tom20; Blue: DAPI. Scale Bar = 20μm. (E) Mitochondrial morphology of MPanc96 cells treated with DMSO or 200nM PD325901 for 48hrs. Green: anti-Tom20; Blue: DAPI. Scale Bar = 20μm. Graph: quantitation of mitochondrial morphologies. n>50 cells, blindly scored by 5 people, 3 independent experiments; Error bar: S.E.M of mean percentages from 1 representative experiment. (F-H) BxPC3 cells expressing scramble or Drp1 shRNA were analyzed by immunoblot (F) then injected into mice and tumor volume was measured over time (G). Tumors were excised and analyzed by immunoblot (H). Blot represents first 7 tumors for each cell type (red boxes). Tubulin, GAPDH: Loading controls. Error bars: S.E.M. of mean tumor volume. ** Two-tailed student t-test, p<0.004.

Figure 2.S3

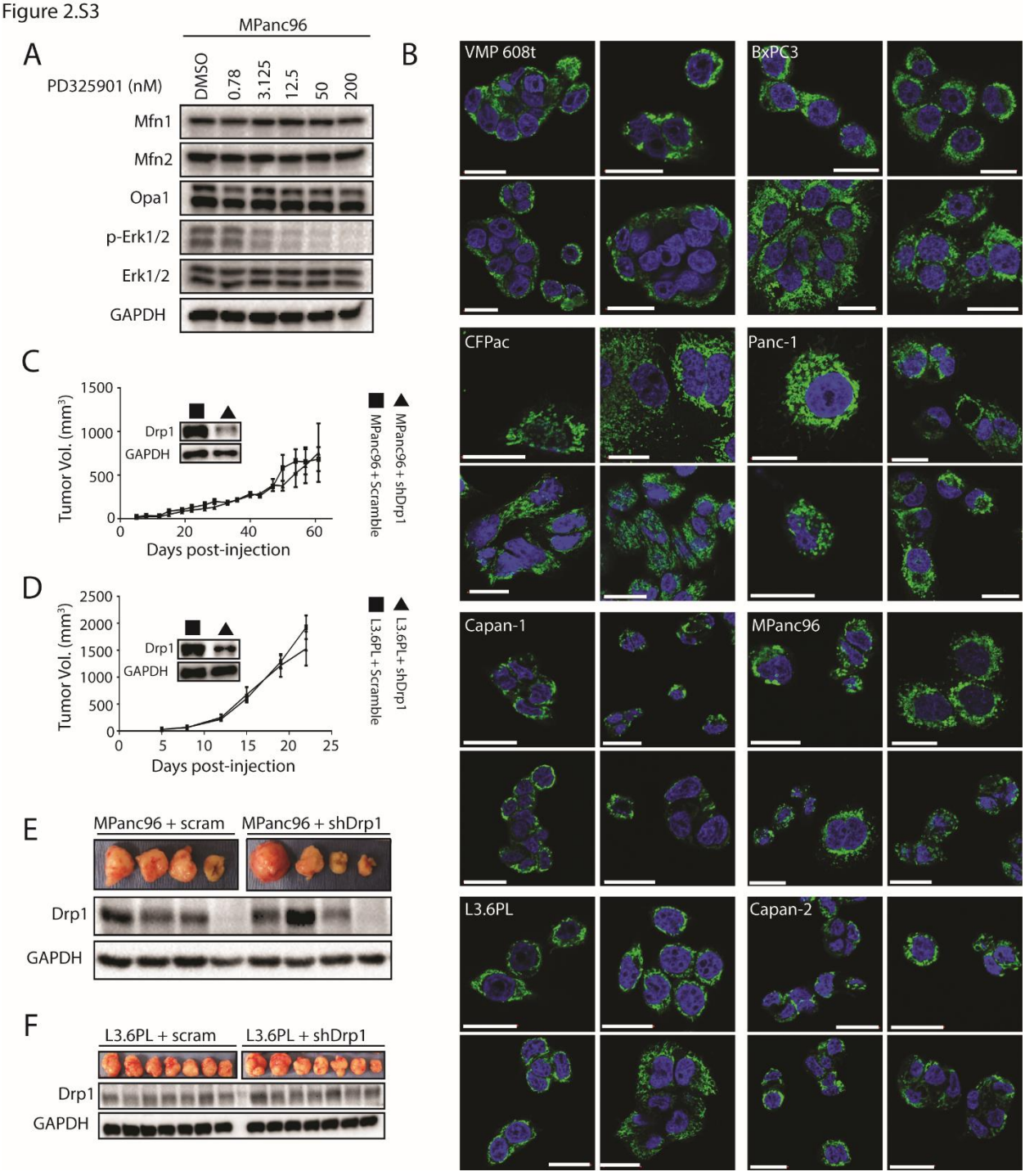
A
MPanc96
PD325901 (nM)
DMSO
0.78
3.125
12.5
50
200
Mfn1
Mfn2
Opa1
p-Erk1/2
Erk1/2
GAPDH
B
VMP 608t
BxPC3
CFPac
Panc-1
Capan-1
MPanc96
L3.6PL
Capan-2
C
Tumor Vol. (mm³)
Drp1
GAPDH
Days post-injection
MPanc96 + Scramble
MPanc96 + shDrp1
D
Tumor Vol. (mm³)
Drp1
GAPDH
Days post-injection
L3.6PL + Scramble
L3.6PL + shDrp1
E
MPanc96 + scram
MPanc96 + shDrp1
Drp1
GAPDH
F
L3.6PL + scram
L3.6PL + shDrp1
Drp1
GAPDH

Figure 2.S3. Analysis of Pancreatic Cancer Cell lines. (Related to Figure 2.4) (Figure 2.S3 C-F contributed by Myers, LJ)

(A) MPanc96 cells were treated with 0.78-200nM PD325901 for 8 hours and the levels of the indicated proteins were analyzed by immunoblot. GAPDH: Loading Control. B. Confocal microscopy of the mitochondrial morphology of 8 patient-derived pancreatic cancer cell lines. Green: anti-Tom20; Blue: DAPI. 4 representative images of each cell line are shown. Scale Bar = 20μm. C-F. Xenograft growth of pancreatic cancer cell lines. MPanc96 (C & E) and L3.6PL (D & F) cells expressing an shRNA targeting either scramble control or Drp1 were analyzed by immunoblot then injected into Nude mice and tumor volume was measured over time. GAPDH: Loading controls. Error bars: S.E.M. of mean tumor volume.

2.2.8 Drp1 is phosphorylated in pancreatic tumor specimens

We also analyzed Drp1 phosphorylation by direct immunohistochemical staining of patient-derived pancreatic cancer specimens, as the majority of pancreatic cancers have mutations in KRAS and/or constitutive MAPK pathway activation (Bos, 1989). Serial sections were cut from 12 formalin-fixed, paraffin-embedded (FFPE) surgically resected pancreatic ductal adenocarcinomas, then stained using hematoxylin and eosin (H&E) as well as antibodies specific for S616-phosphorylated Drp1 and T202/Y204-phosphorylated Erk1/2, with representative images from 6 of the tumors shown in Figure 2.5A. The specificity of the Drp1 antibody was confirmed by staining sections cut from FFPE cell pellets of HEK-TtH cells expressing $HRas^{G12V}$ and Drp1 shRNA in addition to shRNA-resistant Drp1 or $Drp1^{S616A}$ (Figure 2.S4). We detected high to moderate levels (2+/3+) of phospho-Erk staining in a large percentage of the tumor area, but not the surrounding normal tissue, for 10 of the 12 sections (Figure 2.5B). We also observed low to moderate (1+/2+) Drp1 phospho-S616 staining in 11 of the 12 tumors. Consistent with our hypothesis that Erk is upstream of Drp1 phosphorylation, 7 of 12 tumors exhibited a high degree of colocalization between the phospho-Erk and phospho-Drp1 staining while an additional 2 tumors exhibited partial colocalization. Of the remaining 3 tumors, two exhibited non-overlapping phospho-Drp1 and phospho-Erk while one was negative for both (Figure 2.5B). To see if these tumors also exhibited mitochondrial fragmentation, we stained additional sections of two tumors with a fluorescently conjugated antibody that recognizes mitochondria (MTC02). Mitochondria in these sections exhibited a high degree of fragmentation (Figure 2.5C) while cells in areas outside of the tumor boundary exhibited an intermediate mix of mitochondrial morphologies (not shown). Collectively, these data suggest that activation of the MAPK pathway leads to an increase in mitochondrial fission that occurs, at least in part, through Erk2-mediated phosphorylation of Drp1 and that this regulation occurs in human pancreatic cancer.

Figure 2.5

A

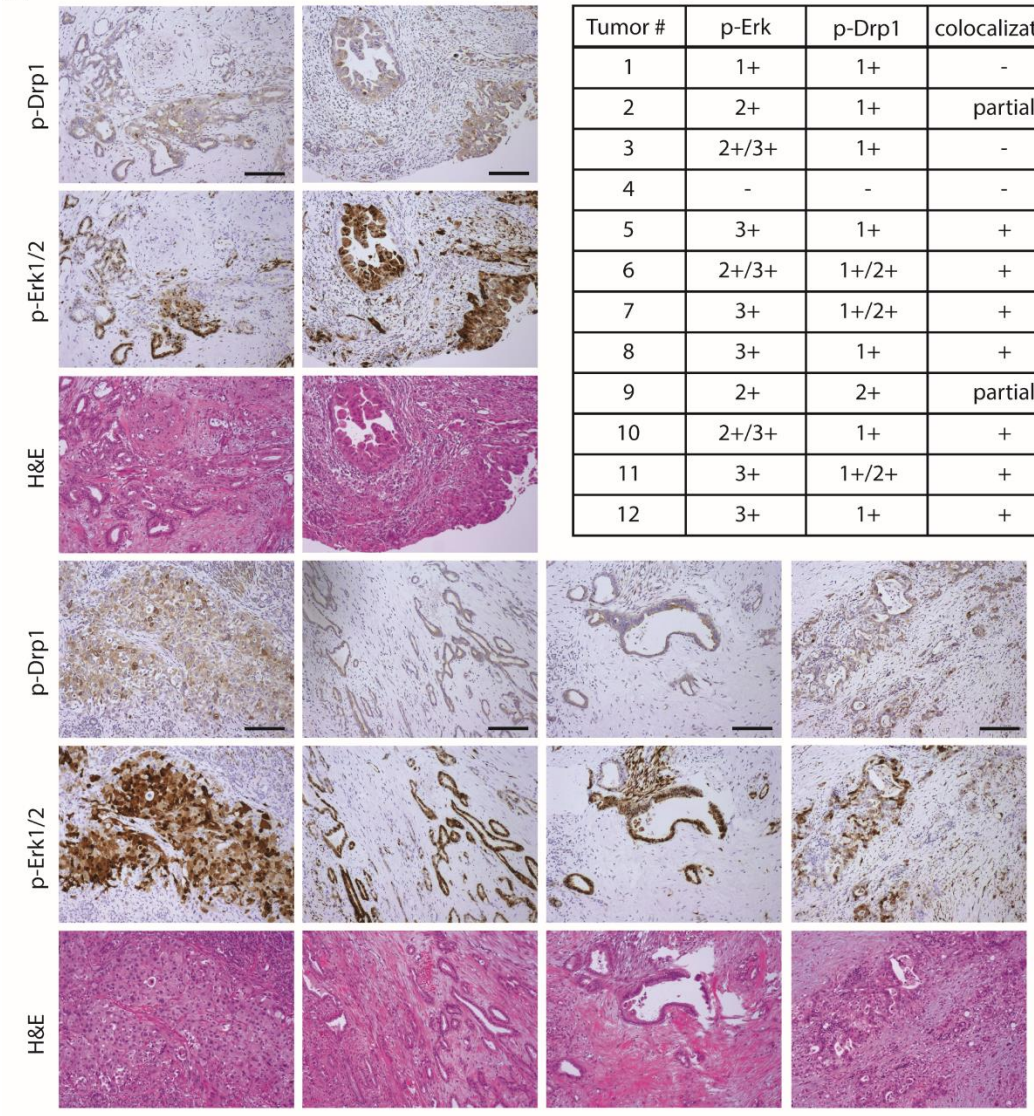

B

Tumor #	p-Erk	p-Drp1	colocalization
1	1+	1+	-
2	2+	1+	partial
3	2+/3+	1+	-
4	-	-	-
5	3+	1+	+
6	2+/3+	1+/2+	+
7	3+	1+/2+	+
8	3+	1+	+
9	2+	2+	partial
10	2+/3+	1+	+
11	3+	1+/2+	+
12	3+	1+	+

C

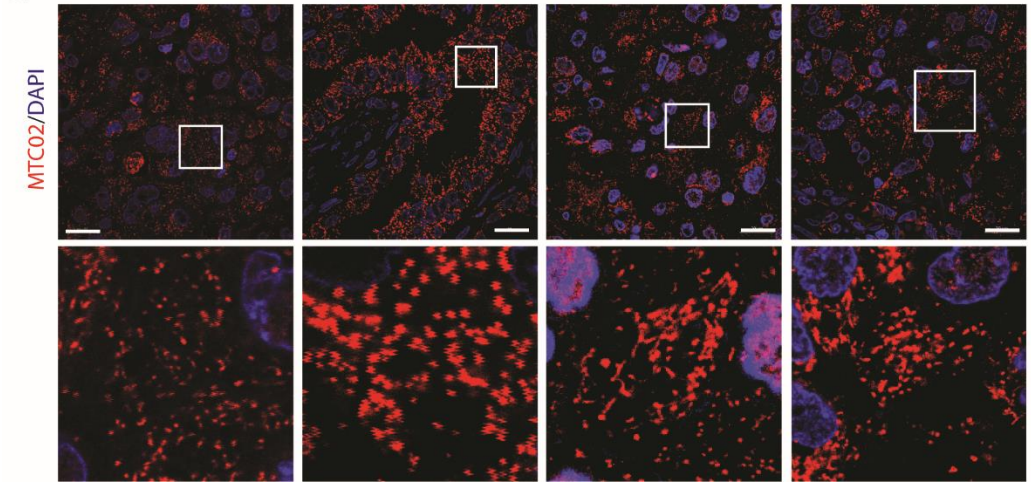

Figure 2.5. Drp1 S616 is phosphorylated in human pancreatic ductal adenocarcinoma (This figure was contributed by Kashatus, JA).

(A) Three serial sections were cut from formalin-fixed, paraffin-embedded sections from 12 pancreatic ductal adenocarcinomas and stained with Hematoxylin and Eosin (H&E) or antibodies against phospho-Drp1 (S616) and phospho-Erk1/2 (T202/Y204). Representative images of colocalization are shown from 6 tumors. Scale Bar = 100μm (IHC). (B) The levels of phospho-Drp1 (S616) and phospho-Erk1/2 (T202/Y204) staining, as well as the degree of co-localization, were determined for each of 12 pancreatic ductal adenocarcinomas examined. (C) Additional sections were cut from two of the tumors (7, 11) and stained with an anti-mitochondria antibody (MTC02) to detect mitochondria (red). Blue: DAPI. Scale Bar = 20μm.

Figure 2.S4

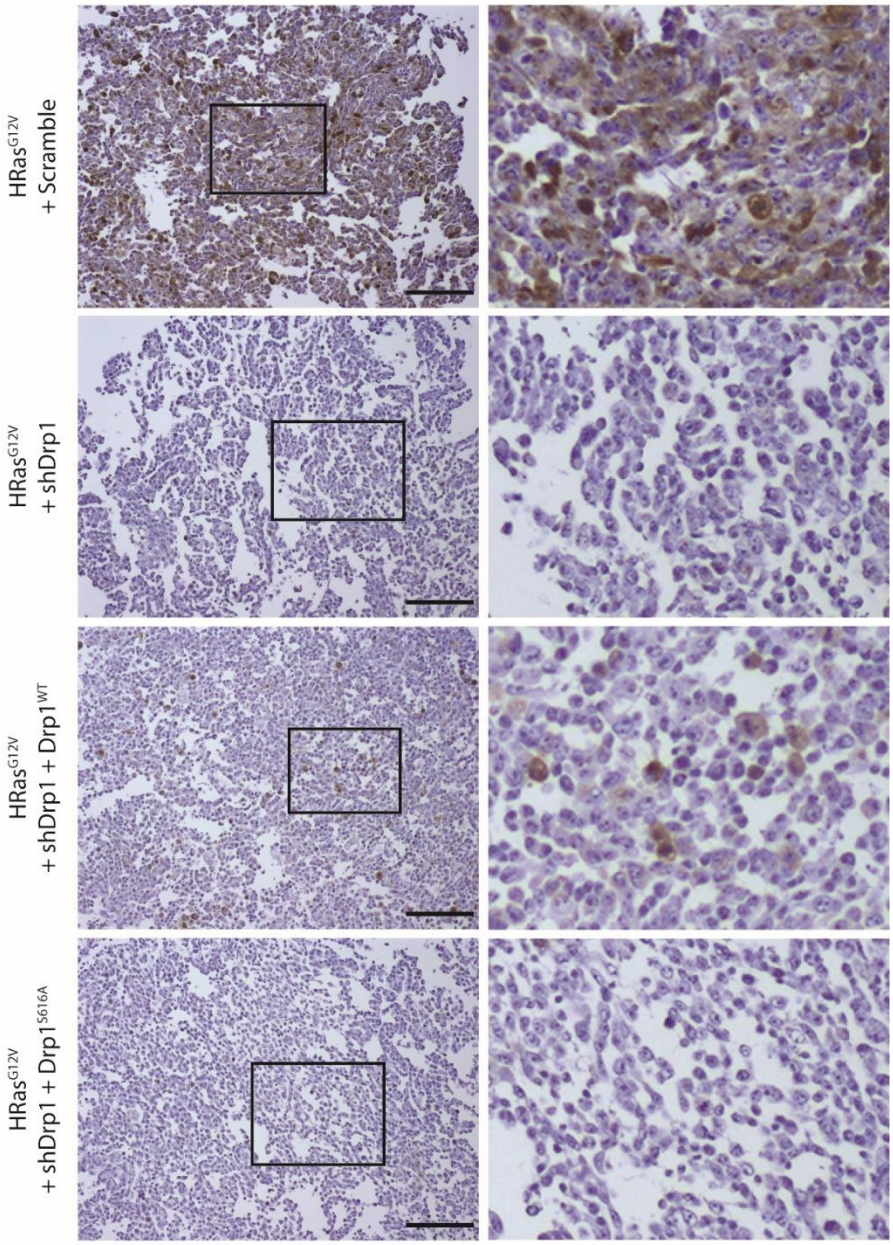
HRas^{G12V} + Scramble
HRas^{G12V} + shDrp1
HRas^{G12V} + shDrp1 + Drp1^{WT}
HRas^{G12V} + shDrp1 + Drp1^{S616A}

Figure 2.S4. Validation of the use of a phospho-specific S616 Drp1 antibody for immunohistochemistry. (Related to Figure 2.5) (This figure was contributed by Kashatus, JA).

HEK-TtH cells were engineered to express Flag-HRasG12V plus an shRNA targeting either scramble control or Drp1 and then rescued with either vector, Flag-Drp1WT or Flag-Drp1S616A. Cell pellets were fixed in formalin, embedded in paraffin and sections were cut and stained using an antibody specific for p-Drp1 (S616). Left image: Scale bar = 100μm; Right image: enlargement of boxed area.

2.2.9 Drp1 S616 phosphorylation is required for Ras-induced mitochondrial fission and tumor growth.

To determine the importance of Drp1 phosphorylation for the phenotypes we have observed, we expressed wildtype or S616A, shRNA-resistant Drp1 in the HEK-TtH cells expressing $HRas^{G12V}$ and Drp1 shRNA. Re-expression of the wildtype, but not the SA mutant restored the levels of Drp1 phosphorylation (Figure 2.6A). Further, expression of wildtype Drp1, but not the mutant, completely restored the highly fragmented phenotype of the $HRas^{G12V}$-expressing cells lost upon knockdown of Drp1 (Figure 2.6B,C). To test the hypothesis that phosphorylation of Drp1 S616 is important for tumor growth, we injected these cells into mice. Knockdown of Drp1 led to a loss of tumor growth and re-expression of wildtype Drp1, but not the SA mutant, restored tumor growth to the levels observed in the scramble control cells (Figure 2.6D-E). These data link the effects of MAPK activation on mitochondrial morphology to the biological requirement of Drp1 for tumor growth and underscore the direct physiological relevance of the Erk2-mediated phosphorylation of Drp1 that we observe.

Figure 2.6

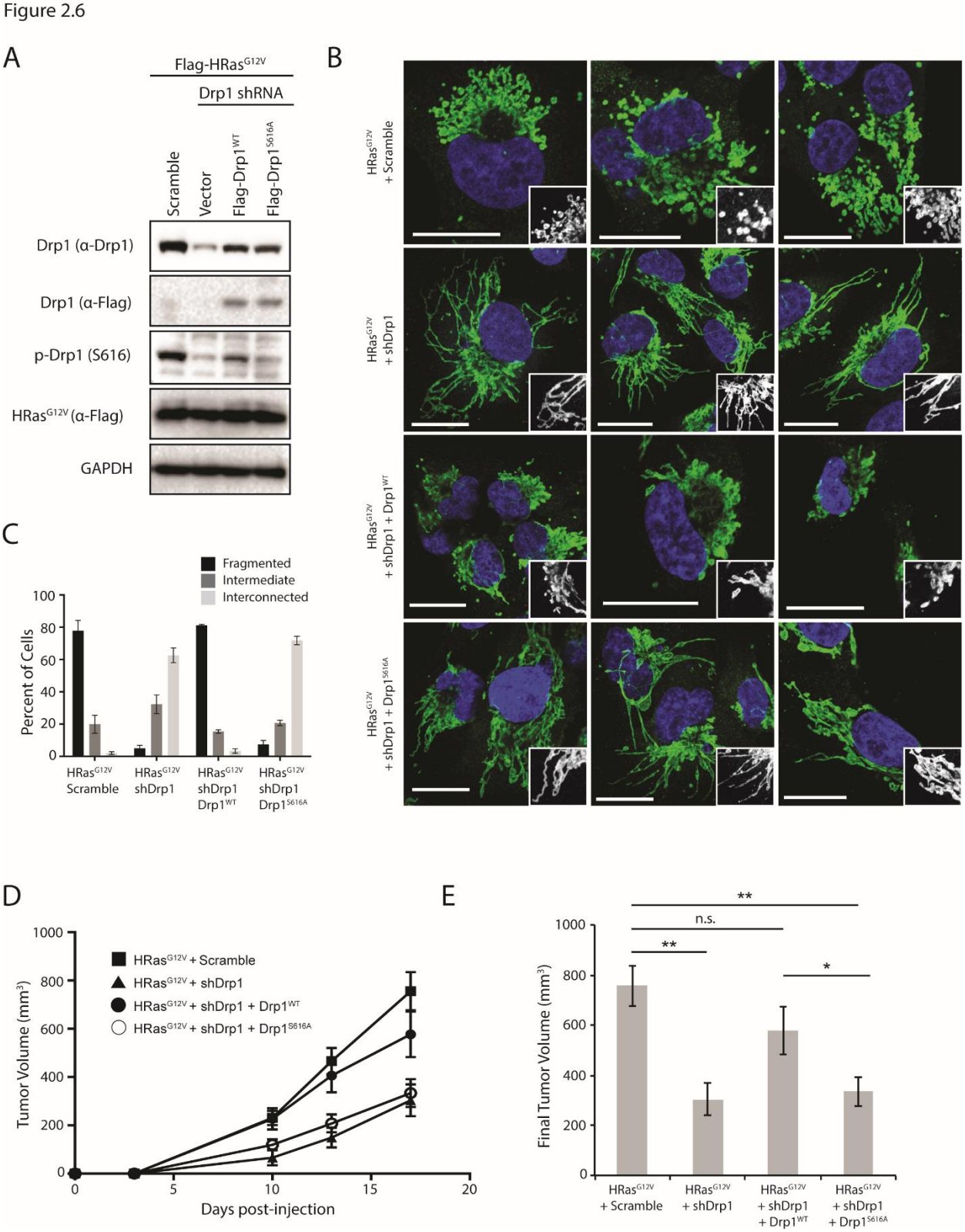
A
Flag-HRas^{G12V}
Drp1 shRNA
Scramble
Vector
Flag-Drp1^{WT}
Flag-Drp1^{S616A}
Drp1 (α-Drp1)
Drp1 (α-Flag)
p-Drp1 (S616)
HRas^{G12V} (α-Flag)
GAPDH
B
HRas^{G12V} + Scramble
HRas^{G12V} + shDrp1
HRas^{G12V} + shDrp1 + Drp1^{WT}
HRas^{G12V} + shDrp1 + Drp1^{S616A}
C
Fragmented
Intermediate
Interconnected
Percent of Cells
HRas^{G12V} Scramble
HRas^{G12V} shDrp1
HRas^{G12V} shDrp1 Drp1^{WT}
HRas^{G12V} shDrp1 Drp1^{S616A}
D
HRas^{G12V} + Scramble
HRas^{G12V} + shDrp1
HRas^{G12V} + shDrp1 + Drp1^{WT}
HRas^{G12V} + shDrp1 + Drp1^{S616A}
Tumor Volume (mm^3)
Days post-injection
E
n.s.
Final Tumor Volume (mm^3)
HRas^{G12V} + Scramble
HRas^{G12V} + shDrp1
HRas^{G12V} + shDrp1 + Drp1^{WT}
HRas^{G12V} + shDrp1 + Drp1^{S616A}

Figure 2.6. Drp1 Serine 616 is required for Ras-induced mitochondrial fission and Ras-induced tumor growth. (Figure 2.6A contributed by Kashatus, DF, Figure 2.6D-E contributed by Kashatus, JA)

(A) HEK-TtH cells were engineered to express Flag-HRas^{G12V} plus an shRNA targeting either scramble or Drp1 and rescued with either vector, Flag-Drp1^{WT} or Flag-Drp1^{S616A}. (B) The mitochondrial morphologies were analyzed. Green: anti-Tom20; Blue: DAPI. (C) Mitochondrial morphologies were quantified in: n>50 cells, blindly scored by 5 people, 3 independent experiments; Error bar: S.E.M of mean percentages from 1 representative experiment. Scale Bar = 20μm. (D-E) Cells were injected into mice and tumor volume measured over time (D). Tumor volumes at day 17 are shown in (E). n=10 tumors per cell line; error bar: S.E.M. of mean tumor volume. Two-tailed student t-test, **p<0.001; *p<0.05; n.s.=p>0.15.

Figure 2.S5

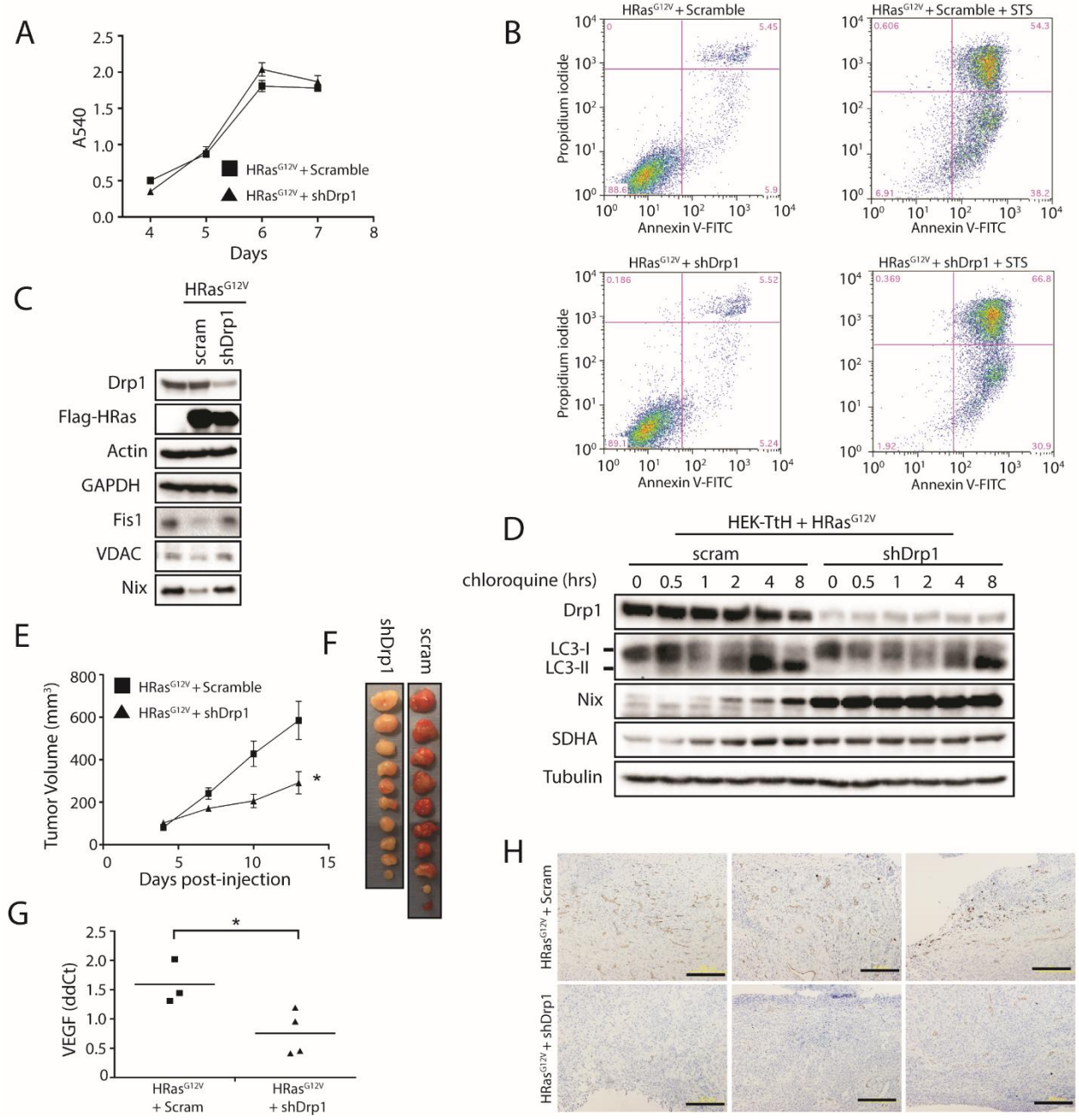
A
A540
Days
HRas^{G12V} + Scramble
HRas^{G12V} + shDrp1
B
HRas^{G12V} + Scramble
HRas^{G12V} + Scramble + STS
HRas^{G12V} + shDrp1
HRas^{G12V} + shDrp1 + STS
Propidium iodide
Annexin V-FITC
C
HRas^{G12V}
scram
shDrp1
Drp1
Flag-HRas
Actin
GAPDH
Fis1
VDAC
Nix
D
HEK-TtH + HRas^{G12V}
scram
shDrp1
chloroquine (hrs)
0 0.5 1 2 4 8 0 0.5 1 2 4 8
Drp1
LC3-I
LC3-II
Nix
SDHA
Tubulin
E
Tumor Volume (mm^3)
Days post-injection
HRas^{G12V} + Scramble
HRas^{G12V} + shDrp1
F
shDrp1
scram
G
VEGF (ddCt)
HRas^{G12V} + Scram
HRas^{G12V} + shDrp1
H
HRas^{G12V} + Scram
HRas^{G12V} + shDrp1

Figure 2.S5. Drp1 knockdown has no effect on proliferation or apoptosis but decreases angiogenesis (This figure was contributed by Kashatus, JA).

(A) MTT assays were performed 4, 5, 6 and 7 days after seeding HEK-TtH cells expressing Flag-HRasG12V plus an shRNA targeting either scramble control or Drp1. B. The same cell lines were left untreated or treated overnight with 1μM staurosporine (STS) then stained with FITC-conjugated Annexin V and propidium iodide and analyzed by flow cytometry. C. Immunoblot analysis of the indicated proteins from HEK-TtH cells with or without HRasG12V and an shRNA targeting either scramble control or Drp1. D. HEK-TtH cells expressing HRasG12V and an shRNA targeting either scramble control or Drp1 were treated with 100μM Chloroquine, harvested at the indicated timepoints and analyzed by immunoblot analysis of the indicated proteins. E. The indicated HEK-TtH cells were injected into Nude mice and tumor volume was measured over time *$p<0.05$. F. Tumors from were removed and photographed. G. RNA was isolated from 3 or 4 size-matched tumors and subjected to quantitative RT-PCR to determine the levels of VEGF. H. Portions of 3 size-matched tumors were formalin fixed and embedded in paraffin then sections were cut and stained for murine CD31. Scale bar = 200μm.

2.3 Discussion

Previous reports have established that tumor cells exhibit a fragmented mitochondrial morphology and that inihibition of the large GTPase, Drp1, which regulates mitochondrial fission, led to decreased tumor cell viability (Arismendi-Morillo, 2009; Rehman et al., 2012). However, the underlying mechnaisms that lead to mitochondrial fragmentation, as well as the changes to cellular processes elicited by mitochondrial fission are not fully understood. Thus, we set out to investigate the mechanisms by which tumor cells achieve mitochondrial fragmentation and what benefits it may provide in the presence of mutant Ras. To that end, we first demonstrated that ectopic mutant HRas expression resulted in increased mitochondrial fragmentation. Subsequent knockdown of Drp1 resulted in mitochondrial elongation, which suggests that Drp1 is promoting mutant HRas-mediated mitochondrial fission (Figure 2.1A). As previous studies have shown that fission can promote tumorigenesis, we next sought to determine if Drp1-mediated mitochondrial fission was promoting tumorigenecity in the presence of mutant HRas. Thus, we showed that expression of Drp1 shRNA resulted in a significant decrease in xenograft tumor growth in immunocompromised mice (Figure 2.1E-G), which suggests that HRas signals to Drp1 to promote xenograft growth.

Due to the persitance of mitochondrial fragmentation throughtout all phases of the cell cycle in our HRas mutant HEK cells, we hypothesized that Ras could be signaling through the constitutively active MAPK pathway to achieve persistent and ubiquitous mitochondrial fragmentation. Upon amino acid sequence analysis, we found that Drp1 is a candidate for phosphorylation by Erk2 at S616, a phosphorylation site on Drp1 that promotes mitochondrial fission. Indeed, *in vitro* kinase assays revealed that Erk2 could phosphorylate Drp1 at S616 (Figure 2.2A). We further demonstrated that pharmacological inhibtion of the MAPK pathway results in decreased Drp1 phosphorylation in a dose dependent manner (Figure 2.2E-F). Conversely, genetic activation of MAPK-pathway components resulted in an increase in Drp1

phosphorylation in a dose dependent manner (Figure 2.2G-J). As Ras activation can lead to signaling through several pathways, there may be other regulators of Drp1 activity downstream of mutant Ras, a possibility that we will examine in more detail later in the discussion. Taken together, these results suggest that HRas-mediated activation of the MAPK pathway leads to increased Drp1 phosphorylation.

As several studies suggest that tumors exhibit increased mitochondrial fragmentation (Inoue-Yamauchi and Oda, 2012) and we previously showed that increased MAPK activity resulted in increased Drp1 phosphorylation, we sought to verify the physiologocial consequence of Drp1 activation through analysis of the mitochondrial morphology. In these experiments, we showed that inhibtion of the MAPK pathway in HRas mutant HEK cells shifted the mitochondria from a fragmented state to an elongated state (Figure 2.3A-B). Further manipulation of the MAPK pathway through genetic upregulation of MAPK pathway components in standard HEK cells induced mitochondrial fragmentation that could be reversed by pharmacological inhibition of MEK (Figure 2.3C-F). Collectively, these data suggest that MAPK-mediated phosphorylation of Drp1 results in increased Drp1 activity and mitochondrial fragmentation.

Due to the prevalence of Ras mutations in cancer, we wanted to test if the Ras-Drp1 axis was intact in pancreatic cancer, which almost exclusively exhibits mutations in KRas (Cox and Der, 2010). Thus we analyzed a panel of human pancreatic cancer cell lines and found varying degrees of Drp1 phosphorylation but robust mitochondrial fragmentation when we analyzed the mitochondrial morphology of these cells (Figure 2.4A,D). We next pharmacologically inhibited the MAPK pathway in the MPanc96 cell line, which displayed the highest Drp1 phosphorylation. Inhibition of MAPK activity resulted in decreased Drp1 phosphorylation as well as mitochondrial elongation (Figure 2.4B-C, E). Furthermore, when we inhibited Drp1 in the BxPC3 cell line, which lacks a Ras mutation but has increased MAPK signaling, we see that we are able to significantly reduce xenograft tumor growth. In order to assess the translational potential of the Ras-Drp1 axis in pancreatic cancer, we also analyzed human pancreatic cancer tumor samples for overlap

between Drp1 and Erk phosphorylation. In a panel of 12 patient samples, we showed that phosphorylated Drp1 expression highly overlapped with phosphorylated Erk1/2 expression (Figure 2.5A-B) and that the mitochondria in this these tissue samples display a fragmented morphology (Figure 2.5C). Taken together, these data demonstarte that in pancreatic cancer with active KRas and MAPK pathway signaling, Erk phosphorylates Drp1 to promote mitochondria fission. Furthermore, these results suggest that in addition to HRas, KRas can also regulate Drp1 and mitochondrial dynamics. Thus, regulation of mitochondrial dynamics may be a putative hallmark of Ras-driven cancers and may warrant further studies to classify mitochondrial morphologies of different Ras-driven cancer types. Such studies are currently underway in our laboratory in an effort to understand if certain mitochondrial phenotypes correlate with tumor behavior and potential responsiveness to therapy.

Finally, we sought to determine the contribution of Drp1 fission activity to xenograft tumor growth. In this experiment, we showed that HEK $HRas^{G12V}$ cells had robust xenograft tumor growth that was compromised by knockdown of Drp1. Resuce of Drp1 knockdown cells with WT Drp1 was able to rescue tumor growth, but rescue with a Drp1 S616A mutant, which is unable to be phosphorylated at Drp1's activating residue, led to tumor volumes comparable to the Drp1 knockdown cells (Figure 2.6). These data suggest that phosphorylation of Drp1 at S616 and by extension, mitochondrial fission, is necessary for xenograft tumor growth in the presence of mutant HRas.

Mitochondrial dynamics have been known to play an important role in a number of human diseases including obesity and type 2 diabetes (Yoon et al., 2011), Parkinson's disease (Lim et al., 2012) and Alzheimer's disease (Su et al., 2010), but the role of mitochondrial fusion and fission in malignancy has only recently begun to be explored (Qian et al., 2013). Consistent with our findings, the majority of studies that have examined mitochondrial morphology in tumor cells support a pro-tumorigenic role for mitochondrial fission (Arismendi-Morillo, 2009; Chen et al., 2014; Hagenbuchner et al., 2013; Inoue-Yamauchi and Oda, 2012; Rehman et al., 2012; Zhang

et al., 2013a; Zhao et al., 2013a). Despite this, the molecular mechanisms through which oncogenic signaling pathways can alter mitochondrial dynamics have not been well defined. Our previous work defined a pathway through which the small GTPase and important Ras effector protein RalA, along with its effector RalBP1, promotes mitochondrial fission during mitosis by promoting the recruitment of Drp1 to the mitochondria and enabling its phosphorylation by Cdk1 (Kashatus et al., 2011). The work presented here identifies an additional pathway downstream of Ras to promote Drp1 activity and mitochondrial fragmentation and underscores the importance of mitochondrial fragmentation for Ras- and MAPK-driven tumor growth. These studies provide one molecular mechanism that underlies the change in mitochondrial morphology we observe in pancreatic cancer cell lines and, potentially, the changes observed by others in a number of different cancer cell lines (Inoue-Yamauchi and Oda, 2012). However, it is important to recognize that Ras can signal through a variety of pathways and that the MAPK-Drp1 axis may not be the only way that Ras can regulate mitochondrial dynamics. Recently, a study by Kim et al. found that Akt activation of Amyloid β (Aβ) led to Drp1 activation and extensive mitochondrial fragmentation in neuronal cells (Kim et al., 2016). This has important ramifications for potential therapies aiming to block Drp1 activation through inhibition of MAPK signaling, as KRas-driven tumors eventually become dependent on PI3K-Akt activation to sustain their tumorigenic phenotypes (Muzumdar et al., 2017). Future studies will require further examination of the role of KRas-driven, PI3K-Akt mediated regulation of mitochondrial dynamics in tumor cells. Nevertheless, our findings demonstrate the importance of MAPK-driven mitochondrial morphological change in a genetically-defined model system of Ras-driven tumor growth.

There are a number of physiological mechanisms that could potentially explain the loss tumor growth observed upon inhibition of Drp1, as the regulation of mitochondrial fusion and fission has been shown to play a role in several physiological processes whose dysregulation are classical “hallmarks” of human cancer (Hanahan and Weinberg, 2011), including apoptosis (Sheridan and Martin, 2010), and proliferation (Mitra et al., 2009; Qian et al., 2012). Our results,

however, suggest that inhibition of Drp1 does not block tumor growth through direct effects on either proliferation or apoptosis (Figure 2.S5A,B). The loss of major tumor suppressor pathways, through expression of SV-40 large and small T antigens in the HEK-TtH cells, may explain why we do not observe the previously documented effects on proliferation and survival and suggests that inhibition of Drp1 may be an effective therapeutic option even in tumors that have disabled their apoptotic and growth arrest capabilities. The rapid proliferation of tumor cells requires a large increase in the production of molecular building blocks and tumors achieve this through increased uptake of both glucose and glutamine, which are used for both ATP generation and biosynthesis (Diaz-Ruiz et al., 2009; Ferreira, 2010; Vander Heiden et al., 2009; Warburg, 1956), and through increased autophagy, which can provide biosynthetic precursors and contribute to the metabolic reprogramming (Lozy and Karantza, 2012; Rosenfeldt and Ryan, 2011). Indeed, Ras-driven tumors in particular exhibit high levels of mitophagy (Kim et al., 2011) and a number of groups over the past several years have shown that autophagy plays an essential role in tumors driven by oncogenic Ras or mutant BRaf (Guo et al., 2011; Lock et al., 2011; Rao et al., 2014; Rosenfeldt et al., 2013; Son et al., 2013; Strohecker et al., 2013). We observe a marked increase in mitochondrial mass and mitochondrial protein levels following knockdown of Drp1 in cells expressing $HRas^{G12V}$ (Figure 2.S1C, 2.S5C). Furthermore, the increased mitochondrial protein levels of Drp1 knockdown cells are unaffected by inhibition of autophagy, suggesting that mitophagy has already been inhibited in these cells (Figure 2.S5D). However, we have no evidence that the inhibition of tumor growth we observe is due to a loss of mitophagy. We do, however, consistently observe a phenotypic difference in the color of the tumors that arise following Drp1 inhibition that suggests a decrease in tumor vasculature (Figures 2.1F, 2.S1F, 2.S5E, 2.S5F). Further, our preliminary analysis indicates that knockdown of Drp1 in HEK-TtH $HRas^{G12V}$ cells results in lower levels of VEGF mRNA and decreased tumor vasculature as measured by staining for CD31 (Figure 2.S5G, 2.S5H). We speculate that MAPK-induced mitochondrial fission may promote the activation of pro-angiogenic signaling pathways, which are

known to be sensitive to mitochondria-derived reactive oxygen species (Ushio-Fukai and Nakamura, 2008; Xia et al., 2007). Further analysis of this phenomenon is warranted to determine whether this regulation plays a significant role in the observed effects.

These potential mechanisms (i.e. - proliferation, apoptosis, metabolism, mitophagy, angiogenesis, etc.) through which mitochondrial fission promotes tumor growth are not mutually exclusive, and changes in mitochondrial morphology may function through different combinations of these and other mechanisms in different types of tumors or in response to different stromal environments. We provide a more extensive discussion of the potential ways that the KRas-Drp1 axis may regulate these cellular processes in cancer cells in chapter 5. It will be important to test these potential mechanisms in a variety of different model systems in order to fully explore the possibility of mitochondrial fission inhibition as a therapeutic approach to cancer treatment.

In conclusion, we show that the MAPK regulation of mitochondrial fission through phosphorylation of the fission-mediating GTPase Drp1 is essential in a model of Ras-driven tumor growth. Furthermore, identification of this pathway provides a mechanistic link between mutations in *RAS* and several physiological changes characteristic of Ras-driven tumors and potentially offers an avenue of therapeutic intervention for the treatment of a wide variety of human cancers.

Chapter 3: High-Throughput detection and quantification of mitochondrial fusion through Imaging Flow Cytometry

*****_This chapter is adapted from Nascimento et al. Cytometry Part A 2016_

3.1 Introduction

Mitochondria are highly dynamic double membrane-bound organelles that are primarily responsible for meeting the energy requirements of the cell (Corrado et al., 2012; Grandemange et al., 2009; Westermann, 2012) and play an essential role in mediating programmed cell death (Corrado et al., 2012). These functions of mitochondria are profoundly influenced by mitochondrial morphology (Chan, 2012), which is characterized by continuous cycles of fusion and fission (Kageyama et al., 2011). Shifts in the balance of fission and fusion can result in rapid changes in mitochondrial morphology and significantly impact mitochondrial function (Cerveny et al., 2007). Analysis of a large number of different cell types reveals a high degree of variability in mitochondrial morphology (Westermann, 2012), ranging from extensive interconnected networks to populations of small, punctuate like structures (Benard and Rossignol, 2008; Kuznetsov et al., 2009). This variability arises as a response to the particular energetic demands of each cell type and to the particular nutrient conditions it encounters. Alterations in the activity of the mitochondrial fusion and fission machinery regulate the morphologies seen among different cell types. The mitochondrial machinery consists of large dynamin-related GTPases (Westermann, 2012) MFN1, MFN2 (outer membrane fusion), OPA1 (inner membrane fusion) and Drp1 (fission) (Chan, 2012). Defects in this machinery result in a wide range of pathologies, from neurodegenerative diseases to cancer (Boland et al., 2013; Corrado et al., 2012; Grandemange et al., 2009; Martin, 2012). Despite its importance in so many cellular and organismal processes, there is currently a lack of robust, quantitative assays to monitor mitochondrial fusion and fission activity. In particular, because mitochondrial morphology is ultimately determined by a balance of

both fission and fusion activity, static pictures of mitochondrial networks are not sufficient to distinguish between the relative contributions of these two processes, despite an increasingly sophisticated set of tools to both generate and analyze these images.

Similar issues limit the utility of even the more robust and quantitative assays of mitochondrial connectedness. For example, the rate of diffusion of a mitochondria-targeted photo-activatable green fluorescent protein (mt-PA-GFP) throughout a mitochondrial network (Kashatus et al., 2015), or the recovery of fluorescence following photobleaching of a region of mitochondrial network, can both provide a quantitative measure of mitochondrial connectedness. However, these assays fail to distinguish the relative contributions of fusion and fission activity to these phenotypes.

To date, the only direct measure of either fusion or fission activity in cells is the Polyethylene glycol (PEG) fusion assay, which measures content mixing between separately labeled fluorescent mitochondria in two cells whose plasma membranes have been fused through the addition of PEG (Cipolat et al., 2004; Graves et al., 2012; Mattenberger et al., 2003). Initially utilized to induce fusion of plant protoplasts (Kao, 1974), treatment with PEG is a widely used method to fuse mammalian cells and has a variety of applications, including the generation of hybridomas (Kao, 1974; Wojcieszyn, 1983; Yang, 2006). In the PEG fusion assay, the degree of colocalization between the fluorescent mitochondrial proteins used in the two cells depends on the level of mitochondrial fusion activity and thus can be measured in a quantitative manner. However, there are several drawbacks to this approach as it is currently applied. First, the frequency of cell-cell fusion events following treatment with PEG is relatively low, and thus acquiring enough events for statistical analysis is a time-consuming and laborious process. Further, the need to manually search for fusion events to analyze under the microscope introduces a potential source of bias. To address these issues, we have developed a high throughput method to analyze and quantify mitochondrial fusion activity by fusing mito-YFP and

mito-DsRed expressing cells and performing imaging flow cytometry (IFC) via the Amnis ImagestreamX MKII (George et al., 2004). Through IFC, we are able to drastically reduce the time required to capture the total fusion events of a cell population in a given experiment. Through the colocalization wizard of the ImagestreamX data processing software, IDEAS®, we have generated a standardized method to quantify the colocalization of mitochondria in fused cell populations.

3.2 Results

3.2.1 Verification of Mitochondrial Morphology in MEF and HEK cells

To investigate the capability of IFC to detect colocalization of fused mitochondria, we generated separate fluorescently labeled sets of Mouse embryonic fibroblasts (MEF) and Human embryonic kidney (HEK) cells that would serve as control and experimental samples. As a negative control for mitochondrial fusion, we utilized MFN1 and MFN2 double knockout (MFN DKO) (Chen et al., 2003b) or OPA1 knockout MEFs (Song et al., 2007) that are expressing mitochondrially targeted YFP (mito-YFP) (Karbowski et al., 2002) or DsRed (mito-DsRed). As MFN1 and MFN2 are involved in the fusion of the outer mitochondrial membrane, their loss prevents mitochondrial fusion resulting in a fragmented mitochondrial morphology. Due to its role in inner mitochondrial membrane fusion, loss of OPA1 also results in mitochondrial fragmentation. We confirmed the loss of MFN1, MFN2 and OPA1 in the red and green labeled sets of MEFs by immunoblot (Figure 3.1A). As expected, the MFN DKO and OPA1 KO MEFs exhibit a fragmented, punctuate and perinuclear mitochondrial morphology indicative of their defect in mitochondrial fusion (Figures 3.1B and 3.1C). In addition to these fusion deficient controls, we established three additional cell lines that express a full complement of fusion machinery (Figure 3.1A) and display a range of mitochondrial morphologies. These include WT MEFs, which exhibit an intermediate mitochondrial morphology (Figure 3.1B) and immortalized HEK cells stably transduced with either an empty vector or flag-HRas^{G12V}. As we have previously shown (Kashatus et al., 2015), the HEK

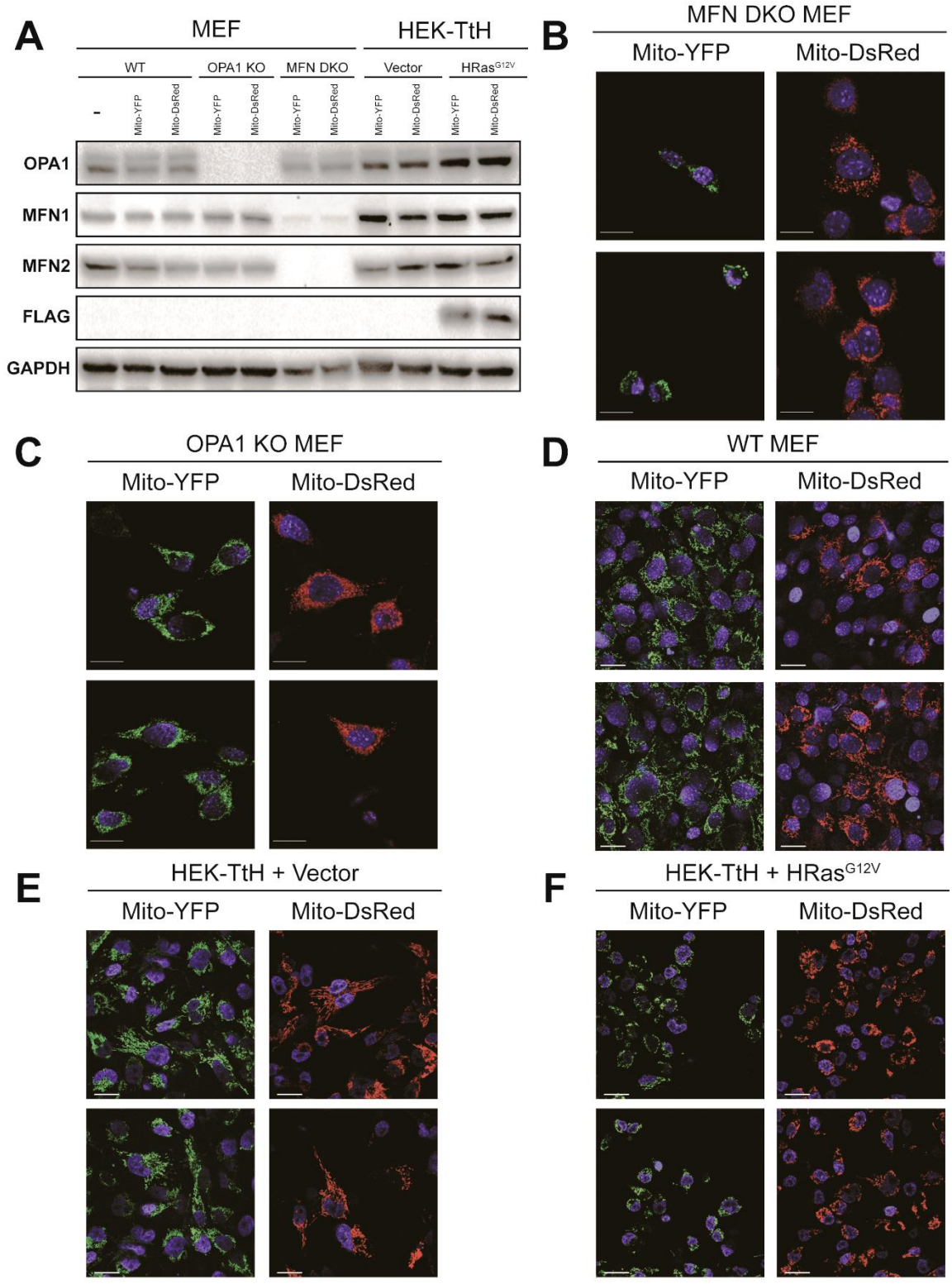
A
MEF
HEK-TtH
WT
OPA1 KO
MFN DKO
Vector
HRasG12V
-
Mito-YFP
Mito-DsRed
OPA1
MFN1
MFN2
FLAG
GAPDH
B
MFN DKO MEF
Mito-YFP
Mito-DsRed
C
OPA1 KO MEF
Mito-YFP
Mito-DsRed
D
WT MEF
Mito-YFP
Mito-DsRed
E
HEK-TtH + Vector
Mito-YFP
Mito-DsRed
F
HEK-TtH + HRasG12V
Mito-YFP
Mito-DsRed

Figure 3.1. Mitochondrial Morphology of MEF and HEK mito-YFP and mito Ds-Red cells. (A) Immunoblot analysis of the expression level of mitochondrial fusion machinery (OPA1, MFN1 and MFN2) as well as Flag-HRas^{G12V} in a panel of separately labeled fluorescent sets (mito-YFP or mito-DsRed) of MEF and HEK cells. GAPDH, loading control. (B-F) Mitochondrial morphologies of the panel of cells examined by immunoblot in (A). Green, mito-YFP; Red, mito-DsRed; Blue, DAPI. Scale bar, 20 μm.

vector alone cells display an intermediate mitochondrial morphology (Figure 3.1E) while $HRas^{G12V}$ cells exhibit a predominantly fragmented mitochondrial morphology characterized by small, punctate and perinuclear mitochondria (Figure 3.1F).

3.2.2 Mitochondrial Fusion Resolved via Confocal Microscopy

In order to confirm that the mitochondrial morphology of the MFN DKO and OPA1 KO MEFs is due to a defect in fusion activity and to explore the fusion activity in our experimental cell lines, we performed the classical PEG fusion assay between the respective red and green labeled subsets of these cells. Labeled cells were co-plated at a ratio of 1:1 red-to-green and treated with 50% PEG/DMEM for two minutes to induce cell-cell fusion followed by several washes and incubated at 37˚ for four hours. Analysis of the mitochondrial morphologies through laser scanning confocal microscopy resulted in expected phenotypes of the knockout MEFs. The OPA1 KO and MFN DKO cells exhibited negligible colocalization between red and green signals as demonstrated by distinct red and green puncta in the cytoplasm of fused cells (Figures 3.2A and 3.2B). Somewhat surprisingly, the WT MEFs display a low degree of colocalization between red and green signals as revealed by the presence of several red and green puncta surrounding colocalized signals (Figure 3.2C). These data suggest that WT MEFs have inherently low fusion activity. As expected, the vector expressing HEK cells demonstrated robust colocalization between red and green signals, indicating a high degree of fusion activity over the four hour time course (Figure 3.2D). In contrast, the $HRas^{G12V}$ expressing cells display reduced colocalization and an increased number of red and green puncta (Figure 3.2E), suggesting a decrease in mitochondrial fusion activity in the presence of mutated HRas. Collectively, these data confirm that colocalization of separately labeled green and red mitochondria in fused cells requires an intact set of mitochondrial fusion machinery and that these cell lines can serve as a suitable system in which to test the capability of IFC to analyze mitochondrial fusion in a quantitative and high-throughput manner.

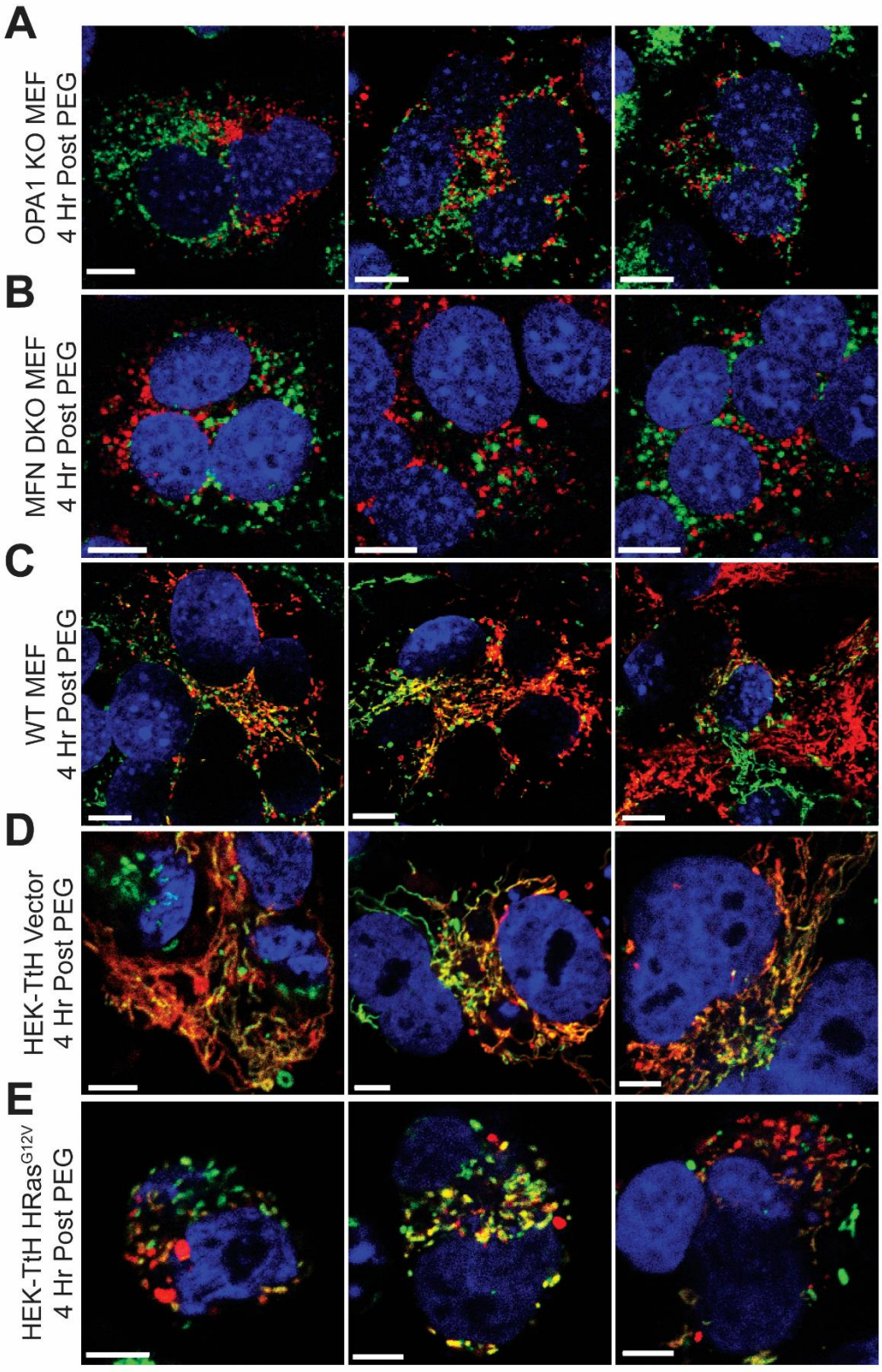
A
OPA1 KO MEF
4 Hr Post PEG
B
MFN DKO MEF
4 Hr Post PEG
C
WT MEF
4 Hr Post PEG
D
HEK-TtH Vector
4 Hr Post PEG
E
HEK-TtH HRas^{G12V}
4 Hr Post PEG

Figure 3.2. Confocal Microscopy 4 Hrs Post PEG Treatment of MEF and HEK cell lines. Mitochondrial morphologies of fused cells containing separate fluorescently labeled sets of OPA1 KO MEFs (A), MFN DKO MEFs (B), WT MEFs (C), HEK-TtH cells stably expressing either vector alone (D) or $HRas^{G12V}$ (E) after treatment with polyethylene glycol (PEG), obtained by laser scanning confocal microscopy. Each column represents a replicate image of the respective cell type. Cells were treated with 50% (wt/vol) PEG 1500/DMEM for 2 minutes, followed by incubation in 10% FBS/DMEM containing Cyclohexamide (33μg/mL) for 4 Hrs, fixed and analyzed by confocal microscopy. Green, mito-YFP; Red, mito-DsRed; Blue, DAPI. Scale bar, 10 μm.

3.2.3 High Throughput Analysis of Mitochondrial Fusion via IFC

Imaging flow cytometry via the ImagestreamX allows for high throughput analysis of a variety of cell characteristics and has only recently been utilized to study aspects of the mitochondria such as protein translocation and mitochondrial localization (Prowse et al., 2012; Wabnitz et al., 2010). We next sought to determine if we could apply the high throughput capability of IFC to characterize and quantify the extent of mitochondrial content mixing by measuring colocalization of mitochondrial fluorescent signals in fused cells. We collected 100,000 events for each cell type, except for the co-expressing YFP/DsRed HEK cells that served as the positive fusion control. We only collected 10000 events for individual mito-YFP and mito-DsRed compensation controls using either mito-YFP or mito-DsRed expressing MEF or HEK cells. Through the IDEAS® 6.0 software, we were able to identify the double positive YFP/DsRed fused cell populations for each cell type (Figure 3.3). Representative IFC images in four channels demonstrate the complete colocalization between YFP and DsRed for the HEK co-expressing cells (Figure 3.4A). As the negative control, we utilized the fusion deficient MFN DKO MEFs and performed the PEG fusion assay between mito-YFP and mito-DsRed expressing cells. Representative IFC images for these cells demonstrate the lack of colocalization between YFP and DsRed (Figure 3.4B). The images acquired by IFC also capture the mitochondrial morphology of the respective positive and negative controls. The HEK cells display a more intermediate mitochondrial morphology (Figure 3.4C) whereas the MFN DKO MEFs exhibit a fragmented, punctuate morphology (Figure 3.4D). Similar results were obtained for the OPA1 KO MEFs (Supporting Information Figure 3.S1). Through the IDEAS® colocalization wizard, we were able to acquire colocalization scores for the double positive populations of the positive and negative controls. For the positive control, the colocalization wizard provided a very high median score of 3.474 with 97.5% of the cell population falling in the colocalized range (Figure 3.4E). The remainder of the population, which didn't fall into the colocalized region, is most likely composed of cells that weren't efficiently transduced with either YFP or DsRed. For the negative control, the

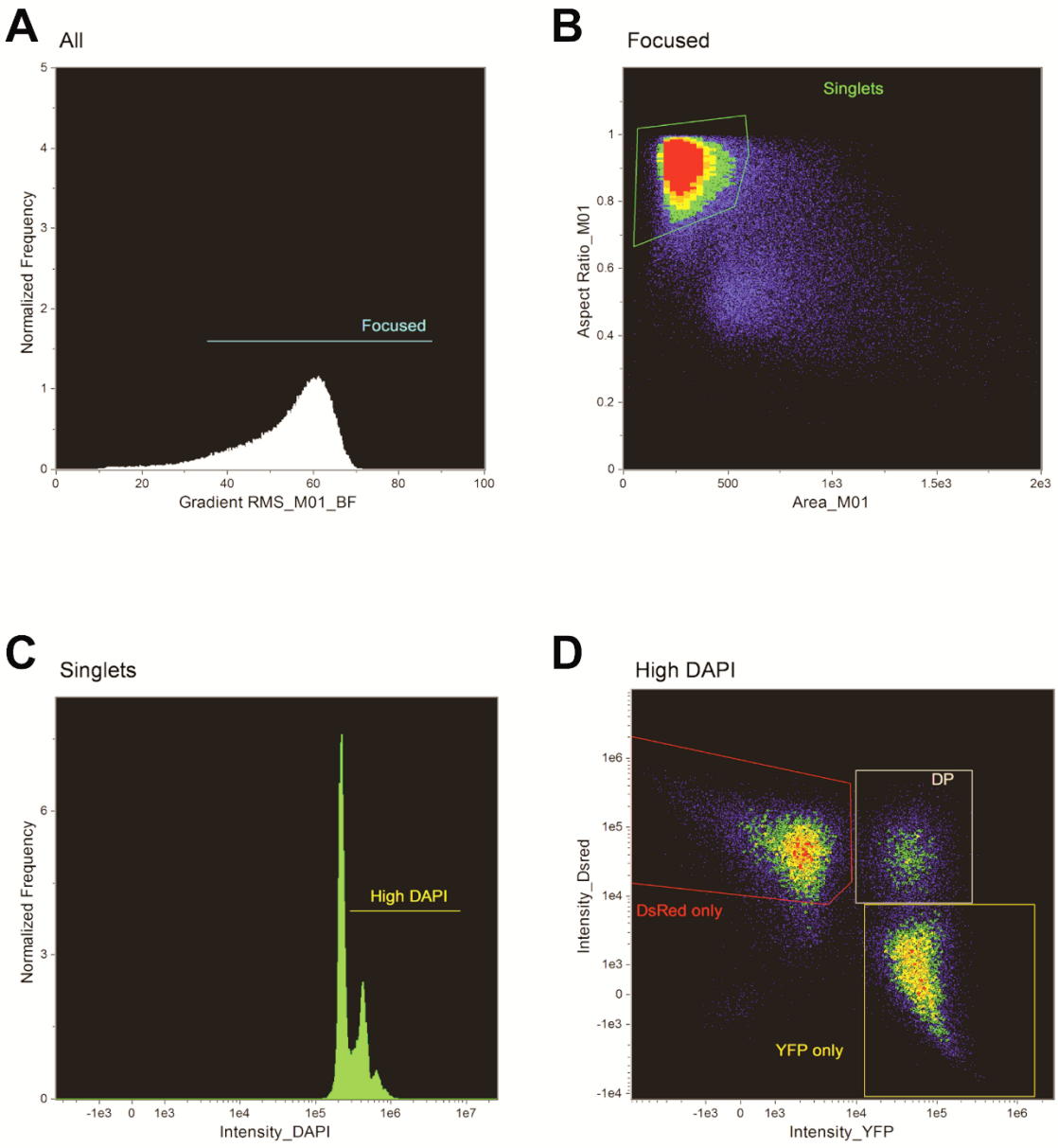
A
All
Normalized Frequency
Gradient RMS_M01_BF
Focused
B
Focused
Singlets
Aspect Ratio_M01
Area_M01
C
Singlets
Normalized Frequency
Intensity_DAPI
High DAPI
D
High DAPI
Intensity_Dsred
Intensity_YFP
DP
DsRed only
YFP only

Figure 3.3. Gating Strategy for identification of double positive Mito-YFP/Mito-DsRed fused cells in the IDEAS Software.

(A) Gating of focused cells according to the gradient RMS feature above 30 arbitrary units. (B) The single cells were gated based on their aspect ratio and area in the brightfield channel. (C) Gating of High DAPI expressing cells was based on high DAPI positivity according to DAPI fluorescence intensity. (D) Gating of the double positive mito-YFP/mito-DsRed expressing cells according to fluorescence intensity of YFP and DsRed.

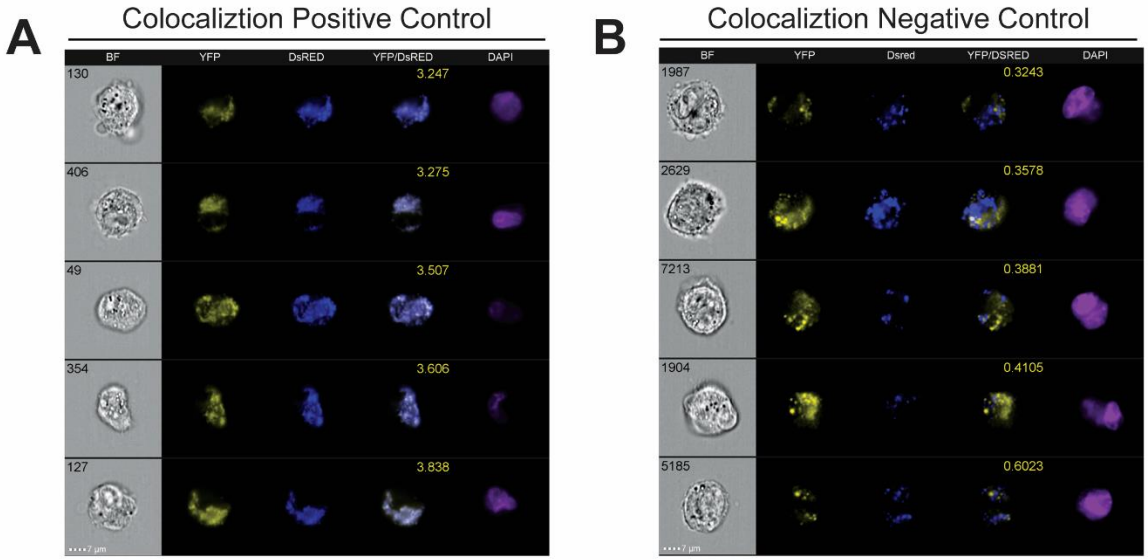

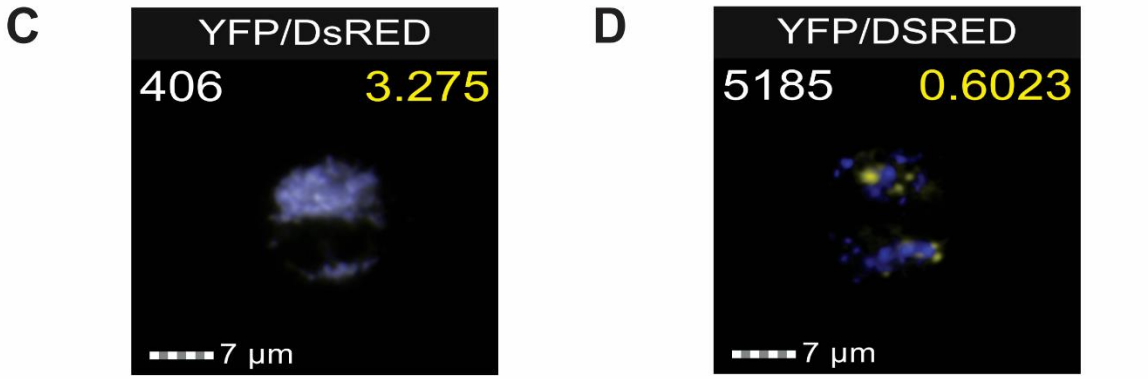

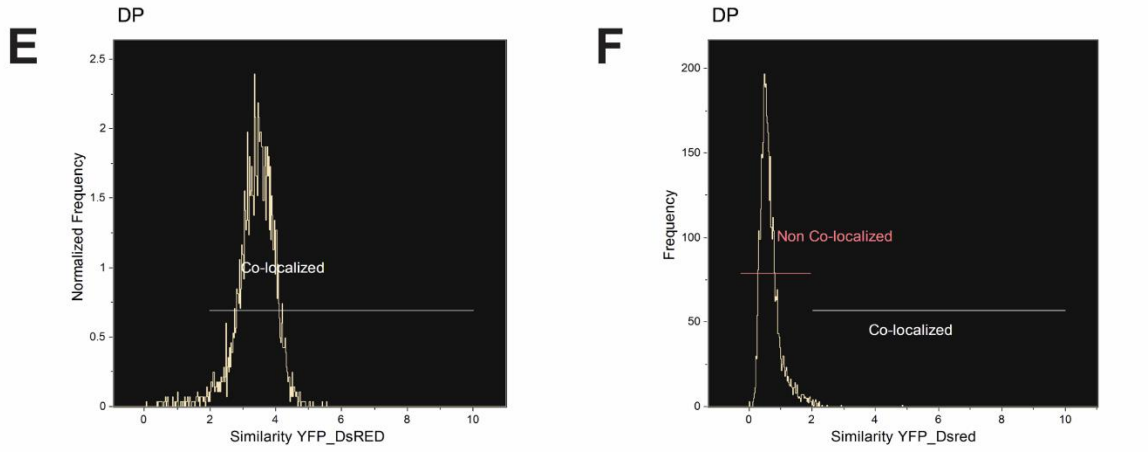

Similarity YFP_DsRED

Population	Count	%Gated	Median
DP & SINGLETS & FOCUSED	2838	100	3.459
Co-localized & DP & SINGLETS & FOCUSED	2768	97.5	3.474

Similarity YFP_Dsred

Population	Count	%Gated	Median
DP & High DAPI & Singlets & Focused	4086	100	0.5893
Co-localized & DP & High DAPI & Singlets & Focused	19	0.47	2.128
Non Co-localized & DP & High DAPI & Singlets & Focused	4061	99.4	0.5872

Figure 3.4. Establishment of colocalized and noncolocalized cutoffs based on Positive and Negative Mitochondrial Fusion Controls.

(A-B) Representative images of HEK-TtH co-expressing Mito-YFP and Mito-DsRed as the positive fusion control (A) or MFN DKO MEFs after PEG treatment as the negative fusion control(B). White number, Cell number; Yellow number, colocalization score. (C-D) Single merged YFP/DsRed Image of positive control (C) or negative control (D). (E-F) Histograms depicting the range of colocalization scores and statistics for the positive control (E) and negative control (F).

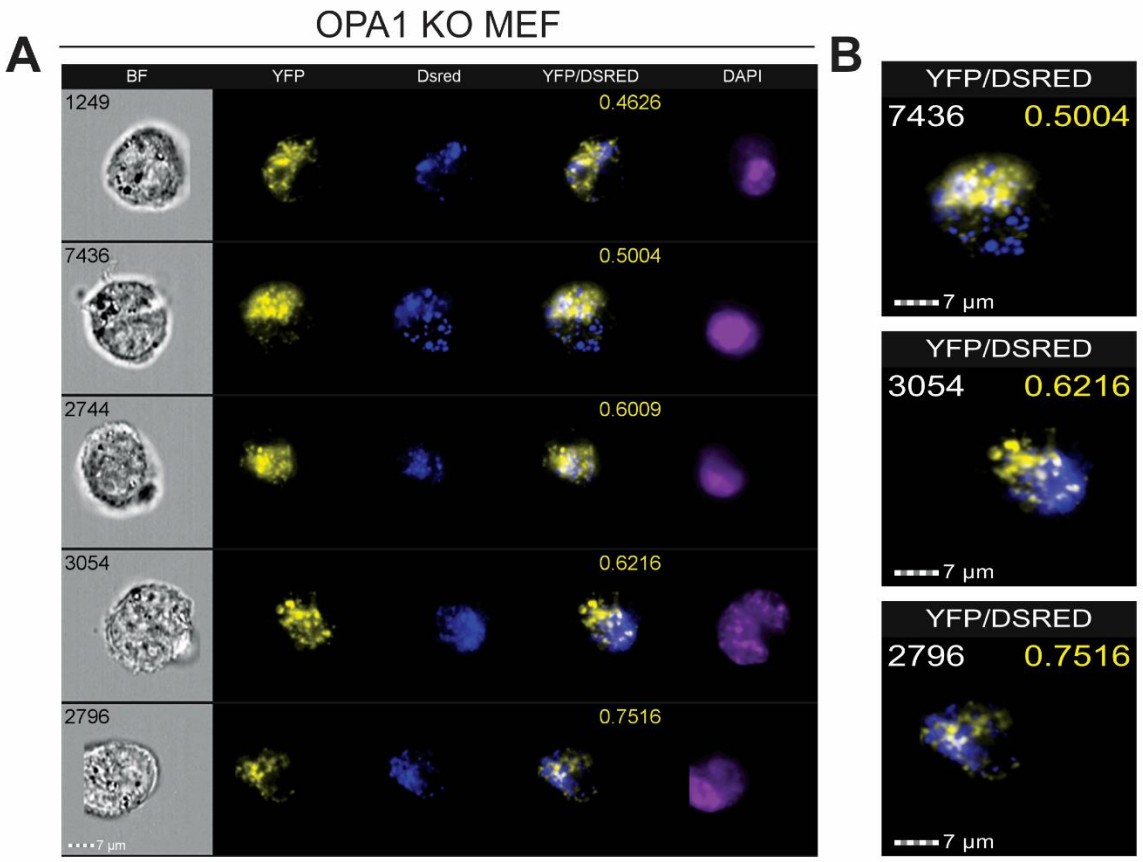

C

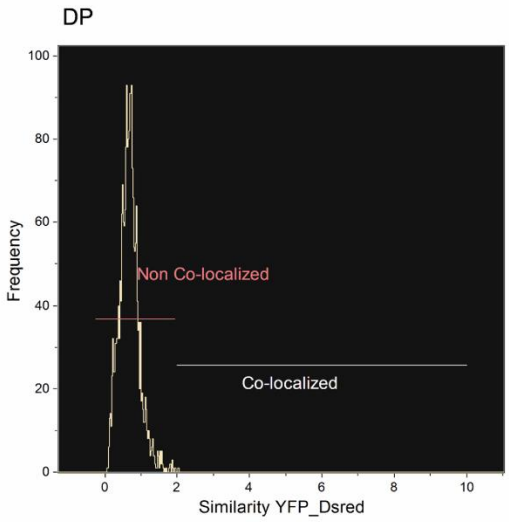

Similarity YFP_Dsred

Population	Count	%Gated	Median
DP & High DAPI & Singlets & Focused	2046	100	0.6641
Co-localized & DP & High DAPI & Singlets & Focused	2	0.1	2.036
Non Co-localized & DP & High DAPI & Singlets & Focused	2043	99.9	0.6637

Figure 3.S1. Establishment of colocalized and noncolocalized cutoffs based Negative Mitochondrial Fusion Controls.

(A-B) Representative images of OPA1 KO MEFs co-expressing Mito-YFP and Mito-DsRed as the negative fusion control after PEG treatment. White number, Cell number; Yellow number, colocalization score. (C) Histograms depicting the range of colocalization scores and statistics.

colocalization wizard produced a very low colocalization median value of 0.5872 for 99.4% of the double positive population, which we identified as non-colocalized (Figure 3.4F). The very small remainder of the cells (0.47%) fell outside the noncolocalized region with a median score of 2.128. Using these results a ≥ 2 cutoff was set for determining colocalization, based on the minimum range of the positive control and the maximum range of the negative control (Figure 3.4E and 3.4F). Taken together, these data demonstrate the ability of the IDEAS® software to generate expected colocalization values (high vs. low) of completely “fused” and fusion deficient mitochondrial populations.

In order to perform an initial test of IFC to measure colocalization in PEG treated cells where we were uncertain of the outcome, we performed the assay on WT MEFs (Figure 3.5). Consistent with the results from the classical PEG fusion analysis of this cell line, we observed a lack of mitochondrial fusion in the IFC images (Figure 3.5A and 3.5B). The merged YFP/DsRed images display distinct red and green signals over large areas within a single cell, suggesting a lack of mitochondrial mobility. Through colocalization analysis of the DP cell population, we found that the majority (96.4%) fell within the non-colocalized region with a median score of .4818 (Figure 3.5C), which matches the low level of colocalization seen in the IFC images (Figure 3.5A and 3.5B). The remaining colocalized population had a median score of 2.204.

3.2.4 Oncogenic Ras expressing cells have impaired Mitochondrial Fusion

Next, we wanted to use IFC to test the mitochondrial fusion capacity of our two HEK cell lines that displayed different mitochondrial fusion activity using the classical PEG fusion assay (Figures 3.2D-E). We have previously shown that expression of oncogenic HRas leads to robust mitochondrial fragmentation in HEK cells due to the upregulation of mitochondrial fission activity (Kashatus et al., 2015). Further, a mt-PA-GFP assay found that the mitochondria in cells expressing oncogenic HRas, but not vector control, remained punctate over an hour-long time course, suggesting a possible defect in their fusion activity (Kashatus et al., 2015). To further test

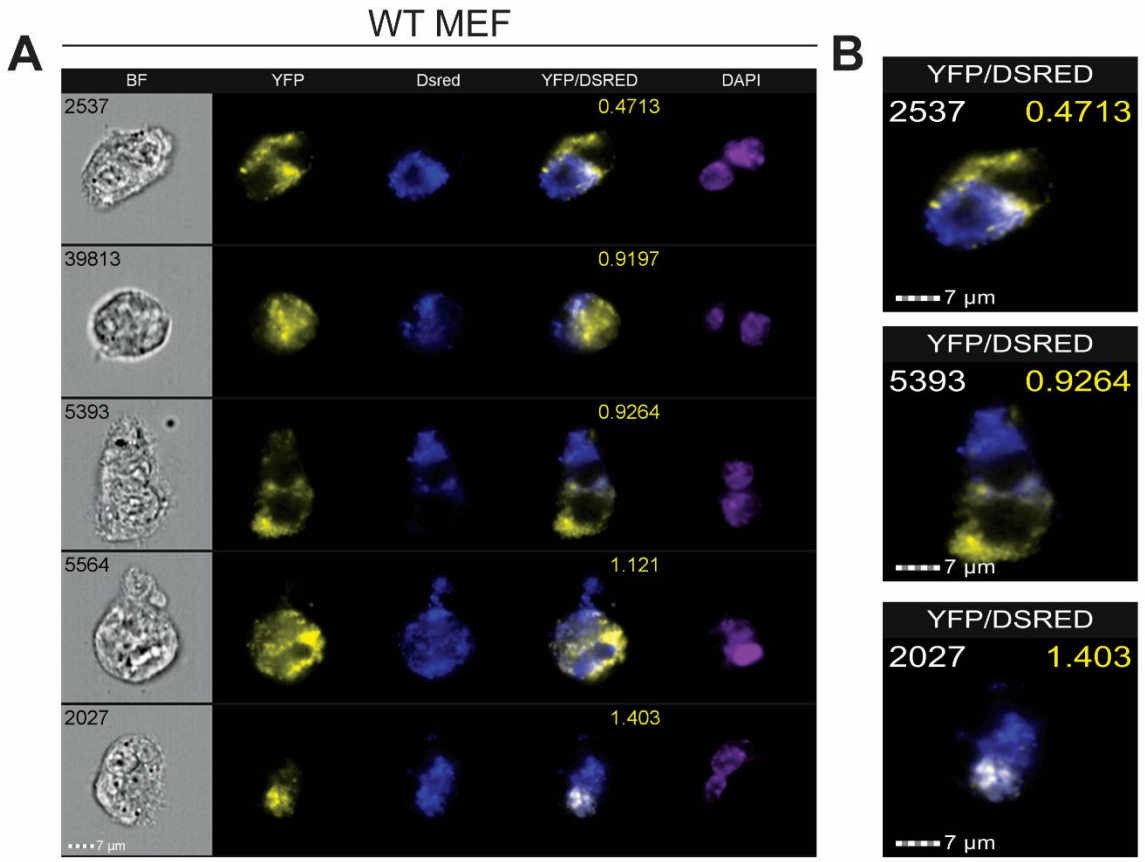

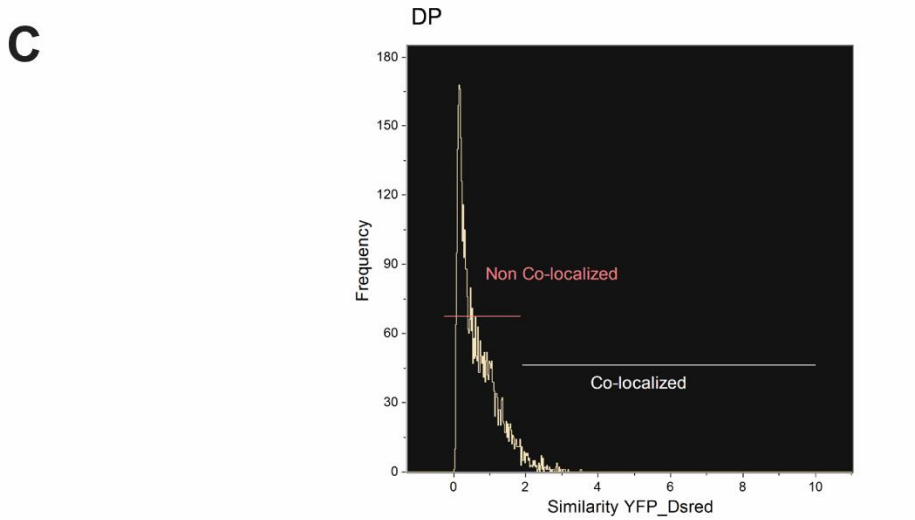

Similarity YFP_Dsred

Population	Count	%Gated	Median
DP & High DAPI & Singlets & Focused	4001	100	0.5096
Co-localized & DP & High DAPI & Singlets & Focused	130	3.25	2.204
Non Co-localized & DP & High DAPI & Singlets & Focused	3855	96.4	0.4818

Figure 3.5. Colocalization Scores for WT MEFs 4 Hrs Post PEG Treatment.

(A) Representative images in five channels of WT MEFs 4Hrs after PEG treatment. (B) Single merged YFP/DsRed images of individual WT MEFs for corresponding colocalization scores (yellow). (C). Histogram demonstrating the range of colocalization scores for the WT MEFs including percentages and median scores of populations in the colocalized and non-colocalized regions.

this hypothesis via IFC, we repeated the PEG fusion assay with the separately labeled HEK cells expressing empty vector or oncogenic $HRas^{G12V}$. We found that HEK cells expressing vector alone achieved a moderate degree of colocalization (Figure 3.6A) which was comparable to what we observed using confocal microscopy (Figure 3.2D). The $HRas^{G12V}$ cells displayed less colocalization in IFC images (Figure 3.6B), also matching what we observed using confocal microscopy (Figure 3.2E). Upon closer inspection of the IFC images (Figures 3.6C and 3.6D), we observe that the mitochondria of each cell type displayed similar mitochondrial morphology to what we observe in Figures 3.2D and 3.2E, respectively. These data suggest that the HEK cells are amenable to PEG treatment and are able to maintain their cellular composition after image capture via IFC. We then ran the colocalization wizard on the gated DP population. For the vector control cells, we obtained a distribution that favored the non-colocalized state (62.3%, median colocalization value 0.8241) versus colocalized (37%, median colocalization value 2.618) (Figure 3.6E). Given that mitochondria are dynamic organelles, these data align with what we would expect from a population of cells with an intermediate mitochondrial morphology in which the mitochondria are constantly undergoing varying degrees of fusion and fission. The $HRas^{G12V}$ cells displayed a distribution where a higher percentage of the fused cells fell within the non-colocalized population (67.9%) and had a lower median colocalization value (.7434) compared to the vector control cells. Conversely, the $HRas^{G12V}$ cells had a lower colocalized population (32.1%) with a lower median colocalization value (2.542) compared to the vector control cells (Figure 3.6F). These data suggest oncogenic HRas may be signaling to downregulate mitochondrial fusion activity. This loss of fusion activity may contribute to the extensive mitochondrial fragmentation observed in HEK $HRas^{G12V}$ cells where we have shown an upregulation of fission activity. This reciprocal regulation of fusion and fission suggests a bimodal role of oncogenic Ras in mediating mitochondrial dynamics. Taken together, these data validate IFC as a viable high-throughput tool to detect and quantify mitochondrial fusion in mammalian cells.

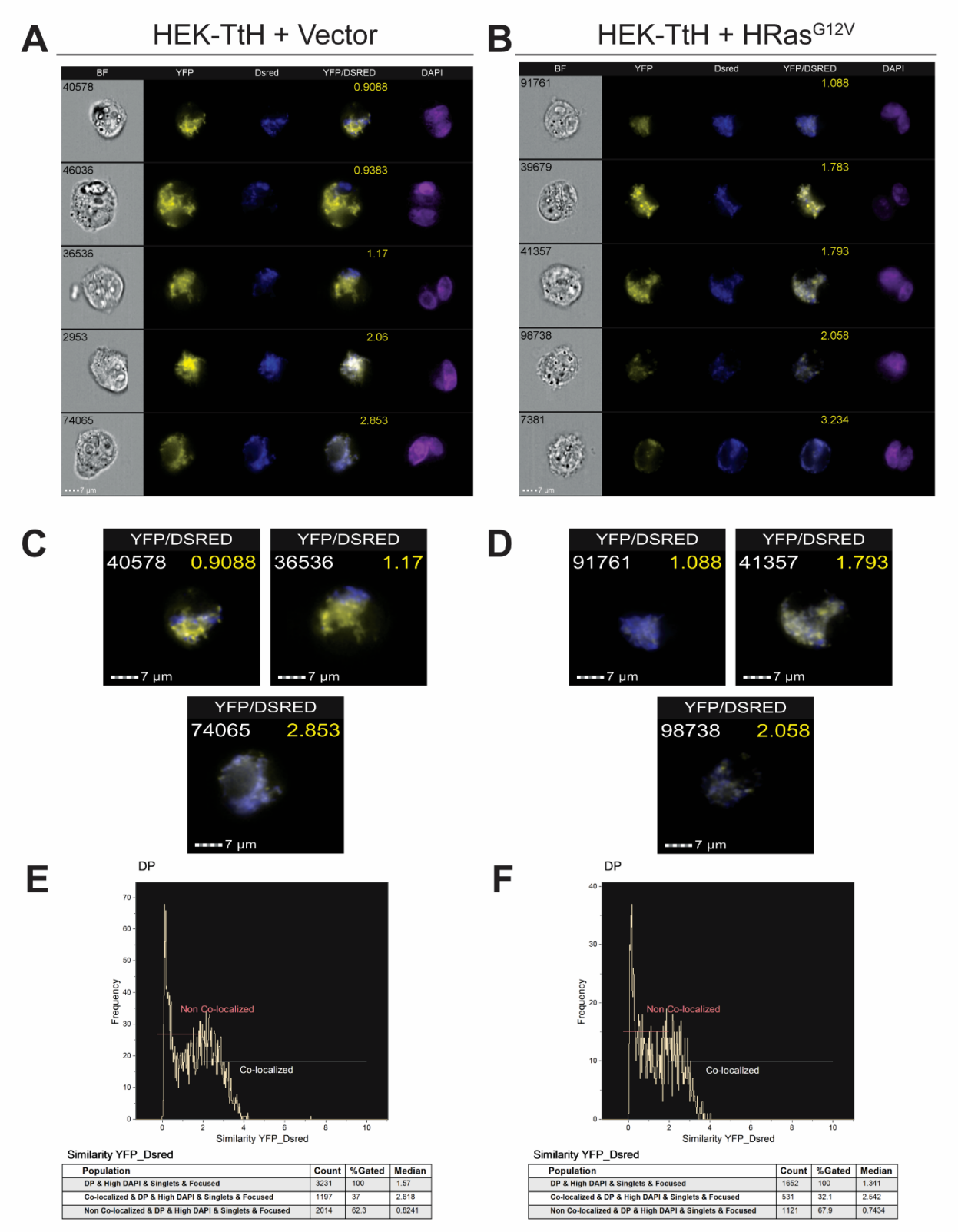
A
HEK-TtH + Vector
BF
YFP
Dsred
YFP/DSRED
DAPI
40578
0.9088
46036
0.9383
36536
1.17
2953
2.06
74065
2.853
7 µm
B
HEK-TtH + HRasG12V
91761
1.088
39679
1.783
41357
1.793
98738
2.058
7381
3.234
C
YFP/DSRED
40578 0.9088
36536 1.17
74065 2.853
D
YFP/DSRED
91761 1.088
41357 1.793
98738 2.058
E
DP
Frequency
Non Co-localized
Co-localized
Similarity YFP_Dsred
Similarity YFP_Dsred
Population | Count | %Gated | Median
DP & High DAPI & Singlets & Focused | 3231 | 100 | 1.57
Co-localized & DP & High DAPI & Singlets & Focused | 1197 | 37 | 2.618
Non Co-localized & DP & High DAPI & Singlets & Focused | 2014 | 62.3 | 0.8241
F
DP
Frequency
Non Co-localized
Co-localized
Similarity YFP_Dsred
Similarity YFP_Dsred
Population | Count | %Gated | Median
DP & High DAPI & Singlets & Focused | 1652 | 100 | 1.341
Co-localized & DP & High DAPI & Singlets & Focused | 531 | 32.1 | 2.542
Non Co-localized & DP & High DAPI & Singlets & Focused | 1121 | 67.9 | 0.7434

Figure 3.6. Colocalization Scores for HEK-TtH Vector and HEK-TtH HRas^{G12V} 4 Hrs Post PEG Treatment.

(A-B) Representative images in five channels of HEK-TtH Vector (A) and HRas^{G12V} cells (B) 4 Hrs after PEG treatment. (C-D) Merged YFP/DsRed images of single cells spanning a range of colocalization scores (yellow) for HEK-TtH Vector (C) and HRas^{G12V} cells (D). (E-F) Histograms illustrating the range of colocalization scores for the Vector alone expressing cells (E) and HRas^{G12V} cells including percentages and median scores of populations in the colocalized and noncolocalized regions.

3.3 Discussion

Mitochondrial fusion and fission are increasingly recognized to regulate several important physiological processes, especially in the context of human disease. Indeed, several studies have established a connection between the dysregulation of mitochondrial dynamics and the pathology of diseases as diverse as Alzheimer's disease (Dupuis, 2013), Parkinson's disease (Rakovic, 2011), diabetes (Gordon, 2015) and cancer (Grandemange et al., 2009). Recently we have shown that oncogenic Ras signaling promotes mitochondrial fragmentation and contributes to tumor growth(Kashatus et al., 2015). These studies underscore the importance of establishing novel high throughput methods to evaluate not just static mitochondrial morphology, but the activity of both mitochondrial fission and mitochondrial fusion machinery in intact cells. Indeed, methods have already been developed to quantify mitochondrial morphology utilizing high-content wide-field fluorescent microscopy in combination with semi-automated data analysis (Leonard et al., 2015). Leonard and colleagues employ automated wide-field fluorescence microscopy to initially capture mitochondrial images from live cells followed by "preprocessing" to enhance fluorescent signal from their images and utilize a machine-learning based algorithm to classify mitochondrial morphologies into four different subtypes. Consequently, they are able to determine changes in distributions of mitochondrial morphologies as a result of treatment with drugs that impair mitochondrial function (Leonard et al., 2015). While developing new methods to quantify changes in mitochondrial morphology, which are vital for proper cellular function, remain an integral part of biological research, there still remains a lack of high throughput methods to directly measure and quantify mitochondrial fusion activity.

Mitochondrial fusion activity can be measured using the PEG fusion assay in which content mixing of separately labeled fluorescent mitochondria in fused cells is used as a readout for mitochondrial fusion activity. The major drawback of this method is that it has traditionally relied on confocal microscopy to survey fusion events and is thus time-consuming and subject to

bias. Furthermore, given the low occurrence of cell-cell fusion events following PEG treatment, it is difficult to collect the number of fusion events required to achieve statistical rigor.

The application of IFC to examine mitochondrial fusion activity provides a high throughput method to automate the acquisition of double positive cell-cell fusion events with which to subsequently analyze colocalization. The colocalization can be assessed in an objective manner as the IDEAS® 6.0 colocalization wizard can measure colocalization of entire mitochondrial networks on a per cell basis. We have demonstrated the ability to acquire expected colocalization scores for cell types that should have low colocalization due to loss of mitochondrial fusion activity (OPA1 KO and Mfn1/2 DKO) and for cells that should have high colocalization due to co-expression of mito-YFP and mito-DsRed. However, one caveat to the technique may be that the colocalization wizard is unable to distinguish the colocalization of healthy vs. dying cell populations, which will have differing mitochondrial dynamics. This may result in attributing colocalization to non-distinct mitochondrial signals. In future experiments, we may be able to utilize a viability dye such as the LIVE/DEAD® Fixable Far Red Stain (Thermo Fisher Scientific) to segregate live cells from dead cells without fluorescence bleed-through into the DAPI, YFP and DsRed channels already utilized by our assay. Another drawback of the application of IFC to measure mitochondrial fusion is that our gating strategy could not eliminate 100% of the false positive fused double positive cells. These are instances in which a red labeled cell and a green labeled cell have not fused together, but are within close enough proximity to each other to exhibit an aspect ratio and DAPI content to be falsely identified as a cell fusion event with noncolocalized mitochondrial signal. The prevalence of these contaminating events was fairly low, however they may result in the overestimation of the noncolocalized population designated by the colocalization wizard. In an attempt to diminish the contribution of falsely identified fused cells, we utilized the IDEAS® 6.0 software's Feature Finder wizard to identify the parameters that could segregate these falsely identified fused cells by defining true sets of cells that contain two distinct nuclei

within a single cell. The Feature Finder identified the features “Nuclear Aspect Ratio” and “Nuclear Symmetry2 Object (M07, Ch07, tight)” as being able to segregate the true fused cells from those that were not. When the truth sets were overlaid on the “Nuclear Aspect Ratio” vs. “Nuclear Symmetry2 Object (M07, Ch07, tight)” plot, a gate was drawn on the events that fell within the region defined by the truth set depicting two nuclei within a single cell membrane, which we defined as “High DAPI & Multi-Nuclei”. We attempted to verify this gate for single, multinucleated cells in the brightfield image by the presence of two nuclei within a continuous cell membrane/cytoplasm. Upon further inspection, we continued to find cells within the gate that appeared to be two cells/nuclei close together with a high aspect ratio, so we proceeded with our original gating strategy in order to obtain a more robust number of events for analysis. The colocalization scores from our original gating strategy and the “High DAPI & Multi-Nuclei” gating strategy were very similar, implying minimal impact of these contaminating events on the final results. Thus, through our original gating strategy (Figure 3.3) we were able to test the mitochondrial fusion capacity of WT MEFs as well as that of cells transformed with oncogenic Ras. We determined that Ras transformed cells had impaired fusion activity compared to vector control cells which suggests that oncogenic Ras may be able to signal to fusion machinery in order to moderately downregulate mitochondrial fusion.

In conclusion, we validate IFC as a viable high throughput tool to detect and measure PEG-mediated mitochondrial fusion activity in mammalian cells. This technique will become invaluable as we seek to unravel the intricacies of mitochondrial dynamics and to understand how the interplay of fusion and fission are regulated in a variety of human diseases.

Chapter 4: Drp1 promotes KRas-driven metabolic changes and pancreatic tumor growth.

**This chapter is adapted from Nagdas et al., manuscript under revision*

4.1 Introduction

Pancreatic ductal adenocarcinoma (PDAC) is the fourth leading cause of cancer-related death in the US (Siegel et al., 2018). With predicted increases in PDAC incidence over the next decade and a 5-year survival rate of approximately 8%, it is projected to be the second leading cause by 2030 (Rahib et al., 2014; Siegel et al., 2018). Up to 90% of PDAC cases harbor an oncogenic *RAS* mutation, almost exclusively in the *KRAS* isoform (Bardeesy and DePinho, 2002; Cox et al., 2014; Ryan et al., 2014). Mutations in the gene encoding KRas render it constitutively GTP-bound, resulting in activation of its downstream effector pathways, including MAPK, PI3K, and RalGDS (di Magliano and Logsdon, 2013; Eser et al., 2014; Pylayeva-Gupta et al., 2011; Shields et al., 2000; Ying et al., 2016; Zeitouni et al., 2016). Activation of these pathways initiates a variety biological processes critical for tumor growth, including cellular growth, proliferation, inhibition of apoptosis and evasion of immune destruction (Hanahan and Weinberg, 2011; Pylayeva-Gupta et al., 2011). In addition, activation of KRas and its effectors promotes metabolic reprogramming in a number of cancers, including PDAC (Cohen et al., 2015; Kimmelman, 2015). For example, oncogenic KRas signaling induces glucose uptake and glycolysis in PDAC in part through activation of the MAPK pathway (Gaglio et al., 2011; Ying et al., 2012). KRas-induced glucose uptake promotes a number of anabolic process essential for cellular growth such as hexosamine and ribose biosynthesis (Ying et al., 2012). In addition, oncogenic KRas promotes a non-canonical use of glutamine for redox homeostasis (Son et al., 2013) and KRas-driven PDAC cells exhibit increased macropinocytosis, allowing them to scavenge extracellular proteins as a source of amino acids (Commisso et al., 2013; Kamphorst et al., 2015). Further, KRas-driven cancer cells utilize autophagy to recycle and restore TCA cycle metabolic intermediates needed for both anabolic and bioenergetics processes (Guo et al., 2011; Yang et al., 2011).

Mitochondria are major hubs of metabolic regulation. Notably, we and others previously demonstrated that oncogenic Ras signaling promotes mitochondrial fragmentation through Erk2-mediated phosphorylation of the large mitochondrial fission GTPase Dynamin-related protein 1 (Drp1) (Kashatus et al., 2015; Serasinghe et al., 2015). Furthermore, we showed that Drp1 expression is necessary for Ras-induced transformation and Ras-driven tumor growth, indicating that Drp1-dependent mitochondrial fragmentation is a critical biological process for Ras/MAPK-mediated tumorigenesis (Kashatus et al., 2015; Serasinghe et al., 2015). Consistent with this, PDAC cell lines and patient samples with hyperactive Ras/MAPK signaling exhibit activated Drp1 and mitochondrial fragmentation, indicating this pathway is physiologically prevalent *in vivo* (Kashatus et al., 2015).

The link between Ras and Drp1-dependent mitochondrial fission joins a growing list of studies connecting oncogenic signaling and mitochondrial biology (Kashatus, 2017; Trotta and Chipuk, 2017; Vyas et al., 2016). A common theme of many of these studies is the dysregulation of mitochondrial morphology and dynamics in a variety of tumor types. Mitochondrial network morphology is maintained through the opposing processes of fusion, mediated by the large GTPases Mitofusin 1 and 2 (Mfn1 and 2) and Optic Atrophy 1 (Opa1), and fission, mediated by Drp1 (Chen and Chan, 2004; van der Bliek et al., 2013). Shifts in the balance of mitochondrial fusion and fission impact mitochondrial function, which can have numerous cell physiological consequences important for tumor growth (Scatena, 2012; Vyas et al., 2016). For example, manipulation of mitochondrial morphology can directly impact cell proliferation (Kashatus et al., 2011; Qian et al., 2012; Taguchi et al., 2007), apoptosis (Martinou and Youle, 2011; Sheridan and Martin, 2010) and metabolism (Roy et al., 2015; Wai and Langer, 2016).

In this study, we sought to investigate the physiological role of Drp1-dependent mitochondrial fragmentation in models of cellular transformation and pancreatic cancer that are driven by endogenous expression of oncogenic KRas. We find that Drp1 is required for KRas-

mediated cell proliferation and cellular transformation in mouse embryonic fibroblasts (MEFs). Mechanistically, Drp1 promotes KRas-induced glycolysis via regulation of the glycolytic enzyme hexokinase-2. In a genetically engineered model of pancreatic cancer, genetic deletion of Drp1 leads to a significant survival advantage over littermates with wildtype Drp1. In addition, we observe a strong selective pressure against loss of Drp1 in KRas-driven murine pancreatic cancer, further demonstrating its importance. Interestingly, tumors that ultimately arise in the absence of Drp1 exhibit profound metabolic reprogramming. Not surprisingly these tumor cells re-express hexokinase-2 and restored glycolytic flux. In addition, Drp1 null tumor cells appear to increase the catabolism of lipids to make up for decreased efficiency of fatty acid oxidation. Collectively, these results indicate that Drp1 is a critical component of KRas-driven metabolic reprogramming and suggest Drp1 inhibition may provide a therapeutic benefit to pancreatic cancer patients.

4.2 Results

4.2.1 Drp1-dependent HK2 expression and glycolysis contribute to KRas-driven cellular transformation

Our previous studies demonstrated that Drp1 is required for subcutaneous tumor growth driven by exogenous expression of $HRas^{G12V}$ (Kashatus et al., 2015). Given the distinct biological roles of HRas and KRas (Hobbs et al., 2016) and the different physiological outcomes of exogenous versus endogenous expression oncogenic Ras (DeNicola et al., 2011), we sought to determine the biological role of Drp1 in the setting of oncogenic KRas. To that end, we isolated mouse embryonic fibroblasts (MEFs) from *Trp53*$^{flox/flox}$ (P), *Kras*$^{LSL\text{-}G12D/+}$; *Trp53*$^{flox/flox}$ (KP), or *Kras*$^{LSL\text{-}G12D/+}$; *Trp53*$^{flox/flox}$; *Drp1*$^{flox/flox}$ (KPD) mice and treated the fibroblasts with adenoviral Cre to induce recombination. Using serial dilution, we isolated clonal cell lines that were $p53^{-/-}$ (P), $KRas^{G12D/+}$; $p53^{-/-}$ (KP), or $KRas^{G12D/+}$; $p53^{-/-}$; $Drp1^{-/-}$ (KPD) (Figure 4.1A). Consistent with our observations in $HRas^{G12V}$-expressing HEK cells (Kashatus et al., 2015), expression of oncogenic

$KRas^{G12D}$ promotes a fragmented mitochondrial morphology (compare P to KP), that reverts to a more connected morphology upon deletion of Drp1 (KPD) (Figure 4.1B).

To determine whether Drp1 contributes to $KRas^{G12D}$-induced cell proliferation, we performed cell counts on MEFs under standard culture conditions. While KP MEF exhibit robust cellular expansion *in vitro*, deletion of Drp1 reduces cell expansion to the levels of the $KRas^{WT}$ MEFs (Figure 4.1C). Identical results were obtained when cell expansion was measured after 24 hours of culture using CellTiter-Glo (Figure 4.1D). Importantly, these effects are observed in two independent sets of clonal cell lines (Figure 4.S1A). Consistent with these effects on proliferation, deletion of Drp1 leads to a loss of KRas-induced soft agar colony formation in both sets of MEFs (Figure 4.1E, Figure 4.S1B). Importantly, re-expression of isoform 2 of murine Drp1 in KPD MEFs rescues colony formation (Figure 4.S1, C and D). Collectively, these data demonstrate that Drp1 is necessary for oncogenic KRas-driven cellular transformation and cell accumulation.

Although a number of potential mechanisms could account for the requirement of Drp1 in KRas-driven transformation, we initially focused on altered metabolism since mitochondria are integral to metabolic regulation. Interestingly, despite regular media changes, we consistently observe differences in media acidification between the cell lines growing in soft agar, indicative of potential differences in glycolytic flux. Specifically, we noted that the media of the KP MEFs quickly becomes acidic (yellow color) while the KPD MEFs appear to maintain a more neutral pH, similar to the P cells (Figure 4.1F). To test how expression of oncogenic Ras and Drp1 impact glycolytic flux, we performed a Glycolysis Stress Test using the Seahorse XF24 Extracellular Flux Analyzer. Consistent with the observed media color changes, we found that glucose-induced extracellular acidification rate (ECAR) and maximal ECAR increase in KP MEFs compared with the P cells (Figure 4.1G, Figure 4.S1E). Furthermore, deletion of Drp1 decreases both glucose-induced and maximal ECAR, suggesting that Drp1 is required for KRas-induced increases in

glycolytic flux (Figure 4.1G, Figure 4.S1E). Interestingly, rescuing Drp1 expression in the KPD MEFs is sufficient to rescue the glycolytic flux to levels seen in KP MEFs (Figure 4.S1F).

KRas can increase glycolytic flux through a variety of mechanisms, including upregulation of glucose transporters (Ying et al., 2012; Yun et al., 2009) and upregulation of hexokinase activity (Patra et al., 2013). Hexokinase-2 (HK2), one of the rate-limiting enzymes of glycolysis, localizes to the mitochondrial outer membrane and is constitutively active in KRas-driven cancers (Patra et al., 2013; Pedersen, 2007). Notably, $KRas^{G12D}$ expression induces a substantial increase in HK2 protein levels that is significantly decreased upon deletion of Drp1 (Figure 4.1, H and I). This loss in HK2 expression appears to be, at least in part, due to decreases in HK2 transcript, as we observe a similar decrease in HK2 mRNA levels in both sets of KDP MEFs by quantitative PCR (Figure 4.S1G).

To determine whether Drp1-dependent regulation of HK2 is sufficient to account for the glycolytic phenotype we observe, we stably overexpressed HK2 in KPD MEFs (Figure 4.1J). Re-expression of HK2 rescues both the glucose-induced- and maximal ECAR to the levels observed in KP cells, suggesting that the loss of HK2 expression is sufficient to explain the loss of glycolytic flux (Figure 4.1K). Next, to determine whether this loss in glycolysis is sufficient to account for the loss of transformation in the KPD MEFs we repeated the soft agar assays and found that overexpression of HK2 in KPD MEFs partially rescues the soft agar growth (Figure 4.1L). Together these data demonstrate that Drp1-dependent regulation of HK2 is required for the $KRas^{G12D}$-induced increase in glycolytic flux and furthermore, this KRas-Drp1-HK2 axis contributes to $KRas^{G12D}$-mediated cellular transformation.

4.2.2 Loss of Drp1 inhibits pancreatic ductal adenocarcinoma progression

To test whether the requirement for Drp1 for KRas-induced transformation extends to an *in vivo* setting, we crossed *Kras*$^{LSL\text{-}G12D/+}$; *Trp53*$^{flox/flox}$; *Pdx-1-CreER*$^{Tg/+}$ mice

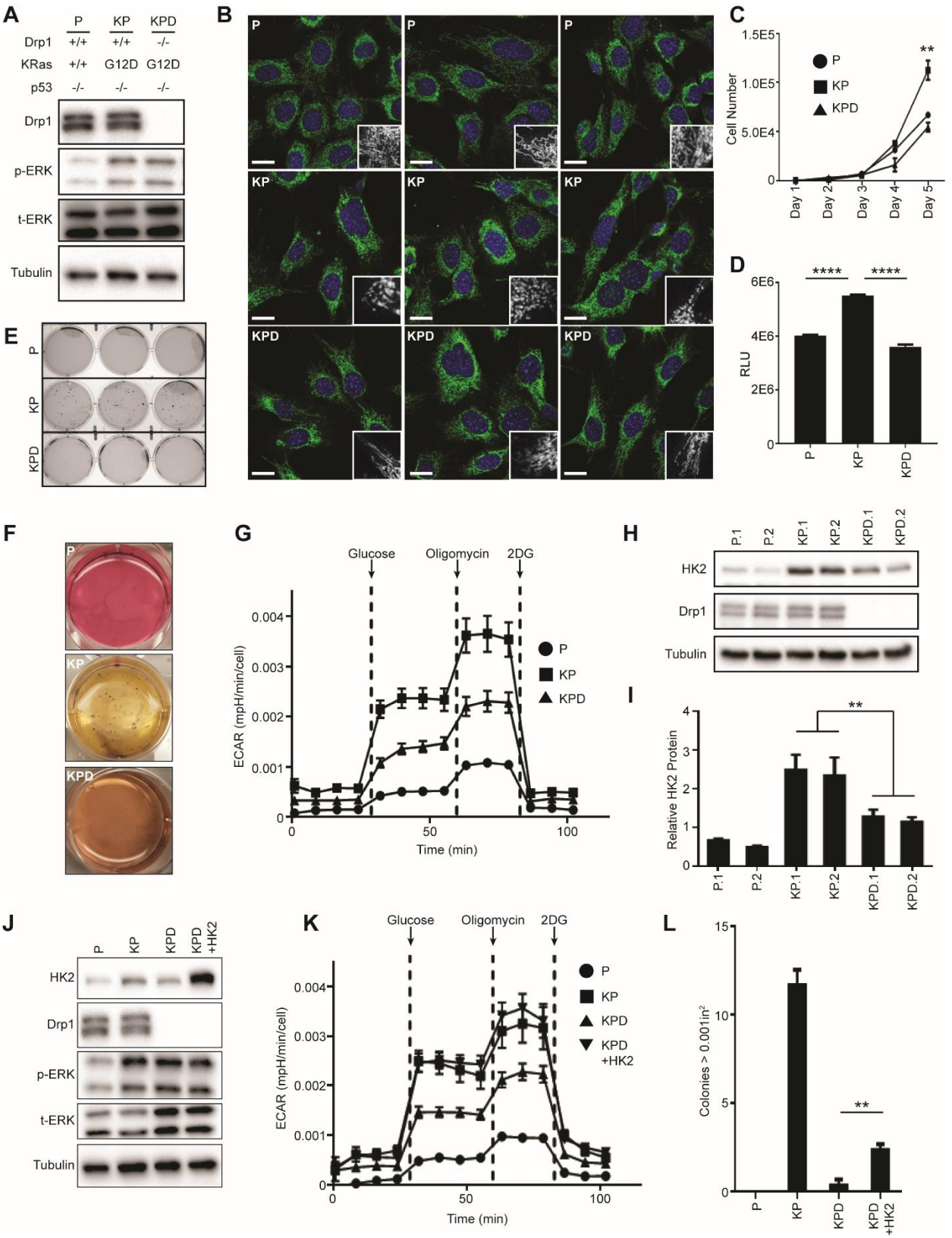
A
P
KP
KPD
Drp1 +/+ +/+ -/-
KRas +/+ G12D G12D
p53 -/- -/- -/-
Drp1
p-ERK
t-ERK
Tubulin
B
P
KP
KPD
C
Cell Number
1.5E5
1.0E5
5.0E4
0
Day 1
Day 2
Day 3
Day 4
Day 5
**
D
RLU
6E6
4E6
2E6
0
****
****
E
F
G
Glucose
Oligomycin
2DG
ECAR (mpH/min/cell)
Time (min)
H
P.1
P.2
KP.1
KP.2
KPD.1
KPD.2
HK2
Drp1
Tubulin
I
Relative HK2 Protein
**
J
P
KP
KPD
KPD +HK2
HK2
Drp1
p-ERK
t-ERK
Tubulin
K
Glucose
Oligomycin
2DG
ECAR (mpH/min/cell)
Time (min)
P
KP
KPD
KPD +HK2
L
Colonies > 0.001in²
**

Figure 4.1. Drp1-dependent HK2 expression and glycolysis contribute to KRas-driven cellular transformation.

(A) Immunoblot analysis of Drp1, phosphorylated Erk (p-Erk) and total Erk (t-Erk) in mouse embryonic fibroblasts (MEFs) with the following genotypes: $p53^{-/-}$ (P), $KRas^{G12D/+}$; $p53^{-/-}$ (KP) and $KRas^{G12D/+}$; $p53^{-/-}$; $Drp^{-/-}$ (KPD). Tubulin = loading control. **(B)** Representative immunofluorescence staining of mitochondrial morphology in the indicated MEFs stained with Tom20 (mitochondria, green) and DAPI (nuclei, blue). Scale bars, 20 μm. Insets, mitochondria zoom. **(C and D)** The indicated cell lines were seeded at equal density and cells were counted daily over a five-day period (**C**, n=3 replicates per cell line, representative result from one of three independent experiments, mean ± SEM, **P<0.01, one-way ANOVA with Tukey's multiple comparison) or analyzed by CellTiter Glo after 24 hours in culture **(D**, n=3 replicates per cell line, representative result from one of four independent experiments, mean ± SEM, ****P<0.0001, one-way ANOVA with Tukey's multiple comparison). **(E and F)** Equal numbers of the indicated cells lines were seeded in soft agar and imaged after 3 weeks (**E**, n=3). Prior to cell staining, wells were imaged to analyze media color (**F**). **(G)** The extracellular acidification rate (ECAR) was analyzed on the indicated MEF lines over a 100-minute time course. Glucose, oligomycin and 2-DG were added at the indicated time points (n=3 replicates per cell line, representative result from one of three independent experiments). **(H and I)** Immunoblot analysis **(H)** and quantitation **(I)** of Hexokinase 2 (HK2) and Drp1 expression in the indicated MEFs (n=3 independent experiments, data are mean ± SEM, **P<0.01, one-way ANOVA with Tukey's multiple comparison **(**cell lines grouped together by genotype)). Tubulin = loading control. **(J)** Immunoblot analysis of HK2, Drp1, p-Erk and t-Erk expression in the indicated MEFs. Tubulin = loading control. **(K)** ECAR was analyzed on the indicated MEF lines over a 100-minute time course (n=3 replicates per cell line, representative result from one of three independent experiments). **(L)** Equal numbers of the indicated cells lines were seeded in soft

agar, and after 3 weeks cell colonies were stained and colonies > 0.001 in^2 were counted (n=3 replicates per cell line, representative result from one of three independent experiments, Data are mean ± SEM. **P<0.01, two-way ANOVA with Tukey's multiple comparison).

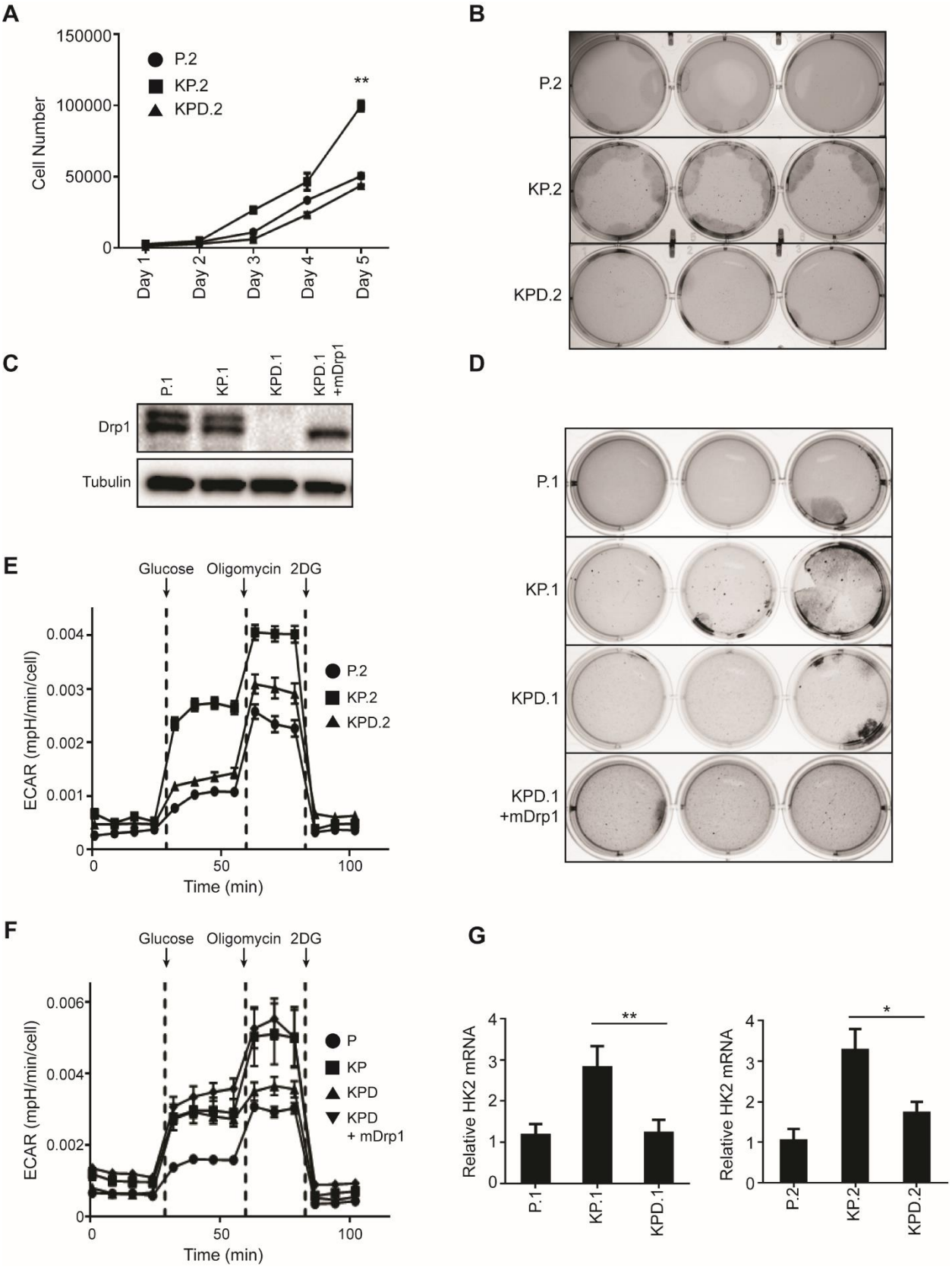
A
150000
100000
50000
0
Cell Number
P.2
KP.2
KPD.2
**
Day 1
Day 2
Day 3
Day 4
Day 5
B
P.2
KP.2
KPD.2
C
P.1
KP.1
KPD.1
KPD.1 +mDrp1
Drp1
Tubulin
D
P.1
KP.1
KPD.1
KPD.1 +mDrp1
E
Glucose
Oligomycin
2DG
ECAR (mpH/min/cell)
0.004
0.003
0.002
0.001
0
50
100
Time (min)
P.2
KP.2
KPD.2
F
Glucose
Oligomycin
2DG
ECAR (mpH/min/cell)
0.006
0.004
0.002
0
50
100
Time (min)
P
KP
KPD
KPD + mDrp1
G
Relative HK2 mRNA
4
3
2
1
0
**
P.1
KP.1
KPD.1
Relative HK2 mRNA
*
P.2
KP.2
KPD.2

Figure 4.S1. Drp1 contributes to KRas-driven glycolysis and cellular transformation.

(A) The indicated cell lines were seeded at equal density and cells were counted daily over a five-day period (n=3 replicates per cell line, representative result from one of three independent experiments, mean ± SEM, **P<0.01, one-way ANOVA with Tukey's multiple comparison). **(B)** Equal numbers of the indicated cells lines were seeded in soft agar and imaged after 3 weeks (n=3). **(C)** Immunoblot analysis of Drp1 in K, KP and KPD MEFs plus KPD MEFs in which murine Drp1 has been stably re-expressed. Tubulin = loading control. **(D)** Equal numbers of the indicated cells lines were seeded in soft agar and imaged after 3 weeks (n=3). **(E and F)** The extracellular acidification rate (ECAR) was analyzed on the indicated MEF lines over a 100-minute time course. Glucose, oligomycin and 2-DG were added at the indicated time points (n=3 replicates per cell line, representative result from one of three independent experiments). **(G)** Real-time qPCR analysis of relative *HK2* mRNA levels in the indicated MEFs (n=3 replicates per cell line, 3 independent experiments, data are aggregate means ± SEM, *P<0.05, **P<0.01, Student's T–test).

(Gidekel Friedlander et al., 2009) to mice with two floxed alleles of *Drp1* (Wakabayashi et al., 2009) to generate KPDC mice. Due to the embryonic lethality of the whole mouse Drp1 knockout (Wakabayashi et al., 2009) and the unknown role of Drp1 in pancreatic development, we employed the tamoxifen-inducible Pdx-1-Cre-ER to have temporal control of recombination. We injected 30 mice of each genotype (*Kras*$^{LSL\text{-}G12D/+}$; *Trp53*$^{flox/flox}$; *Pdx-1-CreER*$^{Tg/+}$; *Drp1*$^{+/+}$ and *Kras*$^{LSL\text{-}G12D/+}$; *Trp53*$^{flox/flox}$; *Pdx-1-CreER*$^{Tg/+}$; *Drp1*$^{flox/flox}$) with tamoxifen after weaning and monitored the mice for tumor development. Consistent with a role for Drp1 in KRas-driven tumor growth *in vivo*, Drp1$^{flox/flox}$ mice exhibit a 45-day survival advantage compared to the Drp1^{WT} mice, which equates to a 38% increase in longevity (Figure 4.2A). Notably, all KPDC mice bore moderately to poorly differentiated PDAC at endpoint, regardless of Drp1 status (Figure 4.2, B and C). The masses of tumors at necropsy were similar between Drp1^{WT} and Drp1^{flox} mice (Figure 4.S2A). In addition, the incidences of various tumor sequelae (e.g. biliary obstruction) were similar between the study arms (Figure 4.S2B), and the animals gained weight at similar trajectories, excluding the possibility that the survival advantage resulted from artificial skewing of the endpoint determination (Figure 4.S2C).

We sought to determine whether Drp1^{flox} mice progress to adenocarcinoma slower than Drp1^{WT} mice, which could contribute to the survival advantage seen in the Drp1^{flox} KPDC mice. Pancreatic cancer is proposed to arise following progression through a series of precursor lesions, with pancreatic intraepithelial neoplasias (PanINs) most abundantly found (Gidekel Friedlander et al., 2009; Guerra and Barbacid, 2013) in the KPC model used in these studies. Pancreata from both Drp1^{flox} and Drp1^{WT} mice exhibit all subtypes of PanINs when analyzed either 40 or 60 days after tamoxifen injection (Figure 4.S2D). Interestingly, neither the number nor type of lesion varies between the two sets of mice at 40 days following tamoxifen injection, suggesting that loss of Drp1 does not impair the earliest stages of tumorigenesis (Figure 4.2D). However, at 60 days following tamoxifen injection, Drp1^{flox} KPDC mice exhibit a decreased number of PanIN3, but not

PanIN1/2 lesions compared to $Drp1^{WT}$ mice, suggesting that loss of Drp1 impairs the progression to PanIN3 and explaining, at least in part, the survival advantage observed for the $Drp1^{flox}$ mice (Figure 4.2D).

The incomplete inhibition of PanIN development and eventual emergence of PDAC in the $Drp1^{flox}$ mice led us to speculate that the $Drp1^{flox}$ mice may experience incomplete Drp1 excision, especially given previously described recombination inefficiencies of CreER transgenes (Magnuson and Osipovich, 2013). To that end, we evaluated Drp1 expression by immunohistochemistry (IHC) in tumors collected at necropsy. Because Drp1 exhibits diffuse cytoplasmic staining, Drp1 positivity was determined by thresholding Drp1 staining to negative controls (Figure 4.S3, A and B). Interestingly, $Drp1^{flox}$ tumors exhibit regions with tumor cells that retain Drp1 expression as well as regions with complete loss of Drp1 (Figure 4.2E). Although at least partial Drp1 recombination can be detected by PCR in all $Drp1^{flox}$ tumors examined (Figure 4.S3C), no $Drp1^{flox}$ adenocarcinomas were found that exhibit complete loss of Drp1 staining in tumor cells (Figure 4.S3D). Furthermore, when we evaluated Drp1 expression on a subset of PanIN3 lesions from $Drp1^{flox}$ mice 60 days after injection, only 2/33 lesions demonstrated complete loss of Drp1 (Figure 4.S3E).

To determine if the heterogeneity in Drp1 loss observed in the adenocarcinomas is recapitulated in mitochondrial morphological heterogeneity, we examined mitochondrial morphology using immunofluorescence. Consistent with our previous observations in patient PDAC specimens (Kashatus et al., 2015), mitochondria from $Drp1^{WT}$ tumors exhibit a highly fragmented morphology (Figure 4.2F). $Drp1^{flox}$ tumors, on the other hand, exhibit a heterogeneous morphology, with regions of highly fragmented mitochondrial staining and other regions with more elongated mitochondrial structures, consistent with the incomplete deletion of Drp1 observed by IHC (Figure 4.2F). Collectively, the data from these mice suggest that Drp1 promotes KRas-

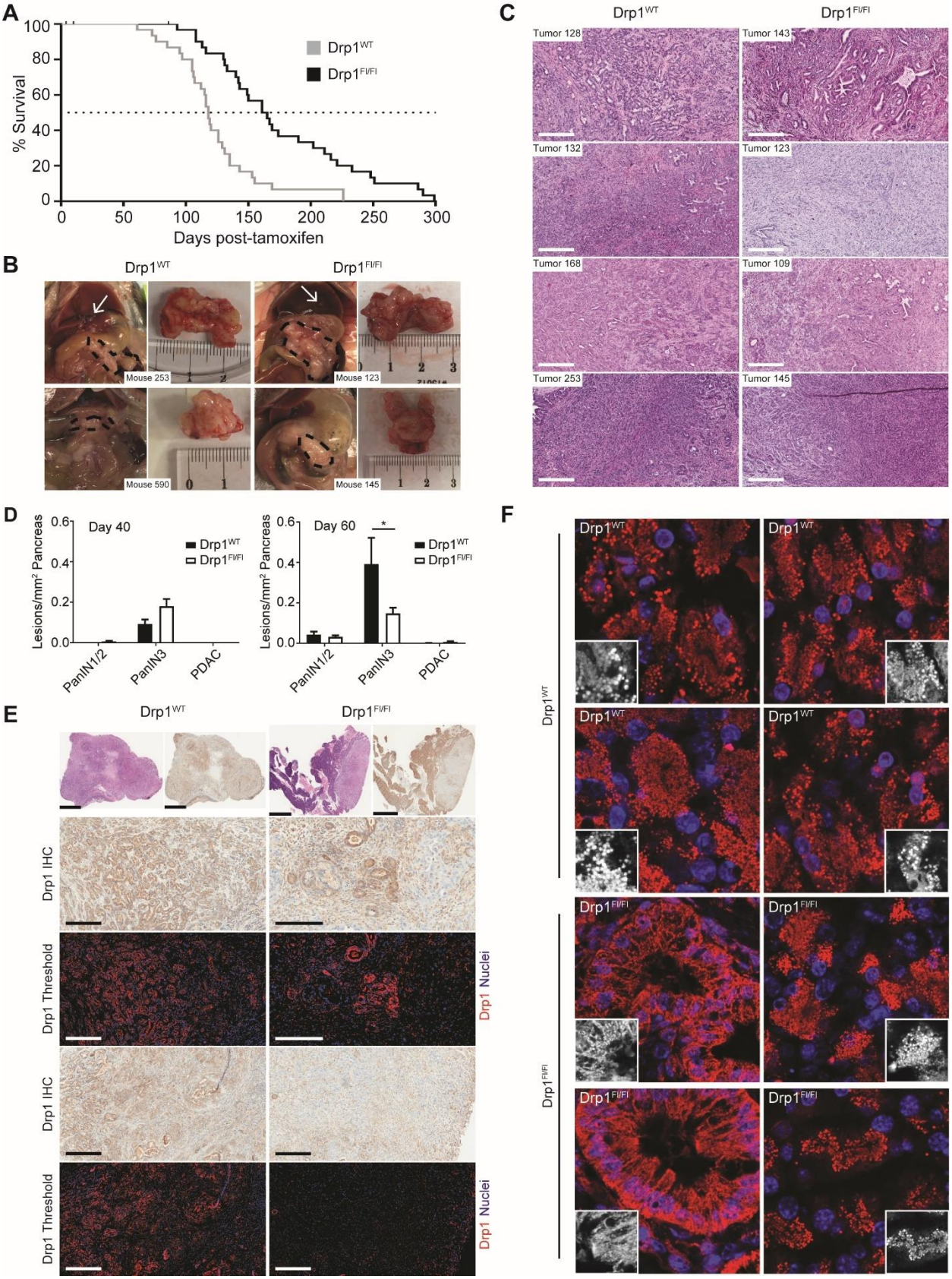
A
% Survival
Days post-tamoxifen
Drp1WT
Drp1FI/FI
B
Drp1WT
Drp1FI/FI
Mouse 253
Mouse 123
Mouse 590
Mouse 145
C
Drp1WT
Drp1FI/FI
Tumor 128
Tumor 143
Tumor 132
Tumor 123
Tumor 168
Tumor 109
Tumor 253
Tumor 145
D
Day 40
Day 60
Lesions/mm² Pancreas
PanIN1/2
PanIN3
PDAC
E
Drp1 IHC
Drp1 Threshold
Drp1 Nuclei
F
Drp1WT
Drp1FI/FI

Figure 4.2. Loss of Drp1 inhibits pancreatic ductal adenocarcinoma progression (This figure was contributed by Nagdas, S & Kashatus, JA).

(A) Overall survival was measured in *Kras*$^{LSL\text{-}G12D/+}$; *Trp53*$^{flox/flox}$; *Drp1*^{WT}; *Pdx-1-CreER*$^{Tg/+}$ mice (grey line) and *Kras*$^{LSL\text{-}G12D/+}$; *Trp53*$^{flox/flox}$; *Drp1*$^{flox/flox}$; *Pdx-1-CreER*$^{Tg/+}$ mice (black line) that had been injected with tamoxifen post-weaning to induce recombination (n=30 mice per group, **** P<0.0001, log-rank (Mantel-Cox) test). **(B)** Representative gross images of pancreatic ductal adenocarcinoma (PDAC; black dashed outline) from mice with the indicated genotype. Liver metastases are indicated with white arrows. **(C)** Tumor sections were generated from mice with the indicated genotypes and stained with hematoxylin & eosin (H&E). Scale bars, 300μm. **(D)** *Kras*$^{LSL\text{-}G12D/+}$; *Trp53*$^{flox/flox}$; *Drp1*^{WT}; *Pdx-1-CreER*$^{Tg/+}$ and *Kras*$^{LSL\text{-}G12D/+}$; *Trp53*$^{flox/flox}$; *Drp1*$^{flox/flox}$; *Pdx-1-CreER*$^{Tg/+}$ mice were euthanized 40 days (left panel; n=4 mice per genotype) or 60 days (right panel; n=6 mice (*Drp1*^{WT}) or 8 mice (*Drp1*$^{flox/flox}$)) after tamoxifen injection and all grades of pancreatic lesions were analyzed and quantified from H&E stained tissue sections (3 sections per mouse, data are mean ± SEM, *P<0.05, two-way ANOVA with Tukey's multiple comparison). **(E)** Immunohistochemical (IHC) analyses of tumors stained for Drp1. Low magnification H&E (top row, left) and corresponding IHC images of tumor (top row, right). High magnification IHC images from regions within tumors of the top panel (rows 2&4). Color deconvoluted image of high magnification IHC image (rows 3&5). Scale bars, 300μm (rows 2-5); 2mm (top row). **(F)** Representative immunofluorescence analysis of mitochondrial morphology in pancreatic tumors harvested from Drp1^{WT} and Drp1$^{flox/flox}$ mice and stained with an anti-mitochondria antibody (red) and DAPI (nuclei, blue). Insets, mitochondria zoom.

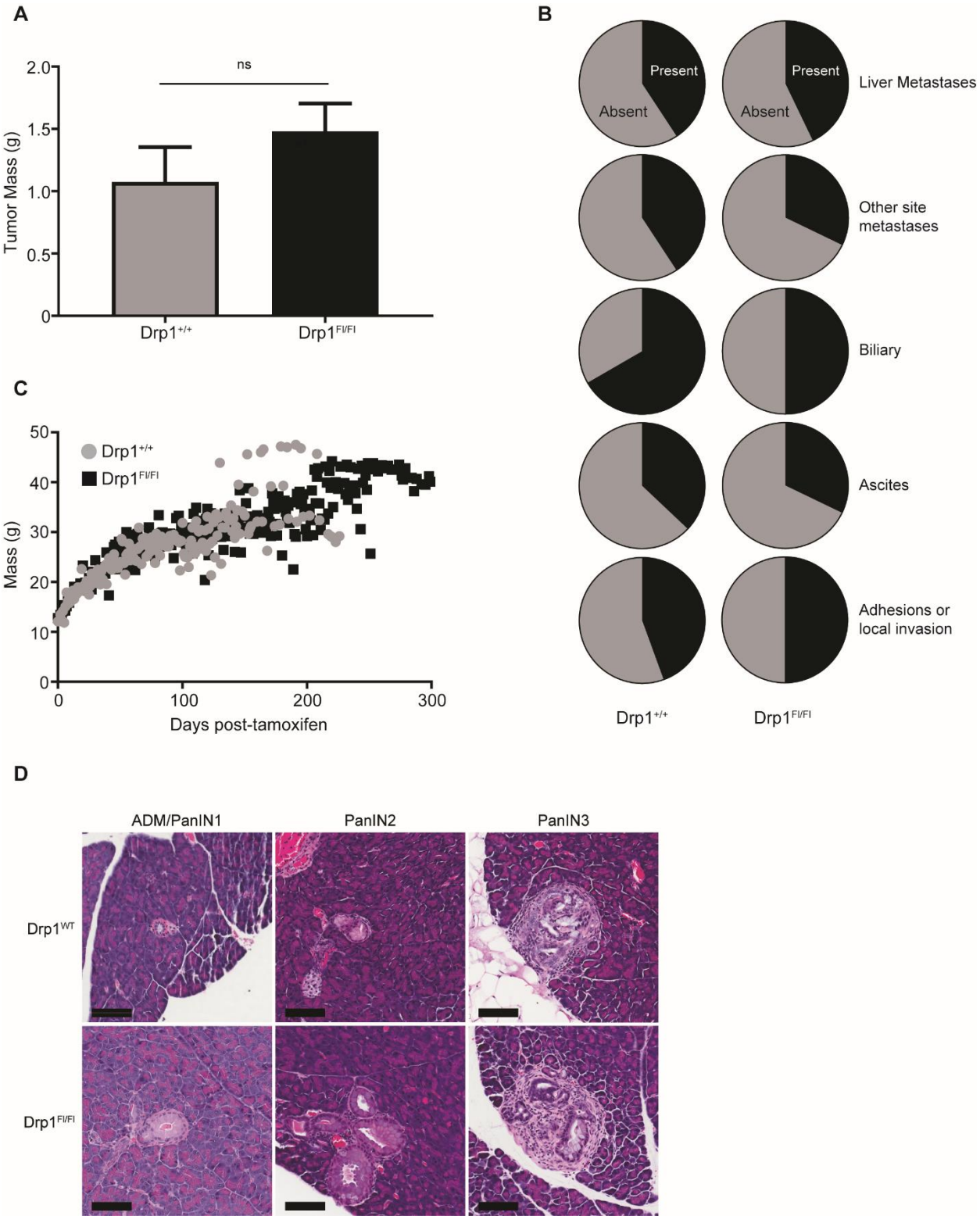
A
ns
Tumor Mass (g)
2.0
1.5
1.0
0.5
0
Drp1+/+
Drp1Fl/Fl
B
Present
Absent
Present
Absent
Liver Metastases
Other site metastases
Biliary
Ascites
Adhesions or local invasion
Drp1+/+
Drp1Fl/Fl
C
Drp1+/+
Drp1Fl/Fl
Mass (g)
50
40
30
20
10
0
0
100
200
300
Days post-tamoxifen
D
ADM/PanIN1
PanIN2
PanIN3
Drp1WT
Drp1Fl/Fl

Figure 4.S2. Incidence of tumor sequelae are comparable between Drp1^{flox} and Drp1^{WT} mice. (This figure was contributed by Nagdas, S).

(A) Tumors were isolated from *Kras*$^{LSL\text{-}G12D/+}$; *Trp53*$^{flox/flox}$; *Drp1^{WT}*; *Pdx-1-CreER*$^{Tg/+}$ and *Kras*$^{LSL\text{-}G12D/+}$; *Trp53*$^{flox/flox}$; *Drp1$^{flox/flox}$*; *Pdx-1-CreER*$^{Tg/+}$ mice and tumor weights were determined at necropsy (n=18 Drp1^{WT}, n=12 Drp1^{flox}, Data are mean ± SEM, n.s. = P>0.05, Student's T-test). **(B),** The presence or absence of the indicated tumor sequelae was evaluated for the indicated sets of mice at necropsy (n=27 Drp1^{WT}, n=28 Drp1^{flox}). **(C)** Enrolled mice were weighed 3X per week following tamoxifen injections until survival endpoints were reached. Weight trajectories as a function of time (n=30 Drp1^{WT} and Drp1^{flox}). **(D)** Pancreata were removed from *Kras*$^{LSL\text{-}G12D/+}$; *Trp53*$^{flox/flox}$; *Drp1^{WT}*; *Pdx-1-CreER*$^{Tg/+}$ and *Kras*$^{LSL\text{-}G12D/+}$; *Trp53*$^{flox/flox}$; *Drp1$^{flox/flox}$*; *Pdx-1-CreER*$^{Tg/+}$ mice at 40 or 60 days following tamoxifen injection. Tissue was fixed and stained with H&E to examine the incidence of the indicated pancreatic lesions. Scale bars, 100 μm.

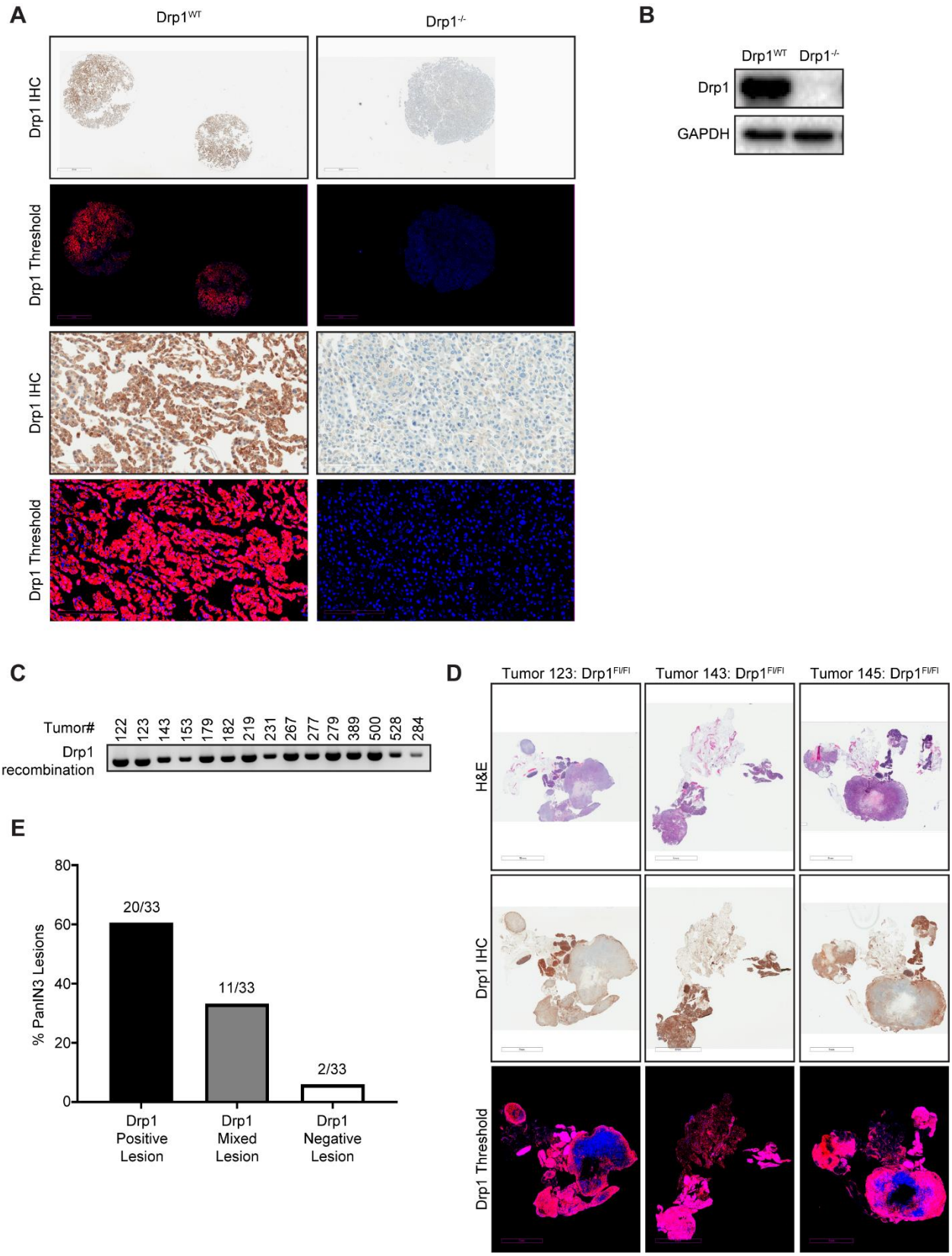
A
Drp1WT
Drp1-/-
Drp1 IHC
Drp1 Threshold
Drp1 IHC
Drp1 Threshold
B
Drp1WT
Drp1-/-
Drp1
GAPDH
C
Tumor#
122
123
143
153
179
182
219
231
267
277
279
389
500
528
284
Drp1 recombination
D
Tumor 123: Drp1Fl/Fl
Tumor 143: Drp1Fl/Fl
Tumor 145: Drp1Fl/Fl
H&E
Drp1 IHC
Drp1 Threshold
E
% PanIN3 Lesions
80
60
40
20
0
20/33
11/33
2/33
Drp1 Positive Lesion
Drp1 Mixed Lesion
Drp1 Negative Lesion

Figure 4.S3. Drp1 expression is heterogeneous in tumors isolated from Drp1^{flox} mice. (This figure was contributed by Nagdas, S).

(A) Cell pellets of Drp1^{WT} and Drp1$^{-/-}$ MEFs were paraffin-embedded and Drp1 expression was analyzed by immunohistochemistry (IHC). Low magnification Drp1 IHC images of cell pellet (top row) with corresponding color deconvoluted image (2nd row). High magnification Drp1 IHC images of cell pellet (3rd row) with corresponding color deconvoluted image (4th row). **(B)** Immunoblot analysis of Drp1 expression in the MEFs used in **(A)**. GAPDH = loading control. **(C)** Cre-mediated recombination at the Drp1 locus was analyzed in DNA from pancreatic tumors isolated from Drp1^{flox} mice. **(D)** Tumors isolated from Drp1^{flox} mice at necropsy were stained with hematoxylin & eosin (H&E; top row), Drp1 IHC (2nd row), and corresponding color deconvoluted image (3rd row) **(E)** Drp1 expression was analyzed by IHC in PanIN3 lesions from Drp1^{flox} mice euthanized 60 days after tamoxifen injection. Lesions in which all morphologically attributable epithelial cells express Drp1 were scored as positive. Lesions in which some, but not all, morphologically attributable epithelial cells within a lesion express Drp1 were scored mixed. Lesions in which no morphologically attributable epithelial cells within a lesion express Drp1 were scored negative.

driven tumor growth in a physiological *in vivo* model of PDAC and that strong selective pressure against the loss of Drp1 leads to selection for cells in which its excision is incomplete.

4.2.3 Drp1$^{-/-}$ tumor cell lines exhibit profound metabolic reprogramming

To further investigate the physiological changes that may occur as a consequence of, or adaption to, the loss of Drp1 *in vivo*, we generated a series of tumor-derived cell lines from both Drp1^{WT} and Drp1^{flox} tumors. Consistent with our IHC results, many clones, but not all, derived from Drp1^{flox} tumors retained one allele of Drp1, providing further evidence of Drp1 retention in our tumors (Figure 4.3A). Drp1^{WT} and Drp1$^{Fl/-}$ cell lines exhibit a punctate, fragmented mitochondrial morphology, demonstrating that one intact allele of Drp1 is sufficient to recapitulate the mitochondrial morphology in KRas-driven cells (Figure 4.3, B and C). Drp1$^{-/-}$ cell lines, on the other hand, exhibit mitochondria with elongated, tubular structures consistent with a loss of mitochondrial fission capability (Figure 4.3C). Importantly, Drp1^{WT} and Drp1$^{-/-}$ cells are both able to form tumors when implanted orthotopically into the pancreas of an immunodeficient mouse, with no difference in tumor volume twenty days after implantation (Figure 4.3D).

Given the decrease in KRas^{G12D}-induced HK2 expression and glycolysis upon deletion of Drp1 in MEFs, we analyzed these parameters in the tumor derived cell lines. Unlike the MEFs, but consistent with the robust tumor growth seen *in vivo*, tumor cells lacking Drp1 express HK2 at levels comparable to those that express Drp1 (Figure 4.3E). Furthermore, there is no impairment in glycolytic flux of radiolabeled glucose in the Drp1$^{-/-}$ tumor cells (Figure 4.3F). These data are consistent with a model in which Drp1$^{-/-}$ cells need to overcome the loss of Drp1-dependent HK2 expression and glycolytic flux in order for tumor progression to occur.

Although Drp1-null tumor cells did not display any glycolytic differences when compared to Drp1^{WT} cells, the intimate relationship between mitochondrial biology and cellular metabolism as well as many findings linking mitochondrial dynamics with bioenergetics

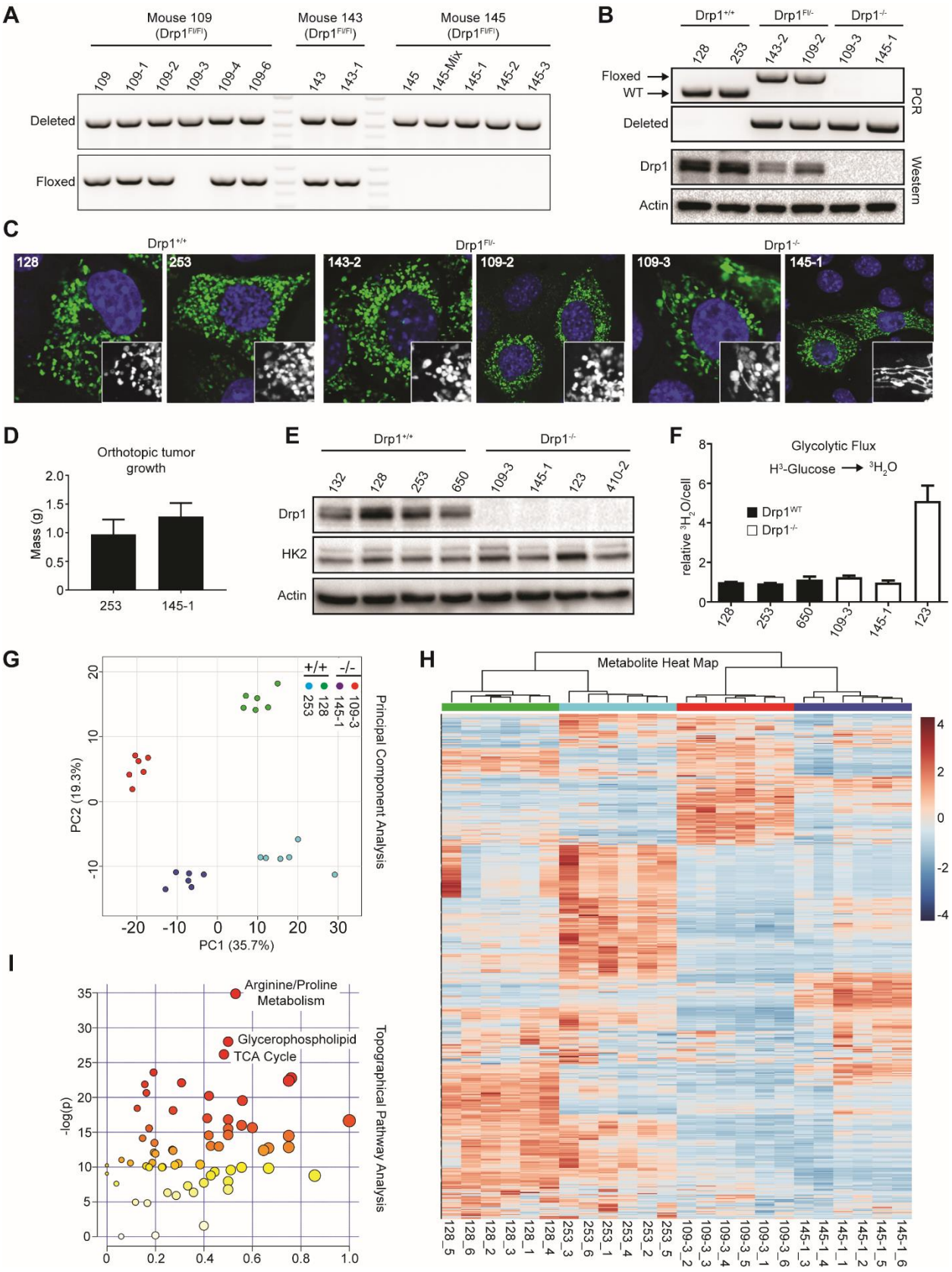
A
Mouse 109 (Drp1Fl/Fl)
Mouse 143 (Drp1Fl/Fl)
Mouse 145 (Drp1Fl/Fl)
109
109-1
109-2
109-3
109-4
109-6
143
143-1
145
145-Mix
145-1
145-2
145-3
Deleted
Floxed
B
Drp1+/+
Drp1Fl/-
Drp1-/-
128
253
143-2
109-2
109-3
145-1
Floxed
WT
Deleted
PCR
Drp1
Actin
Western
C
Drp1+/+
Drp1Fl/-
Drp1-/-
128
253
143-2
109-2
109-3
145-1
D
Orthotopic tumor growth
Mass (g)
253
145-1
E
Drp1+/+
Drp1-/-
132
128
253
650
109-3
145-1
123
410-2
Drp1
HK2
Actin
F
Glycolytic Flux
H3-Glucose → 3H2O
Drp1WT
Drp1-/-
relative 3H2O/cell
128
253
650
109-3
145-1
123
G
+/+
-/-
253
128
145-1
109-3
Principal Component Analysis
PC2 (19.3%)
PC1 (35.7%)
H
Metabolite Heat Map
I
Arginine/Proline Metabolism
Glycerophospholipid
TCA Cycle
-log(p)
Topographical Pathway Analysis

Figure 4.3. Drp1$^{-/-}$ tumor cell lines exhibit profound metabolic reprogramming. (This figure was contributed by Nagdas, S).

(A) PCR was performed on polyclonal (109, 143, 145) tumor-derived cell lines as well as single cell clones derived from those lines (145-Mix is a mix of 6 single cell clones). The reaction in the top panel detects recombination of the Drp1^{flox} allele (i.e. deletion of Drp1) while the reaction in the bottom panel detects the floxed Drp1 allele (i.e. not deleted). **(B)** Identical PCR reactions as in **(A)** and immunoblot analysis for Drp1 were performed on the indicated Drp1^{WT}, Drp1$^{Fl/-}$, or Drp1$^{-/-}$ tumor-derived cell lines (Actin = loading control). **(C)** Representative immunofluorescence staining of mitochondrial morphology in the indicated tumor-derived cell lines transiently transfected with mito-YFP (mitochondria, green) and stained with DAPI (nuclei, blue). **(D)** The indicated Drp1^{WT} and Drp1$^{-/-}$ cell lines were injected orthotopically into the pancreata of immunocompromised mice and tumor mass was measured at 20 days post-injection following necropsy (n=4 mice per cell line, Data are mean ± SEM). **(E)** Immunoblot analysis of HK2 and Drp1 expression in the indicated tumor cell lines (Representative blot, n=3, actin = loading control). **(F)** The indicated tumor cell lines were incubated with ^{3}H-Glucose for two hours and the production of $^{3}H_2O$ was analyzed as a readout of glycolytic flux (n=3 replicates per cell line, 3 independent experiments, data are aggregate means ± SEM). **(G)** Whole metabolomics profiles were generated for six replicates of each of the indicated cell lines and principal component analysis was performed. **(H)** Hierarchical cluster analysis was performed on all of the metabolites detected in **(G)** to identify similarity between the tumor cell lines included in the analysis. **(I)** Topographical pathway enrichment analysis was performed on metabolomics data from Drp1^{WT} and Drp1$^{-/-}$ tumor-derived cell lines to identify pathways with significantly altered metabolites at key metabolite nodes.

(Roy et al., 2015; Wai and Langer, 2016; Zorzano et al., 2010) led us to interrogate additional metabolic differences between our $Drp1^{WT}$ and $Drp1^{-/-}$ cells. To that end, we performed global metabolomics profiling (Metabolon, Inc.) on two $Drp1^{WT}$ and two $Drp1^{-/-}$ cell lines grown under standard culture conditions with 10% serum supplementation (Extended Data File 1). Using MetaboAnalyst (Xia and Wishart, 2010), a web-based platform for processing metabolomics data (http://www.metaboanalyst.ca/), we performed preliminary bioinformatics analysis on the four cell lines. Two-dimensional principle component analysis (PCA) reveals that each cell line clusters distinctly from one another (Figure 4.3G) while hierarchical clustering illustrates that each of the cell lines segregates on independent branches of a metabolite dendrogram (Figure 4.3H), demonstrating the expected tumor cell heterogeneity of the cell lines. Interestingly, Drp1-null cell lines cluster away from $Drp1^{WT}$ cells, particularly along Component 1, the largest contributor to the variance (Figure 4.3G), suggesting that Drp1 expression contributes significantly to the global metabolic phenotype of KRas-driven tumor cells. Further illustrating this point, hierarchical clustering demonstrates that the two $Drp1^{WT}$ cell lines segregate together on an independent branch from the two $Drp1^{-/-}$ cell lines (Figure 4.3H). In addition, the hierarchical clustering heat map demonstrates distinct classes of metabolites clearly dysregulated between $Drp1^{-/-}$ and $Drp1^{WT}$ cells, suggesting that loss of Drp1 leads to distinct metabolic reprogramming either as a direct consequence of, or adaptation to, the loss of Drp1 function (Figure 4.3H).

To gain further insight into potential pathways impacted by loss of Drp1 in the tumor cells, we performed pathway analyses using two independent metabolomics platforms (Metabolon and MetaboAnalyst). We performed Pathway Enrichment analysis (Metabolon) on the set of 350 metabolites significantly different between the pairwise comparison of all $Drp1^{-/-}$ and $Drp1^{WT}$ samples (Figure 4.S4A). In addition, we performed Topographical Pathway analyses on our entire dataset using MetaboAnalyst, which models a metabolite's relative impact on the pathway's end product to identify the metabolic pathways most perturbed by loss of Drp1 (Figure 4.3I).

Consistent with major changes in mitochondrial function upon deletion of Drp1, both metabolomics analysis platforms identified fatty acid metabolism, amino acid metabolism and TCA cycle as potential pathways that contribute to the global metabolic reprogramming that occurs upon loss of Drp1 in our KRas-driven cancer cells.

4.2.4 Loss of Drp1 results in increased lipid catabolism and inefficient mitochondrial function

We chose to further explore lipid metabolism in our Drp1-null tumor cells given its links to mitochondria and its emerging role in KRas-driven cancers (Gouw et al., 2017; Kamphorst et al., 2013; Padanad et al., 2016; Svensson et al., 2016). Careful analysis of individual lipids within the metabolomics data set revealed that while the levels of several phosphatidylcholine and phosphatidylethanolamine species with diverse acyl chain length and saturation status were comparable between our cell lines (Figure 4.4A, Figure 4.S4B, External Database S1), the levels of the corresponding lysolipids and fatty acids were decreased in the two $Drp1^{-/-}$ cell lines compared to the $Drp1^{WT}$ cells (Figure 4.4A, Figure 4.S4B). The decrease in lysolipids and fatty acids could potentially come about through a variety of mechanisms, including decreased import, increased flux into anabolic membrane synthesis and increased catabolic oxidation to produce energy (Figure 4.4B). Interestingly, when added to the media, ^{14}C-labeled palmitate is incorporated into the neutral fatty acid compartment, (phospholipids, triacylglycerols, and cholesterol esters) equivalently in the three $Drp1^{WT}$ and three $Drp1^{-/-}$ cell lines we tested, suggesting that lipids are imported at similar rates in these cell lines and that there is no difference in incorporation into membranes and other neutral lipids (Figure 4.4C). In contrast, $Drp1^{-/-}$ cell lines exhibit decreased oxidation of ^{14}C-labeled palmitate to $^{14}CO_2$ compared to $Drp1^{WT}$ cells (Figure 4.4D). This decrease in lipid-derived CO_2 can arise from a decreased flux of fatty acids into the fatty acid oxidation pathway, or through an incomplete oxidation of the fatty acids with no decrease in flux. Consistent with the latter hypothesis, analysis of acylcarnitine levels revealed that $Drp1^{-/-}$ cells exhibit either increased (C4, C6, C8) or comparable (C14, C16, C18) levels of

acylcarnitines compared to Drp1^{WT} cells (Figure 4.4, A and E). Accumulation of acylcarnitines is associated with abnormal fatty acid oxidation, consistent with a loss of mitochondrial function in the Drp1$^{-/-}$ tumor cells (Kler et al., 1991). To further support this idea, all three of the Drp1$^{-/-}$ tumor cell lines we tested exhibited decreased spare respiratory capacity compared to three Drp1^{WT} lines (Figure 4.4F). In addition, Drp1$^{-/-}$ tumor cells exhibit a significantly higher NAD+/NADH ratio than the Drp1^{WT} cells (Figure 4.4G). Together these results indicate the Drp1$^{-/-}$ tumor cells have decreased mitochondrial oxidative capacity and a decreased ability to respond to bioenergetic demands. To further test this possibility, we seeded equal numbers of Drp1^{WT} and Drp1$^{-/-}$ cell lines under a variety of nutrient conditions and analyzed them after 24 hours by CellTiter Glo. While removal of glucose or glutamine as a carbon source affected both sets of cells equivalently, forcing the cells to rely on mitochondrial metabolism and/or fatty acid oxidation by growing them in media supplemented with only serum or with serum plus galactose had a greater detrimental effect on Drp1$^{-/-}$ cells (Figure 4.4H). Collectively, the metabolic data from these cells lines indicates that successful tumor development in the absence of Drp1 requires first that cells overcome the decrease in HK2-dependent glycolytic flux and second that these cells increase the flux of lipids towards catabolic processes to overcome a decrease in mitochondrial function.

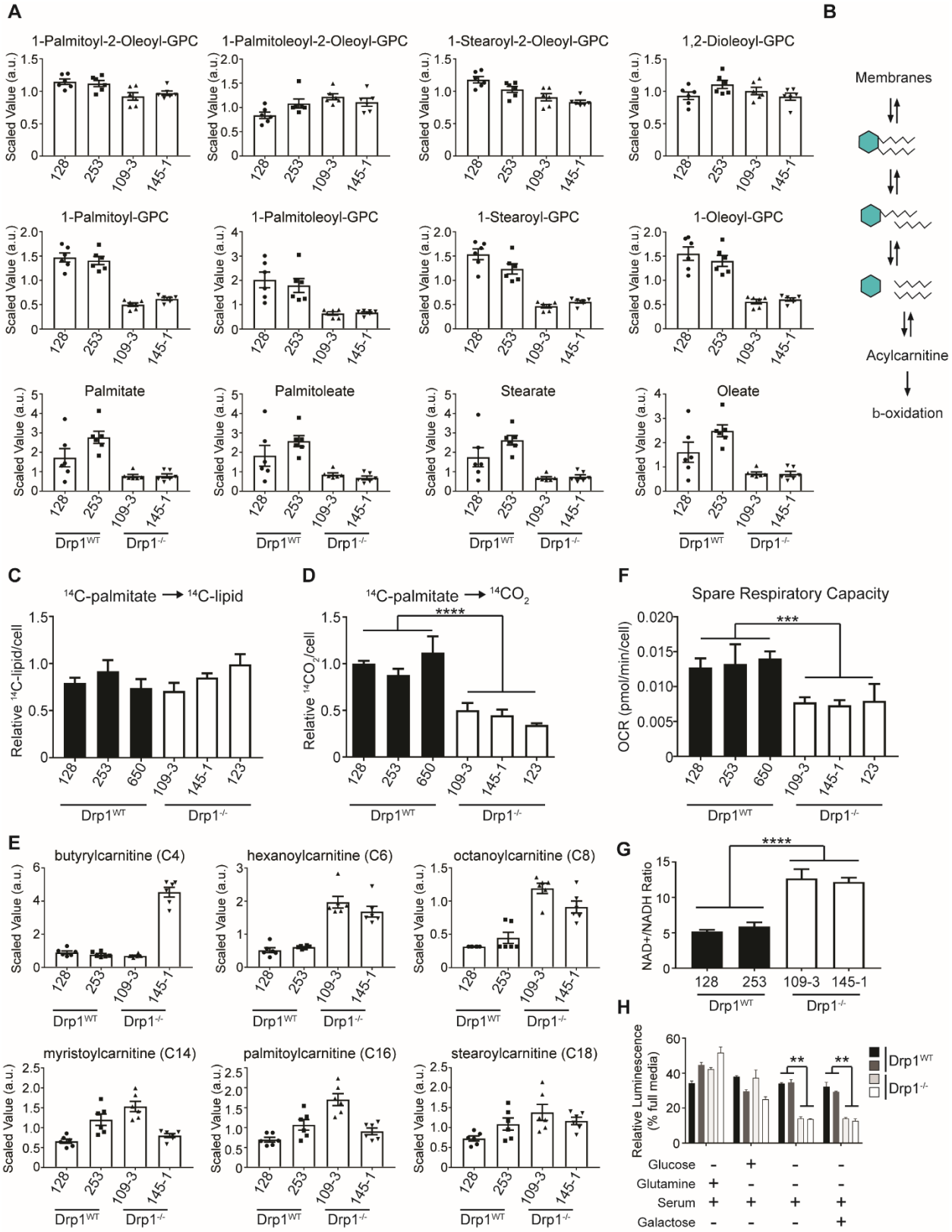
A
1-Palmitoyl-2-Oleoyl-GPC
1-Palmitoleoyl-2-Oleoyl-GPC
1-Stearoyl-2-Oleoyl-GPC
1,2-Dioleoyl-GPC
1-Palmitoyl-GPC
1-Palmitoleoyl-GPC
1-Stearoyl-GPC
1-Oleoyl-GPC
Palmitate
Palmitoleate
Stearate
Oleate
Scaled Value (a.u.)
128
253
109-3
145-1
Drp1WT
Drp1-/-
B
Membranes
Acylcarnitine
b-oxidation
C
14C-palmitate → 14C-lipid
Relative 14C-lipid/cell
650
123
D
14C-palmitate → 14CO2
Relative 14CO2/cell
****
F
Spare Respiratory Capacity
OCR (pmol/min/cell)
***
E
butyrylcarnitine (C4)
hexanoylcarnitine (C6)
octanoylcarnitine (C8)
myristoylcarnitine (C14)
palmitoylcarnitine (C16)
stearoylcarnitine (C18)
G
NAD+/NADH Ratio
H
Relative Luminescence (% full media)
**
Glucose
Glutamine
Serum
Galactose

Figure 4 4. Loss of Drp1 results in increased lipid catabolism and inefficient mitochondrial function. (This figure was contributed by Nagdas S).

(A) The scaled abundance of four phosphatidylcholine (PC) species (top row), the corresponding lyso-PC species (middle row), and corresponding fatty acids (bottom row) from the metabolomics analysis of the indicated $Drp1^{WT}$ and $Drp1^{-/-}$ tumor-derived cell lines (n=6 replicates per cell type, data are mean ± SEM). **(B)** Schematic diagram of phospholipid metabolism showing two potential fates for lyso-lipids and fatty acids in cells. **(C and D)** The indicated tumor cell lines were incubated with ^{14}C-Palmitate for two hours and the production of ^{14}C-labeled neutral lipids and $^{14}CO_2$ were analyzed as readouts of membrane synthesis **(C)** and fatty acid oxidation **(D)**, respectively (n=3 replicates per cell line, 3 independent experiments, data are aggregate means ± SEM, **** P<0.0001, unpaired two-sided Student's T–test **(**cell lines grouped together by genotype)). **(E)** The scaled abundance of 6 different acylcarnitines from the metabolomics analysis of the indicated $Drp1^{WT}$ and $Drp1^{-/-}$ tumor-derived cell lines (n=6 replicates per cell type, data are mean ± SEM). **(F)** The oxygen consumption rate (OCR) was analyzed on the indicated tumor-derived cell lines over a 100-minute time course and used to calculate spare respiratory capacity (n=3 replicates per cell line, 3 independent experiments, data are aggregate means ± SEM, *** P<0.001, unpaired two-sided Student's T–test **(**cell lines grouped together by genotype))**. (G)** The ratio of NAD+/NADH was calculated from the metabolomics analysis of the indicated $Drp1^{WT}$ and $Drp1^{-/-}$ tumor-derived cell lines. (n=6 replicates per cell type, **P<0.0001, Student's T–test **(**cell lines grouped together by genotype)) **(H)** Equal numbers of the indicated $Drp1^{WT}$ and $Drp1^{-/-}$ tumor-derived cell lines were plated in media containing or lacking glucose, glutamine, serum or galactose as indicated and subsequently analyzed by CellTiter-Glo following 24 hours in culture. Data represents relative luminescence as a percentage of the values measured in full media for each cell line (n=3 replicates per cell line, representative result from one of three independent experiments, Data

are mean ± SEM, **P<0.01, unpaired two-sided Student’s T–test **(**cell lines grouped together by genotype)).

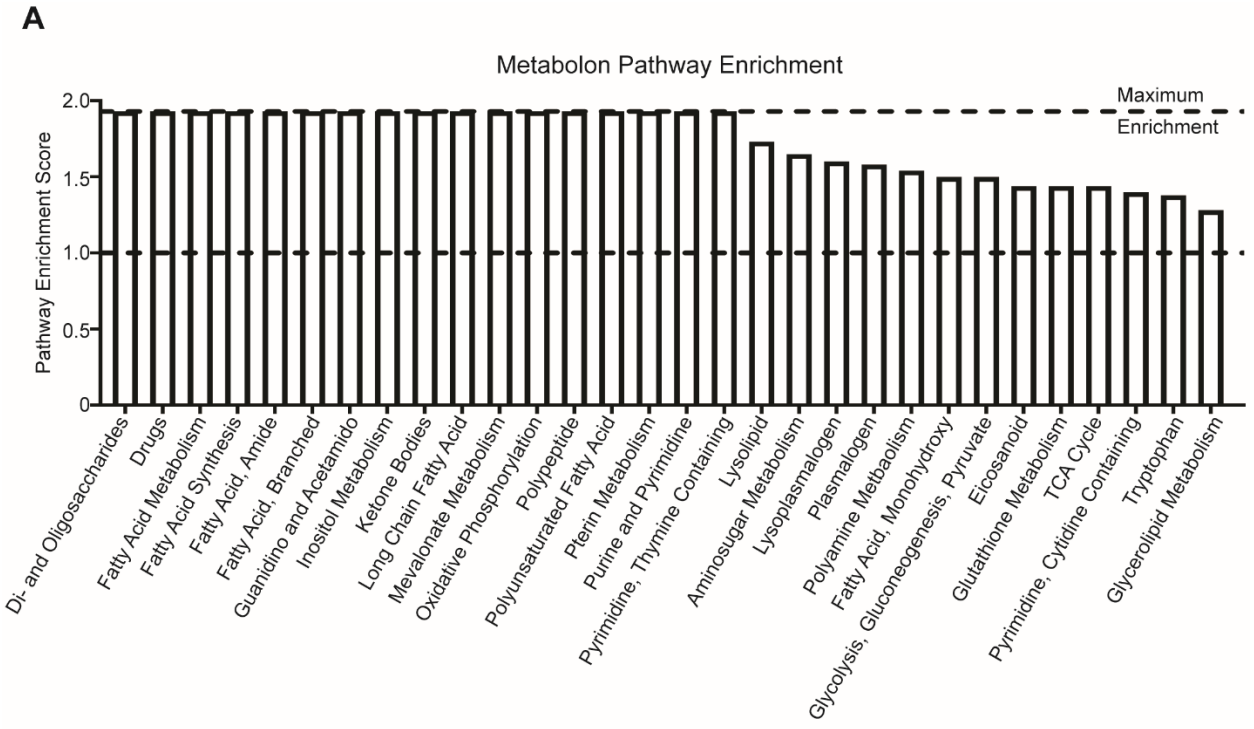
A
Metabolon Pathway Enrichment
Maximum Enrichment
Pathway Enrichment Score
2.0
1.5
1.0
0.5
0
Di- and Oligosaccharides
Drugs
Fatty Acid Metabolism
Fatty Acid Synthesis
Fatty Acid, Amide
Fatty Acid, Branched
Guanidino and Acetamido
Inositol Metabolism
Ketone Bodies
Long Chain Fatty Acid
Mevalonate Metabolism
Oxidative Phosphorylation
Polypeptide
Polyunsaturated Fatty Acid
Pterin Metabolism
Purine and Pyrimidine
Pyrimidine, Thymine Containing
Lysolipid
Aminosugar Metabolism
Lysoplasmalogen
Plasmalogen
Polyamine Metbaolism
Fatty Acid, Monohydroxy
Glycolysis, Gluconeogenesis, Pyruvate
Eicosanoid
Glutathione Metabolism
TCA Cycle
Pyrimidine, Cytidine Containing
Tryptophan
Glycerolipid Metabolism

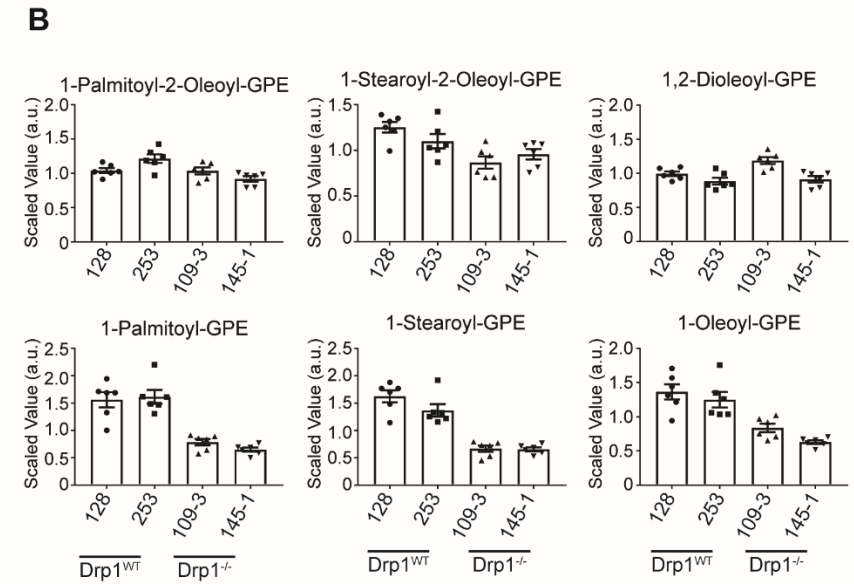
B
1-Palmitoyl-2-Oleoyl-GPE
1-Stearoyl-2-Oleoyl-GPE
1,2-Dioleoyl-GPE
1-Palmitoyl-GPE
1-Stearoyl-GPE
1-Oleoyl-GPE
Scaled Value (a.u.)
128
253
109-3
145-1
Drp1WT
Drp1-/-

Figure 4.S4. Drp1$^{-/-}$ tumor cell lines exhibit metabolic reprogramming. (This figure was contributed by Nagdas, S).

(A) Pathway enrichment analysis was performed on 350 metabolites that were significantly different between the pairwise comparison of all Drp1$^{-/-}$ and Drp1^{WT} tumor-derived cell lines to identify potential metabolic pathways dependent on Drp1. **(B)** The scaled abundance of three phosphatidylethanolamine (PE) species (top row) and the corresponding lyso-PE species (bottom row) from metabolomic analysis of the indicated Drp1^{WT} and Drp1$^{-/-}$ tumor-derived cell lines (n=6 replicates per cell type, data are mean ± SEM).

4.3 Discussion

Throughout this chapter, we demonstrated that MEFs generated from our genetically engineered mouse model with mutant KRas and WT Drp1 (KP cells) recapitulated the signaling and mitochondrial morphology changes we reported in chapter 2. The KP cells have increased MAPK activation as evidenced by increased p-Erk1/2 levels compared to the WT cells (P cells) (Figure 4.1A). There is also an increase in p-Drp1 levels which corresponds with the increase in p-Erk1/2 levels (Figure 4.1A). When we analyzed mitochondrial morphology, we saw more robust mitochondrial fission in the KP cells compared to the control cells (Figure 4.1B). Loss of Drp1 resulted in mitochondrial elongation in the KRas mutant Drp1 null cells (KPD cells) (Figure 4.1B). Upon examination of how loss of Drp1 affects tumorigenic phenotypes, we found that there is a reduction in cell accumulation as well as colony formation in the KPD cells compared to the KP cells (Figure 4.1C, 4.1E). We hypothesized that these changes could be occurring due to differences in cell metabolism and we focused on glycolysis due to its established importance for tumor growth (Jose et al., 2011). We found that loss of Drp1 compromised the increase in glycolytic metabolism induced by activation of KRas (Figure 4.1F-G). We went on to establish that Drp1 is regulating HK2 expression, a key regulator of glycolytic metabolism (Figure 4.1H-I) and that rescue with HK2 could restore glycolysis and partially rescue colony formation (Figure 4.1K-L). Collectively, these data suggest that Drp1-mediated regulation of HK2 expression downstream of KRas is, in part, promoting the tumorigenic properties of the MEF lines.

To determine the effect of Drp1 on pancreatic tumor progression *in vivo*, we generated a tamoxifen-inducible mouse model of pancreatic cancer to conditionally knockout Drp1 in the pancreas. In a survival experiment, the $Drp1^{flox/flox}$ mice exhibit a 45-day survival advantage compared to Drp1 WT mice (Figure 4.2A). The difference in survival was not due to decreased tumor burden as tumor masses at necropsy were comparable between genotypes. Furthermore, both genotypes of mice exhibited moderately to poorly differentiated PDAC. In an attempt to

determine what was causing the difference in survival in the Drp1$^{flox/flox}$ mice, we sought to determine if there was a difference in PanIN progression. Upon inspection of Drp1 WT and Drp1$^{flox/flox}$ mice pancreata at pre-determined endpoints (day 40 and 60 post tamoxifen injection) we found that Drp1$^{flox/flox}$ mice exhibited decreased number of PanIN3 lesions at day 60 (Figure 4.2D), which suggests that the loss of Drp1 may be delaying progression of PanIN2 lesions to PanIN3. To elucidate mechanisms that may account for the similarity in tumor burden at survival-endpoint between genotypes, we decided to test whether there is incomplete recombination in the Drp1$^{flox/flox}$ mice. Unexpectedly, we found regions of Drp1$^{flox/flox}$ tumors that retain Drp1 expression (Figure 4.2E) even though all of the tumors had undergone at least partial recombination. Due to the retained expression of Drp1 in Drp1$^{flox/flox}$ mice, we hypothesized that there may be areas of Drp1$^{flox/flox}$ tumors that display a fragmented mitochondrial morphology as well. Upon immunohistochemical examination of Drp1 in tumor samples from our mice, we found that the Drp1 WT tumors all displayed fragmented mitochondrial morphology whereas the Drp1$^{flox/flox}$ tumors showed heterogeneous mitochondrial morphology (Figure 4.2F) consistent with heterogenous Drp1 expression. These data suggest that there may be a selective pressure to maintain Drp1 expression as well as mitochondrial fission in tumors of Drp1$^{flox/flox}$ mice.

In order to achieve a better understanding of the physiological changes being mediated by Drp1 *in vivo*, we generated a series of tumor-derived cell lines from Drp1 WT or Drp1$^{flox/flox}$ tumors. Drp1 WT and Drp1$^{-/-}$ tumor cell lines had comparable capacity to form tumors after orthotopic injection into the pancreas and suggests that Drp1$^{-/-}$ cells have undergone adaptations after Drp1 loss to maintain tumorigenicity. To further examine possible mechanisms of adaptation, we analyzed these cells for metabolic differences. Unexpectedly, we found that the tumor cell lines display similar HK2 levels and glycolytic metabolism regardless of Drp1 status, which is different than the MEF data (Figure 4.3E-F). In comparing the Drp1 WT and Drp1 null tumor cells, we found that they have similar levels of HK2 as well as similar flux through glycolysis whereas the MEF WT Drp1 cells had increased HK2 levels and glycolysis compared to the Drp1 null cells.

These data are consistent with a model where HK2 expression and glycolysis are important for promoting tumorigenic phenotypes, although we have yet to directly test the contribution of HK2 and glycolysis to tumorigenicity in the tumor cell lines.

Due to comparable levels of glycolysis between the Drp1 WT and Drp1$^{-/-}$ tumor cells, we decided to analyze other potential metabolic differences between the genotypes, so we performed global metabolomic profiling on two sets of Drp1 WT and Drp1$^{-/-}$ cells. Analysis of the metabolomics data revealed that the Drp1 WT cell lines clustered together and away from the Drp1$^{-/-}$ cell lines which themselves clustered together. Furthermore, there are distinct sets of metabolites being dysregulated in Drp1 WT compared to Drp1$^{-/-}$ cells, which suggests that loss of Drp1 results in metabolic rewiring that may be important for maintaining tumorigenicity in the Drp1$^{-/-}$ cells.

Analysis of the metabolic pathways altered by loss of Drp1 revealed changes in fatty acid metabolism, amino acid metabolism as well as TCA cycle intermediates. Due to the links between mitochondria and lipid metabolism, we further examined changes to individual lipid species. We found that lysolipids and fatty acids were decreased in Drp1$^{-/-}$ cells (Figure 4.4A). We hypothesized that the decrease in lysolipids and fatty acids is due to incomplete oxidation of fatty acids as evidenced by the accumulation of acylcarnitines in Drp1$^{-/-}$ cells (Figure 4.4A and E). Studies have shown that acylcarnitine accumulation is indicative of dysfunctional mitochondria, which we verified by the decreased spare respiratory capacity of Drp1$^{-/-}$cells. Taken together, these data suggest that Drp1$^{-/-}$ tumor cells may adapt to the loss of Drp1 by upregulating catabolism and thus accumulation of acylcarnitines at the mitochondria, in an attempt to possibly overcome decreased mitochondrial function.

In summary, in an *in vitro* MEF system, loss of Drp1 results in decreased HK2 expression, which, in part, promotes increased glycolysis in the presence of mutant KRas. The increased glycolysis is also playing a role in promoting the tumorigenic properties of KRas mutant MEFs. A supplementary explanation for the increased glycolysis associated with KRas activation involves

a potential role for Drp1 in mediating KRas-associated glucose uptake, which is upstream of HK2. Studies have shown that mutant KRas expression correlates with increased expression of glucose transporters in lung and colon cancers (Sasaki, 2012; Zhang et al., 2018). As Drp1 has been shown to regulate protein contacts at the plasma membrane (Itoh et al., 2018), it is possible that Drp1 could be involved in promoting glucose transporter stability at the cell surface which would result in increased glucose transporter expression. To test this hypothesis, we could compare the levels of glucose transporters between Drp1 WT and null MEFs. If we see that there is decreased levels of glucose transporters in the null cells, we could perform Drp1 rescue experiments to determine if Drp1 can rescue glucose transporter expression. A relationship between Drp1 and cell surface protein regulation would represent a novel facet of Drp1 function in cancer.

In an *in vivo* model of pancreatic cancer, there is strong selection against loss of Drp1 expression. Tumor cell lines derived from Drp1 null tumors also maintain HK2 expression and flux through glycolysis. Maintenance of glycolysis in the Drp1 null tumor cells raise questions about the validity of the MEF system as a physiologically relevant model to determine the effects of Drp1 on tumor growth. However, several interpretations are available to reconcile the MEF data and the tumor cell line data.

The simplest explanation for the discrepancy between the MEF data and the tumor cell line data is that the changes being mediated by Drp1 are cell-type specific. In other words, there may be no relationship between the effects that Drp1 loss elicits in MEFs and the effects seen in the tumor cell lines. While plausible, this interpretation of the data is unlikely. In the field of cancer research, several studies have established the validity of MEFs as useful *in vitro* systems to model what is happening *in vivo* (Bar-Sagi and Feramisco, 1986; Commisso et al., 2013; DeNicola et al., 2011; Patra et al., 2013; Tuveson, 2004). Additionally, the tumor cell lines were generated from tumor cells that have been growing in their natural environment for over three months. In this time, the cellular stress associated with the tumor microenvironment will have created a selective pressure for those cells that are able to maintain a proliferative advantage. In the MEFs,

we demonstrate that loss of Drp1 is antagonistic to tumorigenic phenotypes. Therefore, it is likely that within the tumor, those cells that were able to overcome the antagonistic effects of Drp1 loss continued to grow and eventually dominated the tumor cell population. This possibility would emphasize the need to look at pancreatic cancer cells at an early timepoint, before any selective pressures arise, to determine if there is a difference between early tumor cells and late tumor cells.

As mentioned previously, one major possibility is that the cells that we derived from the PDAC tumors may have overcome some selective pressure associated with Drp1 loss that resulted in the upregulation of HK2 and subsequently glycolytic metabolism. If this possibility were true, we would predict that acutely after recombination in the pancreatic cells there will be a decrease in HK2 levels and glycolytic metabolism. In order to test this hypothesis, we are treating our Drp1 WT and Drp1 null mice with tamoxifen and will isolate early pancreatic cells 10 days post-injection. These cells should have undergone recombination and should have experienced minimal selective pressure. Once we isolate these cells, we will measure HK2 levels by western and perform glycolytic stress tests to measure differences in glycolytic metabolism. If our hypothesis is true, we expect these early-recombined pancreatic cells to recapitulate the MEF data. However, it is possible that we still may not see any differences between Drp1 WT and null early-recombined cells. If this is the case, one explanation would be that adaptation is occurring even after only 10 days and the Drp1 null cells may have already overcome the initial HK2 downregulation caused by loss of Drp1. In this scenario, we could isolate pancreatic ductal cells from KRas mutant Drp1 WT and Drp1 null mice that haven't been exposed to tamoxifen. We would treat the isolated ductal cells with tamoxifen *in vitro* to induce recombination and determine the effects of acute Drp1 loss.

As we have examined potential ways to reconcile regulation of glycolytic metabolism between MEFs and tumor cells, it is notable that we also found that loss of Drp1 results in defects to mitochondrial metabolism. $Drp1^{-/-}$ tumor cells exhibit mitochondrial dysfunction and

consequently increase the catabolism of cellular lipids to potentially overcome the energy deficit that results. There are also defects in amino acid metabolism as well as the TCA cycle in the $Drp1^{-/-}$ tumor cells. Future studies will aim to elucidate how Drp1 is causing changes to these pathways as well.

The identification of a glycolytic defect in $KRas^{G12D}$-expressing, Drp1-null MEFs is somewhat unexpected, given the previous studies that reveal roles for Drp1 in both mitochondrial and peroxisomal metabolism (Wai and Langer, 2016). However, these findings suggest that inhibition of Drp1 may be a novel means to target tumor cell glycolytic metabolism, given the near universal upregulation of glycolytic flux observed in human tumors (Bensinger and Christofk, 2012). Furthermore, the identification of common vulnerabilities in the tumors that arose in the absence of Drp1 (i.e. - a dependence on lipid oxidation) suggests therapeutic strategies that combine Drp1 inhibition with inhibitors of mitochondrial metabolism may prove both efficacious and robust in the treatment of pancreatic cancer and potentially a wide variety of other malignancies.

Chapter 5: Perspectives

Pancreatic cancer is currently the fourth leading cause of cancer related deaths in the US and is projected to rise to second by 2030. While significant progress has been made in the 5-year survival rate for many other cancer types, pancreatic cancer remains the lowest at roughly 8%. In order to improve patient survival outcomes, it is critical to expand our knowledge of pancreatic cancer development and progression with the goal of finding novel therapeutic targets. The findings described in this thesis provide new insight into the role of Ras-mediated mitochondrial dynamics in cancer progression and physiology. Previous work in the field focused on understanding Drp1 function in normal cellular contexts. For example, previous groups have demonstrated that Drp1 oligomerizes around mitochondria to drive mitochondrial fission and that Drp1-mediated mitochondrial fission promotes equal distribution of mitochondria to daughter cells during mitosis (Bleazard et al., 1999; Taguchi et al., 2007). It was further shown that the RalGEF pathway plays an important role in the process of mitochondrial fission for mitosis by mediating the interactions between Drp1 and one of its activating kinases, Cdk1 (Kashatus et al., 2011). The data presented here develops the understanding of how mitochondrial dynamics can promote disease. Specifically, the data focus on the manner in which cancer signaling pathways can co-opt mitochondrial machinery to change mitochondrial morphology. The change in mitochondrial morphology in turn causes physiological changes within the cell to support tumor growth.

In this dissertation, we first demonstrate that the mitochondrial fission protein Drp1 is a direct substrate of the Ras-mediated MAPK pathway and that the fission activity of Drp1 is necessary for xenograft growth. We next demonstrate that oncogenic Ras can inhibit mitochondrial fusion as well, which suggests that Ras may be acting in a bimodal manner to upregulate fission and simultaneously downregulate fusion. This activity drives mitochondria into a fragmented state that is important for tumor growth. Finally, in an *in vivo* pancreatic cancer

model we demonstrate that Drp1 promotes pancreatic cancer lethality. Tumor cell lines derived from our *in vivo* model that have lost Drp1 display increased lipid catabolism to possibly compensate for dysfunctional mitochondria.

While these data provide a more in-depth understanding of how Ras-mediated regulation of mitochondrial dynamics can support tumor growth, there remain several important questions about how to reconcile the differences in metabolism seen in KRas mutant MEF cell lines and murine-derived tumor cells lines, as well as questions about the broader role of mitochondrial dynamics in cancer. For example, it is still unclear how the regulation of mitochondrial dynamics can affect other cellular processes that are known to promote tumorigenesis such as resistance to apoptosis, increased autophagy and more recently, increased macropinocytosis. Further, the work presented in this thesis only focused on changes in a subset of metabolic pathways in cellular physiology such as aerobic respiration (oxidative phosphorylation), glycolysis and lipid metabolism. How mitochondrial dynamics can cause changes in other types of cellular metabolism important for cancer such as glutamine metabolism will be important areas for further research. In our *in vivo* model, we focus on the consequences of Drp1 loss for tumor cells, however, we didn't explore if mitochondrial fission activity is itself important for tumorigenesis *in vivo*. This important distinction will inform future strategies for targeting mitochondrial dynamics. This chapter sets out to provide some initial insight into these burgeoning questions and ways to potentially test them. Finally, the chapter will explore the potential of Drp1 to serve as a therapeutic target for pancreatic cancer patients.

5.1 How can the metabolic changes happening in MEFs be reconciled with the metabolic changes happening in tumor-derived cell lines?

In chapter 4, we utilized an *in vitro* MEF system derived from our pancreatic cancer mouse model to test the physiological effects associated with loss of Drp1 in an endogenous mutant KRas model. In this system, we found that in the KP cells (KRasG12D, Drp1 WT), Drp1-mediated

HK2 expression promotes increased glycolysis, which partially contributes to KRas-driven anchorage independent growth. Surprisingly, when we studied mouse tumor cells lines generated from our pancreatic cancer model, we were unable to recapitulate the effects of Drp1 loss on HK2 expression and glycolysis. The Drp1 null tumor cells lines had similar levels of HK2 expression as well as flux through glycolysis when compared to the Drp1 WT cells. These results suggest that the relationship between Drp1 and the regulation of glycolysis require further investigation in terms of how to interpret the MEF data in relation to the tumor cell line data.

In chapter 4, we discussed some possible ways to reconcile the MEF data with the tumor cell line data. In this section, we expand on some of those possibilities as well as to offer some preliminary evidence to suggest that there may be a selective pressure to upregulate glycolysis after Drp1 loss.

5.1.1 Are the MEF metabolism data and tumor cell line metabolism data cell-type specific?

As mentioned in the discussion of chapter 4, the simplest explanation to address the differences between the MEF data and the tumor cell line data is that they are merely cell-specific differences. This remains a plausible explanation as the MEFs and pancreatic ductal epithelial cells are structurally different cell types with respective physiological functions that may be too functionally different to be regulated by Drp1 in a similar manner (Mallinjoud et al., 2014). Additionally, there are other important aspects to consider when trying to compare the MEF cells to the tumor cell lines, such as the cell of origin that gave rise to the clones that were used to generate our tumor cell lines. If the cell of origin was an epithelial cell, this would not discredit the argument for cell-specific differences between the MEFs and tumor cell lines as fibroblasts may be too functionally distinct from epithelial cells and would limit direct comparison. However, if tumor cells had undergone epithelial to mesenchymal transition (EMT) before we isolated clones for cell lines, this would open the possibility that the MEF cells could model the metabolism of the early the tumor cells. This is due to the fact that cells that have undergone EMT go through

extensive metabolic rewiring, resulting in an increased dependence on glycolytic metabolism (Morandi et al., 2017). Thus, it is possible that the cell of origin was an epithelial cell that initially lost HK2 expression and reduced glycolysis after Drp1 loss, but subsequently underwent EMT which could have induced the re-expression of HK2 and elevated glycolysis in the clone that what would eventually become a Drp1 null tumor line. To test this possibility, we are currently analyzing our tumor cell lines for expression of mesenchymal markers to determine whether they have undergone EMT.

A more plausible explanation for sustained glycolytic flux in the Drp1 null tumor cells stems from preliminary data that we've generated using a third set of MEFs. Data from this third set of MEFs suggests that there may be a selective pressure to upregulate glycolytic metabolism in response to loss of Drp1. In those experiments, we saw that, after performing the glycolysis stress test on successive passages of cells, there was a rapid increase in maximal glycolysis levels after each successive passage in the Drp1 null cells (Figure 5.1). In the first experiment (Figure 5.1B), with the earliest passage number, the KP cells had the highest glycolysis levels as previously shown, but KPD cells were well below the P cells in their maximal glycolysis. In the following two experiments (Figure 5.1C and 51.D), the KP cells maintained their advantage, however the KPD cells surpassed the P cells in terms of maximal glycolysis levels. These data suggest that very rapidly after Drp1 loss, even in nutrient-rich cell culture conditions, there is a selective pressure to upregulate glycolysis.

In chapter 4, we also suggest using early-recombined pancreatic ductal cells that have undergone minimal selective pressure to determine if we can recapitulate the MEF data in a more physiologically relevant model. While we are still developing the early-recombined Drp1 null cell lines, we have produced an early-recombined Drp1 WT cell line. Without the null cell line, we can't compare the full effect of Drp1 loss on HK2 expression and glycolysis, but we have used a new class of Drp1 inhibitors (Mallat et al., 2018) to treat the early-recombined Drp1 WT cell line and

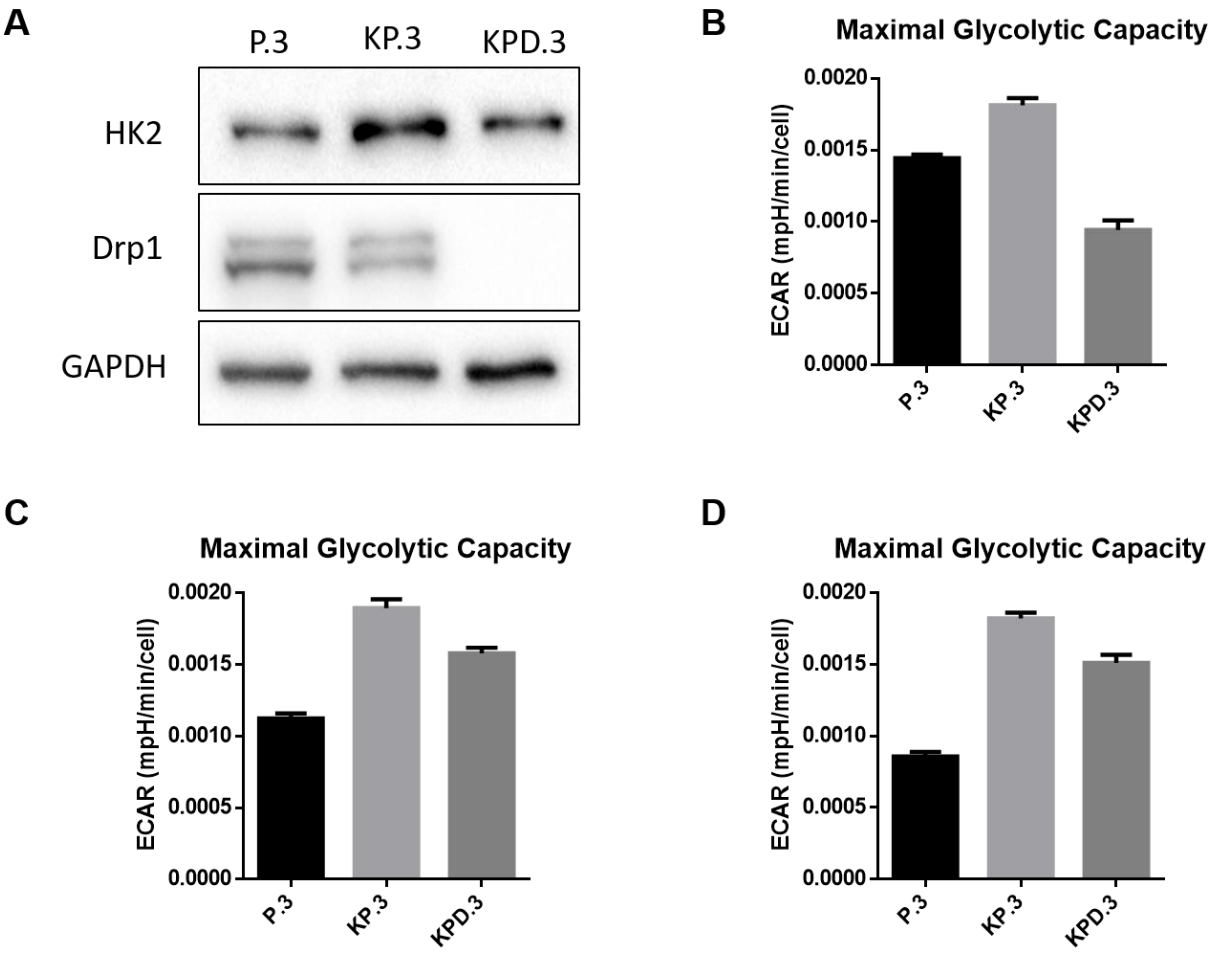
A
P.3
KP.3
KPD.3
HK2
Drp1
GAPDH
B
Maximal Glycolytic Capacity
ECAR (mpH/min/cell)
0.0020
0.0015
0.0010
0.0005
0.0000
P.3
KP.3
KPD.3
C
Maximal Glycolytic Capacity
ECAR (mpH/min/cell)
0.0020
0.0015
0.0010
0.0005
0.0000
P.3
KP.3
KPD.3
D
Maximal Glycolytic Capacity
ECAR (mpH/min/cell)
0.0020
0.0015
0.0010
0.0005
0.0000
P.3
KP.3
KPD.3

Figure 5.1. HK2 expression level and Glycolysis in MEF.3 cells.

(A) Western blot demonstrating HK2 and Drp1 expression level in a third set of P (KRas WT, Drp1 WT), KP (KRasG12D, Drp1 WT) and KPD (KRasG12D, Drp1-/-) cells. GAPDH is used as a loading control. (B-D) Maximal glycolytic capacity of P.3, KP.3 and KPD.3 cells. (B) Earliest passage of MEF.3 cells, (C-D) Maximal glycolytic capacity of subsequent passages of MEF.3 cells.

measure changes in HK2 expression. While the data (not shown) are preliminary we find that in this cell line, inhibition of Drp1 results in decreased expression of HK2. Although preliminary, this result would suggest that initially, loss of Drp1 in the presence of mutant KRas results in decreased HK2 expression and glycolysis and that there may be a selective pressure to upregulate these processes as the tumors adapt to Drp1 loss. In other words, the MEF data could potentially be a physiologically relevant model to examine the effect of Drp1 loss in KRas mutant cells.

The other possibility with the early-recombined pancreatic cell experiment is that we may never see a difference between the Drp1 WT and null cells, regardless of the timepoint at which we isolate the cells. This scenario would suggest that Drp1 doesn't regulate HK2 and glycolytic metabolism in pancreatic cancer cells in the same manner it regulates HK2 and glycolysis in MEF cells. In this instance, we can test for differences between Drp1 WT and null cells in other metabolic processes to determine if we can find a link between MEFs and tumor cells.

5.1.2 What is the role of KRas-mediated stromal cell reciprocal signaling?

Another possibility to consider is the role of KRas-mediated stromal cell reciprocal signaling as a mechanism to explain the absence of a difference between Drp1 WT and tumor cell lines in their Hk2 expression and glycolysis levels. Recently, Tape et al. found that mutant KRas in tumor cells can regulate signaling of surrounding stromal cells. Those KRas-activated stromal cells can in turn reciprocally activate other signaling pathways in the original tumor cells which can essentially double the signaling output of the original tumor cell (Tape et al., 2016). For example, the authors assert that the field previously believed that KRas cell-autonomously regulates AKT signaling. However, they discover that that activation of AKT in PDAC tumor cells is dependent on reciprocal stromal cell signaling. Interestingly, the authors find that the functional consequences of the reciprocal signaling axis includes regulation of protein abundance, transcription, metabolism, proliferation and anchorage independent growth. In terms of the

mitochondrial-associated proteins specifically, KRas-mediated stromal cell reciprocal signaling can restore the expression of HK1 and HK2 as well as VDAC, the receptor for HK2 at the outer mitochondrial membrane (Tape et al., 2016). These data suggest that after tumors have been established and the PDAC stromal response has been developed, KRas in the tumor cells can induce reciprocal signaling in stromal cells to upregulate HK2 levels in the tumor cells. Therefore, if Drp1 loss causes downregulation of HK2, it is possible that the Drp1 null tumor cells may be able to re-express HK2 due to the reciprocal signaling axis. To test this hypothesis, we could knockdown HK2 in the Drp1 WT tumor cells and co-culture them with cancer associated fibroblasts (CAFs), with a set of Drp1 WT-HK2 knockdown cells alone as a negative control. We could measure HK2 levels after the co-culture to see if the CAFs caused an increase in HK2 expression. Previous studies have shown that KRas reciprocally signals to stromal cells via the sonic hedgehog-smoothened-glioma-associated oncogene (SHH-SMO-GLI) pathway. To determine if the reciprocal stromal axis was mediating the HK2 re-expression, we could treat the CAFs with an SHH inhibitory antibody and subsequently measure HK2 expression compared to vehicle control. Collectively, the possibilities outlined in this subchapter and the experiments proposed to test them would provide more insight into the ways in which KRas can overcome the loss of Drp1 to potentially maintain expression of HK2. Thus, the *in vivo* adaptations that may occur in the tumor cells pre-isolation would not occur in the *in vitro* MEF system and would help to explain the discrepancy between the two sets of data.

5.2 What other physiological processes can be regulated by Drp1 and mitochondrial dynamics?

In chapter 4, we focused primarily on the metabolic changes that were being driven by Drp1 in the context of mutant KRas *in vitro* and *in vivo*. For our *in vitro* studies, we utilized MEFS generated from our genetically engineered mice that express mutant KRas with or without Drp1. We found that KRas mutant, Drp1 WT cells had increased glycolytic potential compared to Drp1

null cells. This effect could be partially rescued by re-expressing Drp1 in the null cells. However, there are several other physiological processes important for tumor growth that have been shown to be regulated by KRas. How these cellular mechanisms may be affected by changes in mitochondrial dynamics will be critical to understand how mitochondrial dynamics promote pancreatic cancer. This subchapter will focus on how KRas can cause changes in apoptosis, autophagy and macropinocytosis, how we may go about testing the contribution of mitochondrial dynamics to these KRas-mediated changes and how we could interpret the results of these experiments.

5.2.1 How can Drp1 and mitochondrial dynamics cause changes in apoptosis?

One of the key determinants for the success of chemotherapeutic strategies *in vivo* is the responsiveness of a tumor to apoptosis. In chapter 4, the data demonstrate that loss of Drp1 provides a pancreatic cancer survival benefit of 45 days *in vivo,* which translates to a 38% increase in survival compared to KRas mutant Drp1 WT mice (Figure 4.2A). In an attempt to explain the differences between Drp1 WT and Drp1 null mice, we analyzed the contribution of Drp1 to changes in metabolic profiles of MEFs and cell lines generated from the tumors of the respective mice. The data show that in the MEFs and tumor cell lines, Drp1 causes metabolic rewiring that could contribute to tumor outgrowth of Drp1 WT mice. Interestingly, studies have shown that the metabolic changes in cancer cells could also be promoting changes in apoptotic pathways (Matsuura et al., 2016). Such a relationship may provide additional insight into the difference in survival between WT and null mice.

In the intrinsic apoptosis pathway, an intracellular stressor initiates cleavage of Bid into truncated Bid (tBid). tBid can go on to interact with proapoptotic Bcl-2 family proteins Bax and Bak, which cause mitochondrial outer membrane permeabilization (MOMP). MOMP results in the release of cytochrome C into the cytosol where it can interact with Apaf-1 to create the apoptosome. The apoptosome triggers the caspase cleavage cascade and results in cell death.

In human non-small cell lung cancer (NSCLC) cell lines with mutant KRas, Hata et al. found that there is a downregulation of proapoptotic proteins Bcl-2-like protein 11 (BIM) and p53 upregulated modulator of apoptosis (PUMA) that drives resistance to apoptosis after combinatorial treatment with MEK and PI3K inhibitors (Hata et al., 2014). Furthermore, studies have shown that Hypoxia-Inducible Factor-1 alpha (HIF-1), which can be induced by KRas (Kikuchi et al., 2009), can promote resistance to apoptosis by upregulation of glucose uptake and glycolysis (Dong and Wang, 2004; Kilic et al., 2006). The data presented in chapter 4 suggest that in MEFs with mutant KRas and Drp1 WT, there is an increase in glycolytic potential that is compromised by loss of Drp1. Furthermore, Drp1 WT cells have increased cell accumulation over time as well as superior colony formation in soft agar. As it has been reported that glycolysis can suppress apoptosis, it is tempting to hypothesize that the resistance to apoptosis induced by increased glycolysis may also be promoting increased cell accumulation as well as colony formation in Drp1 WT MEFs. To test this hypothesis, we could repeat the cell accumulation assay over five days with the P, KP and KPD cell lines and stain the cells with an apoptosis marker, such as annexin V, after each harvest. We could analyze the number of apoptotic cells after each day by flow cytometry to determine if there are any differences between the genotypes. If there is less apoptosis in the KP cells compared to the KPD cells, this would suggest that Drp1 is promoting resistance to apoptosis, possibly through increased glycolysis. To directly test the contribution of glycolysis to apoptotic resistance, we could add back HK2 to Drp1 null cells to increase glycolysis and measure apoptosis over time to determine if exogenous HK2 can rescue apoptosis resistance in the null cells. Conversely, we could treat the different genotypes with an inhibitor of glycolysis, such as 2-Deoxyglucose (2-DG) in order to prevent glycolysis-mediated suppression of apoptosis. In this scenario, the KP cells, which normally have increased glycolysis compared to the KPD cells, should become more sensitive to apoptosis over time and we would predict to see more comparable levels of apoptotic cells between the genotypes. Another possibility is that there is no significant difference in apoptosis between the cells. This could be due to the fact that the cells

are grown in full media conditions over the five-day cell accumulation assay and are not experiencing stress inducing conditions that would promote apoptosis. In order to address this caveat, we could perform the cell accumulation assay under different nutrient deprivation conditions to induce apoptosis and test for differences. Alternatively, we could treat with an apoptosis inducer, such as staurosporine, and look for differences in resistance to apoptosis.

5.2.2 How can Drp1 and mitochondrial dynamics cause changes in autophagy?

Aside from the classic hallmarks of cancer, the process of recycling cellular components known as autophagy is gaining appreciation as a mechanism tumor cells use for survival (White, 2015). Briefly, autophagy is regulated by numerous energy/nutrient sensing proteins such as 5' AMP-activated protein kinase (AMPK) and mTOR and by growth factors. These proteins signal to autophagy components such as the unc-51 like autophagy activating kinase (ULK1) kinase complex that initiates the development of phagophores. Additionally, there are several sets of autophagy related gene (ATG) proteins, such as ATG5, that utilize a ubiquitin-like conjugation system to regulate autophagosome maturation (Yang and Klionsky, 2010). Under conditions of stress, such as starvation, phagophores begin to engulf cytosolic contents and will subsequently fuse to become an autophagosome. The autophagosomes will go on to fuse with lysosomes to generate autolysosomes, which have the ability to degrade the cytosolic components. The material produced by the autolysosomes are transported into the cytoplasm where they can be used for cellular processes. Recent findings suggest that autophagy is a feature of Ras-driven cancers (Bryant et al., 2014). In PDAC specifically, studies have shown that tissue samples from patients display high levels of light chain 3 (LC3) protein, which is a marker for autophagosome formation. High LC3 expression correlated with poor patient prognosis (Fujii et al., 2008). Furthermore, Yang et al. showed that loss of ATG5 or pharmacological inhibition of autophagy with chloroquine led to reduced PDAC cell line fitness as well as increased survival in a KRasG12D mouse model of PDAC (Yang et al., 2011).

Interestingly, Yang et al. found that inhibition of autophagy in PDAC cell lines was associated with decreased mitochondrial function (Yang et al., 2011). Data presented in chapter 4 suggests that loss of Drp1 in mouse tumor cell lines results in decreased accumulation of fatty acids as well as decreased mitochondrial respiration (Figure 4.4A). One interpretation proposed in chapter 4 is that the mitochondria in Drp1 null cells utilize more of the fatty acids as energy substrates in an attempt to compensate for dysfunctional mitochondria. Another possibility, corroborated by the previously mentioned study, is that the loss of Drp1 results in decreased autophagic flux in the presence of mutant KRas. Further support for this possibility stems from a study by Zou et al. which showed that in MDA-MB-231 breast cancer cells with mutant KRas, inhibition of Drp1 resulted in suppression of autophagy as well as metabolic reprogramming (Zou et al., 2016). Further still, Guo et al. found that autophagy inhibition in immortalized baby mouse kidney epithelial cells (iBMK) with ectopic mutant KRas expression led to mitochondrial dysfunction (Guo et al., 2011). From a steric perspective, Drp1-mediated mitochondrial fission activity would facilitate the engulfment of mitochondria by autophagosomes due to their reduced size upon fragmentation. This form of mitochondrial autophagy, known as mitophagy is thought to be necessary for mitochondrial quality control (Shirihai et al., 2015). Based on these data, we hypothesize that, in KRas mutant cells with Drp1, Drp1 facilitates the induction of autophagy in order to maintain mitochondrial quality. In order to elucidate the relationship between Ras-induced mitochondrial fission and autophagy, we could treat KRas mutant Drp1 WT and KRas mutant Drp1 null tumor cells with autophagy inhibitors and measure mitochondrial respiration via a mitochondrial stress test. If Drp1 is promoting autophagy to maintain mitochondrial function, the Drp1 WT cells should have decreased respiration, possibly to levels seen in Drp1 null cells, whereas the Drp1 null cells would exhibit negligible effects on their already defective mitochondrial respiration under pharmacological autophagy inhibition. Additionally, we could also perform immunofluorescence colocalization experiments between the mitochondria and autophagy machinery to compare levels of mitochondrial clearance between Drp1 positive and

null cell lines. If Drp1 is promoting autophagy in the context of mutant KRas, we would expect to see increased colocalization between mitochondria and the autophagy machinery in the Drp1 WT cells compared to the null cells. If these hypotheses were to hold true, they would suggest that Drp1 can control autophagy in KRas-driven pancreatic tumors and would support previous findings showing that Drp1 plays a role in regulating autophagy in breast cancer (Zou et al., 2016).

5.2.3 How can Drp1 and mitochondrial dynamics cause changes in macropinocytosis?

Intracellularly, KRas mutant cancer cells use autophagy to recycle cellular components, however they are also able to uptake extracellular material to aid their survival in a process known as macropinocytosis (Bryant et al., 2014). Briefly, macropinocytosis is a form of clathrin-independent endocytosis of heterogeneous vesicles greater than 0.2 μm in diameter. Macropinocytosis is initiated by cytoskeletal rearrangement at the plasma membrane. The membrane becomes ruffled and may eventually fold back onto itself, fusing with the basal membrane, which results in the enclosure of a portion of extracellular fluid (Lim and Gleeson, 2011). These new vesicles are classified as macropinosomes and undergo a process known as “tabulation” to form more spherical structures during the maturation process (Racoosin and Swanson, 1993). The contents of the macropinosomes are degraded if they fuse with lysosomes or are transported back to the plasma membrane (Lim and Gleeson, 2011).

Interestingly, studies have shown that overexpression of oncogenic Ras proteins can induce macropinocytosis (Bar-Sagi and Feramisco, 1986). Commisso et al. discovered that KRas mutant human pancreatic cancer cell lines had increased macropinocytosis compared to wild type Ras expressing cells isolated from the same tumor, which suggests that endogenous mutant KRas can promote macropinocytosis (Commisso et al., 2013). They went on to demonstrate that KRas mutant cells use macropinocytosis as a mechanism to scavenge amino acids such as glutamine, which can provide nutrients for the tumor cell. Furthermore they demonstrated that pharmacological inhibition of macropinocytosis with ethyl isopropyl amiloride (EIPA) resulted in decreased xenograft growth of pancreatic cancer cells (Commisso et al., 2013).

Given the role of mutant KRas in inducing macropinocytosis in tumor cells and that KRas can induce mitochondrial fission, it is possible that there may be a link between mitochondrial fission and macropinocytosis. Studies have shown that, in invasive ovarian cancer cells, mitochondria localize to leading edge lamellipodia, which results in increased mitochondrial mass and ATP concentration in these areas (Cunniff et al., 2016). Further, Cunniff et al. demonstrated that mitochondrial trafficking is necessary for cytoskeletal remodeling at the leading edge. In support of the idea that mitochondrial migration to the leading edge of motile cell supports cytoskeletal remodeling, Zhao et al. showed that Drp1-mediated mitochondrial fission is necessary for accumulation of mitochondria at the leading edge and lamellipodia formation (Zhao et al., 2013b). Together, these studies suggest that Drp1-mediated mitochondrial fission and subsequent mitochondrial trafficking is necessary for the cytoskeletal remodeling that must occur to generate membrane protrusions that facilitate cell motility. Interestingly, macropinocytosis is also dependent on cytoskeletal dynamics and remodeling in order to endocytose extracellular material (Lim and Gleeson, 2011). Based on these observations, it is possible that in PDAC tumors, active KRas signals to promote mitochondrial fission, which in turn promotes the cytoskeletal remodeling necessary for macropinocytosis to occur. To test this hypothesis, we can incubate Drp1 WT and null tumor cells with fluorescently labeled yeast protein and determine if there are any differences in protein uptake by microscopy. We would expect to see that the Drp1 null tumor cells have less uptake of protein. To further test this hypothesis, we could perform live cell imaging on the Drp1 WT and null tumor cells to visualize membrane ruffling. We would predict that the Drp1 null cells, which would have less capacity for membrane remodeling, would exhibit less membrane ruffling. The loss of membrane remodeling and protein uptake in the Drp1 null cells would suggest a role for Drp1 in promoting macropinocytosis in PDAC.

Other extracellular material that can be taken up by macropinocytosis includes mitochondrial contents. Studies show that internalization of functional isolated mitochondria can rescue mitochondrial function as well as cellular viability in cells with depleted mitochondrial DNA.

These effects were dependent on macropinocytosis, as inhibition with EIPA mitigated the rescue (Kitani et al., 2014). Based on the studies presented in this subsection as well as our data, one intriguing possibility is that KRas-mediated Drp1-dependent mitochondrial fission may be a mechanism to fragment mitochondria and prime them for exocytosis. The exported mitochondrial content may then be macropinocytosed by neighboring cells to maintain mitochondrial function and cellular fitness. This idea is completely untested and there is currently no preliminary data from our laboratory to suggest this may be possible. However, studies have shown that mitochondrial proteins and DNA can be secreted out of cells to induce cellular responses in neighboring cells (Unuma et al., 2015). To test this hypothesis experimentally, we could compare KRas mutant MEFs and tumor cells with and without Drp1 for their ability to secrete mitochondrial content. In this experiment, if Drp1-mediated mitochondrial fission is promoting export of mitochondrial content to be macropinocytosed by neighboring cells, we would expect to see more uptake of fluorescently labeled mitochondrial content in Drp1 WT cells compared to Drp1 null cells by either microscopy or flow cytometry. We could repeat this experiment with Drp1 rescue cells to test if there is an increase in mitochondrial content internalization. In chapter 4 we demonstrate that re-expression of Drp1 causes a partial rescue of colony formation as well as glycolytic metabolism. To test the contribution of macropinocytosis to the rescue effects, we could treat Drp1 WT and null MEFs and tumor cells with the macropinocytosis inhibitor EIPA and determine the effects on colony formation and metabolism. Based on our Drp1 rescue data as well as the studies that demonstrate that mitochondrial macropinocytosis can rescue cell viability (Kitani et al., 2014), we would expect that macropinocytosis is playing some role in promoting Drp1 rescue. If we find that there is no difference in macropinocytosis of mitochondrial content between the two cell subsets, this may suggest that Drp1 is not playing a role in promoting mitochondrial uptake, and we could test if Drp1 is regulating uptake of other nutrients sources.

5.3 Does Drp1 promote other types of metabolism important for tumor growth?

In chapter 4, we focused primarily on how Drp1 can cause the changes in glycolysis and lipid metabolism. We found that in MEFs, mutant KRas causes a significant increase in glycolytic metabolism and loss of Drp1 compromises the ability of KRas mutant MEFs to perform maximal glycolysis. The increase in glycolytic metabolism was due, in part, to a Drp1-mediated increase in HK2 levels. As described previously, pancreatic tumor cells generated from our inducible mouse model displayed a distinct metabolic phenotype from the MEF cell lines. The Drp1 WT and Drp1 null cells had comparable levels of glycolytic metabolism whereas they had marked differences in their oxidative metabolism. We showed that the tumor cells had dysfunctional mitochondria and that they increased catabolism of lipids to possibly compensate for reduced mitochondrial respiration. The changes in glycolytic and lipid metabolism encompass some of the key metabolic pathways that have been characterized as critical for tumor growth (Jose et al., 2011). However, there are several types of metabolic pathways that tumor cells can co-opt in order to maintain nutrient levels, amino acid supplies as well as to mitigate ROS toxicity (Kashatus, 2017). This subchapter will cover some of the metabolic pathways that have been previously established as necessary for tumor survival, as well as emerging pathways that have recently gained an appreciation for their role in promoting tumor cell metabolism.

5.3.1 Does Drp1 promote glutamine metabolism in pancreatic cancer?

Along with glycolysis, it has been known for some time that cancer cells also have an increased reliance on glutamine (Bryant et al., 2014). Early studies showed that *in vitro*, proliferating cells preferentially utilized glutamine up to ten times more than any other amino acid (Eagle, 1955). Glutamine is so critical for cancer cell survival because it is involved in a wide range of physiological pathways that are important for growth. Glutamine provides carbon to drive the TCA cycle which results in macromolecular synthesis. Glutamine is also a nitrogen source for the synthesis of nucleotides and nonessential amino acids as well as hexosamine biosynthesis (Dang, 2012; Hensley et al., 2013). Importantly, Son et al. found that, in KRas mutant PDAC,

there is a shift from the classical glutamate dehydrogenase 1 (GLUD1) pathway to the aspartate transaminase pathway (GOT1) to mediate glutaminolysis and stimulate proliferation (Son et al., 2013). In this study, the authors showed that mutant KRas in PDAC cells increased the expression of GOT1 and decreased the expression of GLUD1. GOT1 mediates the conversion of glutamine-derived aspartate into oxaloacetate, which is eventually converted into pyruvate. The conversion of aspartate into pyruvate leads to an increased NADPH/NADP+ ratio in the cell to preserve the cellular redox state (Son et al., 2013).

The majority of glutamine metabolism takes place in the mitochondrial matrix, however the role of mitochondrial dynamics in the regulation of glutamine uptake and utilization remains unknown (Obre and Rossignol, 2015). Briefly, glutamine is incorporated into the cell where it is primarily found in the cytoplasm. Glutamine then gets taken up by the mitochondria and converted into glutamate (Glu) by glutaminase (GLS1). In the mitochondria of pancreatic cancer cells, Glu is converted into aspartate by GOT2 and the aspartate is transported out of the mitochondria into the cytoplasm to eventually become pyruvate (Son et al., 2013). Interestingly, it has been found that mitochondrial fission can increase the expression of GOT2, which would suggest increased aspartate production in cells with fragmented mitochondria (Jacobi et al., 2015). Thus, it has been shown that fragmented mitochondria can promote GOT2 expression and possibly increase cytoplasmic aspartate levels and that KRas can promote aspartate conversion to pyruvate as well as increased Drp1 activity. Based on these findings, it is tempting to speculate that in KRas mutant cells, Drp1 promotes increased glutamine conversion to aspartate, which would promote KRas dependence on glutamine for redox homeostasis. In order to test this hypothesis, we could first measure levels of GOT2 and ROS between Drp1 WT and null MEFs and pancreatic tumor cell lines. If Drp1 is promoting the conversion of glutamine to aspartate, which goes on to maintain redox homeostasis, we would expect to see increased ROS and decreased GOT2 levels in the Drp1 null cells. This would be due to the loss of mitochondrial fission, which would decrease levels of GOT2 and decrease the flux of aspartate out to the cytoplasm. If the Drp1 null cells have

increased ROS and decreased GOT2 levels, we could perform rescue experiments with GOT2 in the Drp1 null cells. In this experiment, we would expect to see that addition of GOT2 to the Drp1 null cells would lead to decreased ROS levels and could potentially rescue some of the tumorigenic properties of the Drp1 null cells. If we don't detect any differences between the Drp1 WT and null cells in their ROS levels, this would suggest that Drp1 doesn't have an effect on glutamine use for redox homeostasis and we could instead test if Drp1 is promoting utilization of glutamine for TCA cycle intermediates, a process that is dependent on mitochondrial function.

5.3.2 Does Drp1 promote stromal metabolism in pancreatic cancer?

In the field of cancer biology there has been a growing appreciation for the microenvironment within tumors that can support their growth and proliferation. One of the prevailing features of pancreatic cancer specifically is an extensive fibrotic stromal response that is evident in the majority of the tumor (Sousa and Kimmelman, 2014). The aggressive stromal reaction leads to impaired vasculature resulting in hypoxic and nutrient deficient regions within the tumor (Feig et al., 2012). Thus, pancreatic tumors utilize a variety of mechanisms to procure the resources required to sustain their growth including macropinocytosis as previously described (Kamphorst et al., 2015). Another recently identified mechanism pancreatic tumors use to acquire resources is dependent on the activity of certain cell types that make up the stroma. Pancreatic stellate cells (PSCs), one of several components of the desmoplastic pancreatic cancer stroma, have been shown to promote nutrient supply to cancer cells. Specifically, Sousa et al. delineated a novel relationship between PSCs and cancer cells whereby PSCs secrete alanine to fuel oxidative metabolism in pancreatic cancer cells. The PSC alanine secretion is dependent on activation of autophagy that is induced by pancreatic cancer cells (Sousa et al., 2016).

Interestingly, studies have shown that Drp1 can promote autophagic flux in breast cancer cells (Zou et al., 2016). However, the role of Drp1 in driving autophagic flux in stromal cancer cells has yet to be explored. As Sousa et al. demonstrated that the ability for PSCs to undergo

autophagy is critical for their secretion of alanine, we would hypothesize that Drp1 is playing a role in PSC-mediated alanine secretion that supports pancreatic tumor metabolism. To test this hypothesis, we could isolate PSCs from our mouse tumors and knockdown Drp1. We could then pharmacologically induce autophagy, in vector control and shDrp1 PSCs and measure changes in protein levels of autophagy markers. We would expect that the shDrp1 PSCs would have decreased induction of autophagy markers such as LC3-II and p62 compared to the vector control cells. Furthermore, we could determine the amounts of LC3-II puncta formed by confocal microscopy. Once again, we would expect to see fewer puncta formed in the shDrp1 PSCs. To determine if loss of Drp1 affects alanine secretion, we could measure vector and shDrp1 PSC-conditioned media and determine alanine levels. We would expect that the shDrp1 cells would have decreased alanine secretion compared to the vector cells. Finally, to determine if loss of Drp1 affects PSC ability to rewire tumor cell metabolism, we could treat our Drp1 WT tumor cells with vector and shDrp1 PSC-conditioned media. We would expect to see less induction of oxidative metabolism in the cells treated with shDrp1 media compared to the cells treated with vector media. These results would suggest that Drp1-mediated regulation of autophagy in stromal PSCs promotes the cross-talk between tumor and microenvironment. These data would also help to identify a novel component of PDAC tumors where Drp1 could be exploited for therapeutic treatment.

5.4 How does mitochondrial shape promote tumorigenic phenotypes in pancreatic cancer?

Thus far the discussion has centered around ways to test whether Drp1 has effects on other types of metabolism as well as other physiological processes that represent some of the hallmarks of cancer. However, we have yet to examine the functional contribution of Drp1-mediated mitochondrial fission to tumor growth *in vivo* and the question remains outstanding in the fields of mitochondrial and cancer biology. Thus, while there have been several studies on the contributions of mitochondrial machinery to tumor growth (Chapter 2) (Kashatus et al., 2015;

Serasinghe et al., 2015), the direct effect of mitochondrial shape is not well understood. In other words, what does it mean for a tumor to have fragmented mitochondria versus fused mitochondria? In this subchapter, we explore if tumors necessarily need fragmented mitochondria per se or whether mitochondrial shape is a by-product of some other function of mitochondrial machinery. We also conceptualize theoretical models with which to tease apart the contributions of Drp1 itself and Drp1-mediated mitochondrial fission to PDAC development. We also explore the role of mitochondrial fusion in pancreatic cancer and discuss potential ways to test whether mitochondrial fusion promotes or inhibits tumor growth.

5.4.1 Is mitochondrial fission necessary for tumor growth?

In the field of mitochondrial research, the contribution of mitochondrial fission activity versus non-fission related activity by mitochondrial fission proteins in tumor growth is an important distinction that remains to be answered in an *in vivo* setting. Once it is understood how mitochondrial machinery proteins are mediating tumorigenic properties, it may be possible to develop new therapies to target either the proteins themselves or instead, to modulate mitochondrial shape if it is found that mitochondrial shape directly dictates tumorigenic potential. In chapter 2, we established that Drp1 was necessary for xenograft tumor growth (Kashatus et al., 2015). We demonstrated that, in HEK cells transformed with HRasG12V, knockdown of Drp1 resulted in a significant reduction of xenograft tumor growth (Figure 2.1 E-G). In order to address the contribution of Drp1-mediated mitochondrial fission to xenograft growth, we performed a rescue experiment with a Drp1 S616A mutant, which is incapable of fragmenting mitochondria. In this experiment, we found that addback of WT Drp1 was able to rescue xenograft growth to HEK scramble control levels (Figure 2.6 D-E). However, addback of the Drp1 S616A mutant was unable to rescue xenograft growth, evidenced by comparable tumor volume to HEK shDrp1 xenografts (Figure 2.6 D-E). These data suggest that downstream of HRasG12V, activation of Drp1 and subsequent mitochondrial fission are driving xenograft tumor growth. In a different

experimental setting, Serasinghe et al. demonstrated that Drp1 null MEFs transduced with HRasG12V were unable to form colonies in soft agar, but addback of WT Drp1 was able to rescue colony formation. However, when they added back a Drp1 S616A mutant, they were unable to rescue colony formation (Serasinghe et al., 2015). Taken together with the xenograft data from chapter 2, these results further suggest that the fission activity of Drp1 is promoting the tumorigenic phenotypes associated with HRasG12V transformed cells. At the physiological level, mitochondrial fission seems to be important for cells in order to promote advancement through the cell cycle as well as maintaining mitochondrial quality, concepts previously reviewed in section 1.5.

While these data are compelling, there are several important factors to consider when trying to extrapolate the interpretations of these findings to a mutant KRas setting. First, several studies have shown that the three Ras isoforms have different functions in different contexts. This is evidenced by the fact that KRas is primarily mutated in lung, colon and pancreatic cancer whereas HRas is mainly mutated in head and neck cancers (Cox and Der, 2010). Furthermore, a study from the Jacks laboratory showed that induction of KRasG12D in colon cancer cells was able to drive tumor progression but induction of NRasG12D was not (Haigis et al., 2008). Second, there are differential effects induced by endogenous expression of a protein versus exogenous expression. Tuveson et al. highlighted that endogenous expression of KRasG12D induced transformation in MEFs whereas ectopic expression of KRasG12D does not cause transformation (Tuveson, 2004). Since our studies and the studies performed by Serasinghe et al. were performed by ectopic expression of HRasG12V, we would need to perform experiments with endogenous KRasG12D in order to obtain an understanding of mitochondrial fission activity that is more applicable to pancreatic cancer. With this rationale in mind, in chapter 4 we demonstrated that MEFs with endogenous KRasG12D and Drp1 expression have increased cell accumulation and display anchorage independent growth compared to Drp1 null cells. To test the dependence

of KRas mutant cells on mitochondrial fission activity for anchorage independent growth we could perform soft agar assay rescue experiments with mouse Drp1 S616A. We would expect that the Drp1 S616A rescue cells would have colony formation to a similar extent as the Drp1 null cells, which would suggest that in an endogenous mutant KRas setting, Drp1-mediated fission is promoting tumorigenic properties *in vitro*. To test the necessity of Drp1-mediated fission activity *in vivo*, we could generate KRasG12D/+, Drp1 S616A, p53 fl/fl mice and repeat our survival experiment with the Drp1 WT, Drp1 null and Drp1 S616A mice. Due to the suggested importance of mitochondrial fission machinery for tumors (Nagdas and Kashatus, 2017), we would expect that the Drp1 S616A mice would have similar survival rates to Drp1 null mice. If we see that the Drp1 S616A mice had worse survival rates than the Drp1 null mice, this would suggest that Drp1 can promote tumor growth in a manner that is not dependent on its fission activity. Such a result would also have ramifications for the therapeutic potential of mitochondrial dynamics. If the tumor promoting properties of Drp1 are not dependent on its fission activity, targeting mitochondrial fission would no longer be therapeutically viable. Thus, therapeutic efforts would shift away from inhibiting fission activity and towards targeting mitochondrial fission proteins directly. In other words, there would be no need to oppose fission by trying to overexpress or activate fusion proteins as a potential therapeutic option. Furthermore, such a result would prompt us to explore and test other ways that Drp1 could promote physiological changes in the cell, which were reviewed in section 5.2.

5.4.2 What is the role of mitochondrial fusion in pancreatic cancer?

As the notion that mitochondrial fission machinery promotes tumor growth appears to be gaining acceptance in the field of cancer research, the reciprocal concept of mitochondrial fusion inhibiting tumor growth seems to be gaining traction as well. While our laboratory has demonstrated that Ras can signal through Erk2 to drive mitochondrial fission, in chapter 3 we demonstrate the ability for HRasG12V to partially inhibit mitochondrial fusion in HEK cells

(Nascimento et al., 2016). Other studies have shown that Ras-MAPK signaling can phosphorylate Mfn1 to inhibit Mfn1 activity, resulting in fragmented mitochondria (Pyakurel et al., 2015a). Furthermore, Mfn2 has been shown to bind and sequester Ras, which leads to MAPK inhibition in rat vascular smooth muscle cells (Chen et al., 2004). Recently, Xu et al. have measured the effect of blocking mitochondrial fusion in breast and lung cancer cells (Xu et al., 2017). In MCF7 and A549 cells, CRISPR/Cas9-mediated knockout of Mfn2 results in increased cell viability, colony formation and invasion capability *in vitro* as well as increased tumor xenograft growth. They go on to demonstrate that Mfn2 binds directly to mTORC2 to inhibit mTORC2/Akt signaling. Interestingly, the interaction between Mfn2 and mTORC2 occurs at the mitochondria, which suggests that elongated mitochondria may function to sequester mTORC2 and interfere with its downstream signaling (Xu et al., 2017). It should also be noted that the cell lines used in these experiments had mutations in the PI3k/Akt pathway (MCF7) or direct KRas mutations (A549), which suggests that mitochondrial fusion is acting to oppose tumor progression downstream of active Ras pathways.

While the role of mitochondrial fusion proteins has been studied in a few cancer types with activated Ras and/or Ras pathways, there are no studies exploring the role of mitochondrial fusion in pancreatic cancer either *in vitro* or *in vivo*. Based on the previous studies, which suggest that mitochondrial fusion can inhibit tumor growth in Ras driven lung cancer cells, we would predict that inhibition of mitochondrial fusion would promote tumorigenic properties in our KRas mutant MEFs and tumor cell lines. To test this hypothesis, we could perform a CRISPR/Cas9 knockout of Mfn2 and/or Mfn1 in our KRas mutant Drp1 WT MEFs and tumor cell lines and compare them to vector control for changes to their tumorigenic properties such as cell accumulation, colony formation and xenograft tumor growth. To determine the role of mitochondrial fusion *in vivo*, we could cross our pdx-cre-LSL-KRasG12D/het, p53 fl/fl mice with Mfn1/Mfn2 double knockout mice to generate an inducible mitochondrial fusion knockout mouse model. Once these mice are

generated, we could repeat the survival experiment comparing the KRas mutant Mfn1/Mfn2 WT to the Mfn1/Mfn2 null for differences in longevity. Based on studies that suggest that Mfn1 and Mfn2 can directly interact with Ras (Chen et al., 2014; Chen et al., 2004), we would predict that loss of these mitochondrial fusion proteins (and by extension mitochondrial fusion) leads to decreased longevity *in vivo*. In these tumor cells, we would expect there to be increased mitochondrial fragmentation due to an inability to fuse. The effects of this loss of fusion would be two-fold: loss of Ras sequestration and further propagation of the physiological effects of fragmented mitochondria. Failure for loss of mitochondrial fusion proteins to affect longevity would suggest that mitochondrial fusion activity doesn't play a role in mediating pancreatic cancer tumorigenesis. While unlikely, this result would focus our research efforts on the role of mitochondrial fission and the other physiological processes that can be regulated by Drp1.

5.5 Can Drp1 serve as a potential biomarker and/or therapeutic target in pancreatic cancer?

The status of the mitochondria in a host of pathologies is beginning to garner a great deal of attention, with a particular interest in how modulation of mitochondrial shape leads to physiological changes (Lima et al., 2018). Throughout this dissertation, several examples have been highlighted regarding the cellular consequences of fragmented versus fused mitochondria. Under physiological conditions, mitochondria display a wide range of morphologies ranging from elongated tubular networks to fragmented punctate structures depending on cellular needs. In times of nutrient deprivation, mitochondria elongate in order to prevent autophagosomal degradation. Preservation of mitochondria in this manner would allow the cell to maximize energy supply (Rambold, 2011). In cancer cells, several studies, including work presented in this dissertation, suggest that fragmented mitochondria provide a survival benefit perhaps by maintaining mitochondrial quality as well as to allow the cell to undergo increased glycolytic metabolism to provide the building blocks for rapid cell growth (Kashatus, 2017; Trotta and Chipuk, 2017). While fragmented mitochondria is not a unique characteristic of all cancer cells, in

pancreatic cancer specifically, work presented in chapter 2 and chapter 4 shows that Ras-mediated mitochondrial fission is driven by activation of Drp1 (Kashatus et al., 2015). Due to the dependence of PDAC cells on Drp1 for mitochondrial fission, Drp1 represents an attractive candidate for therapeutic exploitation. This subchapter will explore the potential of Drp1 as a biomarker for patients with pancreatic cancer as well as the potential for Drp1 to be used as a therapeutic target for future treatment.

5.5.1 Can Drp1 serve as a biomarker for pancreatic cancer?

Currently, there are no clinical studies examining the expression levels of Drp1 protein, total or activated, in tissue samples of pancreatic cancer patients. Some preliminary data from chapter 2 (Figure 2.5) demonstrate that tumor tissue from PDAC patients have moderate phospho-Drp1 immunohistochemistry staining that colocalizes with the much more intense phospho-Erk1/2 staining. These data suggest that the high p-Erk1/2 stain may serve as a proxy marker for p-Drp1 staining. It is possible that patients could be screened based on their p-Erk1/2 levels and further stratified into p-Drp1 positive patients upon a second screen for Drp1 activity. At this point, the p-Drp1 positive patients could be candidates for treatment with drugs that target mitochondrial fission machinery or drugs that activate mitochondrial fusion. However, these data were generated from a sample of 12 tumors and a far larger sample size will be necessary to make significant conclusions. Nonetheless, the overlap between p-Drp1 staining and p-Erk1/2 staining reveals a promising avenue to pursue.

Drp1 expression level in other types of cancer seems to show some promise for the use of Drp1 as a potential biomarker for patient chemo-sensitivity. Recently, Tanwar et al. have performed an analysis of gene expression data found in The Cancer Genome Atlas (TCGA) from epithelial ovarian cancer (EOC) patients (Tanwar et al., 2016). Their analysis revealed that Drp1 co-expressed with a group of genes responsible for cell-cycle transition in what they term the “Drp1-cell-cycle co-expression module” (Drp1-module). They go on to show that knockdown of

Drp1 in EOC cells caused inhibition of cell cycle progression. Furthermore, expression of the Drp1-module correlated with sensitivity to chemotherapy in primary tumors. Interestingly, KRas is mutated in up to 40% of EOC patients (Khabele, 2015), which suggests that the KRas-Drp1 signaling axis in EOC may be involved in mediating the downstream Drp1 cell cycle activity.

In addition to the relationship between Drp1 and cell cycle progression genes in EOC, Tanwar et al. demonstrated a potential link between ovarian cancer stem cell markers and Dp1 (Tanwar et al., 2016). In their study, they analyze the expression of ovarian cancer stem cell markers, such as aldehyde dehydrogenase 1A1 (Aldh1A1), between primary and relapse patient tumor samples. Their analysis revealed an inverse relationship between Aldh1A1 and Drp1 expression where a subset of relapse patient samples expressed high Aldh1A1 and low Drp1. These data suggest that, in a subset of the relapse EOC patients, Drp1 expression may be limiting cancer stemness and may be one way that Drp1-High primary patient tumors are more sensitive to chemotherapy. Thus, the authors suggest that the Drp1-based gene expression signature of primary tumor patients may have some prognostic value for survival post-chemotherapy, as Drp1-High patients may be more likely to respond to chemotherapy.

5.5.2 Can Drp1 serve as a potential therapeutic target in pancreatic cancer?

Data presented in this dissertation align with several studies in the field that suggest Drp1 is a tumor promoting protein. In chapter 2, we demonstrated that knockdown of Drp1 in HEK cells with mutant HRas resulted in reduced xenograft growth that can be rescued by addback of WT Drp1. In chapter 4, we utilized an *in vitro* system more relevant to pancreatic cancer and demonstrated that loss of Drp1 resulted in decreased cell accumulation as well as compromised colony formation. Both of these tumorigenic properties could be rescued by addback of Drp1. We further demonstrate in an *in vivo* model of PDAC, that loss of Drp1 results in a 45-day survival advantage or 38% increase in longevity compared to animals that maintain full Drp1 expression. Several studies corroborate these findings in other Ras-driven cancer types ranging from breast

cancer to melanoma (Serasinghe et al., 2015; Zou et al., 2016). Thus, the data overwhelmingly suggest that targeting Drp1 directly to inhibit its function could provide some therapeutic benefit to cancer patients in general.

Efforts to target Drp1 pharmacologically have been hampered by controversy regarding the specificity of putative Drp1 inhibitors. Initially, Cassidy-Stone et al. identified mitochondrial division inhibitor 1 (Mdivi-1), a quinazolinone derivative, from a chemical library screen using yeast model systems (Cassidy-Stone et al., 2008). In their study, the authors found that Mdivi-1 was able to inhibit mitochondrial fission in yeast and mammalian cells by selectively inhibiting Drp1. Several subsequent studies have utilized Mdivi-1 in cancer models and have shown that Mdivi-1 can cause genomic instability in breast cancer cells (Qian et al., 2012) and is able to cause regression of tumor growth in a xenograft model using lung cancer cells (Rehman et al., 2012). However, recent work by Bordt et al. suggests that Mdivi-1 may have off target effects (Bordt et al., 2017). Bordt et al. showed that Mdivi-1 could reversibly inhibit mitochondrial complex I oxygen consumption. The inhibition of complex I oxygen consumption caused a reduction in the generation of ROS due to reduced electron transport chain activity. Unexpectedly, the authors found that, in a variety of different cell systems including rat cortical neurons, MEFs as well as COS-7 cells, Mdivi-1 treatment was unable to shift mitochondrial morphology to an elongated state. Furthermore, they demonstrated that Mdivi-1 poorly inhibited recombinant human Drp1 GTPase activity. Thus, these results suggest that the conclusions made from previous studies regarding the effects of Mdivi-1 mediated inhibition of Drp1 need to be re-evaluated.

In an effort to allay concerns regarding the off-target effects of Mdivi-1, Mallat et al. have discovered and characterized a new class of small molecule inhibitors with specificity for Drp1 (Mallat et al., 2018). Through the use of a compound library to screen small molecules that could inhibit Drp1 GTPase activity, they discovered a novel class of 1*H*-pyrrole-2-carboxamide compounds that inhibit Drp1 assembly-dependent GTPase activity *in vitro*. Studies show that

cells that have lost mitochondrial fusion ability have decreased levels of mtDNA (Livak and Schmittgen, 2001). The authors suggest that treatment with these small molecules results in restoration of wild type mtDNA copy number in Mfn1 KO MEFs, which suggests that mitochondrial fusion has been restored presumably through inhibition of Drp1. The authors further specify that they have identified both full and partial inhibitors of Drp1. They speculate that the partial inhibitor is selective for the oligomeric form of Drp1 whereas the full inhibitors are able to inhibit the non-assembled cytosolic Drp1 (Mallat et al., 2018). The emergence of partial and full inhibitors of Drp1 may enable researchers to ask specific questions about the mechanisms used by Drp1 to induce mitochondrial fission coincident with the physiological changes to promote tumor growth. Due to the recent discovery of these drugs, they have yet to be tested on any cancer cell lines or *in vivo* models. Nevertheless, the ongoing efforts to find new classes of drugs that can inhibit Drp1 and the rigor being put forth to verify the specificity of these molecules highlights the determination in the field and potential to exploit Drp1 for therapeutic benefit.

The research compiled in this dissertation highlights the strides made in understanding the role of KRas-induced Drp1-mediated mitochondrial fission in cancer. In chapter 2, we established that Ras signals through the MAPK pathway to activate Drp1 whereby Drp1 promotes mitochondrial fission. In chapter 3, we demonstrate that Ras can also inhibit mitochondrial fusion, further shifting mitochondrial morphology into a fragmented state. In chapter 4, we show that in a setting more physiologically relevant to pancreatic cancer, Drp1 promotes tumorigenic properties *in vitro* and *in vivo* settings. Future work on Drp1 and its role in cancer aims to elucidate the ways in which mitochondrial fission causes physiological changes in the cell. While there are still gaps in our knowledge about the physiological consequences of mitochondrial fission for tumor cells, it is becoming increasingly clear that in pancreatic cancers, fragmented mitochondria support tumor growth. Due to this unique phenotype of pancreatic cancer cells, there are extensive efforts

underway to target Drp1 and inhibit this mitochondrial fission, which will hopefully lead to improved patient outcomes.

Chapter 6: Materials and Methods

6.1 Antibodies and reagents

List of antibodies used: α-Drp1, α-Opa1 (BD Transduction Laboratories), α-pS616-Drp1, α-β-tubulin, α-Erk1/2, α-pT202/Y204 Erk1/2, α-Mek, α-CoxIV, α-actin, α-GAPDH, α-BNIP3L/Nix, α-LC3A/B, α-SDHA, α-Mfn1, α-Mfn2, (Cell Signaling Technologies), α-Tom20, α-Raf, α-Fis1 (Santa Cruz Biotechnology), α-Flag (SIGMA), or α-VDAC/Porin (Calbiochem, EMD Millipore).

The chemicals used for our studies were obtained from the following sources: Cyclohexamide was obtained from Sigma-Aldrich (St. Louis, MO). Polyethylene Glycol was obtained from Alfa Aesar (Ward Hill, MA). Accutase was obtained from Innovative Cell Technologies (San Diego, CA) and Triton X-100 was obtained from Amresco (Dallas, TX).

6.2 Cell lines

OPA1 KO and MFN DKO MEFs were purchased from the ATCC (Manassas, VA).Immortalized HEK Vector and $HRas^{G12V}$ cell lines were previously described (Kashatus et al., 2015). The WT MEFs were a generous gift from Dr. Chris Counter.

6.3 Cell Culture

HEK-TtH cells have been described previously (Hahn et al., 1999; Lim et al., 2005). HEK-TtH, HeLa, CFPac and Panc-1 cells were maintained in Dulbecco's Modified Eagle Medium (DMEM - Life Technologies 11965) supplemented with 10% Fetal Bovine Serum (FBS - Life Technologies) and 100 units per ml penicillin, and 100µg/ml streptomycin (pen/strep) (Life Technologies). VMP 608t, BxPC3, L3.6PL and MPanc96 were maintained in RPMI medium (Life Technologies) supplemented with 10% FBS. Capan-1 and Capan-2 were maintained in Iscove's Modified Dulbecco's Medium (IMDM - Life Technologies) supplemented with 10% FBS.

Nutrient-defined media (Figure 4.4H) was made in DMEM (Life Technologies, A14430) and supplemented with 5% FBS, 4mM L-Glutamine (Life Technologies), 5mM D-glucose (Fisher chemicals) or 25mM D-galactose (BD) as indicated. Viable cell numbers were determined by cell counting (Figure 4.1C) or using the CellTiter-Glo Luminescent Cell Viability assay (Promega - Figure 4.1D & 4.4H).

6.4 Plasmids

Two separate Drp1 shRNA sequences (5'-CAGGAGCCAGCTAGATATTAA) (Friedman et al., 2011) or (5' GGACTCTAAACAGGTTACTGA) were cloned into pSuperior-Retro-Neo/GFP or pSuperior-Retro-Puro plasmids (Oligoengine). pSuperior-Retro-Puro-scramble control, pBabe-Bleo $HRas^{G12V}$, pGEX-5X2-$Drp1^{518-736}$ and pBabe-Neo-$Drp1^{K38A}$ were described previously (Hamad et al., 2002; Kashatus et al., 2015). pGEX-5X2-$Drp1^{518-736, S616A}$ and pGEX-4T3-$hErk2^{R67S}$ were generated by site-directed mutagenesis, shRNA-resistant pBabe-Neo-Drp1-flag and pBabe-Neo-$Drp1^{S616A}$-flag were generated by cloning flag-tagged Drp1 (Frank, 2001) into pBabe-Neo then introducing silent mutations at the shRNA recognition sequence and the S616A mutation by site-directed mutagenesis. Mek-DD was generated from human Mek1 (Turski et al., 2012) by mutagenesis and Mek-DD and Raf-22W (Hamad et al., 2002) were cloned into pcDNA3.1. mito-PAGFP was received from Addgene (Plasmid 23348). pDsRed2-Mito was received from Clontech (Plasmid 632421). Transgenes and shRNAs were stably introduced into human HEK-TtH or HeLa cells by retroviral infection as previously described (O'Hayer and Counter, 2006). Transient transfections were performed using FuGENE 6 transfection reagent (Promega) according to the manufacturer's instructions. PD325901 (TSZ chem) was resuspended in DMSO (AMRESCO) at a stock concentration of 10mM and diluted with DMEM to reach the indicated final concentrations.

pBabeBleo empty vector and $HRas^{G12V}$ constructs were previously described (Kashatus et al., 2015). pWZL-Blasti Mito-YFP was generated through PCR amplification of Mito-YFP (Karbowski et al., 2002) (5'-ACCGTCGAATTCGCCACCATGTCCGTCCTGACGCCG-3' and 5'-

GTCGCGGTCGACTTACTTGTACAGCTCGTCCATGCC-3') followed by restriction enzyme digest with EcoRI/SalI and ligation into EcoRI/SalI digested pWZL-Blasti. pWZL-Blasti and pBabeNeo Mito-DsRed were generated by PCR amplification of pDsRed2-Mito (Clontech Laboratories) (5'-ACCGTCGAATTCGCCACCATGTCCGTCCTGACG-3' and 5'-TTTTTTCTCGAGCTACAGGAACAGGTG-3') followed by restriction enzyme digest with EcoRI/XhoI and ligation into EcoRI/XhoI digested pWZL-Blasti or EcoRI/SalI digested pBabeNeo.

6.5 Real-time PCR

6.5.1 For Tumor samples

Total RNA was extracted from a small portion of size-matched frozen xenograft tumors using TRIzol reagent (Life Technologies) according to the manufacturer's protocol. RNA concentration and quality was measured (BioTek Synergy 2 spectrophotometer) and samples were treated with DNase I (New England Biolabs) then inactivated. 1µg RNA per sample was reversed-transcribed (iScript cDNA synthesis kit, BioRad). Real-time PCR was performed on the Applied Biosystems StepOnePlus Real-Time PCR System employing SensiFast SYBR (Bioline) green detection chemistry. Ct was calculated for each sample reaction using hβ2M gene as an internal control. The following primers were used: β2M forward (5'-CTATCCAGCGTACTCCAAAG), β2M reverse (5'-ACAAGTCTGAATGCTCCACT); VEGF forward (5'-AGGAGGAGGGCAGAATCATCA), VEGF reverse (5'-CTCGATTGGATGGCAGTAGCT). The real-time PCR conditions were 95°C for 2 min, followed by 40 cycles of 95°C for 5 sec and 65°C for 30 sec. After the last PCR cycle, each sample was subject to thermal melting curve analysis to check for non-specific product formation.

6.5.2 For cell lines

Cells were harvested from culture and total RNA was extracted using TRIzol reagent (Life Technologies) according to the manufacturer's protocol. Samples were treated with DNase I (New

England Biolabs), inactivated, and RNA concentration and quality was measured (NanoDrop). 1µg RNA per sample was reversed-transcribed (iScript cDNA synthesis kit, BioRad). Real-time PCR was performed on the Applied Biosystems StepOnePlus Real-Time PCR System using Power SYBR green (Life Technologies) detection chemistry. ΔΔCt was calculated for each sample reaction using UbC and ActB genes as housekeeping controls. The real-time PCR conditions were 95°C for 2 min, followed by 40 cycles of 95°C for 5 sec and 65°C for 30 sec. After the last PCR cycle, each sample was subject to thermal melting curve analysis to check for non-specific product formation. Primers used: HK2 Forward (5'-TGATCGCCTGCTTATTCACGG-3'), Reverse (5'-AACCGCCTAGAAATCTCCAGA-3'), ActB Forward (5'-TGACGTTGACATCCGTAAAG-3'), Reverse (5'-GAGGAGCAATGATCTTGATCT-3'), UbC Forward (5'-GCCCAGTGTTACCACCAAGA-3'), Reverse (5'-CCCATCACACCCAAGAACA-3').

6.6 Flow Cytometry

For apoptosis measurement the indicated HEK-TtH cells were harvested by trypsinization, washed with cold PBS and resuspended in 1X Binding Buffer (10mM HEPES, pH 7.4; 140mM NaCl; 2.5mM $CaCl_2$) at 10^6 cells/ml. 100µl of each cell suspension was transferred to a 5ml flow tube to which Annexin V-FITC (BD Pharmingen) and 15µg/ml Propidium Iodide (PI) (Sigma) were added. Cells incubated 15 minutes at RT in the dark, then 400µl of 1X Binding Buffer was added to each tube and cells were analyzed immediately on a FACSCalibur Benchtop Analyzer (Becton Dickinson/Cytek). For mitochondrial mass measurement the indicated cell lines were engineered to stably express mitochondrially-targeted YFP. Cells were then harvested by trypsinization, washed with cold PBS, resuspended in PBS at $5x10^6$ cells/ml and analyzed immediately on a FACSCalibur Benchtop Analyzer (Becton Dickinson/Cytek). For membrane potential measurement the indicated cells lines were harvested by trypsinization, counted and adjusted to a density of 10^6 cells/ml in full culture media. Cells were incubated with 50nM TMRE (Biotium) for

30 minutes at 37°C, 5% CO_2, then washed once with PBS, resuspended in PBS/0.2% BSA and analyzed immediately on a FACSCalibur Benchtop Analyzer (Becton Dickinson/Cytek).

6.7 Mitochondrial Stress Test (MST)/ Glycolysis Stress Test (GST)

6.7.1 MST for HEK cells

Oxygen consumption rate (OCR) was measured using a Seahorse XF24 Extracellular Flux Analyzer with the XF Cell Mito Stress Test Kit. Cells were seeded at $8X10^4$ cells per well in 100µl DMEM (Invitrogen 11965) containing 10% FBS and allowed to attach for 2 hours. 150µl DMEM-10% FBS was added per well and cells incubated overnight in 5% CO_2 humidified incubator. Prior to assay run, cells were changed into assay media, unbuffered DMEM (Invitrogen 12800) pH 7.4 and subjected to sequential injections of Oligomycin (1µM), FCCP (0.3µM), rotenone (1µM) and antimycin A (0.75µM). Spare respiratory capacity was calculated by dividing the OCR response to FCCP by the basal respiration, having subtracted the non-mitochondrial respiration previously. All values were normalized to cell number per wells setup in parallel.

6.7.2 MST/GST for MEFs and Tumor cell lines

Oxygen Consumption Rate (OCR) for MST assays and Extracellular Acidification Rate (ECAR) for GST assays were measured using a Seahorse XF24 Extracellular Flux Analyzer. GST media was made using serum-free DMEM without glucose, glutamine, pyruvate, sodium bicarbonate (Sigma-Aldrich) adjusted to pH 7.4. The day before the experiment, the 24-well cell culture microplates were coated with 50 µL of poly-D-lysine (Millipore) at 10 µg/cm^2/sterile water. The following morning, the plate was washed once with 200 µL of PBS and allowed to air-dry. Cells were plated (40,000 cells per well for MEFs, 125,000 for mouse tumor cell lines) in at least triplicate for each condition the day of the experiment in 100 µL of GST media per well for GST assay and 100 µL per well in unbuffered, serum-free DMEM adjusted to pH 7.4 (MST media) for the MST assay. Cells were then centrifuged at 500RPM for 1 min and supplemented with 575 µL

of GST media or MST media and immediately placed into the analyzer to begin assay. During the GST assay, glucose (BD), oligomycin (Millipore) and 2-deoxyglucose (Chem-Impex) were injected to a final concentration of 10mM, 2 µM and 100mM, respectively. For the MST assay, oligomycin, BAM15 (Cayman) and Rotenone and Antimycin A (Sigma) were injected to a final concentration of 2 µM, 10 µM, 1 µM and 2µM, respectively. At the end of each experiment, each assay was normalized to cell number counted from a sister plate that was seeded concurrently with the experimental plate.

6.8 Drug Treatments

PD325901 (TSZ chem) was resuspended in DMSO (AMRESCO) at a stock concentration of 10mM and diluted with DMEM to reach the indicated final concentrations. Staurosporine (ENZO) was resuspended in DMSO at a stock concentration of 1mM. Chloroquine diphosphate salt (MP Biomedicals) was resuspended in water at a stock concentration of 100mM.

6.9 MTT Assay

The described HEK-TtH cells were plated at 400 cells/well in 5 X 96-well plates and incubated for 72 hours. One plate was assayed every 24 hours by adding 15µl of 5mg/ml 3-(4,5-Dimethyl- 2-thiazolyl)-2,5-diphenyl-2H-tetrazolium bromide (MTT; Sigma). After 4 hours at 37°C, medium was removed and cells were resuspended in 100µl DMSO. Absorbencies were recorded at 540nm (Martin and Clynes, 1993).

6.10 Protein Analysis

Whole cell lysates were prepared in RIPA buffer and equivalent protein amounts (generally 50 or 100µg) were resolved by SDS-Page. Alternatively, equal cell numbers were lysed directly in SDS-Page sample loading buffer and resolved by SDS-Page. Gels were transferred to PVDF membranes and immunoblotted with the indicated antibodies.

6.11 Xenografts

6.11.1 Subcutaneous Xenografts

$2.5X10^6$ (Figure 2.1, 2.S1), $5X10^6$ (Figure 2.4, 2.S3) or $1X10^7$ (Figure 2.6) cells were resuspended in phosphate buffered saline (PBS), mixed 1:1 with Matrigel and injected subcutaneously into the flanks of SCID/beige (Charles River Laboratory), or Athymic Nude-*FoxN1^{nu}* mice (Harlan). Tumor volumes were determined twice per week and calculated as (length X width^2)□/6. Mice were sacrificed when the tumors reached 1000mm^3 or the mice exhibited signs of moribundity, at which point tumors were removed and weighed. Tumors were halved at harvest and formalin-fixed paraffin-embedded or flash frozen. Experiments were approved by the Duke University Institutional Animal Care and Use Committee and the University of Virginia Animal Care and Use Committee.

6.11.2 Orthotopic Xenografts

Orthotopic xenografts of the clonal tumor-derived cell lines were performed as previously described (Walters et al., 2013). Briefly, 100,000 cells suspended in media were injected into the tail of the pancreas. After 3 weeks, mice were euthanized and tumors were excised, weighed and measured via calipers at necropsy.

6.12 Mito-PAGFP assay

HEK-TtH or HEK-TtH HRas^{G12V} cells were plated on glass bottom microwell dishes (MatTek) and transiently co-transfected with 1ug each pDsRed2-Mito and mito-PAGFP. The next day, cells were imaged on an LSM700 confocal microscope (Zeiss) equipped with a 63x oil objective, heated stage and 5% CO_2 incubation. Positively transfected cells were identified as containing red fluorescent mitochondria. A 4μm-wide ROI strip was selected and activated by a single pulse 405-nm laser. Red and green fluorescent Z-stacks (10 slices, 0.7μm each) were acquired before and immediately following activation, then every 15 minutes for 1 hour. Images

show z-stack reconstruction of representative cells at each timepoint. 5-10 cells were assayed per condition.

6.13 Immunofluorescence

The described HEK-TtH, HeLa or pancreatic cancer cell lines were plated on glass microslides the previous day, then mitochondria were visualized by one of the following methods: (1) Cells were treated with 100nM MitoTracker Red CMXRos (Life Technologies) for 30 minutes, fixed, permeabilized and mounted immediately in Prolong Gold antifade reagent with DAPI (Life Technologies); (2) Cells were fixed, permeabilized and incubated with α-Tom20 primary antibody in conjunction with an α-rabbit Alexa-488 secondary antibody (Life Technologies); (3) Cells were engineered to stably express mitochondria-targeted YFP (BD Biosciences). A Zeiss LSM 700 confocal microscope with 63X oil objective was used for imaging. A cell was judged to have fragmented mitochondria if fewer than 25% of the mitochondria visible in the cell had a length 5 times its width and highly interconnected if greater than 75% of the mitochondria had a length 5 times its width. For quantitation, greater than 50 cells per cell type were blindly analyzed by 3-5 people.

Immunofluorescence on FFPE sections was performed as previously described (Wang et al., 2014). Briefly, FFPE sections were deparaffinized and antigen-retrieved using high pH conditions. Sections were then washed, blocked, and incubated with anti-Mitochondria antibody, clone 113–1, Cy3 conjugate (EMD Millipore) overnight. Slides were incubated with $CuSO_4$ to reduce autofluorescence and mounted with Prolong Gold antifade reagent with DAPI (Life Technologies). Images were taken with a Zeiss LSM 700 Confocal with a 63× oil objective or Zeiss LSM 710 Multiphoton microscope with a 63× (NA 1.4) objective.

6.14 *In Vitro* Kinase Assays

Recombinant GST-Drp1$^{518\text{-}736}$, GST-Drp1$^{518\text{-}736,S616A}$ and GST-Erk2^{R67S} were purified from bacteria using glutathione-sepharose-4B (GE) and eluted with 15mM glutathione (Sigma) in

elution buffer. Proteins were dialyzed overnight in 2L elution buffer and concentrated with an Amicon Ultra 10K centrifugal filter device (Millipore). In vitro kinase reactions were performed as described (Levin-Salomon et al., 2008). Briefly, 500ng GST-Erk2^{R67S} was incubated with 500ng of either GST, GST-Drp1$^{518-736}$, or GST-Drp1$^{518-736,S616A}$ in 25μl 1X Kinase Buffer, incubated for 30 minutes at 30°C then terminated with the addition of 25μl SDS-Page sample loading buffer and resolved by SDS-Page followed by either autoradiography (Hot) or immunoblot (Cold).

6.15 ***PEG Fusion Assay***

For the PEG fusion assay, a total of 20 million separately labeled fluorescent MEF cells expressing mito-YFP or mito-DsRed or 40 million separately labeled HEK cells were seeded at a 1:1 ratio in 143 x 22 mm tissue culture dish and allowed to incubate for 12-16 hours. The cells were then washed once with PBS and incubated in Serum Free (SF) DMEM/Cyclohexamide (CHX) (33 μg/ml) solution for 30 min to inhibit de novo protein synthesis. The cells were then incubated with 5 mL of a 50% (wt/vol) solution of PEG 1500 in SF DMEM for 2 min. Following treatment, the cells were washed three times with a solution of 10% FBS/DMEM/CHX and were left to incubate for 4 hours in 10% FBS/DMEM/CHX.

6.16 ***Sample Preparation and Data Evaluation by Imaging Flow Cytometry***

Following PEG treatment, cells were washed twice with DNAse I/PBS (10 units/mL, New England Biolabs) and dissociated using 3 mL of Accutase for 5 min at room temp. The cells were collected in 10 mL of PBS and spun at 1000 rpm for 15 min. The cells were resuspended in 4 mL of PBS and gently filtered through 100 micron filter mesh (Genessee) into 4 mL of a 4% Formaldehyde/PBS mixture to bring the final solution to a concentration of 2% FA/PBS. The cells remained at RT for 10 min with intermittent agitation. The cells were then spun at 2000 rpm for 5 min. The cells were resuspended in 8 mL of DNAse I/PBS and respun at 2000 rpm. The cells were then resuspended in 1 mL of DAPI (1μg/mL, Thermo Fisher Scientific) in 0.1%Triton X-100/DNAse I/PBS. The cells were spun one final time at 2000 rpm for 5 min and resuspended in

50-80 µL of DAPI/0.1% Triton X-100/DNAse I/PBS. The cells are stored at 4˚ C overnight. We utilized 10 million unstained MEF cells for unstained and DAPI compensation controls. 10 million mito-YFP or mito-DsRed cells were also prepared in this manner for YFP and DsRed compensation controls.

Mito-YFP was excited with 20mW of 488nm laser and emission collected in Channel 2 (480-560nm; camera 1), Mito-DsRed was excited with 200mW of 561nm laser and emission collected in Channel 4 (595-660nm; camera1) and DAPI was excited with 20mW of 405nm laser and emission collected in Channel 7 (420-505nm; camera 2). Brightfield images were collected in both Channel 1 (camera 1) and Channel 9 (camera 2) for insuring the same image location across both cameras. Samples were acquired using the 60X magnification option and a minimum of 100,000 DAPI positive events were collected whenever cell concentrations allowed. Individual mito-YFP, mito-DsRed and DAPI fluorescent controls were collected (without brightfield & 758nm scatter laser) for determining spectral overlap (compensation) across image channels. Compensation was performed using the Compensation wizard in IDEAS® 6.0 software.

Compensated data files were analyzed with IDEAS® 6.0 software utilizing the gating strategy in Figure 3. First, we selected well focused cells in the brightfield channel by gating on high gradient RMS (Figure 3A). From this focused population of cells we next gated on single cells with an aspect ratio between 0.6 and 1 and an area ranging from 100-500 units in the brightfield channel (Figure 3B). From the population of focused single cells, we then gated on cells expressing high DAPI staining (Figure 3C). Finally, within the high DAPI gate, we segregated the cell populations based on YFP and DsRed intensity and we selected the double positive (DP) YFP/DsRed population to run the IDEAS® 6.0 software colocalization wizard (Figure 3D). The colocalization wizard uses the Bright-detail Similarity feature to quantify the degree to which two probes are colocalized. The algorithm uses a log transformed Pearson’s correlation efficient of the localized spots within the masked area of two images. The higher the “similarity” score, the

more colocalization between the images. The only exception to this gating strategy was the positive control HEK cell population which co-expresses YFP and DsRed. As these cells did not undergo PEG-mediated cell fusion, they did not need to be isolated through the high DAPI gate. For colocalization analysis of the HEK co-expressing population, after gating on well focused cells and singlets, we segregated by YFP and DsRed intensity and chose the DP population to run the colocalization wizard (Figure 4). Random images from the colocalized and non-colocalized populations were reviewed to determine the accuracy of the algorithm.

6.17 Mouse Strains and Tamoxifen Injections

LSL-KRas$^{G12D/+}$; *TP53*$^{flox/flox}$ mice were provided by Dr. Kwon Park (University of Virginia), *Drp1*$^{flox/flox}$ mice were published previously (Wakabayashi et al., 2009), and *Pdx1-Cre-ER*^{TM} mice were purchased from Jackson Laboratory. These three lines were intercrossed to produce *LSL-KRas*$^{G12D/+}$; *TP53*$^{flox/flox}$; *Drp1*$^{flox/flox}$; *Pdx1-Cre-ER*^{TM} or *LSL-KRas*$^{G12D/+}$; *TP53*$^{flox/flox}$; *Drp1*^{WT}; *Pdx1-Cre-ER*^{TM} (KPDC) mice for subsequent studies. Mice from independent litters were analyzed to control for mixed background effects. The primers used for genotyping were previously described (Gidekel Friedlander et al., 2009; Wakabayashi et al., 2009) and are listed in Extended Data Table 1. Mice with the desired genotypes were treated with tamoxifen on postnatal days 22, 24, and 26 by intraperitoneal injection (IP) of 9mg/40g body weight in corn oil. In accordance with institutional guidelines, mice were monitored and euthanized when they reached pre-determined endpoints to analyze pancreatic intraepithelial neoplasia (PanIN), exhibited features associated with disease, or lost greater than 15-20% of an animal's maximal body weight for the survival endpoints. All animal studies and procedures were approved by the University of Virginia Institutional Animal Care and Use Committee.

6.18 Histology and Immunohistochemistry

12 HIPAA de-identified pancreatic carcinoma specimens, present as formalin-fixed, paraffin-embedded blocks, were obtained from the University of Virginia Biorepository and Tissue Research Facility (BTRF). Tissue sections were cut from each block at 4μm thick intervals. Antigen retrieval and deparaffinization were performed in PT Link (Dako, Glostrup, Denmark) using low pH for p-DRP1 and high pH for p-Erk, EnVision FLEX Target Retrieval Solution (Dako) for 20 min at 97°C. Immunohistochemistry was performed on a robotic platform (Autostainer, Dako). Endogenous peroxidases were blocked with peroxidase and alkaline Phosphatase blocking reagent (Dako) before incubating the sections with p-Drp1 at 1:25 dilution for 60 minutes and p-Erk at 1:200 dilution for 30 minutes at room temperature. Antigen–antibody complex was detected using Envision™ Dual Link (Dako) followed by incubation with 3,3'-diaminobenzidine tetrahydrochloride (DAB+) chromogen (Dako). All slides were subsequently counterstained with hematoxylin then dehydrated, cleared and mounted for assessment. Immunofluorescence on formalin-fixed paraffin-embedded (FFPE) sections was performed as previously described (Wang et al., 2011) on 2 of the 12 HIPAA de-identified pancreatic carcinoma specimens. Briefly, FFPE sections were deparaffinized and antigen-retrieved, washed and blocked then incubated with anti-Mitochondria antibody, clone 113-1, Cy3 conjugate (EMD Millipore) overnight. Slides were incubated with $CuSO_4$ to reduce autofluorescence and mounted with Prolong Gold antifade reagent with DAPI. Images were taken with a Zeiss LSM 710 Multiphoton microscope with a 20x (NA 0.8) or 63x (NA 1.4) objective.

Entire pancreata were isolated from euthanized mice and fixed in 10% buffered formalin (Fisher Scientific) and embedded in paraffin. For pancreata dedicated to the PanIN investigation arm, tissue 3 serial sections were cut at approximately 100μm, 300μm, and 500μm of depth. Formalin-fixed paraffin-embedded (FFPE) tissue sections were cut at 4-5μm thick intervals. One section of each set of serial sections was stained with routine hematoxylin and eosin stain (H&E),

with the other sections dedicated for immunohistochemical analysis of Drp1 or mitochondrial immunofluorescence. Antigen retrieval and deparaffinization were performed in PT Link (Dako, Glostrup, Denmark) using low pH and EnVision FLEX Target Retrieval Solution (Dako) for 20 min at 97°C. Immunohistochemistry was performed on a robotic platform (Autostainer, Dako). Endogenous peroxidases were blocked with peroxidase and alkaline Phosphatase blocking reagent (Dako) before incubating the sections with antibody for DRP1 (Ab184247 - Abcam, 1: 1,000 for 30 min at room temperature). Antigen–antibody complex was detected using Envision^{TM} Dual Link (Dako) followed by incubation with 3,3'-diaminobenzidine tetrahydrochloride (DAB+) chromogen (Dako). All the slides were counterstained with hematoxylin subsequently; they were dehydrated, cleared and mounted for the assessment.

For analysis of angiogenesis, FFPE blocks of size-matched HEK-TtH; HRas^{G12V} and HEK-TtH; HRas^{G12V}; shDrp1 tumors were sectioned by the University of Virginia Research Histology Core for IHC as mentioned above, stained for mouse CD31-mouse (Abcam) and visualized on an Olympus BX51 microscope with a 20X objective.

6.19 PanIN Histologic Analyses

Slides were digitally scanned using an Aperio ScanScope (SC System) with a 20× objective to obtain digital slides. PanIN and PDAC lesions were identified and quantified on the digital slides stained with H&E using ImageScope software (Leica Biosystems) in concert with Fiji/ImageJ software. Detailed protocol provided below. A pathologist reviewed all H&E stained slides.

Using the ImageScope "Annotations" tool, individual PanIN and PDAC lesions were traced by hand. The ImageScope software determined areas of individual lesions. Lymph nodes were also identified, traced, and areas determined for total pancreatic parenchyma area determination. Images of the H&E stained pancreatic sections were deconvoluted using Fiji/ImageJ's code. The hematoxylin portion of the deconvoluted image was used to determine total tissue area. The areas of the lymph node traces were subtracted to determine total pancreatic parenchyma area.

6.20 Generation of Mouse Embryonic Fibroblasts and Tumor-Derived Cell Lines

To generate MEFs, we isolated E13.5-E14.5 aged embryos from pregnant mothers, removed fetal heart and liver structures, and digested the remaining tissue both mechanically and enzymatically with 0.1% Trypsin (Sigma) for 5 minutes at 37^{o}C. After discarding the undigested tissue, the cell suspension was cultured overnight in DMEM supplemented with 10% FBS and pen/strep. Cells were transduced with AAV-CMV-Cre-GFP (UNC Vector Core) to promote recombination at the indicated alleles. Cells were serially diluted and plated in 96-well plates. Single cell clones were identified, expanded and genotyped to confirm recombination.

To generate the tumor-derived cell lines, approximately a 10mm^3 piece of a tumor was isolated at time of necropsy from mice outlined previously. The isolated tumor was minced followed by enzymatic digestion with 2mg/ml Collagenase IV (MP Biomedical) in DMEM supplemented with 10% FBS for 30 minutes at 37^{o}C. Digested and undigested tumor tissues were cultured overnight in DMEM supplemented with 10% FBS and pen/strep. After removal of undigested tissue, adherent cells were isolated, serially diluted and plated in 96-well plates. Where indicated, single cell clones were identified, expanded and genotyped as described above.

6.21 Genotyping of Cell Lines

Cells were harvested from culture plates and centrifuged at 1,000RPM for 5 minutes at 4^{o}C. Cell pellets were resuspended in 200µL DNA Lysis Buffer and incubated at 55^{o}C for at least 1 hour. The lysate was incubated with 95µL 5M NaCl to precipitate proteins and centrifuged at 3,000RPM for 15 minutes at 4^{o}C. DNA was precipitated with isopropanol, resuspended in water, and used for genotyping analysis as described:

KRAS$^{LSL\text{-}G12D/+}$

Forward: 5'-CTAGCCACCATGGCTTGAGT-3’

Forward: 5'-ATGTCTTTCCCCAGCACAGT-3’

Reverse: 5'-TCCGAATTCAGTGACTACAGATG-3’

TRP53

Forward: 5'-CACAAAAACAGGTTAAACCCAG-3’

Reverse: 5'-AGCACATAGGAGGCAGAGAC-3’

PDX1-CreER$^{Tg/+}$

Forward: 5’-GATCTCCGGTATTGAAACTCCAGC-3’

Reverse: 5’-GCTAAACATGCTTCATCGTCGG-3’

DRP1 (Floxed Allele)

Forward: 5’-ACCAAAGTAAGGAATAGCTGTTG-3’

Reverse: 5’-ATGCGCTGATAATACTATCAACC-3’

DRP1 (Recombined Allele)

Forward: 5’-CACTGAGAGCTCTATATGTAGGC-3’

Reverse: 5’-ATGCGCTGATAATACTATCAACC-3’

6.22 Soft Agar Colony Formation Assay

Soft agar assay was performed as described previously (Borowicz et al., 2014). Briefly, 6-well dishes were coated with 3 mL of 1.5% Seaplaque Agarose (Lonza)/DMEM for the bottom-layer and allowed to solidify for 30 min at room temperature or stored at 4°. Once the bottom layer was solidified, 4 x 10^4 cells were seeded in 3 mL of 0.5% Seaplaque Agarose/DMEM in triplicate and placed in 4° for 10 min to solidify and then kept at 37° for three weeks. Cells were fed with 200 µL 1X DMEM every 3-4 days. After three weeks, any residual media was aspirated and cells

were stained with 300 µL of Nitroblue Tetrazolium Chloride (Alfa Aesar, 1mg/mL/PBS) and incubated at 37C° overnight. The following morning cells were imaged using a BioRad ChemiDoc Imaging System. Colonies were quantified using ImageJ.

6.23 Metabolomics

Metabolomics analyses were performed by Metabolon, Inc. (Durham, North Carolina, USA). Tumor-derived cell lines were grown to 70% confluence in 15cm dishes, with a fresh media change one day before harvest. Cells were recovered by trypsinization. The cell pellets were washed once in PBS then pelleted again, removing all supernatant before flash freezing 100ul packed cell pellets for shipment. Proteins were precipitated with methanol under vigorous shaking for 2 minutes followed by centrifugation. The resulting extract was divided into four fractions: two for analysis by two separate reverse phase (RP)/UPLC-MS/MS methods with positive ion mode electrospray ionization (ESI), one for analysis by RP/UPLC-MS/MS with negative ion mode ESI, and one for analysis by HILIC/UPLC-MS/MS with negative ion mode ESI. Instrument variability was determined to be 3% by calculating the median relative standard deviation (RSD) for the quality control standards that were added to each sample prior to injection into the mass spectrometers. Overall process variability was determined to be 9% by calculating the median RSD for all endogenous metabolites (i.e., non-instrument standards) present in 100% of the pooled matrix samples. Experimental samples were randomized across the platform run with QC samples spaced evenly among the injections.

Raw data was extracted, peak-identified and QC processed using Metabolon's hardware and software. Compounds were identified by comparison to library entries of purified standards or recurrent unknown entities. Metabolon maintains a library based on authenticated standards that contain the retention time/index (RI), mass to charge ratio (m/z), and chromatographic data (including MS/MS spectral data) on all molecules present in the library. Peaks were quantified using area-under-the-curve. Data was normalized to total protein as determined by Bradford

assay to account for differences in metabolite levels due to differences in the amount of material present in each sample.

6.24 Radiotracer Metabolic Flux Studies

Cells were harvested from culture the day of assay and 275,000 cells were seeded per well in a 24-well plate in DMEM supplemented with 10% FBS. After 3 hours of incubation, the cells were washed 1× in PBS and then incubated in assay media supplemented with either ^{3}H-glucose (Perkin Elmer) for glycolysis determination or ^{14}C-Palmitate (Perkin Elmer) for oxidative metabolism and/or neutral lipid incorporation determination. For determination of oxidative metabolism, a CO_2 trap with 2M NaOH, was placed in the wells. The wells were sealed and cells were incubated for 2 hours.

For evaluation of glycolysis, 1N HCl was added to the wells with ^{3}H-glucose stop all reactions and all the liquid was collected into an Eppendorf tube. The tube was placed in a scintillation vial containing an equivalent volume of water and allowed to equilibrate overnight. After equilibration, scintillation cocktail fluid was mixed (Optiphase Super, Perkin Elmer) and vials were counted on a scintillation counter (LS6500, Beckman Coulter).

For determination of oxidative metabolism, the assay media and CO_2 trap was transferred to new wells and sealed. 2M perchloric acid was injected into each sealed well to release CO_2 in the media to be captured in the CO_2 trap. The wells were resealed and allowed to incubate at room temperature for at least 1 hour. After incubation, the NaOH was removed from the trap into scintillation vials, scintillation cocktail fluid was mixed and vials were counted on a scintillation counter.

For evaluation of neutral lipid incorporation, the assay media was removed, cells were washed 1× in PBS, and trypsin dissolved in water was added. After cells detached, lipids were extracted using chlorophorm:methanol method. Specifically, the cell suspension was transferred to a 1:2

chlorophorm:methanol mixture and vortexed. The mixture was then sonicated for 10 minutes, centirifuged at 1000RPM for 10 minutes, and lipids were removed. The lipids were dried, scintillation cocktail fluid was mixed, and vials were counted on a scintillation counter.

6.25 Reagent Formulations

RIPA buffer: 1% NP-40, 20mM Tris pH 8.0, 137mM NaCl, 10% glycerol, 2mM EDTA SDS-Page sample loading buffer: 4% SDS, 100mM Tris pH 6.8, 2% 2-mercaptoethanol, 20% glycerol, 10µg/ml Bromophenol Blue

GST Elution Buffer: 100mM Tris pH 8.0, 120mM NaCl

Kinase Buffer: 20mM HEPES, 10mM MgCl2, 25mM β-glycerophosphate, 1mM Sodium orthovanadate, 100µM Dithiothreitol (DTT) and 100µM Adenosine triphosphate (ATP) with (Hot) or without (Cold) 1µCi γ-^{32}P-ATP

List of References

Al-Mehdi, A. B., Pastukh, V. M., Swiger, B. M., Reed, D. J., Patel, M. R., Bardwell, G. C., Pastukh, V. V., Alexeyev, M. F., and Gillespie, M. N. (2012). Perinuclear mitochondrial clustering creates an oxidant-rich nuclear domain required for hypoxia-induced transcription. Science signaling *5*, ra47.
Alagesan, B., Contino, G., Guimaraes, A. R., Corcoran, R. B., Deshpande, V., Wojtkiewicz, G. R., Hezel, A. F., Wong, K.-K., Loda, M., Weissleder, R.*, et al.* (2015). Combined MEK and PI3K inhibition in a mouse model of pancreatic cancer. Clinical cancer research : an official journal of the American Association for Cancer Research *21*, 396-404.
Albright, C. F. G., B.W.; Liu, J.; Vito, M.; Weinberg, R.A. (1993). Characterization of a guanine nucleotide dissociation stimulator for a *ras*-related GTPase. EMBO *12*, 339-347.
Appels, N. M. G. M., Beijnen, J. H., and Schellens, J. H. M. (2005). Development of Farnesyl Transferase Inhibitors: A Review. The Oncologist *10*, 565-578.
Archer, S. L. (2013). Mitochondrial dynamics--mitochondrial fission and fusion in human diseases. The New England journal of medicine *369*, 2236-2251.
Arismendi-Morillo, G. (2009). Electron microscopy morphology of the mitochondrial network in human cancer. The international journal of biochemistry & cell biology *41*, 2062-2068.
Asano, T., Yao, Y., Zhu, J., Li, D., Abbruzzese, J. L., and Reddy, S. A. (2005). The rapamycin analog CCI-779 is a potent inhibitor of pancreatic cancer cell proliferation. Biochemical and Biophysical Research Communications *331*, 295-302.
Asano, T., Yao, Y., Zhu, J., Li, D., Abbruzzese, J. L., and Reddy, S. A. G. (2004). The PI 3-kinase/Akt signaling pathway is activated due to aberrant Pten expression and targets transcription factors NF-κB and c-Myc in pancreatic cancer cells. Oncogene *23*, 8571.
Bar-Sagi, D., and Feramisco, J. (1986). Induction of membrane ruffling and fluid-phase pinocytosis in quiescent fibroblasts by ras proteins. Science *233*, 1061-1068.
Barbacid, M. (1987). ras Genes. Annual Review of Biochemistry *56*, 779-827.
Bardeesy, N., Aguirre, A. J., Chu, G. C., Cheng, K.-h., Lopez, L. V., Hezel, A. F., Feng, B., Brennan, C., Weissleder, R., Mahmood, U.*, et al.* (2006). Both p16^{Ink4a} and the p19^{Arf}-p53 pathway constrain progression of pancreatic adenocarcinoma in the mouse. Proceedings of the National Academy of Sciences *103*, 5947-5952.
Bardeesy, N., and DePinho, R. A. (2002). Pancreatic cancer biology and genetics. Nature Reviews Cancer *2*, 897.
Benanti, J. A., and Galloway, D. A. (2004). Normal Human Fibroblasts Are Resistant to RAS-Induced Senescence. Molecular and cellular biology *24*, 2842-2852.
Benard, G., and Karbowski, M. (2009). Mitochondrial fusion and division: Regulation and role in cell viability. Seminars in Cell & Developmental Biology *20*, 365-374.
Benard, G., and Rossignol, R. (2008). Ultrastructure of the mitochondrion and its bearing on function and bioenergetics. Antioxidants & redox signaling *10*, 1313-1342.
Benard, G. e. a. (2007). Mitochondrial bioenergetics and structural network organization. J Cell Sci *120*, 838-848.
Bender, T., and Martinou, J.-C. (2016). The mitochondrial pyruvate carrier in health and disease: To carry or not to carry? Biochimica et Biophysica Acta (BBA) - Molecular Cell Research *1863*, 2436-2442.
Bensinger, S. J., and Christofk, H. R. (2012). New aspects of the Warburg effect in cancer cell biology. Seminars in Cell & Developmental Biology *23*, 352-361.
Bleazard, W., McCaffery, J. M., King, E. J., Bale, S., Mozdy, A., Tieu, Q., Nunnari, J., and Shaw, J. M. (1999). The dynamin-related GTPase Dnm1 regulates mitochondrial fission in yeast. Nature cell biology *1*, 298-304.

Boland, M. L., Chourasia, A. H., and Macleod, K. F. (2013). Mitochondrial Dysfunction in Cancer. Frontiers in oncology *3*, 292.
Bordt, E. A., Clerc, P., Roelofs, B. A., Saladino, A. J., Tretter, L., Adam-Vizi, V., Cherok, E., Khalil, A., Yadava, N., Ge, S. X*., et al.* (2017). The Putative Drp1 Inhibitor Mdivi-1 is a Reversible Mitochondrial Complex I Inhibitor that Modulates Reactive Oxygen Species. Developmental cell *40*, 583-594.e586.
Boriack-Sjodin, P. A. M., S.M.; Bar-Sagi, D.; Kuriyan, J. (1998). The structural basis of the activation of Ras by Sos. Nature *394*, 337-343.
Borowicz, S., Van Scoyk, M., Avasarala, S., Karuppusamy Rathinam, M. K., Tauler, J., Bikkavilli, R. K., and Winn, R. A. (2014). The soft agar colony formation assay. J Vis Exp, e51998.
Bos, J. L. (1989). ras Oncogenes in Human Cancer: A Review. Cancer Res *49*, 4682-4689.
Brown, K., Yang, P., Salvador, D., Kulikauskas, R., Ruohola-Baker, H., Robitaille, A. M., Chien, A. J., Moon, R. T., and Sherwood, V. (2017). WNT/β-catenin signaling regulates mitochondrial activity to alter the oncogenic potential of melanoma in a PTEN-dependent manner. Oncogene *36*, 3119-3136.
Brunet, A. (1994). Constitutively active mutants of MAP kinase kinase (MEK1) induce growth factor-relaxation and oncogenicity when expressed in fibroblasts. Oncogene *9*, 3379-3387.
Bruns, C. J., Harbison, M. T., Kuniyasu, H., Eue, I., and Fidler, I. J. (1999). In vivo selection and characterization of metastatic variants from human pancreatic adenocarcinoma by using orthotopic implantation in nude mice. Neoplasia *1*, 50-62.
Bryant, K. L., Mancias, J. D., Kimmelman, A. C., and Der, C. J. (2014). KRAS: feeding pancreatic cancer proliferation. Trends in biochemical sciences.
Caino, M. C., Ghosh, J. C., Chae, Y. C., Vaira, V., Rivadeneira, D. B., Faversani, A., Rampini, P., Kossenkov, A. V., Aird, K. M., Zhang, R*., et al.* (2015). PI3K therapy reprograms mitochondrial trafficking to fuel tumor cell invasion. Proceedings of the National Academy of Sciences *112*, 8638-8643.
Carlson, S. M., Chouinard, C. R., Labadorf, A., Lam, C. J., Schmelzle, K., Fraenkel, E., and White, F. M. (2011). Large-scale discovery of ERK2 substrates identifies ERK-mediated transcriptional regulation by ETV3. Science signaling *4*, rs11.
Carpenter, C. L. D., B.C.; Auger, K.R.; Cohen, B.; Schaffhausen, B.S.; Cantley, L.C. (1990). Purification and characterization of phosphoinositide 3-kinase from rat liver. The Journal of biological chemistry *256*, 19704-19711.
Cassidy-Stone, A., Chipuk, J. E., Ingerman, E., Song, C., Yoo, C., Kuwana, T., Kurth, M. J., Shaw, J. T., Hinshaw, J. E., Green, D. R., and Nunnari, J. (2008). Chemical inhibition of the mitochondrial division dynamin reveals its role in Bax/Bak-dependent mitochondrial outer membrane permeabilization. Developmental cell *14*, 193-204.
Castellano, E., and Downward, J. (2011). RAS Interaction with PI3K: More Than Just Another Effector Pathway. Genes & cancer *2*, 261-274.
Cerveny, K. L., Tamura, Y., Zhang, Z., Jensen, R. E., and Sesaki, H. (2007). Regulation of mitochondrial fusion and division. Trends in cell biology *17*, 563-569.
Chan, D. C. (2012). Fusion and fission: interlinked processes critical for mitochondrial health. Annual review of genetics *46*, 265-287.
Chan, T. O. R., U.; Chan, A.M.; Kimmelman, A.C.; Rittenhouse, S.E.; Panayotou, G.; Tsichlis, P. (2002). Small GTPases and tyrosine kinases coregulate a molecular switch in the phosphoinositide 3-kinase regulatory subunit. Cancer cell *1*, 181-191.
Chang, C. R., and Blackstone, C. (2007). Cyclic AMP-dependent protein kinase phosphorylation of Drp1 regulates its GTPase activity and mitochondrial morphology. The Journal of biological chemistry *282*, 21583-21587.
Chang, C. R., and Blackstone, C. (2010). Dynamic regulation of mitochondrial fission through modification of the dynamin-related protein Drp1. Annals of the New York Academy of Sciences *1201*, 34-39.

Chang, F., Steelman, L. S., Lee, J. T., Shelton, J. G., Navolanic, P. M., Blalock, W. L., Franklin, R. A., and McCubrey, J. A. (2003). Signal transduction mediated by the Ras/Raf/MEK/ERK pathway from cytokine receptors to transcription factors: potential targeting for therapeutic intervention. Leukemia *17*, 1263-1293.
Chen, H., and Chan, D. C. (2004). Mitochondrial Dynamics in Mammals. In Current Topics in Developmental Biology, G.P. Schatten, ed. (Academic Press), pp. 119-144.
Chen, H., Detmer, S. A., Ewald, A. J., Griffin, E. E., Fraser, S. E., and Chan, D. C. (2003a). Mitofusins Mfn1 and Mfn2 coordinately regulate mitochondrial fusion and are essential for embryonic development. The Journal of cell biology *160*, 189-200.
Chen, H., Detmer, S. A., Ewald, A. J., Griffin, E. E., Fraser, S. E., and Chan, D. C. (2003b). Mitofusins Mfn1 and Mfn2 coordinately regulate mitochondrial fusion and are essential for embryonic development. The Journal of cell biology *160*, 189-200.
Chen, K.-H., Dasgupta, A., Ding, J., Indig, F. E., Ghosh, P., and Longo, D. L. (2014). Role of mitofusin 2 (Mfn2) in controlling cellular proliferation. The FASEB Journal *28*, 382-394.
Chen, K.-H., Guo, X., Ma, D., Guo, Y., Li, Q., Yang, D., Li, P., Qiu, X., Wen, S., Xiao, R.-P., and Tang, J. (2004). Dysregulation of HSG triggers vascular proliferative disorders. Nature cell biology *6*, 872.
Chong, H., and Guan, K. L. (2003). Regulation of Raf through phosphorylation and N terminus-C terminus interaction. The Journal of biological chemistry *278*, 36269-36276.
Chou. C.H.; Lin, C., Yang, M.; Wei, C.; Liao, H.; Lin, R.; Tu, W.; Kao, T.; Hsu, C.; Cheng, J.; Chou, A.; Lee, C.; Loh, J.; Howng, S.; Hong, Y. (2012). GSK3beta-Mediated Drp1 Phosphorylation Induced Elongated Mitochondrial Morphology against Oxidative Stress. PloS one *7*, 1-13.
Christofk, H. R., Vander Heiden, M. G., Harris, M. H., Ramanathan, A., Gerszten, R. E., Wei, R., Fleming, M. D., Schreiber, S. L., and Cantley, L. C. (2008). The M2 splice isoform of pyruvate kinase is important for cancer metabolism and tumour growth. Nature *452*, 230.
Cipolat, S., Martins de Brito, O., Dal Zilio, B., and Scorrano, L. (2004). OPA1 requires mitofusin 1 to promote mitochondrial fusion. Proceedings of the National Academy of Sciences of the United States of America *101*, 15927-15932.
Cohen, R., Neuzillet, C., Tijeras-Raballand, A., Faivre, S., de Gramont, A., and Raymond, E. (2015). Targeting cancer cell metabolism in pancreatic adenocarcinoma. Oncotarget *6*, 16832-16847.
Collado, M., Gil, J., Efeyan, A., Guerra, C., Schuhmacher, A. J., Barradas, M., Benguría, A., Zaballos, A., Flores, J. M., Barbacid, M.*, et al.* (2005). Senescence in premalignant tumours. Nature *436*, 642.
Collins, M. A., Bednar, F., Zhang, Y., Brisset, J. C., Galban, S., Galban, C. J., Rakshit, S., Flannagan, K. S., Adsay, N. V., and Pasca di Magliano, M. (2012). Oncogenic Kras is required for both the initiation and maintenance of pancreatic cancer in mice. J Clin Invest *122*, 639-653.
Commisso, C., Davidson, S. M., Soydaner-Azeloglu, R. G., Parker, S. J., Kamphorst, J. J., Hackett, S., Grabocka, E., Nofal, M., Drebin, J. A., Thompson, C. B.*, et al.* (2013). Macropinocytosis of protein is an amino acid supply route in Ras-transformed cells. Nature *497*, 633-637.
Conroy, T., Desseigne, F., Ychou, M., Bouché, O., Guimbaud, R., Bécouarn, Y., Adenis, A., Raoul, J.-L., Gourgou-Bourgade, S., de la Fouchardière, C.*, et al.* (2011). FOLFIRINOX versus Gemcitabine for Metastatic Pancreatic Cancer. New England Journal of Medicine *364*, 1817-1825.
Corrado, M., Scorrano, L., and Campello, S. (2012). Mitochondrial dynamics in cancer and neurodegenerative and neuroinflammatory diseases. International journal of cell biology *2012*, 729290.
Cox, A. D., and Der, C. J. (2010). Ras history: The saga continues. Small GTPases *1*, 2-27.
Cox, A. D., Fesik, S. W., Kimmelman, A. C., Luo, J., and Der, C. J. (2014). Drugging the undruggable RAS: Mission Possible? Nature Reviews Drug Discovery *13*, 828.
Cunniff, B., McKenzie, A. J., Heintz, N. H., and Howe, A. K. (2016). AMPK activity regulates trafficking of mitochondria to the leading edge during cell migration and matrix invasion. Molecular Biology of the Cell *27*, 2662-2674.

Cutler, R. S., R.M.; Saracino, M.R.; Morrison, D.K. (1998). Autoregulation of the Raf-1 serine/threonine kinase. Proceedings of the National Academy of Sciences of the United States of America *95*, 9214-9219.
Dajee, M., Tarutani, M., Deng, H., Cai, T., and Khavari, P. A. (2002). Epidermal Ras blockade demonstrates spatially localized Ras promotion of proliferation and inhibition of differentiation. Oncogene *21*, 1527.
Dang, C. V. (2012). Links between metabolism and cancer. Genes & development *26*, 877-890.
Davies, V. J., Hollins, A. J., Piechota, M. J., Yip, W., Davies, J. R., White, K. E., Nicols, P. P., Boulton, M. E., and Votruba, M. (2007). Opa1 deficiency in a mouse model of autosomal dominant optic atrophy impairs mitochondrial morphology, optic nerve structure and visual function. Human Molecular Genetics *16*, 1307-1318.
de Groof, A. J. C., te Lindert, M. M., van Dommelen, M. M. T., Wu, M., Willemse, M., Smift, A. L., Winer, M., Oerlemans, F., Pluk, H., Fransen, J. A. M., and Wieringa, B. (2009). Increased OXPHOS activity precedes rise in glycolytic rate in H-RasV12/E1A transformed fibroblasts that develop a Warburg phenotype. Molecular Cancer *8*, 54.
Deer, E. L., González-Hernández, J., Coursen, J. D., Shea, J. E., Ngatia, J., Scaife, C. L., Firpo, M. A., and Mulvihill, S. J. (2010). Phenotype and genotype of pancreatic cancer cell lines. Pancreas *39*, 425.
Delettre, C. L., G.; Griffoin, JM.; et al. (2000). Nuclear gene OPA1, encoding a mitochondrial dynamin-related protein, is mutated in dominant optic atrophy. Nat Gen *26*, 207-210.
Demarquoy, J., and Le Borgne, F. (2015). Crosstalk between mitochondria and peroxisomes. World Journal of Biological Chemistry *6*, 301-309.
DeNicola, G. M., Karreth, F. A., Humpton, T. J., Gopinathan, A., Wei, C., Frese, K., Mangal, D., Yu, K. H., Yeo, C. J., Calhoun, E. S*., et al.* (2011). Oncogene-induced Nrf2 transcription promotes ROS detoxification and tumorigenesis. Nature *475*, 106-109.
di Magliano, M. P., and Logsdon, C. D. (2013). Roles for KRAS in Pancreatic Tumor Development and Progression. Gastroenterology *144*, 1220-1229.
Diaz-Ruiz, R., Uribe-Carvajal, S., Devin, A., and Rigoulet, M. (2009). Tumor cell energy metabolism and its common features with yeast metabolism. Biochimica et Biophysica Acta (BBA) - Reviews on Cancer *1796*, 252-265.
Diep, C. H., Munoz, R. M., Choudhary, A., Von Hoff, D. D., and Han, H. (2011). Synergistic effect between erlotinib and MEK inhibitors in KRAS wild-type human pancreatic cancer cells. Clinical Cancer Research *17*, 2744-2756.
Dong, Z., and Wang, J. (2004). Hypoxia Selection of Death-resistant Cells: A ROLE FOR Bcl-XL. Journal of Biological Chemistry *279*, 9215-9221.
Downward, J. (2003). Targeting RAS signalling pathways in cancer therapy. Nature Reviews Cancer *3*, 11.
Drayton, S., Rowe, J., Jones, R., Vatcheva, R., Cuthbert-Heavens, D., Marshall, J., Fried, M., and Peters, G. (2003). Tumor suppressor p16INK4a determines sensitivity of human cells to transformation by cooperating cellular oncogenes. Cancer cell *4*, 301-310.
Dupuis, L. (2013). Mitochondrial quality control in neurodegenerative diseases. Biochimie.
Duvezin-Caubet, S., Jagasia, R., Wagener, J., Hofmann, S., Trifunovic, A., Hansson, A., Chomyn, A., Bauer, M. F., Attardi, G., Larsson, N. G*., et al.* (2006). Proteolytic processing of OPA1 links mitochondrial dysfunction to alterations in mitochondrial morphology. The Journal of biological chemistry *281*, 37972-37979.
Eagle, H. (1955). Nutrition Needs of Mammalian Cells in Tissue Culture. Science *122*, 501-504.
Ehses, S., Raschke, I., Mancuso, G., Bernacchia, A., Geimer, S., Tondera, D., Martinou, J. C., Westermann, B., Rugarli, E. I., and Langer, T. (2009). Regulation of OPA1 processing and mitochondrial fusion by m-AAA protease isoenzymes and OMA1. The Journal of cell biology *187*, 1023-1036.

El-Deiry, W. S., Tokino, T., Velculescu, V. E., Levy, D. B., Parsons, R., Trent, J. M., Lin, D., Mercer, W. E., Kinzler, K. W., and Vogelstein, B. (1993). WAF1, a potential mediator of p53 tumor suppression. Cell *75*, 817-825.
Eser, S., Schnieke, A., Schneider, G., and Saur, D. (2014). Oncogenic KRAS signalling in pancreatic cancer. Br J Cancer *111*, 817-822.
Faris, J. E., Blaszkowsky, L. S., McDermott, S., Guimaraes, A. R., Szymonifka, J., Huynh, M. A., Ferrone, C. R., Wargo, J. A., Allen, J. N., Dias, L. E*., et al.* (2013). FOLFIRINOX in Locally Advanced Pancreatic Cancer: The Massachusetts General Hospital Cancer Center Experience. The Oncologist *18*, 543-548.
Feig, C., Gopinathan, A., Neesse, A., Chan, D. S., Cook, N., and Tuveson, D. A. (2012). The pancreas cancer microenvironment. Clinical cancer research : an official journal of the American Association for Cancer Research *18*, 4266-4276.
Fernandez-Medarde, A., and Santos, E. (2011). Ras in cancer and developmental diseases. Genes & cancer *2*, 344-358.
Ferreira, L. M. R. (2010). Cancer metabolism: The Warburg effect today. Experimental and Molecular Pathology *89*, 372-380.
Fiorini, C., Cordani, M., Padroni, C., Blandino, G., Di Agostino, S., and Donadelli, M. (2015). Mutant p53 stimulates chemoresistance of pancreatic adenocarcinoma cells to gemcitabine. Biochimica et Biophysica Acta (BBA) - Molecular Cell Research *1853*, 89-100.
Fleming, J. B., Shen, G.-L., Holloway, S. E., Davis, M., and Brekken, R. A. (2005). Molecular Consequences of Silencing Mutant KRAS in Pancreatic Cancer Cells: Justification for KRAS Directed Therapy. Molecular Cancer Research *3*, 413-423.
Frank, S. G., B.; Bergmann-Leitner, E.S.; Leitner, W.W.; Robert, E.G.; Catez, F.; Smith, C.L.; Youle, R.J. (2001). The Role of Dynamin-Related Protein 1, a Mediator of Mitochondrial Fission, in Apoptosis. Developmental cell *1*, 515-525.
Franke, T. F. K., D.R.; Cantley, L.C.; Toker, A. (1997). Direct Regulation of the *Akt* Proto-Oncogene Product by Phosphatidylinositol-3,4-biphosphate. Science *275*, 665-667.
Friedman, J. R., Lackner, L. L., West, M., DiBenedetto, J. R., Nunnari, J., and Voeltz, G. K. (2011). ER tubules mark sites of mitochondrial division. Science *334*, 358-362.
Friedman, J. R., and Nunnari, J. (2014). Mitochondrial form and function. Nature *505*, 335-343.
Fujii, S., Mitsunaga, S., Yamazaki, M., Hasebe, T., Ishii, G., Kojima, M., Kinoshita, T., Ueno, T., Esumi, H., and Ochiai, A. (2008). Autophagy is activated in pancreatic cancer cells and correlates with poor patient outcome. Cancer Science *99*, 1813-1819.
Funes, J. M., Quintero, M., Henderson, S., Martinez, D., Qureshi, U., Westwood, C., Clements, M. O., Bourboulia, D., Pedley, R. B., Moncada, S., and Boshoff, C. (2007). Transformation of human mesenchymal stem cells increases their dependency on oxidative phosphorylation for energy production. Proceedings of the National Academy of Sciences *104*, 6223-6228.
Gaglio, D., Metallo, C. M., Gameiro, P. A., Hiller, K., Danna, L. S., Balestrieri, C., Alberghina, L., Stephanopoulos, G., and Chiaradonna, F. (2011). Oncogenic K-Ras decouples glucose and glutamine metabolism to support cancer cell growth. Mol Syst Biol *7*, 523.
Gan, X., Huang, S., Wu, L., Wang, Y., Hu, G., Li, G., Zhang, H., Yu, H., Swerdlow, R. H., Chen, J. X., and Yan, S. S. (2014). Inhibition of ERK-DLP1 signaling and mitochondrial division alleviates mitochondrial dysfunction in Alzheimer's disease cybrid cell. Biochimica et biophysica acta *1842*, 220-231.
George, T. C., Basiji, D. A., Hall, B. E., Lynch, D. H., Ortyn, W. E., Perry, D. J., Seo, M. J., Zimmerman, C. A., and Morrissey, P. J. (2004). Distinguishing modes of cell death using the ImageStream multispectral imaging flow cytometer. Cytometry A *59*, 237-245.
Gidekel Friedlander, S. Y., Chu, G. C., Snyder, E. L., Girnius, N., Dibelius, G., Crowley, D., Vasile, E., DePinho, R. A., and Jacks, T. (2009). Context-Dependent Transformation of Adult Pancreatic Cells by Oncogenic K-Ras. Cancer cell *16*, 379-389.

GISTG (1987). Further evidence of effective adjuvant combined radiation and chemotherapy following curative resection of pancreatic cancer. Cancer *59*, 2006-2010.
Gomes, L. C., Di Benedetto, G., and Scorrano, L. (2011). During autophagy mitochondria elongate, are spared from degradation and sustain cell viability. Nature cell biology *13*, 589-598.
Gomes, L. C., and Scorrano, L. (2013). Mitochondrial morphology in mitophagy and macroautophagy. Biochimica et biophysica acta *1833*, 205-212.
Gordon, J. W. J. W. (2015). Targeting skeletal muscle mitochondria to prevent type 2 diabetes in youth. Biochemistry and cell biology, 1-14.
Gouw, A. M., Eberlin, L. S., Margulis, K., Sullivan, D. K., Toal, G. G., Tong, L., Zare, R. N., and Felsher, D. W. (2017). Oncogene KRAS activates fatty acid synthase, resulting in specific ERK and lipid signatures associated with lung adenocarcinoma. Proceedings of the National Academy of Sciences of the United States of America *114*, 4300-4305.
Grandemange, S., Herzig, S., and Martinou, J. C. (2009). Mitochondrial dynamics and cancer. Seminars in cancer biology *19*, 50-56.
Graves, J. A., Wang, Y., Sims-Lucas, S., Cherok, E., Rothermund, K., Branca, M. F., Elster, J., Beer-Stolz, D., Van Houten, B., Vockley, J., and Prochownik, E. V. (2012). Mitochondrial Structure, Function and Dynamics Are Temporally Controlled by c-Myc. PloS one *7*, e37699.
Griparic, L., Kanazawa, T., and van der Bliek, A. M. (2007). Regulation of the mitochondrial dynamin-like protein Opa1 by proteolytic cleavage. The Journal of cell biology *178*, 757-764.
Guerra, C., and Barbacid, M. (2013). Genetically engineered mouse models of pancreatic adenocarcinoma. Molecular Oncology *7*, 232-247.
Guo, J. Y., Chen, H. Y., Mathew, R., Fan, J., Strohecker, A. M., Karsli-Uzunbas, G., Kamphorst, J. J., Chen, G., Lemons, J. M., Karantza, V.*, et al.* (2011). Activated Ras requires autophagy to maintain oxidative metabolism and tumorigenesis. Genes & development *25*, 460-470.
Guo, X., Chen, K.-H., Guo, Y., Liao, H., Tang, J., and Xiao, R.-P. (2007). Mitofusin 2 Triggers Vascular Smooth Muscle Cell Apoptosis via Mitochondrial Death Pathway. Circulation Research *101*, 1113-1122.
Gysin, S., Lee, S.-H., Dean, N. M., and McMahon, M. (2005). Pharmacologic Inhibition of RAF→MEK→ERK Signaling Elicits Pancreatic Cancer Cell Cycle Arrest Through Induced Expression of p27^{Kip1}. Cancer Research *65*, 4870-4880.
Hagenbuchner, J., Kuznetsov, A. V., Obexer, P., and Ausserlechner, M. J. (2013). BIRC5/Survivin enhances aerobic glycolysis and drug resistance by altered regulation of the mitochondrial fusion/fission machinery. Oncogene *32*, 4748-4757.
Hahn, W. C., Counter, C. M., Lundberg, A. S., Beijersbergen, R. L., Brooks, M. W., and Weinberg, R. A. (1999). Creation of human tumour cells with defined genetic elements. Nature *400*, 464.
Haigis, K. M., Kendall, K. R., Wang, Y., Cheung, A., Haigis, M. C., Glickman, J. N., Niwa-Kawakita, M., Sweet-Cordero, A., Sebolt-Leopold, J., Shannon, K. M.*, et al.* (2008). Differential effects of oncogenic K-Ras and N-Ras on proliferation, differentiation and tumor progression in the colon. Nature genetics *40*, 600-608.
Hamad, N. M., Elconin, J. H., Karnoub, A. E., Bai, W., Rich, J. N., Abraham, R. T., Der, C. J., and Counter, C. M. (2002). Distinct requirements for Ras oncogenesis in human versus mouse cells. Genes & development *16*, 2045-2057.
Hanahan, D., and Weinberg, R. A. (2011). Hallmarks of cancer: the next generation. Cell *144*, 646-674.
Harada, T., Chelala, C., Bhakta, V., Chaplin, T., Caulee, K., Baril, P., Young, B. D., and Lemoine, N. R. (2008). Genome-wide DNA copy number analysis in pancreatic cancer using high-density single nucleotide polymorphism arrays. Oncogene *27*, 1951-1960.
Harder, Z., Zunino, R., and McBride, H. (2004). Sumo1 conjugates mitochondrial substrates and participates in mitochondrial fission. Current biology : CB *14*, 340-345.

Harvey, J. J. (1964). AN UNIDENTIFIED VIRUS WHICH CAUSES THE RAPID PRODUCTION OF TUMOURS IN MICE. Nature (London) *204*, 1104-1105.
Hata, A. N., Yeo, A., Faber, A. C., Lifshits, E., Chen, Z., Cheng, K. A., Walton, Z., Sarosiek, K. A., Letai, A., Heist, R. S*., et al.* (2014). Failure to induce apoptosis via BCL-2 family proteins underlies lack of efficacy of combined MEK and PI3K inhibitors for KRAS mutant lung cancers. Cancer research *74*, 3146-3156.
Hayes, T. K., Neel, N. F., Hu, C., Gautam, P., Chenard, M., Long, B., Aziz, M., Kassner, M., Bryant, K. L., Pierobon, M*., et al.* (2016). Long-Term ERK Inhibition of KRAS-Mutant Pancreatic Cancer Is Associated with MYC Degradation and Senescence-like Growth Suppression. Cancer cell *29*, 75-89.
Hensley, C. T., Wasti, A. T., and DeBerardinis, R. J. (2013). Glutamine and cancer: cell biology, physiology, and clinical opportunities. The Journal of Clinical Investigation *123*, 3678-3684.
Hezel, A. F., Kimmelman, A. C., Stanger, B. Z., Bardeesy, N., and DePinho, R. A. (2006). Genetics and Biology of Pancreatic Ductal Adenocarcinoma. Genes & development *20*, 1218-1249.
Hobbs, G. A., Der, C. J., and Rossman, K. L. (2016). RAS isoforms and mutations in cancer at a glance. Journal of Cell Science *129*, 1287-1292.
Holcomb, B., Yip-Schneider, M. T., Matos, J. M., Dixon, J., Kennard, J., Mahomed, J., Shanmugam, R., Sebolt-Leopold, J., and Schmidt, C. M. (2008). Pancreatic Cancer Cell Genetics and Signaling Response to Treatment Correlate with Efficacy of Gemcitabine-Based Molecular Targeting Strategies. Journal of Gastrointestinal Surgery *12*, 288-296.
Horn, S. R., Thomenius, M. J., Johnson, E. S., Freel, C. D., Wu, J. Q., Coloff, J. L., Yang, C.-S., Tang, W., An, J., Ilkayeva, O. R*., et al.* (2011). Regulation of mitochondrial morphology by APC/C(Cdh1)-mediated control of Drp1 stability. Molecular Biology of the Cell *22*, 1207-1216.
Hruban, R. H., Adsay, N. V., Albores-Saavedra, J., Compton, C., Garrett, E. S., Goodman, S. N., Kern, S. E., Klimstra, D. S., Kloppel, G., Longnecker, D. S*., et al.* (2001). Pancreatic Intraepithelial Neoplasia: A new nomenclature and classification system for pancreatic duct lesions. Am J Surgical Path *25*, 579-586.
Hruban, R. H., and Fukushima, N. (2007). Pancreatic adenocarcinoma: update on the surgical pathology of carcinomas of ductal origin and PanINs. Mod Pathol *20 Suppl 1*, S61-70.
Hu, Y., Lu, W., Chen, G., Wang, P., Chen, Z., Zhou, Y., Ogasawara, M., Trachootham, D., Feng, L., Pelicano, H*., et al.* (2011). K-rasG12V transformation leads to mitochondrial dysfunction and a metabolic switch from oxidative phosphorylation to glycolysis. Cell Research *22*, 399.
Hustinx, S. R., Leoni, L. M., Yeo, C. J., Brown, P. N., Goggins, M., Kern, S. E., Hruban, R. H., and Maitra, A. (2005). Concordant loss of MTAP and p16/CDKN2A expression in pancreatic intraepithelial neoplasia: evidence of homozygous deletion in a noninvasive precursor lesion. Modern Pathology *18*, 959.
Iacobuzio-Donahue, C. A., Fu, B., Yachida, S., Luo, M., Abe, H., Henderson, C. M., Vilardell, F., Wang, Z., Keller, J. W., Banerjee, P*., et al.* (2009). DPC4 Gene Status of the Primary Carcinoma Correlates With Patterns of Failure in Patients With Pancreatic Cancer. Journal of Clinical Oncology *27*, 1806-1813.
Ingerman, E., Perkins, E. M., Marino, M., Mears, J. A., McCaffery, J. M., Hinshaw, J. E., and Nunnari, J. (2005). Dnm1 forms spirals that are structurally tailored to fit mitochondria. The Journal of cell biology *170*, 1021-1027.
Inoue-Yamauchi, A., and Oda, H. (2012). Depletion of mitochondrial fission factor DRP1 causes increased apoptosis in human colon cancer cells. Biochem Biophys Res Commun *421*, 81-85.
Ishihara, N., Nomura, M., Jofuku, A., Kato, H., Suzuki, S. O., Masuda, K., Otera, H., Nakanishi, Y., Nonaka, I., Goto, Y*., et al.* (2009). Mitochondrial fission factor Drp1 is essential for embryonic development and synapse formation in mice. Nature cell biology *11*, 958-966.
Ishihara, N. F., Y.; Toshihiko, O.; Mihara, K. (2006). Regulation of mitochondrial morphology through proteolytic cleavage of OPA1. EMBO *25*, 2966-2977.
Itoh, K., Adachi, Y., Yamada, T., Suzuki, T. L., Otomo, T., McBride, H. M., Yoshimori, T., Iijima, M., and Sesaki, H. (2018). A brain-enriched Drp1 isoform associates with lysosomes, late endosomes and the plasma membrane. Journal of Biological Chemistry.

Jacobi, D., Liu, S., Burkewitz, K., Kory, N., Knudsen, Nelson H., Alexander, Ryan K., Unluturk, U., Li, X., Kong, X., Hyde, Alexander L*., et al.* (2015). Hepatic Bmal1 Regulates Rhythmic Mitochondrial Dynamics and Promotes Metabolic Fitness. Cell metabolism *22*, 709-720.
Jose, C., Bellance, N., and Rossignol, R. (2011). Choosing between glycolysis and oxidative phosphorylation: a tumor's dilemma? Biochimica et biophysica acta *1807*, 552-561.
Kageyama, Y., Zhang, Z., and Sesaki, H. (2011). Mitochondrial division: molecular machinery and physiological functions. Current opinion in cell biology *23*, 427-434.
Kamphorst, J. J., Cross, J. R., Fan, J., de Stanchina, E., Mathew, R., White, E. P., Thompson, C. B., and Rabinowitz, J. D. (2013). Hypoxic and Ras-transformed cells support growth by scavenging unsaturated fatty acids from lysophospholipids. Proceedings of the National Academy of Sciences of the United States of America *110*, 8882-8887.
Kamphorst, J. J., Nofal, M., Commisso, C., Hackett, S. R., Lu, W., Grabocka, E., Vander Heiden, M. G., Miller, G., Drebin, J. A., Bar-Sagi, D*., et al.* (2015). Human pancreatic cancer tumors are nutrient poor and tumor cells actively scavenge extracellular protein. Cancer research *75*, 544-553.
Kao, K. M., MR. (1974). A Method for High-Frequency Intergenic Fusion of Plant Protoplasts. Planta *115*, 355-367.
Karbowski, M., Arnoult, D., Chen, H., Chan, D. C., Smith, C. L., and Youle, R. J. (2004). Quantitation of mitochondrial dynamics by photolabeling of individual organelles shows that mitochondrial fusion is blocked during the Bax activation phase of apoptosis. The Journal of cell biology *164*, 493-499.
Karbowski, M., Lee, Y. J., Gaume, B., Jeong, S. Y., Frank, S., Nechushtan, A., Santel, A., Fuller, M., Smith, C. L., and Youle, R. J. (2002). Spatial and temporal association of Bax with mitochondrial fission sites, Drp1, and Mfn2 during apoptosis. The Journal of cell biology *159*, 931-938.
Karbowski, M., Neutzner, A., and Youle, R. J. (2007). The mitochondrial E3 ubiquitin ligase MARCH5 is required for Drp1 dependent mitochondrial division. The Journal of cell biology *178*, 71-84.
Karnoub, A. E., and Weinberg, R. A. (2008). Ras oncogenes: split personalities. Nature reviews Molecular cell biology *9*, 517-531.
Kashatus, Nascimento, A., Myers, L. J., Sher, A., Byrne, F. L., Hoehn, K. L., Counter, C. M., and Kashatus, D. F. (2015). Erk2 phosphorylation of Drp1 promotes mitochondrial fission and MAPK-driven tumor growth. Molecular cell *57*, 537-551.
Kashatus, D. F. (2017). The regulation of tumor cell physiology by mitochondrial dynamics. Biochemical and Biophysical Research Communications.
Kashatus, D. F., Lim, K. H., Brady, D. C., Pershing, N. L., Cox, A. D., and Counter, C. M. (2011). RALA and RALBP1 regulate mitochondrial fission at mitosis. Nature cell biology *13*, 1108-1115.
Kastan, M. B., Onyekwere, O., Sidransky, D., Vogelstein, B., and Craig, R. W. (1991). Participation of p53 Protein in the Cellular Response to DNA Damage. Cancer Research *51*, 6304-6311.
Kastenhuber, E. R., and Lowe, S. W. (2017). Putting p53 in Context. Cell *170*, 1062-1078.
Khabele, D. (2015). KRAS in Ovarian Cancer. My Cancer Genome https://wwwmycancergenomeorg/content/disease/ovarian-cancer/kras/
Kikuchi, H., Pino, M. S., Zeng, M., Shirasawa, S., and Chung, D. C. (2009). Oncogenic KRAS and BRAF differentially regulate hypoxia-inducible factor-1alpha and -2alpha in colon cancer. Cancer Res *69*, 8499-8506.
Kilic, M., Kasperczyk, H., Fulda, S., and Debatin, K. M. (2006). Role of hypoxia inducible factor-1 alpha in modulation of apoptosis resistance. Oncogene *26*, 2027.
Kim, D. I., Lee, K. H., Gabr, A. A., Choi, G. E., Kim, J. S., Ko, S. H., and Han, H. J. (2016). Aβ-Induced Drp1 phosphorylation through Akt activation promotes excessive mitochondrial fission leading to neuronal apoptosis. Biochimica et Biophysica Acta (BBA) - Molecular Cell Research *1863*, 2820-2834.

Kim, J. H., Kim, H. Y., Lee, Y. K., Yoon, Y. S., Xu, W. G., Yoon, J. K., Choi, S. E., Ko, Y. G., Kim, M. J., Lee, S. J*., et al.* (2011). Involvement of mitophagy in oncogenic K-Ras-induced transformation: overcoming a cellular energy deficit from glucose deficiency. Autophagy *7*, 1187-1198.
Kimmelman, A. C. (2015). Metabolic Dependencies in RAS-Driven Cancers. Clinical cancer research : an official journal of the American Association for Cancer Research *21*, 1828-1834.
Kinsella, B. T. E., R.A.; Maltese, W.A. (1991). Carboxyl-terminal Isoprenylation of *ras*-related GTP-binding Protiens Encoded by *rac1*, *rac2*, and *ralA**. The Journal of biological chemistry *266*, 9786-9794.
Kitani, T., Kami, D., Matoba, S., and Gojo, S. (2014). Internalization of isolated functional mitochondria: involvement of macropinocytosis. Journal of Cellular and Molecular Medicine *18*, 1694-1703.
Kler, R. S., Jackson, S., Bartlett, K., Bindoff, L. A., Eaton, S., Pourfarzam, M., Frerman, F. E., Goodman, S. I., Watmough, N. J., and Turnbull, D. M. (1991). Quantitation of Acyl-CoA and Acylcarnitine Esters Accumulated during Abnormal Mitochondrial Fatty Acid Oxidation. Journal of Biological Chemistry *266*, 22932-22938.
Klimstra, D. S., and Longnecker, D. S. (1994). K-ras mutations in pancreatic ductal proliferative lesions. The American Journal of Pathology *145*, 1547-1550.
Klinkenbijl, J. H., Jeekel, J., Sahmoud, T., van Pel, R., Couvreur, M. L., Veenhof, C. H., Arnaud, J. P., Gonzalez, D. G., de Wit, L. T., Hennipman, A., and Wils, J. (1999). Adjuvant Radiotherapy and 5-Fluorouracil After Curative Resection of Cancer of the Pancreas and Periampullary Region: Phase III Trial of the EORTC Gastrointestinal Tract Cancer Cooperative Group. Annals of Surgery *230*, 776-776.
Kolch, W. (2000). Meaningful relationships: the regulation of the Ras/Raf/MEK/ERK pathway by protein interactions. Biochem J *351*, 289-305.
Kolch, W. H., G.; Lloyd, P.; Rapp, U.R. (1991). Raf-1 protein kinase is required for growth of induced NIH/3T3 cells. Nature *349*, 426-428.
Konstantinidis, I., Warshaw, A., Allen, J., Blaszkowsky, L., Castillo, C., Deshpande, V., Hong, T., Kwak, E., Lauwers, G., Ryan, D*., et al.* (2013). Pancreatic ductal adenocarcinoma: is there a survival difference for R1 resections versus locally advanced unresectable tumors? What is a "true" R0 resection? Annals of Surgery *257*, 731-736.
Koshiba, T., Detmer, S. A., Kaiser, J. T., Chen, H., McCaffery, J. M., and Chan, D. C. (2004). Structural basis of mitochondrial tethering by mitofusin complexes. Science *305*, 858-862.
Kuznetsov, A. V., Hermann, M., Saks, V., Hengster, P., and Margreiter, R. (2009). The cell-type specificity of mitochondrial dynamics. The international journal of biochemistry & cell biology *41*, 1928-1939.
Labrousse, A. M. Z., M.D.; et al. (1999). C. elegans Dynamin-Related Protein DRP-1 Controls Severing of the Mitochondrial Outer Membrane. Molecular cell *4*, 815-826.
Laptenko, O., and Prives, C. (2006). Transcriptional regulation by p53: one protein, many possibilities. Cell Death And Differentiation *13*, 951.
Lee, J. E., Westrate, L. M., Wu, H., Page, C., and Voeltz, G. K. (2016). Multiple dynamin family members collaborate to drive mitochondrial division. Nature *540*, 139.
Lee, Y. J., Jeong, S. Y., Karbowski, M., Smith, C. L., and Youle, R. J. (2004). Roles of the mammalian mitochondrial fission and fusion mediators Fis1, Drp1, and Opa1 in apoptosis. Mol Biol Cell *15*, 5001-5011.
Leonard, A. P., Cameron, R. B., Speiser, J. L., Wolf, B. J., Peterson, Y. K., Schnellmann, R. G., Beeson, C. C., and Rohrer, B. (2015). Quantitative analysis of mitochondrial morphology and membrane potential in living cells using high-content imaging, machine learning, and morphological binning. Biochimica et biophysica acta *1853*, 348-360.
Li, D., Xie, K., Wolff, R., and Abbruzzese, J. L. (2004). Pancreatic cancer. The Lancet *363*, 1049-1057.
Li, J., Li, Y., Jiao, J., Wang, J., Li, Y., Qin, D., and Li, P. (2014). Mitofusin 1 is Negatively Regulated by miR-140 in Cardiomyocyte Apoptosis. Molecular and cellular biology, MCB. 00774-00713.

Liesa, M., and Shirihai, O. S. (2013). Mitochondrial dynamics in the regulation of nutrient utilization and energy expenditure. Cell metabolism *17*, 491-506.
Lim, J. P., and Gleeson, P. A. (2011). Macropinocytosis: an endocytic pathway for internalising large gulps. Immunology And Cell Biology *89*, 836.
Lim, K.-H., Ancrile, B. B., Kashatus, D. F., and Counter, C. M. (2008). Tumour maintenance is mediated by eNOS. Nature *452*, 646.
Lim, K.-H., Baines, A. T., Fiordalisi, J. J., Shipitsin, M., Feig, L. A., Cox, A. D., Der, C. J., and Counter, C. M. (2005). Activation of RalA is critical for Ras-induced tumorigenesis of human cells. Cancer cell *7*, 533-545.
Lim, K.-H., O'Hayer, K., Adam, S. J., Kendall, S. D., Campbell, P. M., Der, C. J., and Counter, C. M. (2006). Divergent Roles for RalA and RalB in Malignant Growth of Human Pancreatic Carcinoma Cells. Current Biology *16*, 2385-2394.
Lim, K.-L., Ng, X.-H., Grace, L. G.-Y., and Yao, T.-P. (2012). Mitochondrial Dynamics and Parkinson's Disease: Focus on Parkin. Antioxidants & redox signaling *16*, 935-949.
Lim, K. H., and Counter, C. M. (2005). Reduction in the requirement of oncogenic Ras signaling to activation of PI3K/AKT pathway during tumor maintenance. Cancer cell *8*, 381-392.
Lima, A. R., Santos, L., Correia, M., Soares, P., Sobrinho-Simões, M., Melo, M., and Máximo, V. (2018). Dynamin-Related Protein 1 at the Crossroads of Cancer. Genes *9*, 115.
Liu, P., Cheng, H., Roberts, T. M., and Zhao, J. J. (2009). Targeting the phosphoinositide 3-kinase (PI3K) pathway in cancer. Nature reviews Drug discovery *8*, 627-644.
Livak, K. J., and Schmittgen, T. D. (2001). Analysis of Relative Gene Expression Data Using Real-Time Quantitative PCR and the 2−ΔΔCT Method. Methods *25*, 402-408.
Livingstone, L. R., White, A., Sprouse, J., Livanos, E., Jacks, T., and Tlsty, T. D. (1992). Altered cell cycle arrest and gene amplification potential accompany loss of wild-type p53. Cell *70*, 923-935.
Lock, R., Roy, S., Kenific, C. M., Su, J. S., Salas, E., Ronen, S. M., and Debnath, J. (2011). Autophagy facilitates glycolysis during Ras-mediated oncogenic transformation. Molecular Biology of the Cell *22*, 165-178.
Lozy, F., and Karantza, V. (2012). Autophagy and cancer cell metabolism. Seminars in cell & developmental biology *23*, 395-401.
Luo, J., Manning, B. D., and Cantley, L. C. (2003). Targeting the PI3K-Akt pathway in human cancer: Rationale and promise. Cancer cell *4*, 257-262.
Macdonald, P. J., Francy, C. A., Stepanyants, N., Lehman, L., Baglio, A., Mears, J. A., Qi, X., and Ramachandran, R. (2015). Distinct Splice Variants of Dynamin-related Protein 1 Differentially Utilize Mitochondrial Fission Factor as an Effector of Cooperative GTPase Activity. The Journal of biological chemistry *291*, 493-507.
Macdonald, P. J., Stepanyants, N., Mehrotra, N., Mears, J. A., Qi, X., Sesaki, H., and Ramachandran, R. (2014). A dimeric equilibrium intermediate nucleates Drp1 reassembly on mitochondrial membranes for fission. Molecular Biology of the Cell *25*, 1905-1915.
Magnuson, M. A., and Osipovich, A. B. (2013). Pancreas-specific Cre driver lines and considerations for their prudent use. Cell metabolism *18*, 9-20.
Maitra, A., Adsay, N. V., Argani, P., Iacobuzio-Donahue, C., De Marzo, A., Cameron, J. L., Yeo, C. J., and Hruban, R. H. (2003). Multicomponent Analysis of the Pancreatic Adenocarcinoma Progression Model Using a Pancreatic Intraepithelial Neoplasia Tissue Microarray. Modern Pathology *16*, 902.
Mallat, A., Uchiyama, L. F., Lewis, S. C., Fredenburg, R. A., Terada, Y., Ji, N., Nunnari, J., and Tseng, C. C. (2018). Discovery and characterization of selective small molecule inhibitors of the mammalian mitochondrial division dynamin, DRP1. Biochemical and Biophysical Research Communications *499*, 556-562.

Mallinjoud, P., Villemin, J.-P., Mortada, H., Polay Espinoza, M., Desmet, F.-O., Samaan, S., Chautard, E., Tranchevent, L.-C., and Auboeuf, D. (2014). Endothelial, epithelial, and fibroblast cells exhibit specific splicing programs independently of their tissue of origin. Genome Research *24*, 511-521.
Martin, L. J. (2012). Biology of mitochondria in neurodegenerative diseases. Progress in molecular biology and translational science *107*, 355-415.
Martin, R. G., Ii, Scoggins, C. R., Egnatashvili, V., Staley, C. A., McMasters, K. M., and Kooby, D. A. (2009). Arterial and venous resection for pancreatic adenocarcinoma: Operative and long-term outcomes. Archives of Surgery *144*, 154-159.
Martin, T. D., Samuel, J. C., Routh, E. D., Der, C. J., and Yeh, J. J. (2011). Activation and Involvement of Ral GTPases in Colorectal Cancer. Cancer Research *71*, 206-215.
Martinou, J.-C., and Youle, R. J. (2011). Mitochondria in Apoptosis: Bcl-2 family Members and Mitochondrial Dynamics. Developmental cell *21*, 92-101.
Matallanas, D., Birtwistle, M., Romano, D., Zebisch, A., Rauch, J., von Kriegsheim, A., and Kolch, W. (2011). Raf family kinases: old dogs have learned new tricks. Genes & cancer *2*, 232-260.
Matsuura, K., Canfield, K., Feng, W., and Kurokawa, M. (2016). Chapter Two - Metabolic Regulation of Apoptosis in Cancer. In International Review of Cell and Molecular Biology, K.W. Jeon, and L. Galluzzi, eds. (Academic Press), pp. 43-87.
Mattenberger, Y., James, D. I., and Martinou, J.-C. (2003). Fusion of mitochondria in mammalian cells is dependent on the mitochondrial inner membrane potential and independent of microtubules or actin. FEBS Letters *538*, 53-59.
Maurer, T., Garrenton, L. S., Oh, A., Pitts, K., Anderson, D. J., Skelton, N. J., Fauber, B. P., Pan, B., Malek, S., Stokoe, D*., et al.* (2012). Small-molecule ligands bind to a distinct pocket in Ras and inhibit SOS-mediated nucleotide exchange activity. Proceedings of the National Academy of Sciences *109*, 5299-5304.
Meeusen, S., DeVay, R., Block, J., Cassidy-Stone, A., Wayson, S., McCaffery, J. M., and Nunnari, J. (2006). Mitochondrial inner-membrane fusion and crista maintenance requires the dynamin-related GTPase Mgm1. Cell *127*, 383-395.
Meeusen, S., McCaffery, J. M., and Nunnari, J. (2004). Mitochondrial fusion intermediates revealed in vitro. Science *305*, 1747-1752.
Meeusen, S. L., and Nunnari, J. (2005). How mitochondria fuse. Current opinion in cell biology *17*, 389-394.
Mitra, K. (2013). Mitochondrial fission-fusion as an emerging key regulator of cell proliferation and differentiation. BioEssays : news and reviews in molecular, cellular and developmental biology *35*, 955-964.
Mitra, K., Wunder, C., Roysam, B., Lin, G., and Lippincott-Schwartz, J. (2009). A hyperfused mitochondrial state achieved at G1-S regulates cyclin E buildup and entry into S phase. Proceedings of the National Academy of Sciences of the United States of America *106*, 11960-11965.
Miyashita, T. (1994). Tumor suppressor p53 is a regulator of bcl-2 and bax gene expression in vitro and in vivo. Oncogene *9*, 1799-1805.
Modolell, I., Guarner, L., and Malagelada, J. R. (1999). Vagaries of clinical presentation of pancreatic and biliary tract cancer. Annals of oncology : official journal of the European Society for Medical Oncology *10 Suppl 4*, 82-84.
Montagut, C., and Settleman, J. (2009). Targeting the RAF–MEK–ERK pathway in cancer therapy. Cancer letters *283*, 125-134.
Moore, P. S., Sipos, B., Orlandini, S., Sorio, C., Real, F. X., Lemoine, N. R., Gress, T., Bassi, C., Klöppel, G., and Kalthoff, H. (2001). Genetic profile of 22 pancreatic carcinoma cell lines. Virchows Archiv *439*, 798-802.

Morandi, A., Taddei, M. L., Chiarugi, P., and Giannoni, E. (2017). Targeting the Metabolic Reprogramming That Controls Epithelial-to-Mesenchymal Transition in Aggressive Tumors. Frontiers in oncology *7*, 40.
Moreno-Sánchez, R., Rodríguez-Enríquez, S., Marín-Hernández, A., and Saavedra, E. (2007). Energy metabolism in tumor cells. FEBS Journal *274*, 1393-1418.
Moskaluk, C. A., Hruban, R. H., and Kern, S. E. (1997). Gene Mutations in the Intraductal Precursors of Human Pancreatic Adenocarcinoma. Cancer Research *57*, 2140-2143.
Muzumdar, M. D., Chen, P. Y., Dorans, K. J., Chung, K. M., Bhutkar, A., Hong, E., Noll, E. M., Sprick, M. R., Trumpp, A., and Jacks, T. (2017). Survival of pancreatic cancer cells lacking KRAS function. Nat Commun *8*, 1090.
Nagdas, S., and Kashatus, D. F. (2017). The Interplay between Oncogenic Signaling Networks and Mitochondrial Dynamics. Antioxidants (Basel) *6*.
Nascimento, A., Lannigan, J., and Kashatus, D. (2016). High-throughput detection and quantification of mitochondrial fusion through imaging flow cytometry. Cytometry A *89*, 708-719.
Neel, Martin, T. D., Stratford, J. K., Zand, T. P., Reiner, D. J., and Der, C. J. (2011). The RalGEF-Ral Effector Signaling Network: The Road Less Traveled for Anti-Ras Drug Discovery. Genes & cancer *2*, 275-287.
Neel, Rossman, K. L., Martin, T. D., Hayes, T. K., Yeh, J. J., and Der, C. J. (2012). The RalB Small GTPase Mediates Formation of Invadopodia through a GTPase-Activating Protein-Independent Function of the RalBP1/RLIP76 Effector. Molecular and cellular biology *32*, 1374-1386.
Neoptolemos , J. P., Stocken , D. D., Friess , H., Bassi , C., Dunn , J. A., Hickey , H., Beger , H., Fernandez-Cruz , L., Dervenis , C., Lacaine , F.*, et al.* (2004). A Randomized Trial of Chemoradiotherapy and Chemotherapy after Resection of Pancreatic Cancer. New England Journal of Medicine *350*, 1200-1210.
O'Hayer, K. M., and Counter, C. M. (2006). A Genetically Defined Normal Human Somatic Cell System to Study Ras Oncogenesis In Vivo and In Vitro. In Methods in Enzymology, (Academic Press), pp. 637-647.
Obre, E., and Rossignol, R. (2015). Emerging concepts in bioenergetics and cancer research: metabolic flexibility, coupling, symbiosis, switch, oxidative tumors, metabolic remodeling, signaling and bioenergetic therapy. The international journal of biochemistry & cell biology *59*, 167-181.
Olichon, A. E., L.J.; Descoins, E.; et al. (2002). The human dynamin-related protein OPA1 is anchored to the mitochondrial inner membrane facing the inter-membrane space. FEBS *523*, 171-176.
Ortiz-Sandoval, C. G., Hughes, S. C., Dacks, J. B., and Simmen, T. (2014). Interaction with the effector dynamin-related protein 1 (Drp1) is an ancient function of Rab32 subfamily proteins. Cellular Logistics *4*, e986399.
Otera, H., Wang, C., Cleland, M. M., Setoguchi, K., Yokota, S., Youle, R. J., and Mihara, K. (2010). Mff is an essential factor for mitochondrial recruitment of Drp1 during mitochondrial fission in mammalian cells. The Journal of cell biology *191*, 1141-1158.
Pacold, M. E. S., S.; Perisic, O.; Lara-Gonzalez, S.; Davis, C.T.; Walker, E.H.; Hawkins, P.T.; Stephens, L.; Eccleston, J.F.; Williams, R.L. (2000). Crystal Structure and Functional Analysis of Ras Binding to Its Effector Phosphoinositide 3-Kinase γ. Cell *103*, 931-943.
Padanad, M. S., Konstantinidou, G., Venkateswaran, N., Melegari, M., Rindhe, S., Mitsche, M., Yang, C., Batten, K., Huffman, K. E., Liu, J.*, et al.* (2016). Fatty Acid Oxidation Mediated by Acyl-CoA Synthetase Long Chain 3 Is Required for Mutant KRAS Lung Tumorigenesis. Cell reports *16*, 1614-1628.
Paola, M., Alvaro, M.-H., Miriam, G.-A., Maricruz, A.-R., Julio, R.-L., and Paulina, C.-H. (2017). Mitochondrial dynamics and cancer. Tumor Biology *39*, 1010428317698391.
Patra, K. C., Wang, Q., Bhaskar, P. T., Miller, L., Wang, Z., Wheaton, W., Chandel, N., Laakso, M., Muller, W. J., Allen, E. L.*, et al.* (2013). Hexokinase 2 is required for tumor initiation and maintenance and its systemic deletion is therapeutic in mouse models of cancer. Cancer cell *24*, 213-228.

Pedersen, P. L. (2007). Warburg, me and Hexokinase 2: Multiple discoveries of key molecular events underlying one of cancers' most common phenotypes, the "Warburg Effect", i.e., elevated glycolysis in the presence of oxygen. J Bioenerg Biomembr *39*, 211-222.
Pitts, K. R., McNiven, M. A., and Yoon, Y. (2004). Mitochondria-specific Function of the Dynamin Family Protein DLP1 Is Mediated by Its C-terminal Domains. Journal of Biological Chemistry *279*, 50286-50294.
Pomerantz, J., Schreiber-Agus, N., Liégeois, N. J., Silverman, A., Alland, L., Chin, L., Potes, J., Chen, K., Orlow, I., Lee, H.-W*., et al.* (1998). The Ink4a Tumor Suppressor Gene Product, p19Arf, Interacts with MDM2 and Neutralizes MDM2's Inhibition of p53. Cell *92*, 713-723.
Prieto, J., León, M., Ponsoda, X., Sendra, R., Bort, R., Ferrer-Lorente, R., Raya, A., López-García, C., and Torres, J. (2016). Early ERK1/2 activation promotes DRP1-dependent mitochondrial fission necessary for cell reprogramming. Nature Communications *7*, 11124.
Prowse, A. B., Chong, F., Elliott, D. A., Elefanty, A. G., Stanley, E. G., Gray, P. P., Munro, T. P., and Osborne, G. W. (2012). Analysis of mitochondrial function and localisation during human embryonic stem cell differentiation in vitro. PloS one *7*, e52214.
Pyakurel, A., Savoia, C., Hess, D., and Scorrano, L. (2015a). Extracellular Regulated Kinase Phosphorylates Mitofusin 1 to Control Mitochondrial Morphology and Apoptosis. Molecular cell.
Pyakurel, A., Savoia, C., Hess, D., and Scorrano, L. (2015b). Extracellular Regulated Kinase Phosphorylates Mitofusin 1 to Control Mitochondrial Morphology and Apoptosis. Molecular cell *58*, 244-254.
Pylayeva-Gupta, Y., Grabocka, E., and Bar-Sagi, D. (2011). RAS oncogenes: weaving a tumorigenic web. Nature Reviews Cancer *11*, 761.
Qian, W., Choi, S., Gibson, G. A., Watkins, S. C., Bakkenist, C. J., and Van Houten, B. (2012). Mitochondrial hyperfusion induced by loss of the fission protein Drp1 causes ATM-dependent G2/M arrest and aneuploidy through DNA replication stress. J Cell Sci *125*, 5745-5757.
Qian, W., Wang, J., and Van Houten, B. (2013). The role of dynamin-related protein 1 in cancer growth: a promising therapeutic target? Expert opinion on therapeutic targets *17*, 997-1001.
Quilliam, L. A. H., S.Y.; Rabun, K.M.; Wei, W.; Park, W.; Broek, D.; Der, C.J. (1994). Membrane-targeting potentiates guanine nucleotide exchange factor CDC25 and SOS1 activation of Ras transforming activity. Proceedings of the National Academy of Sciences of the United States of America *91*, 8512-8516.
Racoosin, E. L., and Swanson, J. A. (1993). Macropinosome maturation and fusion with tubular lysosomes in macrophages. The Journal of cell biology *121*, 1011-1020.
Rahib, L., Smith, B. D., Aizenberg, R., Rosenzweig, A. B., Fleshman, J. M., and Matrisian, L. M. (2014). Projecting cancer incidence and deaths to 2030: the unexpected burden of thyroid, liver, and pancreas cancers in the United States. Cancer Res *74*, 2913-2921.
Rajalingam, K., Schreck, R., Rapp, U. R., and Albert, S. (2007). Ras oncogenes and their downstream targets. Biochimica et biophysica acta *1773*, 1177-1195.
Rakovic, A. G. A. K. J. B. N. P., P.; Lohmann K.; Klein C. (2011). Mutations in PINK1 and Parkin Impair Ubiquitination of Mitofusins in Human Fibroblasts. PloS one *6*, 1-13.
Rambold, S. A. K. B. E. N. L.-S., J. (2011). Tubular network formation protects mitochondria from autophagosomal degradation during nutrient starvation. PNAS *108*, 10190-10195.
Rao, S., Tortola, L., Perlot, T., Wirnsberger, G., Novatchkova, M., Nitsch, R., Sykacek, P., Frank, L., Schramek, D., Komnenovic, V*., et al.* (2014). A dual role for autophagy in a murine model of lung cancer. Nature Communications *5*, 3056.
Rayess, H., Wang, M. B., and Srivatsan, E. S. (2012). Cellular senescence and tumor suppressor gene p16. International journal of cancer Journal international du cancer *130*, 1715-1725.
Rehman, J., Zhang, H. J., Toth, P. T., Zhang, Y., Marsboom, G., Hong, Z., Salgia, R., Husain, A. N., Wietholt, C., and Archer, S. L. (2012). Inhibition of mitochondrial fission prevents cell cycle progression in lung cancer. FASEB journal : official publication of the Federation of American Societies for Experimental Biology *26*, 2175-2186.

Rosenfeldt, M. T., O'Prey, J., Morton, J. P., Nixon, C., MacKay, G., Mrowinska, A., Au, A., Rai, T. S., Zheng, L., Ridgway, R.*, et al.* (2013). p53 status determines the role of autophagy in pancreatic tumour development. Nature *504*, 296-300.
Rosenfeldt, M. T., and Ryan, K. M. (2011). The multiple roles of autophagy in cancer. Carcinogenesis *32*, 955-963.
Rossignol, R., Gilkerson, R., Aggeler, R., Yamagata, K., Remington, S. J., and Capaldi, R. A. (2004). Energy Substrate Modulates Mitochondrial Structure and Oxidative Capacity in Cancer Cells. Cancer Research *64*, 985-993.
Roy, M., Reddy, P. H., Iijima, M., and Sesaki, H. (2015). Mitochondrial Division and Fusion in Metabolism. Current opinion in cell biology *33*, 111-118.
Rozenblum, E., Schutte, M., Goggins, M., Hahn, S. A., Panzer, S., Zahurak, M., Goodman, S. N., Sohn, T. A., Hruban, R. H., Yeo, C. J., and Kern, S. E. (1997). Tumor-suppressive Pathways in Pancreatic Carcinoma. Cancer Research *57*, 1731-1734.
Ryan, D. P., Hong, T. S., and Bardeesy, N. (2014). Pancreatic Adenocarcinoma. The New England journal of medicine *371*, 1039-1049.
Ryan, J. J., Marsboom, G., Fang, Y.-H., Toth, P. T., Morrow, E., Luo, N., Piao, L., Hong, Z., Ericson, K., Zhang, H. J.*, et al.* (2013). PGC1α-mediated Mitofusin-2 Deficiency in Female Rats and Humans with Pulmonary Arterial Hypertension. American Journal of Respiratory and Critical Care Medicine *187*, 865-878.
Samuels, Y., and Velculescu, V. E. (2004). Oncogenic Mutations of PIK3CA in Human Cancers. Cell Cycle *3*, 1221-1224.
Santel, A. F., M.T. (2001). Control of mitochondrial morphology by a human mitofusin. J Cell Sci *114*, 867-874.
Sasaki, H. (2012). Overexpression of GLUT1 correlates with Kras mutations in lung carcinomas. Molecular medicine reports *5*, 599-602.
Scarlett, C. J., Salisbury, E. L., Biankin, A. V., and Kench, J. (2011). Precursor lesions in pancreatic cancer: morphological and molecular pathology. Pathology *43*, 183-200.
Scatena, R. (2012). Mitochondria and Cancer: A Growing Role in Apoptosis, Cancer Cell Metabolism and Dedifferentiation. In Advances in Mitochondrial Medicine, R. Scatena, P. Bottoni, and B. Giardina, eds. (Dordrecht: Springer Netherlands), pp. 287-308.
Scheffzek, K., Ahmadian, M. R., Kabsch, W., Wiesmüller, L., Lautwein, A., Schmitz, F., and Wittinghofer, A. (1997). The Ras-RasGAP Complex: Structural Basis for GTPase Activation and Its Loss in Oncogenic Ras Mutants. Science *277*, 333-339.
Schell, John C., Olson, Kristofor A., Jiang, L., Hawkins, Amy J., Van Vranken, Jonathan G., Xie, J., Egnatchik, Robert A., Earl, Espen G., DeBerardinis, Ralph J., and Rutter, J. (2014). A Role for the Mitochondrial Pyruvate Carrier as a Repressor of the Warburg Effect and Colon Cancer Cell Growth. Molecular cell *56*, 400-413.
Schlieman, M. G., Fahy, B. N., Ramsamooj, R., Beckett, L., and Bold, R. J. (2003). Incidence, mechanism and prognostic value of activated AKT in pancreas cancer. British Journal of Cancer *89*, 2110-2115.
Schrepfer, E., and Scorrano, L. (2016). Mitofusins, from Mitochondria to Metabolism. Molecular cell *61*, 683-694.
Schubbert, S., Shannon, K., and Bollag, G. (2007). Hyperactive Ras in developmental disorders and cancer. Nat Rev Cancer *7*, 295-308.
Scorrano, L. (2013). Keeping mitochondria in shape: a matter of life and death. European journal of clinical investigation *43*, 886-893.
Sebolt-Leopold, J. S., and Herrera, R. (2004). Targeting the mitogen-activated protein kinase cascade to treat cancer. Nature Reviews Cancer *4*, 937.

Serasinghe, M. N., Wieder, S. Y., Renault, T. T., Elkholi, R., Asciolla, J. J., Yao, J. L., Jabado, O., Hoehn, K., Kageyama, Y., Sesaki, H., and Chipuk, J. E. (2015). Mitochondrial division is requisite to RAS-induced transformation and targeted by oncogenic MAPK pathway inhibitors. Molecular cell *57*, 521-536.
Serrano, M., Lin, A. W., McCurrach, M. E., Beach, D., and Lowe, S. W. (1997). Oncogenic ras Provokes Premature Cell Senescence Associated with Accumulation of p53 and p16INK4a. Cell *88*, 593-602.
Sheridan, C., and Martin, S. J. (2010). Mitochondrial fission/fusion dynamics and apoptosis. Mitochondrion *10*, 640-648.
Shieh, S.-Y., Ikeda, M., Taya, Y., and Prives, C. (1997). DNA Damage-Induced Phosphorylation of p53 Alleviates Inhibition by MDM2. Cell *91*, 325-334.
Shields, J. M., Pruitt, K., McFall, A., Shaub, A., and Der, C. J. (2000). Understanding Ras: 'it ain't over 'til it's over'. Trends in cell biology *10*, 147-154.
Shin, S. Y., Rath, O., Choo, S. M., Fee, F., McFerran, B., Kolch, W., and Cho, K. H. (2009). Positive- and negative-feedback regulations coordinate the dynamic behavior of the Ras-Raf-MEK-ERK signal transduction pathway. J Cell Sci *122*, 425-435.
Shirihai, O. S., Song, M., and Dorn, G. W., 2nd (2015). How mitochondrial dynamism orchestrates mitophagy. Circ Res *116*, 1835-1849.
Siegel, R. L., Miller, K. D., and Jemal, A. (2018). Cancer statistics, 2018. CA: A Cancer Journal for Clinicians *68*, 7-30.
Smirnova, E. G., L.; et al. (2001). Dynamin-related Protein Drp1 Is Required for Mitochondrial Division in Mammalian Cells. Mol Biol Cell *12*, 2245-2256.
Smirnova, E. S., D. et al. (1998). A Human Dynamin-related Protein Controls the Distribution of Mitochondria. The Journal of cell biology *143*, 351-358.
Smith, S. C., Oxford, G., Baras, A. S., Owens, C., Havaleshko, D., Brautigan, D. L., Safo, M. K., and Theodorescu, D. (2007). Expression of Ral GTPases, Their Effectors, and Activators in Human Bladder Cancer. Clinical Cancer Research *13*, 3803-3813.
Son, J., Lyssiotis, C. A., Ying, H., Wang, X., Hua, S., Ligorio, M., Perera, R. M., Ferrone, C. R., Mullarky, E., Shyh-Chang, N*., et al.* (2013). Glutamine supports pancreatic cancer growth through a KRAS-regulated metabolic pathway. Nature *496*, 101-105.
Song, Z., Chen, H., Fiket, M., Alexander, C., and Chan, D. C. (2007). OPA1 processing controls mitochondrial fusion and is regulated by mRNA splicing, membrane potential, and Yme1L. The Journal of cell biology *178*, 749-755.
Soubannier, V., and McBride, H. M. (2009). Positioning mitochondrial plasticity within cellular signaling cascades. Biochimica et biophysica acta *1793*, 154-170.
Sousa, C. M., Biancur, D. E., Wang, X., Halbrook, C. J., Sherman, M. H., Zhang, L., Kremer, D., Hwang, R. F., Witkiewicz, A. K., Ying, H*., et al.* (2016). Pancreatic stellate cells support tumour metabolism through autophagic alanine secretion. Nature *536*, 479-483.
Sousa, C. M., and Kimmelman, A. C. (2014). The complex landscape of pancreatic cancer metabolism. Carcinogenesis *35*, 1441-1450.
Stanton, V. P. N., D.W.; Laudano, A.P.; Cooper, G.M. (1989). Definition of the human raf amino-terminal regulatory region by deletion mutagenesis. Molecular and cellular biology *9*, 639-647.
Steelman, L. S. C., W.H.; Abrams, S.L.; et al. (2011). Roles of the Raf/MEK/ERK and PI3K/PTEN/Akt/mTOR pathways in controlling growth and sensitivity to therapy-implications for cancer and aging. Aging *3*, 192-222.
Stokes, J. B., Adair, S. J., Slack-Davis, J. K., Walters, D. M., Tilghman, R. W., Hershey, E. D., Lowrey, B., Thomas, K. S., Bouton, A. H., and Hwang, R. F. (2011). Inhibition of focal adhesion kinase by PF-562,271 inhibits the growth and metastasis of pancreatic cancer concomitant with altering the tumor microenvironment. Molecular cancer therapeutics *10*, 2135-2145.

Strack, S., and Cribbs, J. T. (2012). Allosteric modulation of Drp1 mechanoenzyme assembly and mitochondrial fission by the variable domain. Journal of Biological Chemistry *287*, 10990-11001.
Strohecker, A. M., Guo, J. Y., Karsli-Uzunbas, G., Price, S. M., Chen, G. J., Mathew, R., McMahon, M., and White, E. (2013). Autophagy Sustains Mitochondrial Glutamine Metabolism and Growth of BRAF(V600E)–Driven Lung Tumors. Cancer discovery *3*, 10.1158/2159-8290.CD-1113-0397.
Su, B., Wang, X., Bonda, D., Perry, G., Smith, M., and Zhu, X. (2010). Abnormal Mitochondrial Dynamics—A Novel Therapeutic Target for Alzheimer's Disease? Molecular neurobiology *41*, 87-96.
Svensson, R. U., Parker, S. J., Eichner, L. J., Kolar, M. J., Wallace, M., Brun, S. N., Lombardo, P. S., Van Nostrand, J. L., Hutchins, A., Vera, L.*, et al.* (2016). Inhibition of acetyl-CoA carboxylase suppresses fatty acid synthesis and tumor growth of non-small cell lung cancer in preclinical models. Nature medicine *22*, 1108-1119.
Taguchi, N., Ishihara, N., Jofuku, A., Oka, T., and Mihara, K. (2007). Mitotic phosphorylation of dynamin-related GTPase Drp1 participates in mitochondrial fission. The Journal of biological chemistry *282*, 11521-11529.
Tanwar, D. K., Parker, D. J., Gupta, P., Spurlock, B., Alvarez, R. D., Basu, M. K., and Mitra, K. (2016). Crosstalk between the mitochondrial fission protein, Drp1, and the cell cycle is identified across various cancer types and can impact survival of epithelial ovarian cancer patients. Oncotarget *7*, 60021-60037.
Tape, Christopher J., Ling, S., Dimitriadi, M., McMahon, Kelly M., Worboys, Jonathan D., Leong, Hui S., Norrie, Ida C., Miller, Crispin J., Poulogiannis, G., Lauffenburger, Douglas A., and Jørgensen, C. (2016). Oncogenic KRAS Regulates Tumor Cell Signaling via Stromal Reciprocation. Cell *165*, 910-920.
Toshiyuki, M., and Reed, J. C. (1995). Tumor suppressor p53 is a direct transcriptional activator of the human bax gene. Cell *80*, 293-299.
Trahey, M. M., F. (1987). A Cytoplasmic Protein Stimulates Normal N-ras p21 GTPase, but Does Not Affect Oncogenic Mutants. Science *238*, 542-545.
Trotta, A. P., and Chipuk, J. E. (2017). Mitochondrial dynamics as regulators of cancer biology. Cellular and molecular life sciences : CMLS *74*, 1999-2017.
Tsai, F. D., Lopes, M. S., Zhou, M., Court, H., Ponce, O., Fiordalisi, J. J., Gierut, J. J., Cox, A. D., Haigis, K. M., and Philips, M. R. (2015). K-Ras4A splice variant is widely expressed in cancer and uses a hybrid membrane-targeting motif. Proceedings of the National Academy of Sciences of the United States of America *112*, 779-784.
Turski, M. L., Brady, D. C., Kim, H. J., Kim, B.-E., Nose, Y., Counter, C. M., Winge, D. R., and Thiele, D. J. (2012). A Novel Role for Copper in Ras/Mitogen-Activated Protein Kinase Signaling. Molecular and cellular biology *32*, 1284-1295.
Tuveson, D. A., Shaw, A. T., Willis, N. A. et al. (2004). Endogenous oncogenic K-ras^{G12D} stimulates proliferation and widespread neoplastic and developmental defects. Cancer cell *5*, 375-387.
Unuma, K., Aki, T., Funakoshi, T., Hashimoto, K., and Uemura, K. (2015). Extrusion of mitochondrial contents from lipopolysaccharide-stimulated cells: Involvement of autophagy. Autophagy *11*, 1520-1536.
van der Bliek, A. M., Shen, Q., and Kawajiri, S. (2013). Mechanisms of mitochondrial fission and fusion. Cold Spring Harbor perspectives in biology *5*.
Vander Heiden, M. G., Cantley, L. C., and Thompson, C. B. (2009). Understanding the Warburg Effect: The Metabolic Requirements of Cell Proliferation. Science (New York, NY) *324*, 1029-1033.
Vanhaesebroeck, B. W., M.J.; Kotani, K; Stein, R.; Warne, PH.; Zvelebil, M.J.; Higashi, K.; Volinia, S.; Downward , J.; Waterfield, M.D. (1997). P110 δ, a novel phosphoinositide 3-kinase in leukocytes. Proceedings of the National Academy of Sciences of the United States of America *94*, 4330-4335.
Vauthey, J. N., and Dixon, E. (2009). AHPBA/SSO/SSAT Consensus Conference on Resectable and Borderline Resectable Pancreatic Cancer: rationale and overview of the conference. Annals of surgical oncology *16*, 1725-1726.

Vigil, D., Martin, T. D., Williams, F., Yeh, J. J., Campbell, S. L., and Der, C. J. (2010). Aberrant Overexpression of the Rgl2 Ral Small GTPase-specific Guanine Nucleotide Exchange Factor Promotes Pancreatic Cancer Growth through Ral-dependent and Ral-independent Mechanisms. Journal of Biological Chemistry *285*, 34729-34740.
Visvader, Jane E., and Lindeman, Geoffrey J. (2012). Cancer Stem Cells: Current Status and Evolving Complexities. Cell Stem Cell *10*, 717-728.
Von Hoff , D. D., Ervin , T., Arena , F. P., Chiorean , E. G., Infante , J., Moore , M., Seay , T., Tjulandin , S. A., Ma , W. W., Saleh , M. N*., et al.* (2013). Increased Survival in Pancreatic Cancer with nab-Paclitaxel plus Gemcitabine. New England Journal of Medicine *369*, 1691-1703.
Vyas, S., Zaganjor, E., and Haigis, M. C. (2016). Mitochondria and Cancer. Cell *166*, 555-566.
Wabnitz, G. H., Goursot, C., Jahraus, B., Kirchgessner, H., Hellwig, A., Klemke, M., Konstandin, M. H., and Samstag, Y. (2010). Mitochondrial translocation of oxidized cofilin induces caspase-independent necrotic-like programmed cell death of T cells. Cell Death Dis *1*, e58.
Wai, T., and Langer, T. (2016). Mitochondrial Dynamics and Metabolic Regulation. Trends in Endocrinology & Metabolism *27*, 105-117.
Wakabayashi, J., Zhang, Z., Wakabayashi, N., Tamura, Y., Fukaya, M., Kensler, T. W., Iijima, M., and Sesaki, H. (2009). The dynamin-related GTPase Drp1 is required for embryonic and brain development in mice. The Journal of cell biology *186*, 805-816.
Walters, D. M., Stokes, J. B., Adair, S. J., Stelow, E. B., Borgman, C. A., Lowrey, B. T., Xin, W., Blais, E. M., Lee, J. K., Papin, J. A*., et al.* (2013). Clinical, Molecular and Genetic Validation of a Murine Orthotopic Xenograft Model of Pancreatic Adenocarcinoma Using Fresh Human Specimens. PloS one *8*, e77065.
Wang, C.-C., Bajikar, S. S., Jamal, L., Atkins, K. A., and Janes, K. A. (2014). A time- and matrix-dependent TGFBR3–JUND–KRT5 regulatory circuit in single breast epithelial cells and basal-like premalignancies. Nature cell biology *16*, 345-356.
Warburg, O. (1956). On the Origin of Cancer Cells. Science *123*, 309-314.
Waterham , H. R., Koster , J., van Roermund , C. W. T., Mooyer , P. A. W., Wanders , R. J. A., and Leonard , J. V. (2007). A Lethal Defect of Mitochondrial and Peroxisomal Fission. New England Journal of Medicine *356*, 1736-1741.
Weinberg, F., Hamanaka, R., Wheaton, W. W., Weinberg, S., Joseph, J., Lopez, M., Kalyanaraman, B., Mutlu, G. M., Budinger, G. R. S., and Chandel, N. S. (2010). Mitochondrial metabolism and ROS generation are essential for Kras-mediated tumorigenicity. Proceedings of the National Academy of Sciences *107*, 8788-8793.
Weissmueller, S., Manchado, E., Saborowski, M., Morris, J. P., Wagenblast, E., Davis, C. A., Moon, S.-H., Pfister, N. T., Tschaharganeh, D. F., Kitzing, T*., et al.* (2014). Mutant p53 drives pancreatic cancer metastasis through cell-autonomous PDGF receptor beta signaling. Cell *157*, 382-394.
Welsch, M. E., Kaplan, A., Chambers, J. M., Stokes, M. E., Bos, P. H., Zask, A., Zhang, Y., Sanchez-Martin, M., Badgley, M. A., Huang, C. S*., et al.* (2017). Multivalent Small-Molecule Pan-RAS Inhibitors. Cell *168*, 878-889.e829.
Westermann, B. (2010). Mitochondrial fusion and fission in cell life and death. Nature reviews Molecular cell biology *11*, 872-884.
Westermann, B. (2012). Bioenergetic role of mitochondrial fusion and fission. Biochimica et biophysica acta *1817*, 1833-1838.
White, E. (2015). The role for autophagy in cancer. The Journal of Clinical Investigation *125*, 42-46.
Whyte, D. B., Kirschmeier, P., Hockenberry, T. N., Nunez-Oliva, I., James, L., Catino, J. J., Bishop, W. R., and Pai, J.-K. (1997). K- and N-Ras Are Geranylgeranylated in Cells Treated with Farnesyl Protein Transferase Inhibitors. Journal of Biological Chemistry *272*, 14459-14464.

Wojcieszyn, J. W. S., R.A.; Lumley-Sap, K.; Jacobson, K.A. (1983). Studies on the Mechanism of Polyethylene Glycol-mediated Cell Fusion using Fluorescent Membrane and Cytoplasmic Probes. The Journal of cell biology *96*, 151-159.
Wright, L. P., and Philips, M. R. (2006). Thematic review series: lipid posttranslational modifications. CAAX modification and membrane targeting of Ras. Journal of lipid research *47*, 883-891.
Xia, J., and Wishart, D. S. (2010). MetPA: a web-based metabolomics tool for pathway analysis and visualization. Bioinformatics *26*, 2342-2344.
Xiang, J.-F., Wang, W.-Q., Liu, L., Xu, H.-X., Wu, C.-T., Yang, J.-X., Qi, Z.-H., Wang, Y.-Q., Xu, J., Liu, C*., et al.* (2016). Mutant p53 determines pancreatic cancer poor prognosis to pancreatectomy through upregulation of cavin-1 in patients with preoperative serum CA19-9 ≥ 1,000 U/mL. Scientific Reports *6*, 19222.
Xu, K., Chen, G., Li, X., Wu, X., Chang, Z., Xu, J., Zhu, Y., Yin, P., Liang, X., and Dong, L. (2017). MFN2 suppresses cancer progression through inhibition of mTORC2/Akt signaling. Scientific Reports *7*, 41718.
Yang, J., Shen MH. (2006). Polyethylene glycol-mediated cell fusion. Methods in molecular biology *325*, 59-66.
Yang, S., Wang, X., Contino, G., Liesa, M., Sahin, E., Ying, H., Bause, A., Li, Y., Stommel, J. M., Dell'Antonio, G*., et al.* (2011). Pancreatic cancers require autophagy for tumor growth. Genes & development *25*, 717-729.
Yang, Z., and Klionsky, D. J. (2010). Mammalian autophagy: core molecular machinery and signaling regulation. Current opinion in cell biology *22*, 124-131.
Yarbrough, W. G., Buckmire, R. A., Bessho, M., and Liu, E. T. (1999). Biologic and Biochemical Analyses of p16 INK4a Mutations From Primary Tumors. JNCI: Journal of the National Cancer Institute *91*, 1569-1574.
Ychou, M., Conroy, T., Seitz, J. F., Gourgou, S., Hua, A., Mery-Mignard, D., and Kramar, A. (2003). An open phase I study assessing the feasibility of the triple combination: oxaliplatin plus irinotecan plus leucovorin/ 5-fluorouracil every 2 weeks in patients with advanced solid tumors. Annals of Oncology *14*, 481-489.
Ying, H., Dey, P., Yao, W., Kimmelman, A. C., Draetta, G. F., Maitra, A., and DePinho, R. A. (2016). Genetics and biology of pancreatic ductal adenocarcinoma. Genes & development *30*, 355-385.
Ying, H., Elpek, K. G., Vinjamoori, A., Zimmerman, S. M., Chu, G. C., Yan, H., Fletcher-Sananikone, E., Zhang, H., Liu, Y., Wang, W*., et al.* (2011). Pten is a major tumor suppressor in pancreatic ductal adenocarcinoma and regulates an NF-κB-cytokine network. Cancer discovery *1*, 158-169.
Ying, H., Kimmelman, A. C., Lyssiotis, C. A., Hua, S., Chu, G. C., Fletcher-Sananikone, E., Locasale, J. W., Son, J., Zhang, H., Coloff, J. L*., et al.* (2012). Oncogenic Kras maintains pancreatic tumors through regulation of anabolic glucose metabolism. Cell *149*, 656-670.
Yoon, Y., Galloway, C. A., Jhun, B. S., and Yu, T. (2011). Mitochondrial Dynamics in Diabetes. Antioxidants & redox signaling *14*, 439-457.
Youle, R. J., and Karbowski, M. (2005). Mitochondrial fission in apoptosis. Nature Reviews Molecular Cell Biology *6*, 657.
Yu, T., Robotham, J. L., and Yoon, Y. (2006). Increased production of reactive oxygen species in hyperglycemic conditions requires dynamic change of mitochondrial morphology. Proceedings of the National Academy of Sciences of the United States of America *103*, 2653-2658.
Yu, T. J., B.S.; Yoon, Y. (2011). High-Glucose Stimulation Increases Reactive Oxygen Species Production Through the Calcium and Mitogen-Activated Protein Kinase-Mediated Activation of Mitochondrial Fission. Antioxidants & redox signaling *14*, 425-435.
Yuan, T. L., and Cantley, L. C. (2008). PI3K pathway alterations in cancer: variations on a theme. Oncogene *27*, 5497-5510.

Yun, J., Rago, C., Cheong, I., Pagliarini, R., Angenendt, P., Rajagopalan, H., Schmidt, K., Wilson, J. K. V., Markowitz, S., Zhou, S.*, et al.* (2009). Glucose Deprivation Contributes to the Development of KRAS Pathway Mutations in Tumor Cells. Science (New York, NY) *325*, 1555.
Zeitouni, D., Pylayeva-Gupta, Y., Der, C. J., and Bryant, K. L. (2016). KRAS Mutant Pancreatic Cancer: No Lone Path to an Effective Treatment. Cancers (Basel) *8*.
Zhang, B., Davidson, M. M., Zhou, H., Wang, C., Walker, W. F., and Hei, T. K. (2013a). Cytoplasmic irradiation results in mitochondrial dysfunction and DRP1-dependent mitochondrial fission. Cancer research *73*, 6700-6710.
Zhang, G.-E., Jin, H.-L., Lin, X.-K., Chen, C., Liu, X.-S., Zhang, Q., and Yu, J.-R. (2013b). Anti-Tumor Effects of Mfn2 in Gastric Cancer. International Journal of Molecular Sciences *14*, 13005-13021.
Zhang, Q., Jeppesen, D. K., Higginbotham, J. N., Demory Beckler, M., Poulin, E. J., Walsh, A. J., Skala, M. C., McKinley, E. T., Manning, H. C., Hight, M. R.*, et al.* (2018). Mutant KRAS Exosomes Alter the Metabolic State of Recipient Colonic Epithelial Cells. Cellular and Molecular Gastroenterology and Hepatology *5*, 627-629.e626.
Zhang, Y., Xiong, Y., and Yarbrough, W. G. (1998). ARF Promotes MDM2 Degradation and Stabilizes p53: ARF-INK4a Locus Deletion Impairs Both the Rb and p53 Tumor Suppression Pathways. Cell *92*, 725-734.
Zhao, J., Liu, T., Jin, S., Wang, X., Qu, M., Uhlen, P., Tomilin, N., Shupliakov, O., Lendahl, U., and Nister, M. (2011). Human MIEF1 recruits Drp1 to mitochondrial outer membranes and promotes mitochondrial fusion rather than fission. The EMBO journal *30*, 2762-2778.
Zhao, J., Zhang, J., Yu, M., Xie, Y., Huang, Y., Wolff, D., Abel, P., and Tu, Y. (2013a). Mitochondrial dynamics regulates migration and invasion of breast cancer cells. Oncogene *32*, 4814-4824.
Zhao, J., Zhang, J., Yu, M., Xie, Y., Huang, Y., Wolff, D. W., Abel, P. W., and Tu, Y. (2013b). Mitochondrial dynamics regulates migration and invasion of breast cancer cells. Oncogene *32*, 4814-4824.
Zimmermann, G., Papke, B., Ismail, S., Vartak, N., Chandra, A., Hoffmann, M., Hahn, S. A., Triola, G., Wittinghofer, A., Bastiaens, P. I. H., and Waldmann, H. (2013). Small molecule inhibition of the KRAS–PDEδ interaction impairs oncogenic KRAS signalling. Nature *497*, 638.
Zorzano, A., Liesa, M., Sebastián, D., Segalés, J., and Palacín, M. (2010). Mitochondrial fusion proteins: Dual regulators of morphology and metabolism. Seminars in Cell & Developmental Biology *21*, 566-574.
Zou, P., Liu, L., Zheng, L. D., Payne, K. K., Manjili, M. H., Idowu, M. O., Zhang, J., Schmelz, E. M., and Cheng, Z. (2016). Coordinated Upregulation of Mitochondrial Biogenesis and Autophagy in Breast Cancer Cells: The Role of Dynamin Related Protein-1 and Implication for Breast Cancer Treatment. Oxidative Medicine and Cellular Longevity *2016*, 4085727.
Züchner, S., Mersiyanova, I. V., Muglia, M., Bissar-Tadmouri, N., Rochelle, J., Dadali, E. L., Zappia, M., Nelis, E., Patitucci, A., Senderek, J.*, et al.* (2004). Mutations in the mitochondrial GTPase mitofusin 2 cause Charcot-Marie-Tooth neuropathy type 2A. Nature Genetics *36*, 449.